



Università
Ca'Foscari
Venezia

Scuola Dottorale di Ateneo
Graduate School

Dottorato di ricerca in Scienze Chimiche
Ciclo XXVIII
Anno di discussione 2015

Supramolecular organization of dyketopyrrolopyrrole derivatives

Settore scientifico disciplinare di afferenza: CHIM/06

Tesi di Dottorato di Ester Vagnozzi, matricola 810846

Coordinatore del Dottorato
Prof. Maurizio Selva

Tutore del Dottorando
Prof. Ottorino De Lucchi

Co-tutore del Dottorando
Dr. Giuseppe Borsato

SUPRAMOLECULAR ORGANIZATION OF DIKETOPYRROLOPYRROLE DERIVATIVES

1. WATER SOLUBLE DPPs

1.1 High Performance Pigments	13
1.2 DPP	14
1.2.1 Physical and chemical properties	14
a) UV-Vis	14
b) Fluorescence	15
c) X-Ray structure analysis	16
d) Chemical properties	16
1.2.2 Industrial synthesis	17
1.3 Supramolecular polymers	19
1.3.1 Noncovalent interactions used in supramolecular polymerizations	21
a) Hydrogen bond	21
b) π -interactions	25
c) Metal coordination	25
1.4 Supramolecular polymers in water	28
1.5 Self-healing materials	33
1.6 Supramolecular polymer derived from DPP: <i>longchain</i> -DPP	36
1.7 Aim	38
1.8 Synthesis of water soluble DPPs	40
1.8.1 Synthesis of TEG-DPP	40
1.8.2 Synthesis of monoTEG-DPP	45
1.8.3 TEG-DPP characterization in solution	48
a) UV-Vis spectroscopy	48
b) UV-Vis temperature-dependent analysis	49
c) NMR temperature-dependent analysis	58
d) Dynamic light scattering analysis	60
1.8.4 TEG-DPP characterization in the solid state	62
a) Differential scanning calorimetry analysis	62
b) Polarised optical microscopy analysis	63
c) Atomic force microscopy analysis	64
d) Scanning electron microscopi analysis	65

1.8.5 Mono TEG-DPP characterization in solution	66
a) UV-Vis spectroscopy	67
b) UV-Vis temperature-dependent analysis	68
1.8.6 Mono TEG-DPP characterization in the solid state	75
a) Differential scanning calorimetry analysis	75
b) Polarised optical microscopy analysis	75
c) Atomic force microscopy analysis	77
d) Scanning electron microscopy analysis	78
1.9 Conclusions	79
1.10 Experimental Section	81
1.10.1 General	81
1.10.2 Synthetic procedures	82
Appendix A	91
A1 Supramolecular polymerizations	91
A1.1 Isodesmic model	93
A1.2 Cooperative model	97
Bibliography	101

2 DOSY CHARACTERIZATION OF LONGCHAIN-DPP AND TEG-DPP

2.1	Introduction: measuring High-Resolution Diffusion by NMR Spectroscopy	107
2.1.1	Concepts of Molecular Diffusion in Isotropic Systems	107
2.1.2	The 2D DOSY Technique	108
2.1.3	Applications of NMR Diffusion Measurements in Supramolecular Chemistry	109
2.2	Aim	115
2.3	Synthesis of DOSY references	116
2.3.1	Dosy characterization	117
2.4	Conclusions	119
2.5	Experimental Section	120
2.5.1	General	120
2.5.2	Synthetic procedures	120
	Bibliography	123

3 LIQUID CRYSTALS BASED ON DPPs

3.1	Dendritic architecture	127
3.2	Dendrimers: design and synthesis	128
3.2.1	Synthetic Methodologies	131
	a) Divergent method	131
	b) Convergent procedures	131
3.3	Liquid Crystals	133
3.3.1	Mesophase of calamitic mesogens	134
3.3.2	Mesophase of discotic mesogens	136
3.4	Liquid-Crystal dendrimers	138
3.4.1	LC dendrimers with terminal mesogens	138
3.4.2	Main chain liquid crystal dendrimers	139
3.4.3	Intrinsic dendromesogens	141
3.5	Aim	143
3.6	Synthetic strategy	146
3.6.1	Synthesis of G1 pinacol boronic ester	147
3.6.2	Synthesis and characterization of G1-pDPP	150
3.6.3	Synthesis of G1.1 pinacol boronic ester	153
3.6.4	Synthesis and characterization of G1.1-pDPP	156
3.6.5	Synthesis of G2 pinacol boronic ester	158
3.6.6	Synthesis and characterization of G2-pDPP	161
3.6.7	Synthesis of methyl protected DPP dendrimers	163
	a) Synthesis and characterization of G1.1-methylDPP	163
	b) Synthesis and characterization of G2-methylDPP	165
3.7	Synthesis of N-functionalized DPP	167
3.7.1	Synthesis and characterization of G1-DPP	167
3.7.2	Synthesis of DPP-G2	169
3.7.3	Synthesis and characterization of G1-DPP spacer	171
3.7.4	Synthesis and characterization of G2-DPP spacer	173

3.8	Conclusions	175
3.9	Experimental Section	179
3.9.1	General	179
3.9.2	Synthetic procedures	180
	Bibliography	201

Acronyms and abbreviations

(CD ₃) ₂ SO	Dimethyl Sulfoxide-d6
1D	One Directional Order
2D	Two Directional Orders
ACN	Acetonitrile
AcOEt	Ethyl Acetate
AFM	Atomic Force Microscope
B ₂ pin ₂	Bis(pinacolato)diboron
BTAs	Trialkylbenzene-1,3,5-Tricarboxamides
C ₅ -NH ₂	Calix[5]Arene
C ₇ D ₈	Toluene-d8
CD	<i>Circular Dichroism</i>
CD ₂ Cl ₂	Dichloromethane-d2
CD ₃ CN	Acetonitrile-d3
CDCl ₃	Chloroform-d
Col _h	Hexagonal Columnar Phase
Col _o	Oblique Columnar Phase
Col _r	Rectangular Columnar Phase
Col _s	Square Columnar Phase
CP	Covalent/Conventional Polymer
D	Diffusion Coefficient
D ₂ O	Deuterium Oxide
C ₆ D ₆	Benzene-d6
DCM	Dichloromethane
DGEBA	Bisphenol A Diglycidyl Ether
DIC	N,N'-Diisopropylcarbodiimide
DLS	Dynamic Light Scattering
DMAP	4-Dimethylaminopyridine
DME	Dimethoxyethane
DMF	Dimethylformamide
DMSO	Dimethyl Sulfoxide
DMSO-d6	Dimethyl Sulfoxide-d6
DNA	Deoxyribonucleic Acid
DOSY	Diffusion-Ordered Spectroscopy
DP	Degree of Polymerization
DPP	Diketopyrrolopyrrole
DSC	Differential Scanning Calorimetry
DTBP	Di- <i>tert</i> -Butyl Peroxide
EA	Elementar Analysis
EDAC	1-Ethyl-3-(3-dimethylaminopropyl)carbodiimide
EFG	Electrophilic Functional Group
EFM	Electric Force Microscopy

ESI-MS	Electrospray Ionization – Mass Spectroscopy
EtOH	Ethanol
FC	Flash Chromatography
FFT	Fast Fourier Transformation
G1	First Generation
G2	Second Generation
HBP	Hydrogen-Bonding Brush Polymer
HPLC	<i>High Performance Liquid Chromatography</i>
HPPs	High Performance Pigments
ILT	Inverse Laplace Transformation
IR	Infrared
ITC	Isothermal Titration Calorimetry
LC	Liquid Crystal
MCH	Methylcyclohexane
Mebip	2,6-Bis(19-methylbenzimidazolyl)pyridine
MeOH	Methanol
MW	Molecular Weight
N*	Nematic Chiral Phase or Cholesteric phase
NFG	Nucleophilic Functional Group
NIR	Near-Infrared Spectroscopy
NMP	N-Methyl-2-Pyrrolidone
NMR	Nuclear Magnetic Resonance
PA-amide	Polyacrylate Amide
PAMAM	Poly(amido)amines
PC ₇₀ BM	[6,6]-Phenyl-C71-butyric acid methyl ester
PCE	Solar Cell Efficiency
PEG	<i>Polyethylene Glycol</i>
Pery-2	Amphiphilic Perylene
POM	Polarised Optical Microscopy
PPI	Poly(propylene)imines
ROS	Reactive Oxygen Species
SANS	Small-Angle Neutron Scattering
SEC	Exclusion Chromatography
SEM	<i>Scanning Electron Microscopy</i>
SmA	Smectic A phase
SmC	Smectic C phase
SP	Supramolecular Polymer
t-Boc	Di- <i>tert</i> -Butyl Dicarbonate
<i>t</i> -BuLi	<i>tert</i> -Butyllithium
t-BuOK	Potassium <i>tert</i> -Butoxide
TEG	Tri-(Ethylene Glycol)
TFA	Trifluoroacetic Acid
T _g	Glass Transition Temperature
TGA	Thermogravimetric Analysis
TGMDA	Tetraglycidyl Methylene Dianiline

THF	Tetrahydrofuran
TIPB	Tryisopropyl Borate
TLC	Thin Layer Chromatography
TMS	Tetramethylsilane
TNF	4,5,7-Trinitrofluorenone-2-Carboxylate
TPA	Two Photon Absorption
TPE	Thermoplastic Elastomer
TPEM	Two Photons Excitation Microscopy
UDETA	1-(2-Aminoethyl)-2-Imidazolidone
UPy	Ureidopyrimidinone
UV	Ultraviolet
Vis	Visible
VPO	Oligo(<i>p</i> -Phenylene Vinylenes)
XRD	X-Ray Diffraction
ϵ	Molar Extinction Coefficient
λ	Wavelength

Abbreviations of synthesised compounds

BrDPP	3,6-bis(4-bromophenyl)pyrrolo[3,4-c]pyrrole-1,4(2H,5H)-dione
BrDPP-Boc	di-tert-butyl 3,6-bis(4-bromophenyl)-1,4-dioxopyrrolo[3,4-c]pyrrole-2,5(1H,4H)-dicarboxylate
G1 Pinacol boronic ester	4,4,5,5-tetramethyl-2-(3,4,5-tris((4-(dodecyloxy)benzyl)oxy)phenyl)-1,3,2-dioxaborolane
G1.1 Pinacol boronic ester	4,4,5,5-tetramethyl-2-(4-((3,4,5-tris((4-(dodecyloxy)benzyl)oxy)benzyl)oxy)phenyl)-1,3,2-dioxaborolane
G1.1-methylDPP	2,5-dimethyl-3,6-bis(4'-((3,4,5-tris((4-(dodecyloxy)benzyl)oxy)benzyl)oxy)-[1,1'-biphenyl]-4-yl)pyrrolo[3,4-c]pyrrole-1,4(2H,5H)-dione
G1.1-pDPP	3,6-bis(4'-((3,4,5-tris((4-(dodecyloxy)benzyl)oxy)benzyl)oxy)-[1,1'-biphenyl]-4-yl)pyrrolo[3,4-c]pyrrole-1,4(2H,5H)-dione
G1.1-pDPP Boc	di-tert-butyl 1,4-dioxo-3,6-bis(4'-((3,4,5-tris((4-(dodecyloxy)benzyl)oxy)benzyl)oxy)-[1,1'-biphenyl]-4-yl)pyrrolo[3,4-c]pyrrole-2,5(1H,4H)-dicarboxylate
G1-DPP	3,6-diphenyl-2,5-bis(3,4,5-tris((4-(dodecyloxy)benzyl)oxy)benzyl)pyrrolo[3,4-c]pyrrole-1,4(2H,5H)-dione
G1-DPP spacer	bis(3,4,5-tris((4-(dodecyloxy)benzyl)oxy)benzyl) 2,2'-(1,4-dioxo-3,6-diphenylpyrrolo[3,4-c]pyrrole-2,5(1H,4H)-diyl)diacetate
G1-pDPP	3,6-bis(3',4',5'-tris((4-(dodecyloxy)benzyl)oxy)-[1,1'-biphenyl]-4-yl)pyrrolo[3,4-c]pyrrole-1,4(2H,5H)-dione
G1-pDPP Boc	di-tert-butyl 1,4-dioxo-3,6-bis(3',4',5'-tris((4-

	(dodecyloxy)benzyl)oxy)-[1,1'-biphenyl]-4-yl)pyrrolo[3,4-c]pyrrole-2,5(1H,4H)-dicarboxylate
G2 Pinacol boronic ester	2-(3,5-bis((3,4,5-tris((4-(dodecyloxy)benzyl)oxy)benzyl)oxy)phenyl)-4,4,5,5-tetramethyl-1,3,2-dioxaborolane
G2-DPP	2,5-bis(3,5-bis((3,4,5-tris((4-(dodecyloxy)benzyl)oxy)benzyl)oxy)benzyl)-3,6-diphenylpyrrolo[3,4-c]pyrrole-1,4(2H,5H)-dione
G2-DPP spacer	C ₂₉₂ H ₄₁₂ N ₂ O ₃₄ ; M. W. 4494,39
G2-methylDPP	3,6-bis(3',5'-bis((3,4,5-tris((4-(dodecyloxy)benzyl)oxy)benzyl)oxy)-[1,1'-biphenyl]-4-yl)-2,5-dimethylpyrrolo[3,4-c]pyrrole-1,4(2H,5H)-dione
G2-pDPP	3,6-bis(3',5'-bis((3,4,5-tris((4-(dodecyloxy)benzyl)oxy)benzyl)oxy)-[1,1'-biphenyl]-4-yl)pyrrolo[3,4-c]pyrrole-1,4(2H,5H)-dione
G2-pDPP Boc	di-tert-butyl 3,6-bis(3',5'-bis((3,4,5-tris((4-(dodecyloxy)benzyl)oxy)benzyl)oxy)-[1,1'-biphenyl]-4-yl)-1,4-dioxopyrrolo[3,4-c]pyrrole-2,5(1H,4H)-dicarboxylate
<i>Longchain</i> -DPP	3,6-bis(3',4',5'-tris(dodecyloxy)-[1,1'-biphenyl]-4-yl)pyrrolo[3,4-c]pyrrole-1,4(2H,5H)-dione
<i>Longchain</i> -DPP Boc	di-tert-butyl 1,4-dioxo-3,6-bis(3',4',5'-tris(dodecyloxy)-[1,1'-biphenyl]-4-yl)pyrrolo[3,4-c]pyrrole-2,5(1H,4H)-dicarboxylate
Methyl BrDPP	3,6-bis(4-bromophenyl)-2,5-dimethylpyrrolo[3,4-c]pyrrole-1,4(2H,5H)-dione
Methyl <i>longchain</i> -DPP	2,5-dimethyl-3,6-bis(3',4',5'-tris(dodecyloxy)-[1,1'-biphenyl]-4-yl)pyrrolo[3,4-c]pyrrole-1,4(2H,5H)-dione
Mono BrDPP	3-(4-bromophenyl)-6-phenylpyrrolo[3,4-c]pyrrole-1,4(2H,5H)-dione
Mono BrDPP-Boc	di-tert-butyl 3-(4-bromophenyl)-1,4-dioxo-6-phenylpyrrolo[3,4-c]pyrrole-2,5(1H,4H)-dicarboxylate
Mono TEG-DPP	3-phenyl-6-(3',4',5'-tris(2-(2-(2-methoxyethoxy)ethoxy)ethoxy)-[1,1'-biphenyl]-4-yl)pyrrolo[3,4-c]pyrrole-1,4(2H,5H)-dione
Mono TEG-DPP Boc	di-tert-butyl 1,4-dioxo-3-phenyl-6-(3',4',5'-tris(2-(2-(2-methoxyethoxy)ethoxy)ethoxy)-[1,1'-biphenyl]-4-yl)pyrrolo[3,4-c]pyrrole-2,5(1H,4H)-dicarboxylate
TEG-DPP	3,6-bis(3',4',5'-tris(2-(2-(2-methoxyethoxy)ethoxy)ethoxy)-[1,1'-biphenyl]-4-yl)pyrrolo[3,4-c]pyrrole-1,4(2H,5H)-dione
TEG-DPP Boc	di-tert-butyl 1,4-dioxo-3,6-bis(3',4',5'-tris(2-(2-(2-methoxyethoxy)ethoxy)ethoxy)-[1,1'-biphenyl]-4-yl)pyrrolo[3,4-c]pyrrole-2,5(1H,4H)-dicarboxylate
TEG-pinacol boronic ester	4,4,5,5-tetramethyl-2-(3,4,5-tris(2-(2-(2-methoxyethoxy)ethoxy)ethoxy)phenyl)-1,3,2-dioxaborolane
Tosyl-TEG	2-(2-(2-methoxyethoxy)ethoxy)ethyl 4-methylbenzenesulfonate

1 WATER SOLUBLE DPPs

1.1 High Performance Pigments

High Performance Pigments (HPP) are organic pigments possessing excellence of performance, application permanence, compatibility with health, safety and environmental issues, good profitability in value-in-use to the consumer and return of investment to the producer. In the pigment literature the term HPP appears for the first time in the mid-sixties. Nowadays, a large number of studies about these special organic pigments exist, their applications are numerous and mostly exploit the light and weather fastness of these molecules and their good tinctorial properties.¹

HPPs encompass a wide variety of pigments, including phthalocyanines (blue and green), indanthrone, quinacridone, perylene, diketopyrrolopyrrole, naphthol, carbazole violet, benzimidazolone, azo condensations, metal complex pigments and isoindolinone. In Table 1.1 we report some examples of HPPs.

In this dissertation it is examined in depth the molecule of diketopyrrolopyrrole (DPP), best known as Ferrari Red.

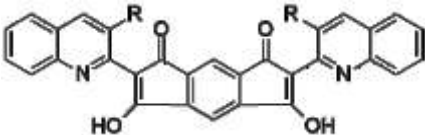
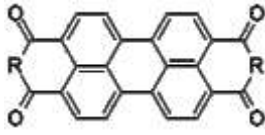
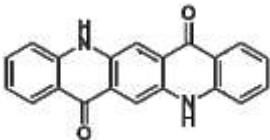
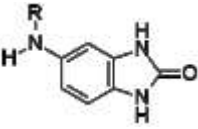
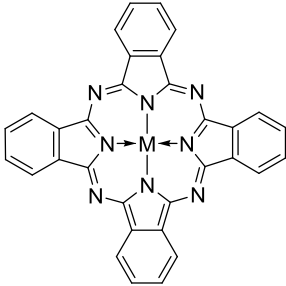
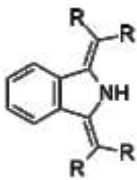
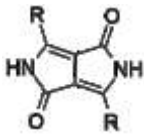
<i>Quinophthalones</i>		<i>Perylenes</i>	
			
<i>Quinacridone</i>		<i>Benzimidazolones</i>	<i>Anthraquinones</i>
			
<i>Phthalocyanines</i>		<i>Isoindolines</i>	<i>Diketopyrrolopyrroles</i>
			
			

Table 1.1 Chemical structures of some HPPs.

1.2 DPP

DPP is a bicyclic 8π electron system containing two lactam units (Figure 1.1). The molecule is virtually planar, the two phenyl rings are twisted out of the pyrrolopyrrole plane by 7° . DPP main physical properties are an absorption in the visible region with a molar extinction coefficient of $33000 \text{ (dm}^2 \text{ mol}^{-1}\text{)}$, high melting point ($> 350^\circ \text{C}$) and low solubility ($< 110 \text{ mg/L}$ in DMF at 25°C) as a consequence of hydrogen intermolecular bonding and π - π stacking among adjacent molecular planes. Insolubility is the main cause of the low reactivity and high chemical-physical stability of DPP.²

Like many other pigments classes, DPP pigments are fluorescent in solution, whereas in the solid state DPP is a vivid red. DPP compounds comprise a number of bright and stable orange-red coloured pigments: changing the substituents at the *para*- and *meta*-position of the two phenyl rings attached to the DPP chromophore unit is possible to extend the colour of the final pigments to the blue-violet. Light and weather fastness are two important features that permit to use these substrates in the automotive industry and in general in painting and tinting applications.

In recent years research on DPPs has focused on optical, electrochemical and electroluminescent properties and on the synthesis of conjugated DPP polymers with the aim to formulate new derivatives of DPP for different applications, mainly in the organic photovoltaic field.

1.2.1 Physical and chemical properties

a) UV-Vis

As shown in Figure 1.1, all DPP pigments show a bathochromic shift of the maximum absorption in the solid state with respect to the maximum absorption in solution. This shift is due to the strong intermolecular interactions, such as hydrogen bonding, π - π stacking and van der Waals interactions in the solid state. The solid state absorption maxima of DPP depend strongly on the nature and position of the substituent.³

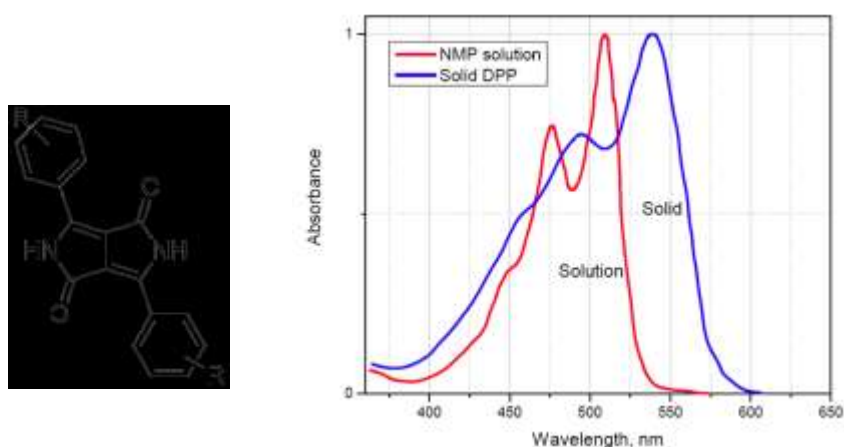


Figure 1.1 Absorption spectra of DPP in solution (NMP) and in the solid state (evaporated film).

In Table 1.2 it is reported the absorption maxima (λ_{\max}) of differently substituted DPPs measured in solution and in the solid state together with the ϵ values.

R	Shade ^a	Absorption maxima λ_{\max} (nm)		$\Delta\lambda_{\max}$	ϵ_{\max} (dm ² mol ⁻¹) ^c
		In solution ^b	In solid state		
<i>m</i> -CF ₃	Orange-yellow	509	518	9	25500
<i>m</i> -Cl	Orange	512	528	16	27000
H	Yellow-red	504	538	34	33000
<i>p</i> -Br	Blue-red	515	555	40	35000
<i>p</i> -N(CH ₃) ₂	Violet-blue	554	603	51	81500

Table 1.2 Absorption maxima (λ) of different substituted DPPs. (a) In plasticized PVC pigmented with 0.2 % DPP derivative; (b) measured in NMP; (c) molar extinction coefficient wavelength of maximum absorption in solution.

b) Fluorescence

DPP pigments fluoresce in solution. The Figure 1.2 shows the absorption and emission spectra of DPP in solution of chloroform. The Stokes shifts (difference between positions of the band maxima of the absorption and emission spectra of the same electronic transition) are in the range 10-15 nm and the fluorescence quantum yields are about 60 %. Through N substitution, both the solubility and the Stokes shift can be increased.⁴

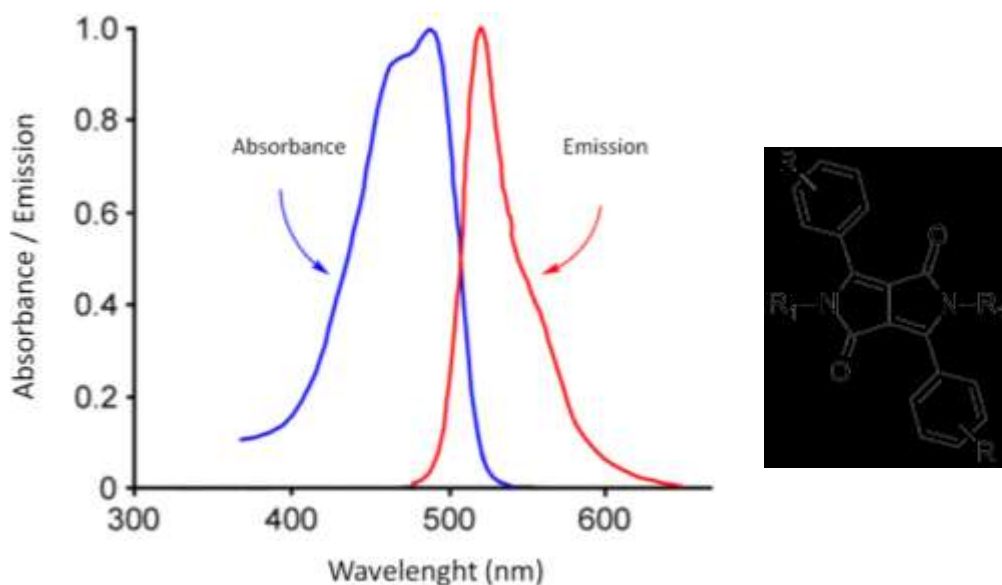


Figure 1.2 Absorption and emission spectra of DPP in chloroform.

c) Single X-ray structure analysis

The intra and intermolecular arrangements of the DPP molecules in solid state were studied by single X-ray structure analysis. The crystal lattice is determined by two types of interactions: hydrogen bonds and π - π stacking interactions, as shown in Figure 1.3. The hydrogen bonds occurring between the amide groups of DPP are relatively strong and the H \cdots O distance is 1.82 Å. The π - π interactions act perpendicularly to the chromophore's plane of DPP. The smallest distance among the DPP molecules is 3.34 Å.⁵

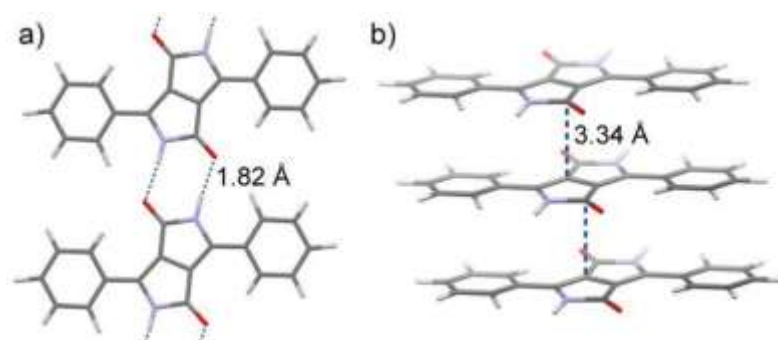


Figure 1.3 Intermolecular interactions between two DPP molecules in the crystal lattice: (a) hydrogen bonds, (b) π - π stacking.

d) Chemical properties

The molecular structure of DPP has different reactive centers such as the aryl rings that undergo electrophilic and nucleophilic reactions and the bicyclic lactam chromophoric unit with three different functional groups: (1) double bonds, (2) C=O and (3) secondary (NH) that may potentially undergo structural modification for further derivatization⁶.

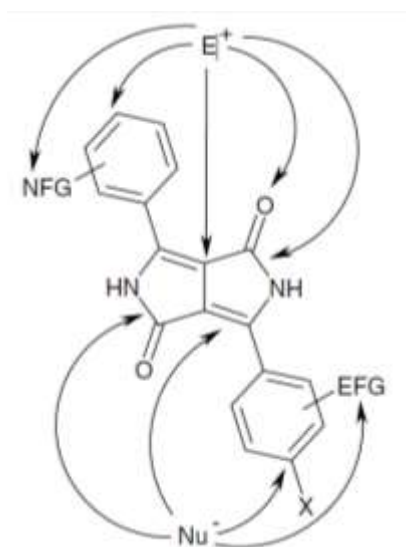


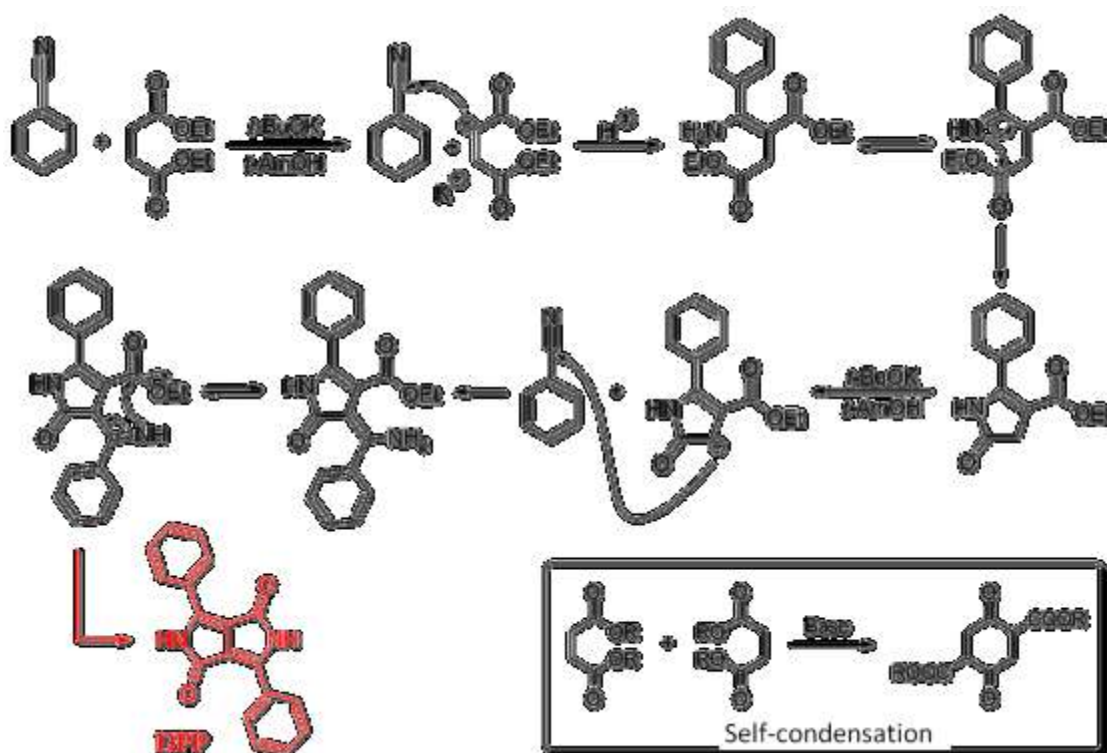
Figure 1.4 Potential reactive centers in a diaryl-DPP derivative. EFG: electrophilic functional group; NFG: nucleophilic functional group; X: halogen.

1.2.2 DPP Industrial Synthesis

In the early 1970s, Farnum et al.⁷ obtained the DPP molecule as a by-product. They understood its great potential and noted the unusual properties of this compound: its brightness, its colour and the low solubility and they realized to have synthesized an organic pigment. Then, they tried to optimize the reaction conditions to improve the yields and published their work as a kind of curiosity.

After ten years the industrial synthesis of DPP was developed by researchers at Ciba-Geigy.⁸ Their synthetic strategy is still the most important and most frequently used. The major advantages of this procedure are the easy availability of the starting materials, its simplicity, the broad spectrum of usable nitriles and the yields of the produced pigments. Furthermore, the isolation and purification of the final product is extremely simple and fast (filtration and washing with alcohol is usually sufficient).

In the procedure, benzonitrile reacts with dialkyl succinate in the presence of alkali metal alkoxides to form DPP. They prove that best results are obtained with succinates of tertiary or secondary alcohols, with tertiary alkoxides as bases and in tertiary alcohols as solvents. The tertiary alkoxides are considered the best bases because they have sufficient basicity to deprotonate the succinic acid esters and they are too weak as nucleophiles to undergo nucleophilic addition to the cyano group of the nitriles. The low electrophilicity of nitriles requires high temperatures in order to obtain the nucleophilic addition of the anions generated from succinic esters.⁹



Scheme 1.1 Succinic method of DPP synthesis.

As depicted in the insert of Scheme 1.1, succinic esters with strong steric hindrance have an important role to limit the dimerization reaction by the Claisen condensation mechanism.

Best yields in the synthesis of DPP can be obtained from unhindered aromatic nitriles, in particular for the electron poor ones. The synthesis of DPP compounds using terephthalonitrile, benzonitrile, 2-methylbenzonitrile, and 4-dimethylaminobenzonitrile gives the corresponding DPPs with 80 %, 63 %, 7 % and 3.7 % yields.¹⁰

1.3 Supramolecular polymers

DPPs, as quinacridones, indigos and other organic pigments promote H-bonding between $-NH$ hydrogens (donor) and carbonyl groups (acceptor), reminiscent of the same type of H-bonding interactions present in proteins.¹¹ The interplay of H-bonding and π -stacking develops high lattice energies and gives at these structures the opportunity to self-assemble through supramolecular polymers in solution and in the solid state.

In supramolecular polymers (SP) monomers are held together and organized by means noncovalent interactions, such as hydrogen bonding, metal coordination and host-guest interactions. On the contrary conventional polymers (CP) are characterized by the repetition of monomeric units held together by covalent bonds. In Figure 1.5 the two types of polymers are displayed.

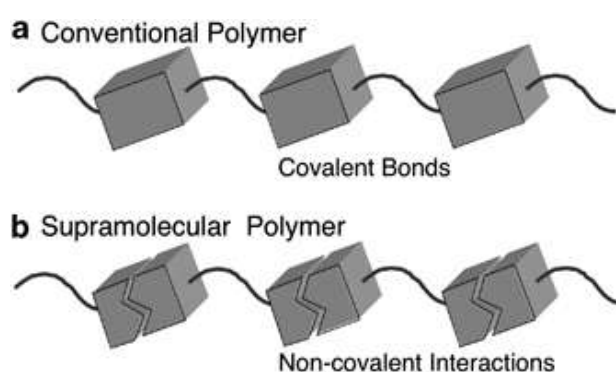


Figure 1.5 Schematic representation of a CP (a) and a SP (b).¹²

Nylon is the first example of synthetic supramolecular polymer: the main features of this material are the result of cooperative hydrogen bonds, as shown in Figure 1.6.

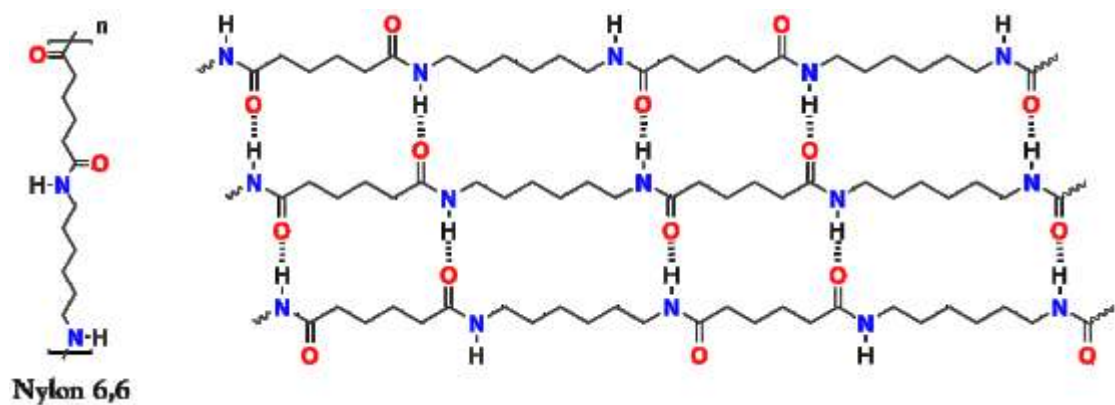


Figure 1.6 Monomeric structure of Nylon and hydrogen bonds of the polymer.

Supramolecular systems are presented also in nature: DNA is the best known self-assembled structure in biological systems. It exists in a double helical form.¹³ The two single strands are held together by a number of hydrogen bonds, involving acidic hydrogen atoms, oxygen and nitrogen atoms of the purine and pyrimidine bases in order to maintain the double helical structure,¹⁴ as shown in Figure 1.7.

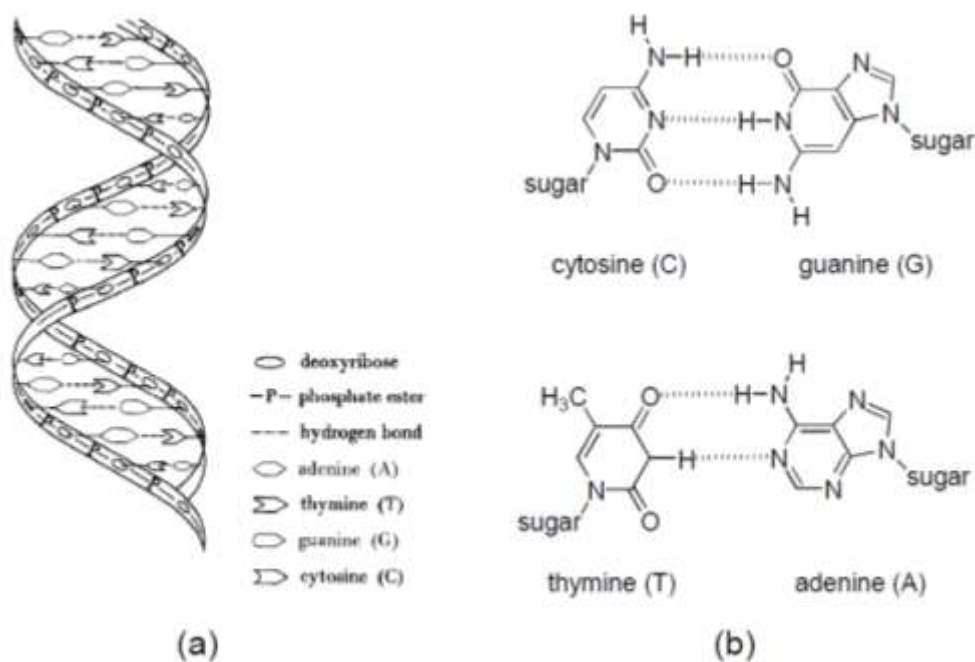


Figure 1.7 Complementary base pairing in DNA helical structure **(a)** and base pairing in DNA (guanine and cytosine form triple hydrogen bonds; adenine and thymine form double hydrogen bonds) **(b)**.

Architectural and dynamic parameters, such as degree of polymerization (DP), lifetime of the chain, its conformation, depend on the strength of noncovalent interactions. Supramolecular polymerizations are thermodynamically controlled,¹⁵ thus the lengths and polymer properties highly depend upon concentration and temperature. Moreover also pH and monomers purity can influence the DP. In Figure 1.8 it is shown the different mechanism between the conventional and the supramolecular polymerization.



Figure 1.8 Mechanism of conventional polymerization and of supramolecular polymerization.

In the last few years, interest on supramolecular chemistry has grown exponentially: these polymers seem to be promising and smart materials able to be turned on and off by external stimuli. Recent studies concern self-healing materials, optoelectronic materials and medical materials.

1.3.1 Non covalent interactions used in supramolecular polymerizations

a) Hydrogen Bond

The hydrogen bond is a type of dipole-dipole attraction between an electronegative atom and a hydrogen atom bonded to another electronegative atom, such as nitrogen, oxygen, or fluorine. Hydrogen bonds are the most useful interactions for encouraging molecules to self-assemble into well-defined aggregates even if they are weaker than covalent and ionic bonds, with an energy typically between 5 and 30 kJ/mol.

A single hydrogen bond is not strong enough to produce supramolecular polymers. However, both the strength and the directionality can be improved by introducing multiple hydrogen bonds to fabricate hydrogen bonding arrays. Furthermore, when arrays of donor (D) and acceptor sites (A) are introduced, also the selectivity of the system can be increased. Indeed, the order of (D) and (A) sites influences the binding strength.

Jorgensen et al.¹⁶ were the first to point out this theory. They demonstrated, that although the DAA–AAD and ADA–DAD arrays have the same number of hydrogen bonds, the binding constant of DAA–AAD arrays (Figure 1.9, **2**) is significantly higher than that of ADA–DAD arrays **1** (Figure 1.9) ($K_a \approx 10^4$ vs 10^2 M⁻¹), due to the additional attractive secondary electrostatic interactions in DAA–AAD arrays. Later Zimmerman et al.¹⁷ confirmed that the AAA–DDD arrays **3** (Figure 1.9) have a higher binding constant ($K_a > 10^5$ M⁻¹ in CDCl₃), on account of the solely attractive secondary interactions.

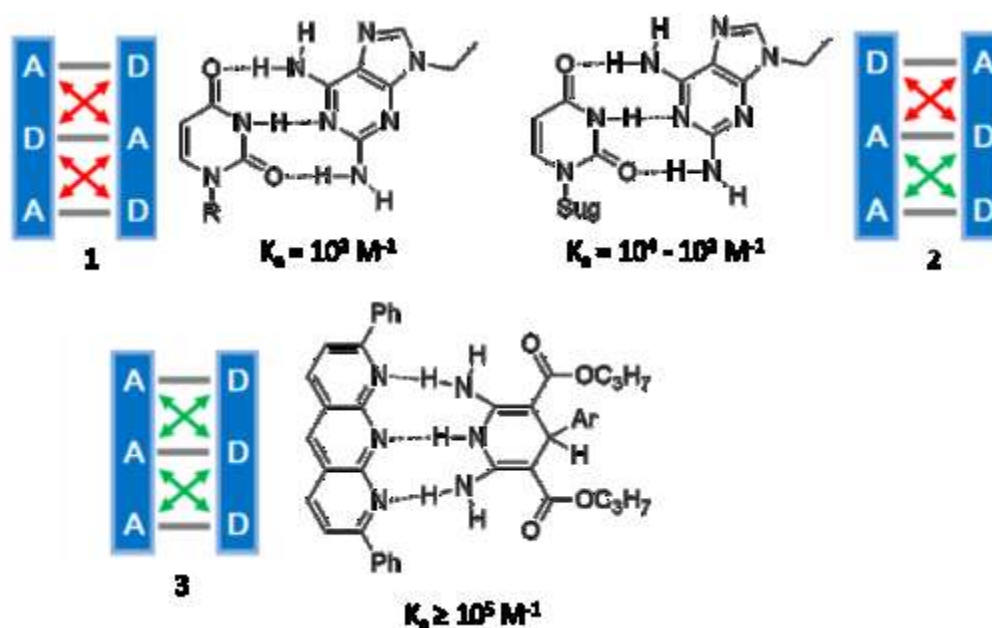


Figure 1.9 Multiple hydrogen bonding arrays and their binding constants.

Lehn et al.¹⁸ synthesized the first main chain supramolecular polymer in the 1990's. Bifunctional diamidopyridine and uracil derivatives were mixed to form linear polymeric chains via triple hydrogen-bonding interactions, as shown in Figure 1.10. The chirality of the spacer (tartaric acid) leads to a partial elastic structure.¹⁹

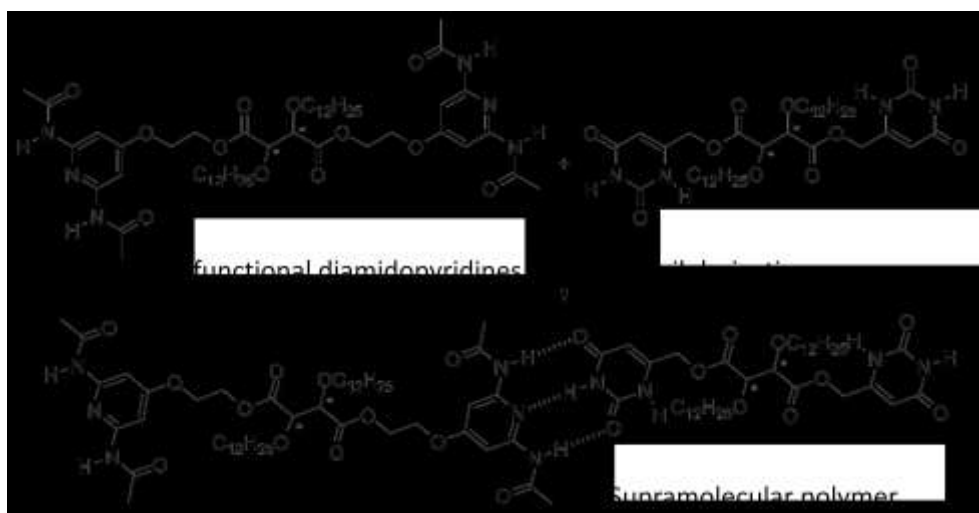


Figure 1.10 Supramolecular polymer LC via triple hydrogen bonds, synthesized by Lehn.

Lehn's group synthesized also a rod rigid supramolecular polymer²⁰ to investigate the possibilities of this new class of materials. In this system, a rigid 9,10-dialkoxyanthracene core connects the hydrogen bonded group with an imide group, as shown in Figure 1.11.

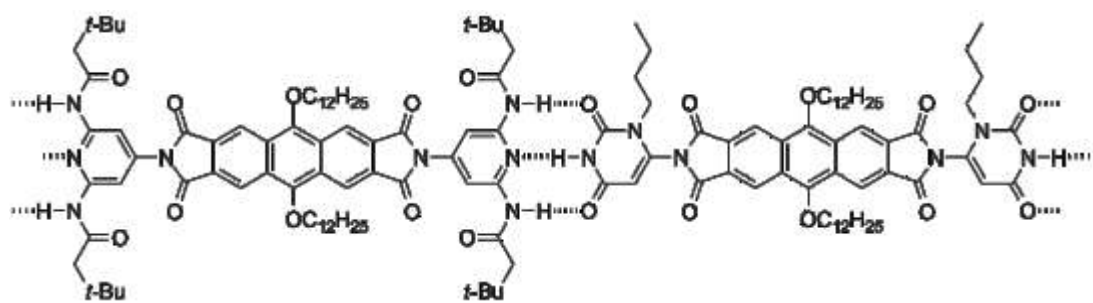


Figure 1.11 LC supramolecular polymer based on a rod rigid core.

To achieve supramolecular polymers with a high degree of polymerization (*i.e.* polymers with a higher number of repeating units), multiple hydrogen bonding arrays are necessary. In 1997 Meijer et al.²¹ introduced a bifunctional AADD type monomers, containing two UPy end groups, that were able to form linear supramolecular polymers, as shown in Figure 1.12. The molecular mass of the supramolecular polymers can be modulated varying the concentration of the solution and the solvent. Since then, this unit has been widely used for constructing supramolecular polymers.

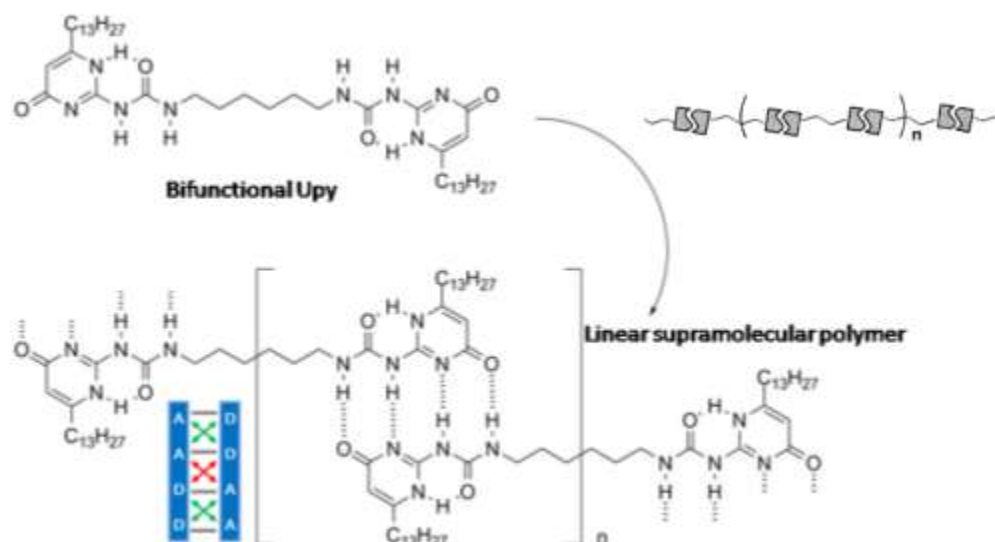


Figure 1.12 Linear supramolecular polymer (Urypy) synthesized by Meijer et al.

Another important example is represented in Figure 1.14. Discotic molecules with a large aromatic core permit to achieve polymers with high degree of polymerization and well-defined architectures in all solvent types. These polymeric structures are obtained with high DP even in dilute solution (10^{-6} M hexane), on account of their large association constant (10^8 M).²² In the example, the supramolecular aggregation of disks, due to hydrogen bonds and stacking interactions, results optimized in a helical column.



Figure 1.13 Monomer with chiral and achiral chains.

Moreover the chirality placed in the sidechains of the molecule (Figure 1.13, **C** or **D**) is amplified in the supramolecular helical polymer. This phenomenon is known as “sergeant and soldier effect”: the chiral monomer imposes a supramolecular chiral structure upon achiral monomers.²³ Furthermore, only a small percent of disks with chiral sidechains (only 4 % of Sergeant) in achiral disks (Soldiers) manages to develop helical polymers of one helicity exclusively.²⁴

In Figure 1.14 we report a schematic representation of “sergeant and soldier effect”.



Figure 1.14 Sergeant and soldier mechanism.

b) π -Interactions

The π - π stacking interactions are another kind of noncovalent forces with an important role in self-assembly and molecular recognition processes. They are weakly directional and weaker than hydrogen bonds: calculations give about $10 \text{ kJ}\cdot\text{mol}^{-1}$ for typical aromatic-aromatic interactions in comparison with $15\text{-}40 \text{ kJ}\cdot\text{mol}^{-1}$ for moderate hydrogen bonds among neutral molecules.²⁵

At the supramolecular level, the aromatic rings can interact in different ways: stacked arrangement (face-to face, perfect alignment, offset, slipped, parallel displaced) and edge- or point-to-face, T-shaped conformations, as shown in Figure 1.15.²⁶

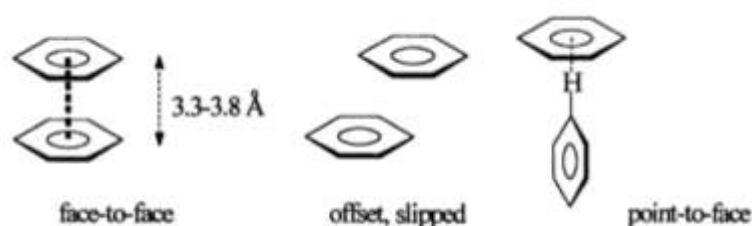


Figure 1.15 Stacked arrangement.

Supramolecular polymers organized through π - π interactions allow electron transfer perpendicular to the molecular planes upon excitation of the chromophores.

Alkoxy substituted triphenylenes are an example of compounds able to give π - π stacking. Ringsdorf et al.²⁷ demonstrated that these donor molecular structures, shown in Figure 1.16, can self-assemble in solution forming alternating donor-acceptor supramolecular polymers by doping them with equimolar amounts of electron acceptors such as the (-)-menthol 3,5-dinitrobenzoate. The formation of these supramolecular systems of donor-acceptor is favoured by apolar solvent. In more polar solvents the triphenylenes alone do not polymerize and consequently donor-acceptor polymers with low DP are obtained. Moreover even if chiral, these molecules do not form a supramolecular chiral polymer. This behaviour is typical of molecules arranged in an unordered assembly. Furthermore, the mixing of alkoxytriphenylene with a chiral bulky substrate, as for example a derived from (-)-menthol 3,5-dinitrobenzoate, introduces supramolecular chirality in the columns.¹⁵

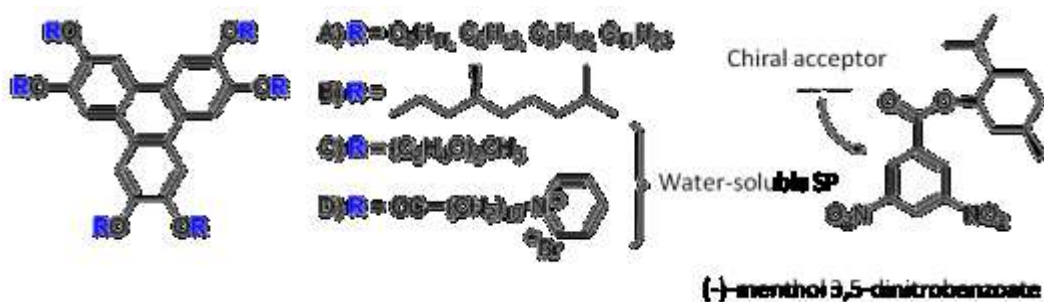


Figure 1.16 Apolar triphenylene and menthol group.

The menthol group enters in the alkyl side-chains of the triphenylene and induces a noncooperative helical twist into the columns. In this manner CD effect is induced in the chromophore of the triphenylene.

Phthalocyanines and porphyrins, shown in Figure 1.17, are an important example of molecules able to develop aromatic-aromatic supramolecular interactions. They have a significantly larger core than triphenylenes which allows stronger arene-arene interactions.²⁸ Their optical and electronic properties can change easily by the incorporation of a different metal in the core.

Phthalocyanines usually dimerize and only at higher concentrations they manage to form oligomers. We can observe phthalocyanines self-assembled in helical aggregates when crown ethers and chiral alkoxy side-chains are present in the periphery of these molecules. This effect can be turned off by the addition of a potassium salt that overrules the twist imposed by the chiral side-chains.²⁹

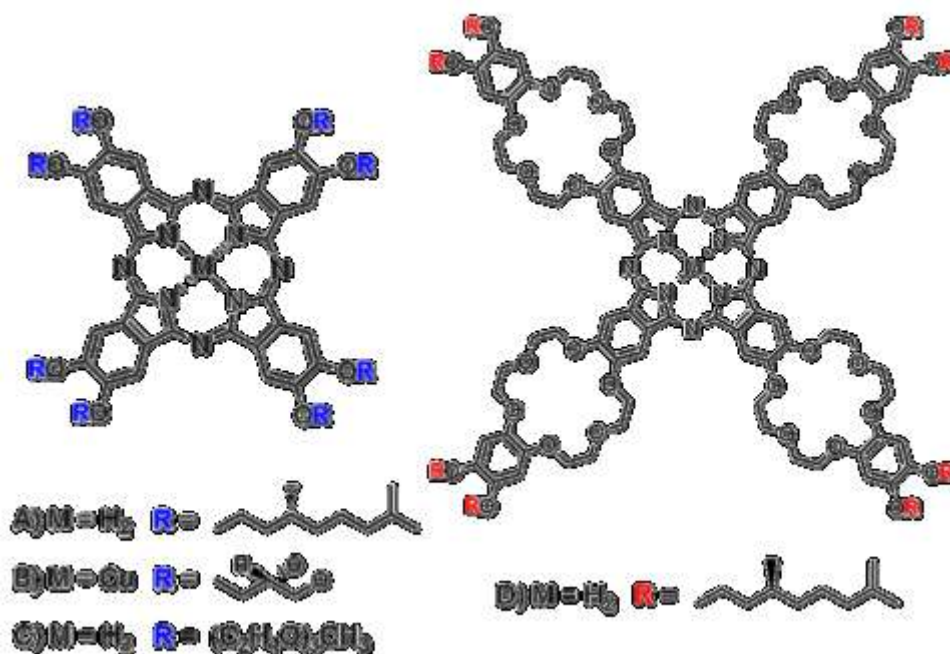


Figure 1.17 Discotic molecules based on phthalocyanines.

c) Metal coordination

Metal coordination bonds have been used to synthesize a large number of supramolecular complexes. Metal containing polymers combine the properties of organic polymers with the magnetic, electronic, optical and catalytic potential metals. In metallosupramolecular polymers the metal-ligand coordination is reversible and dynamic. Furthermore not all metal coordination bonds are reversible because most of them are held together with kinetically stable metal-ligand interactions.

Multidentate ligands and multivalent metal ions permit to increase the binding constant (K) and in this way also the degree of polymerization increases.

In 2000 Hunter's group³⁰ synthesized high molecular coordination polymers based on porphirins. A porphirin, which has six coordination sites, is provided with two pendant pyridine groups and cobalt atom. They determine the size of aggregates with $^1\text{H-NMR}$ diffusion and with the size exclusion chromatography (SEC). They demonstrate that **(a)** forms aggregates significantly larger than monofunctional compounds **(c)**, which cannot grow beyond the dimeric state. In this way molecules **(c)** can control and stop the polymerization (Figure 1.18).

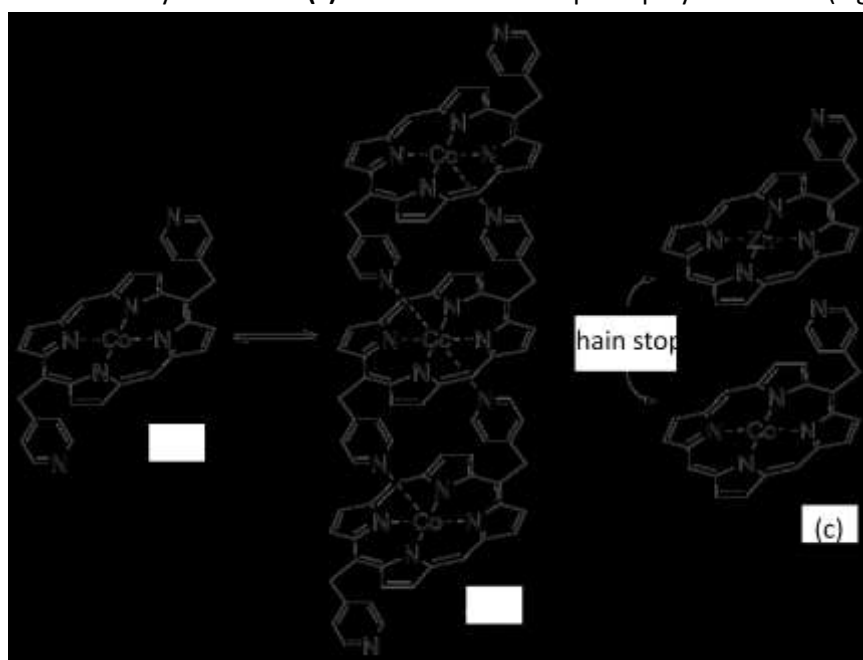


Figure 1.18 Metal coordination polymer, synthesized by Hunter's group.

1.4 Supramolecular polymers in water

Supramolecular polymerizations are mostly known in organic and non-polar solvents and interesting material properties have been observed studying specific monomers, such as ureido-pyrimidones or bis-ureas that can aggregate into very long chains.

Apart from biological systems, there are not many examples of self-assembled materials in water: controlling the aggregate shape, size and stability for aqueous-based one-dimensional supramolecular polymers is difficult. At the same time, the ability to do so is highly important in view of a number of applications, in functional soft matter including electronics, biomedical engineering, and sensors.³¹ Thus, the aqueous medium is the goal of supramolecular chemistry.³²



Figure 1.19 Cover picture of the number of *Angewandte Chemie* journal about “*Supramolecular chemistry in water*”.³²

In this paragraph we present three examples of water soluble supramolecular polymers: the first and the second have been synthesized by Boutellier’s group whereas the third has been synthesized by Meijer’s group.

The amphiphilic perylene derivative synthesized by Boutellier’s group^{31, 33} exhibits a large hydrophobic aromatic core, surrounded by four hydrophilic arms, as shown in Figure 1.20, (a).

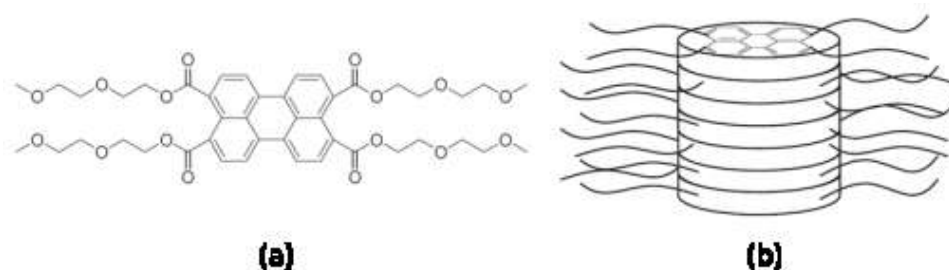


Figure 1.20 (a) Pery-2 structure, synthesized by Boutellier. **(b)** Schematic representation of its supramolecular aggregation.

This molecule permits to self-assemble in water in one-dimensional column by π - π cofacial overlap and hydrophobic interactions, as shown in Figure 1.20, **(b)**. The four hydrophilic branches ensure the water solubility of the structure.

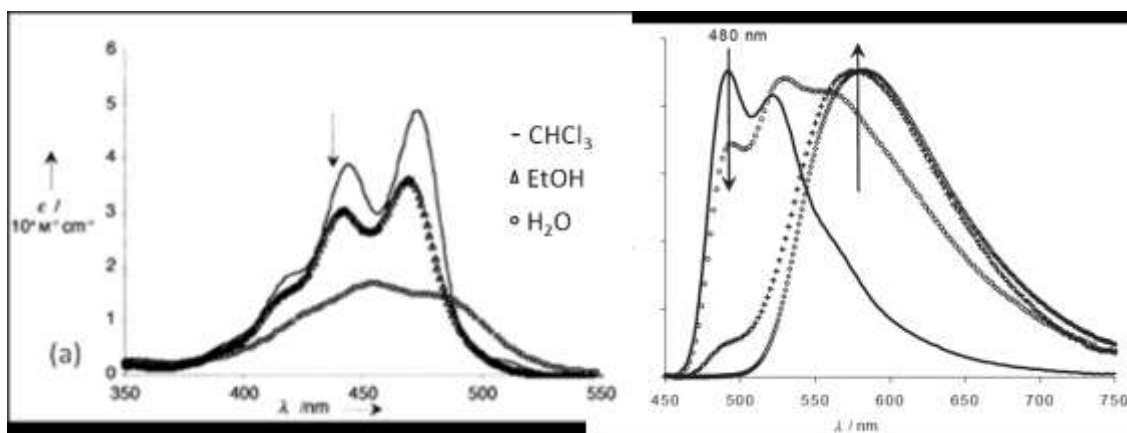


Figure 1.21 (a) UV-Vis spectra of solutions of Pery-2 (10^{-4} M) in several solvents: chloroform, ethanol and water. **(b)** Fluorescence in water for four concentrations ($c= 4 \cdot 10^{-7}$ M, 10^{-5} M, 10^{-4} M, 10^{-2} M) with λ_{exc} at 425 nm.

UV-Vis spectra in Figure 1.21, **(a)** show the absorption of the compound for three different solvents: the molecular structure is not aggregated in chloroform while in more polar solvent molecules polymerize and the spectral signals are shifted. This phenomenon is maximised in water. At the fluorescence analysis they observed how the polymer self-assembles increasing the concentration of solution, Figure 1.21, **(b)**.

In addition, solutions of Pery-2 (in D_2O at $25^\circ C$) at different concentrations are studied using small-angle neutron scattering (SANS) to verify the expected wire-like structure (Figure 1.22). In this way for $q > 0.01 \text{ \AA}^{-1}$, they obtained three satisfying fits and they established a constant rod diameter ($2r= 24 \text{ \AA}$), as shown in Figure 1.22 **(a)**. While, once obtained all the thermodynamic parameters, they calculated number average degree of polymerization of Pery-2 versus concentration in water, as displayed in Figure 1.22 **(b)**.

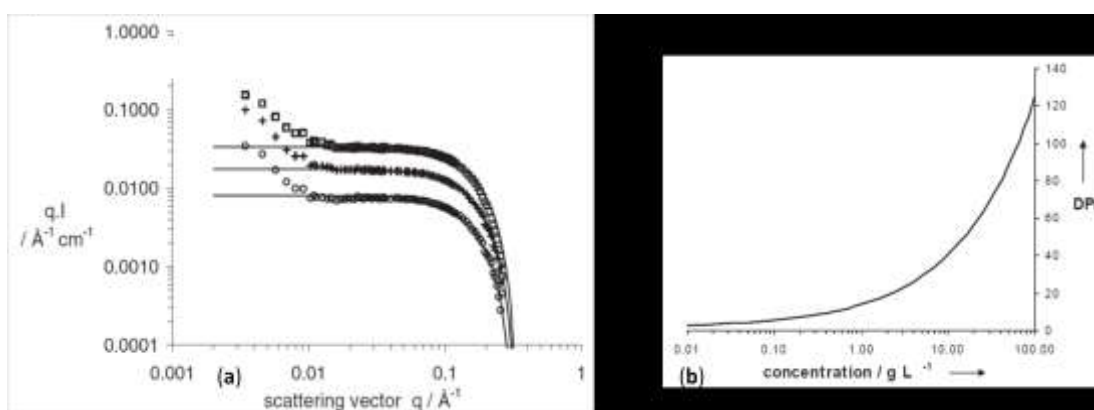


Figure 1.22 SANS data for solutions of Pery-2 in D_2O at different concentrations **(a)**; DP_n versus concentration of Pery-2 in water, **(b)**.

Boutlier's group³⁴ synthesized also a water soluble bis-urea. This molecular structure comprises three parts, as displayed in Figure 1.23: (1) the center of the molecule, a bis-urea motif; (2) alkyl spacers and (3) ethylene oxide oligomers. These hydrophilic chains should

assure a good solubility in several low-polarity organic solvents. Moreover, they demonstrate that a good solubility in water and acetonitrile is guaranteed by ethylene oxide chain formed by 7 units.

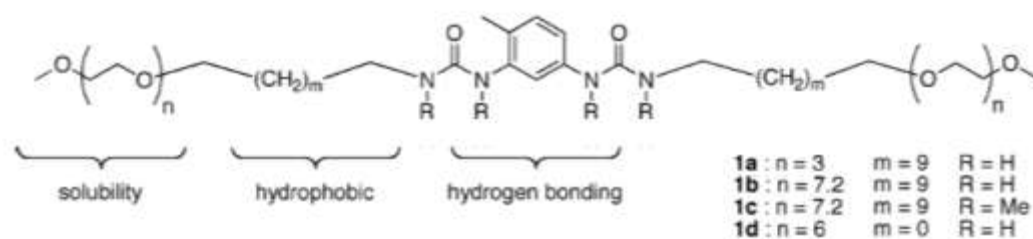


Figure 1.23 Bis-urea structure synthesized by Boutellier et al..

The presence of both hydrogen-bonding and hydrophobic groups ensures that self-assembly occurs in water, aprotic polar solvents, or nonpolar solvents. The supramolecular aggregation has been characterised through small-angle neutron scattering (SANS) and isothermal titration calorimetry (ITC). In Figure 1.24, **(a)**, it is reported the scattered intensity for very diluted solutions of this molecule in the three deuterated solvents (D_2O , CD_3CN and C_7D_8).

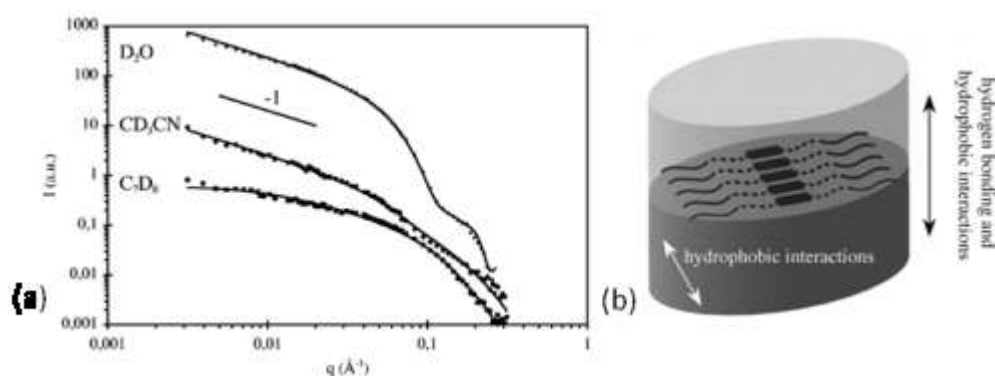


Figure 1.24 SANS analysis **(a)**; representation of aggregated species **(b)**.

The dimensions of the scattering objects can be deduced from a fit calculated according to a suitable geometrical model. The obtained values demonstrate that in CD_3CN and in C_7D_8 any aggregated species are present, whereas in D_2O they identified very long filaments with a large cross-section. In Figure 1.24, **(b)**, the schematic representation of the supramolecular polymer in D_2O is proposed according to the fitting result. In the end the stability of the filament has been tested with ITC.

Another important example of supramolecular polymer in water has been synthesized by Mejer et al.³⁵ They propose the creation of columnar architectures in water by bifunctional ureido-s-triazines provided with penta(ethylene oxide) side chains; the structure is represented in Figure 1.25.

This structure self-assembles in water, leading to helical columns via cooperative stacking of the hydrogen-bonded pairs (DADA array). The geometry of this system is verified using SANS experiments, obtaining a column radius of 16 Å.

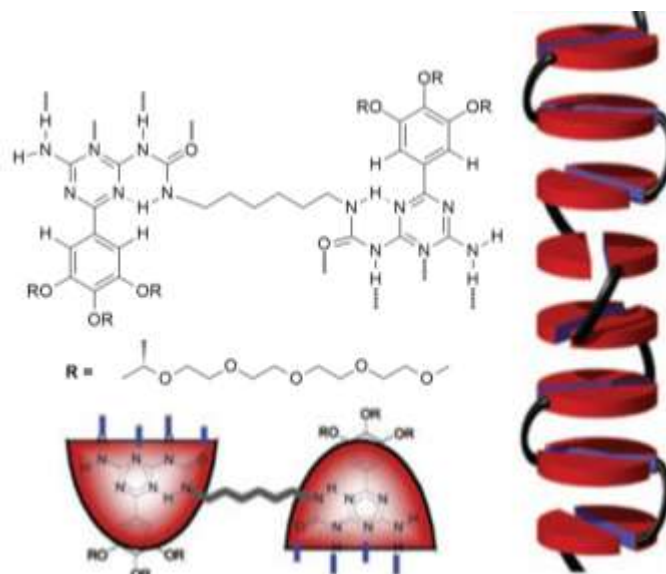


Figure 1.25 Columnar architecture synthesized by Meijer.

The self-assembly of this compound in water is investigated with temperature-dependent UV-Vis and Circular Dichroism (CD) spectroscopy, as reported in Figure 1.26. Increasing temperature, a gradual blue-shift absorption is recorded from 292 to 288 nm. These changes indicate the coincidental loss of positional order of the molecules within the columns (CD) and loss of intermolecular hydrogen bonding (UV-Vis). Moreover, a $2 \cdot 10^{-4}$ M aqueous solution becomes turbid above 353 K. This effect is due to the phase separation between the oligo (ethylene oxide) side chain and the water.

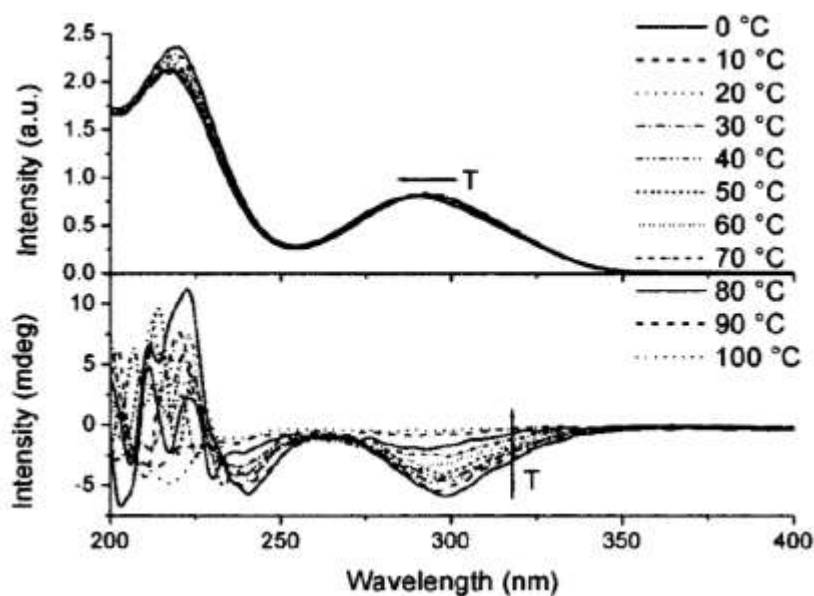


Figure 1.26 UV-Vis (upper) and CD spectra (lower) of substrate in water ($2.4 \cdot 10^{-4}$ M) at different temperatures.

This structure has been studied also with fluorescence, as shown in Figure 1.27: in water the fluorescence of this compound is quenched if it is compared with the fluorescence of this molecule in other solvents, as chloroform or acetone. The fluorescence intensity increases increasing the temperature. This behaviour suggests that at low temperature the molecules

are not molecular dispersed and that hydrophobic stacking interactions among the ureido-s-triazine units cause the strong quenching of the fluorescence.³⁶

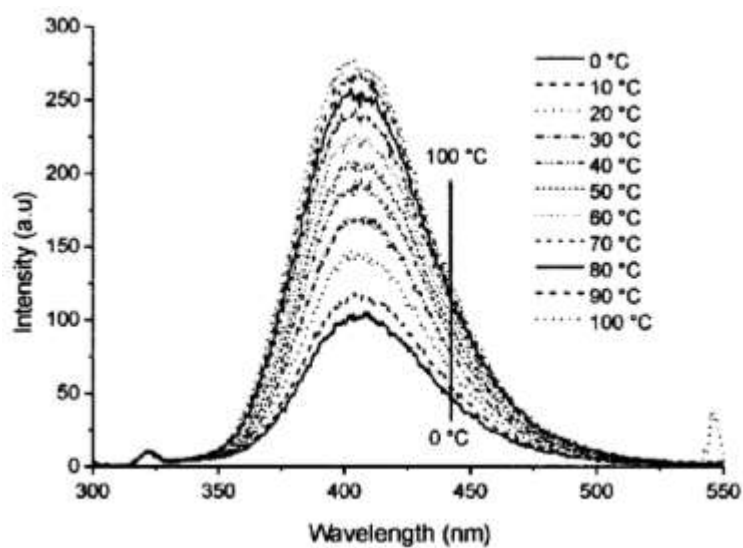


Figure 1.27 Fluorescence spectra in water recorded at $5 \cdot 10^{-6}$ M with λ_{exc} at 290 nm.

Using UV-Vis, Fluorescence and CD Mejer et al. proved the formation of highly ordered aggregates in water. Furthermore, they proved that the self-assembly process on the basis of the combination of noncovalent interactions is a hierarchical process with the solvophobic interactions occurring at lower concentrations than the solvent sensitive hydrogen bonds. Continuing these studies will allow the generation of a variety of ordered supramolecular architectures in water.

1.5 Self-healing materials

In the last decade, the development of polymers that can spontaneously repair themselves after mechanical damage would significantly improve the safety, lifetime, energy efficiency and environmental impact of man-made materials.³⁷ Self-healing materials are polymers, metals, ceramics and their composites that when damaged through thermal, mechanical, ballistic or other means have the ability to heal and restore the material to its original set of properties. The inspiration for these new smart materials comes from the biological system: the human blood clotting system; it contains a network of capillaries that deliver healing chemicals to damaged areas.³⁸

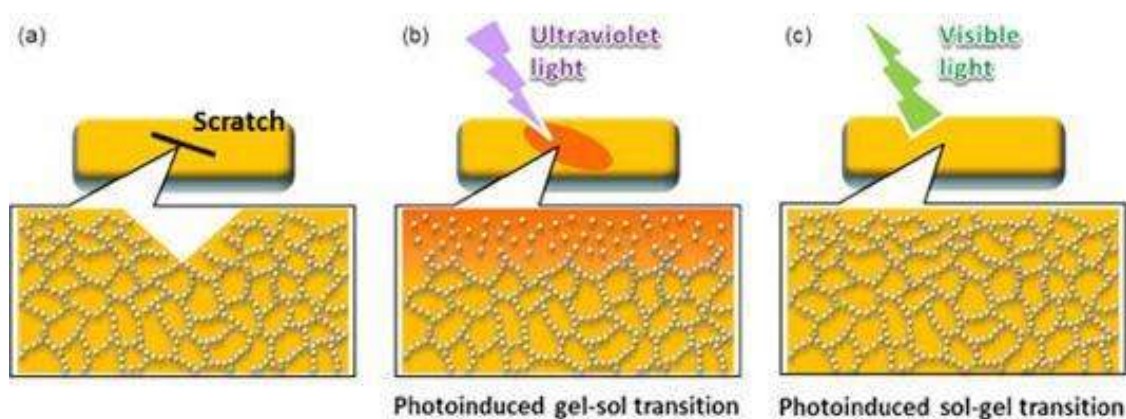


Figure 1.28 Schematic representation of the self-healing process: (a) damaged material, (b) ultra light exposition; (c) supramolecular reorganization.

In particular, supramolecular polymer based materials seem to be promising systems in order to integrate and develop complex self healing structures for many different applications such as building, furniture, textiles. Self-healing process can be influenced by external stimuli, such as changes in temperature and pH and light exposition. A schematic representation of the self-healing process is shown in Figure 1.28.

An important example of self-healing material has been described by Rowan's group:³⁹ they synthesized a metallo-supramolecular polymer that can be mended through exposure to light, Figure 1.29.

These new polymers are based on a macromonomer comprising a rubbery, amorphous poly(ethylene-co-butylene) core with 2,6-bis(19-methylbenzimidazolyl)pyridine (Mebip) ligands at the termini. To test their structures, they deliberately damaged a thick film of the polymers by applying well-defined cuts with a depth of 50–70 % of the film thickness. These samples are subsequently exposed to ultraviolet radiation with a wavelength of 320–390 nm and an intensity of 950 mW cm⁻². Under these conditions, two consecutive exposures of 30 s are sufficient to completely heal the cuts. In this way, the original properties could be restored.

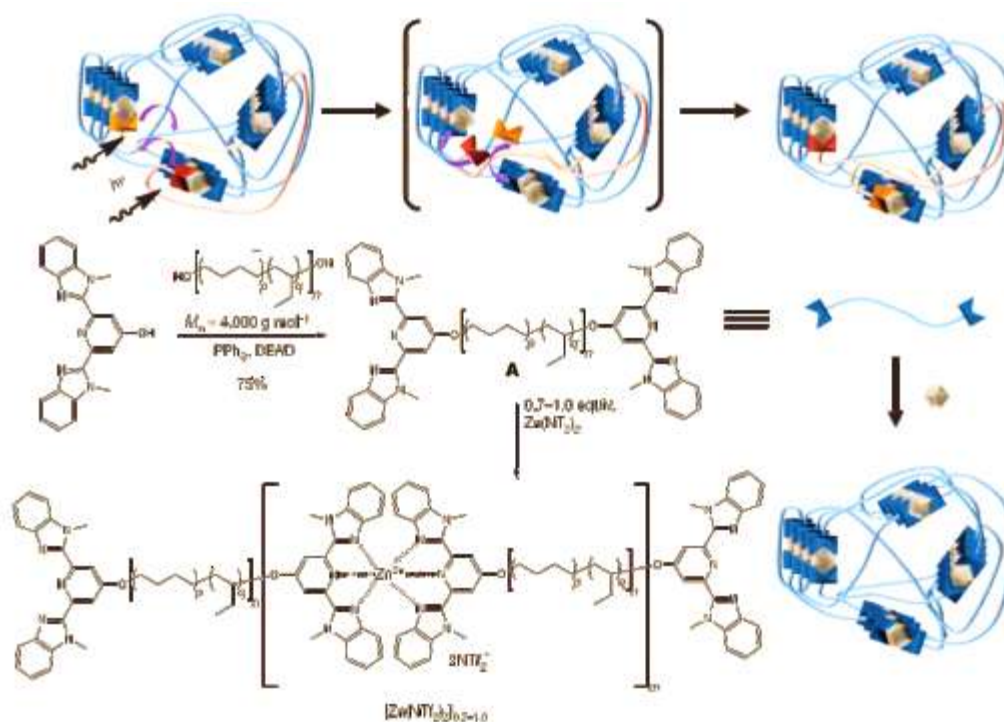


Figure 1.29 Mechanism and synthesis of photohealable metallosupramolecular polymer, synthesized by Rowan's group.

Another important example is described by Guan's group:⁴⁰ they prepare a novel multiphase design that can combine stiffness and spontaneous healing in a thermoplastic elastomeric system. The key of their work is to program dynamic healing motifs (hydrogen bonds) in the soft phase of a hard-soft multiphase system (Figure 1.31), merging the unique properties of hybrid polymers (stiffness and toughness) with those of dynamic supramolecular assemblies (autonomic healing). They develop a hydrogen-bonding brush polymer (HBP) that self-assembles into a two-phase morphology that behaves as a true thermoplastic elastomer (TPE). The HBP consists of a 'hard' backbone (high T_g) and 'soft' brushes (low T_g) carrying polyvalent hydrogen-bonding sites for dynamic supramolecular assembly. For their self-healing TPE system (Figure 1.30, **(a)**), they chose a polystyrene backbone as the hard phase and polyacrylate amide (PA-amide) brushes as the soft phase. Processed from a polar solvent, the brush polymer should collapse into a core-shell nanostructure with a hard polystyrene core and a soft PA-amide shell. Hydrogen bonding-directed supramolecular assembly of the PA-amide brushes should lead to the formation of a dynamic microphase separated nanostructure that can be reversibly broken and reformed, affording spontaneous self-healing behaviour (Figure 1.30, **(b)**).

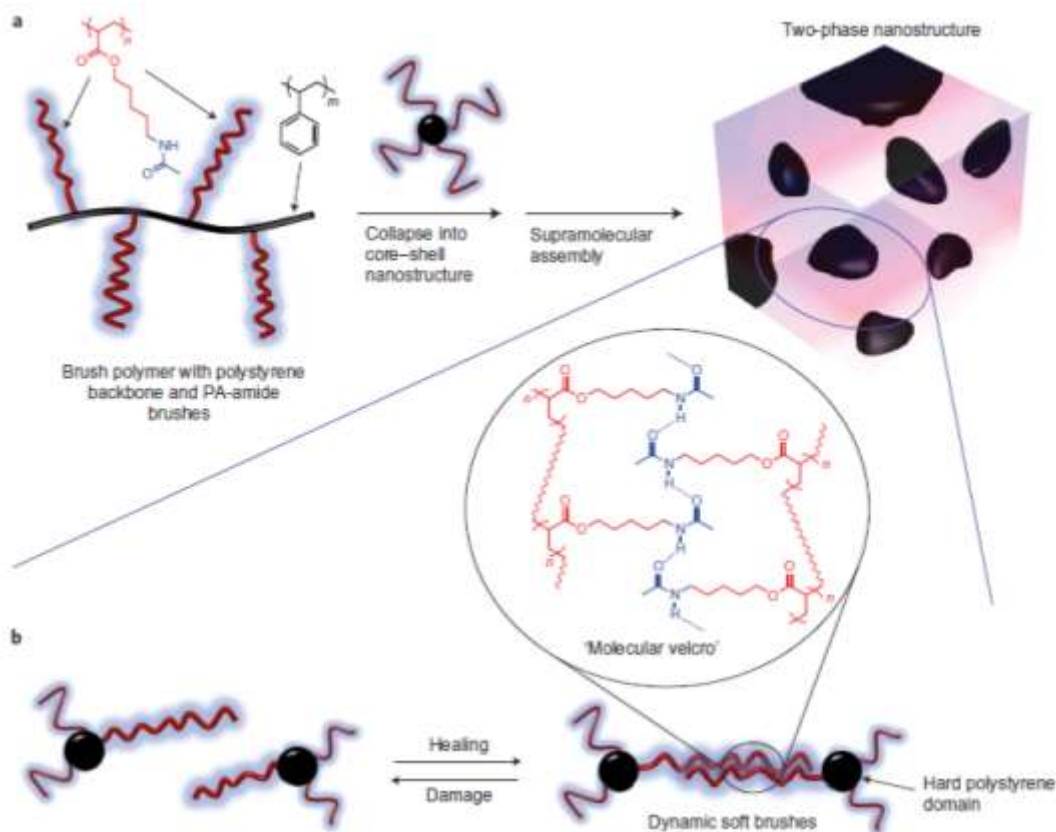


Figure 1.30 Multiphase self-healing brush polymer system. **(a)** The hydrogen bonds self-assemble into a two phase nanostructure morphology; **(b)** the supramolecular connections between soft brushes can rupture reversibly under stress.

It is reported a last example of self-healing material synthesized by Michaud's group.⁴¹ In their work, they start from a single reactive prepolymer, functionalized with a defined number of hydrogen bonds, to prepare a series of networks presenting different ratios of diepoxide and tetraepoxide. In this way, they manage to increase the number of chemical cross-links, improving the material resistance, without changing the concentration of hydrogen bonds in order to preserve a high self-healing ability.

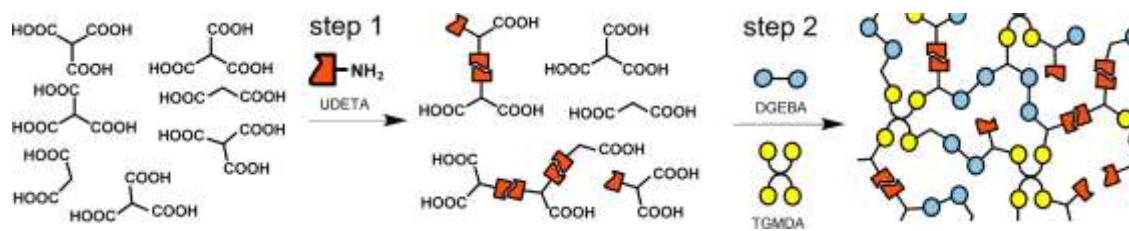


Figure 1.31 Synthetic strategy to generate insoluble hybrid networks. First step: amidation of poly(carboxylic acid)s. Second step: cross-linking with a variable amount of the difunctional DGEBA and the tetrafunctional TGMDA epoxy resins.

In Figure 1.31, it is reported the synthetic strategy that they use to improve the creep resistance and thermomechanical properties of cured materials.

1.6 Supramolecular polymer derived from DPP: *longchain*-DPP

The first supramolecular polymer derived from DPP is the Long Chain-DPP that used its H-bonded network and π - π stacking to produce new supramolecular aggregates. The synthetic steps to obtain this molecule are shown in Figure 1.32.

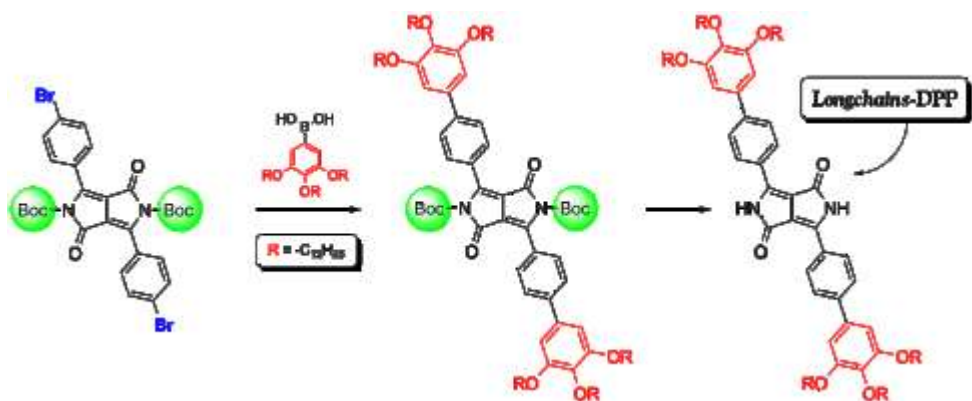


Figure 1.32 Synthesis of *Longchain*-DPP.

The main physical properties of this compound are strong fluorescence in solution, high molar extinction coefficient ($22519 \text{ dm}^2 \text{ mol}^{-1}$) and thermal stability.

The supramolecular self-assembly has been investigated with temperature-dependent UV-Vis experiments. The UV absorption analysis in Figure 1.33, (a), is referred to a $1.4 \times 10^{-5} \text{ M}$ solution of *longchain*-DPP in methylcyclohexane (MCH) and it is performed from 298 and 368 K in steps of 10° C . Equilibrium between different chemical species generates seven isosbestic points.

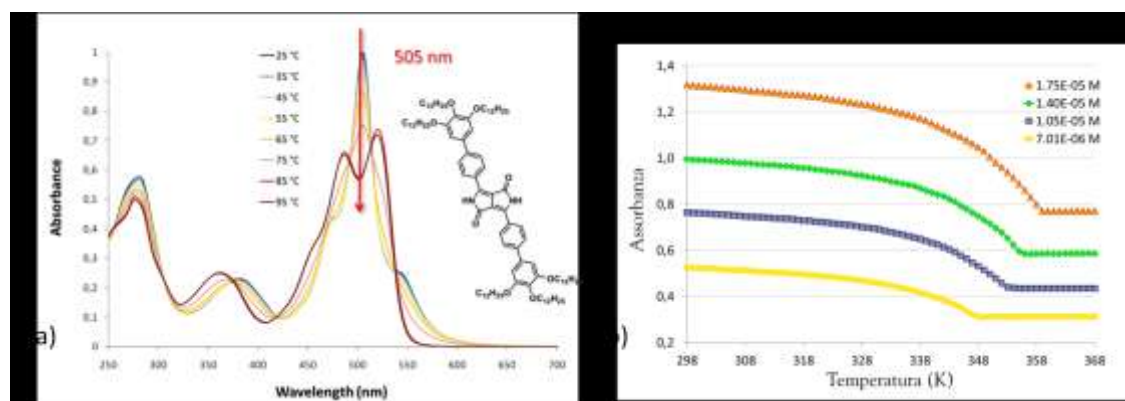


Figure 1.33 (a) Temperature-dependent UV-Vis spectra of *longchain*-DPP in MCH ($c = 1.4 \times 10^{-5} \text{ M}$). (b) Experimental data of *longchain*-DPP obtained in temperature-dependent experiments at the wavelength of 505 nm.

The most pronounced variation of absorbance is observed at 505 nm, hence T-dependent UV absorptions are recorded at this wavelength. The curves recorded at this λ suggest a cooperative process, described by nucleation-elongation mechanism.

Furthermore, the morphology of this molecule has been characterised by scanning electron microscopy (SEM) and epifluorescence microscopy (EFM). The aspect is clearly fibrous; as shown in Figure 1.34.

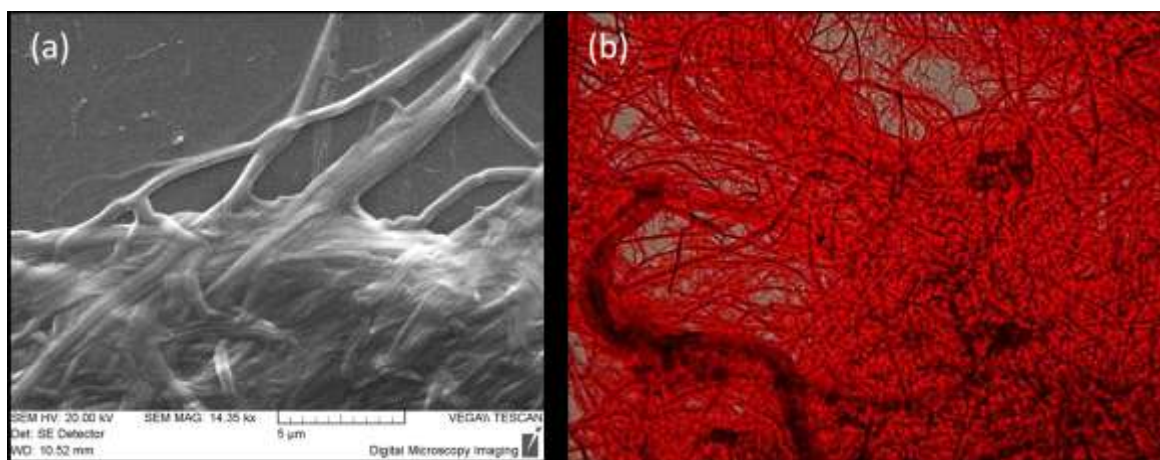


Figure 1.34 Fibers structures of *longchain-DPP* at SEM (a) and at EFM (b).

1.7 Aim

The starting point of this work is the **longchain-DPP** reported in paragraph 1.6. In this dissertation we describe the synthesis of two new DPPs able to develop supramolecular polymers in water.

There are different examples in the literature of supramolecular polymers in water and some of their structure have been already reported in paragraph 1.4. An important inspiration for this work is the system synthesized by Bouteiller's group, shown in Figure 1.35 and already described in paragraph 1.4: the center of the molecule is a bisurea, able to develop strong hydrogen bonds. The hydrogen-bonding group is linked to alkyl spacers and these hydrophobic groups are linked to ethylene oxide oligomers, important substituents to guarantee solubility in polar solvents.⁴²

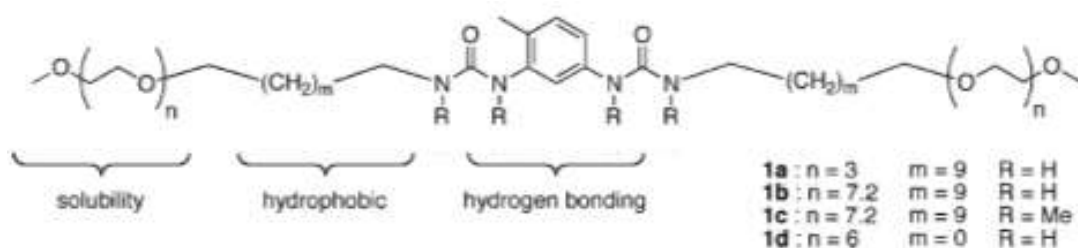


Figure 1.35 Design and structure of bis-urea.

In this chapter, it is presented a first study of two supramolecular polymers in water based on the structure of DPP. A supramolecular system with the same features of that described by Boutillier has been synthesized: the hydrophobic DPP molecule has been combined with the hydrophilic tri-(ethylene glycol) (TEG).

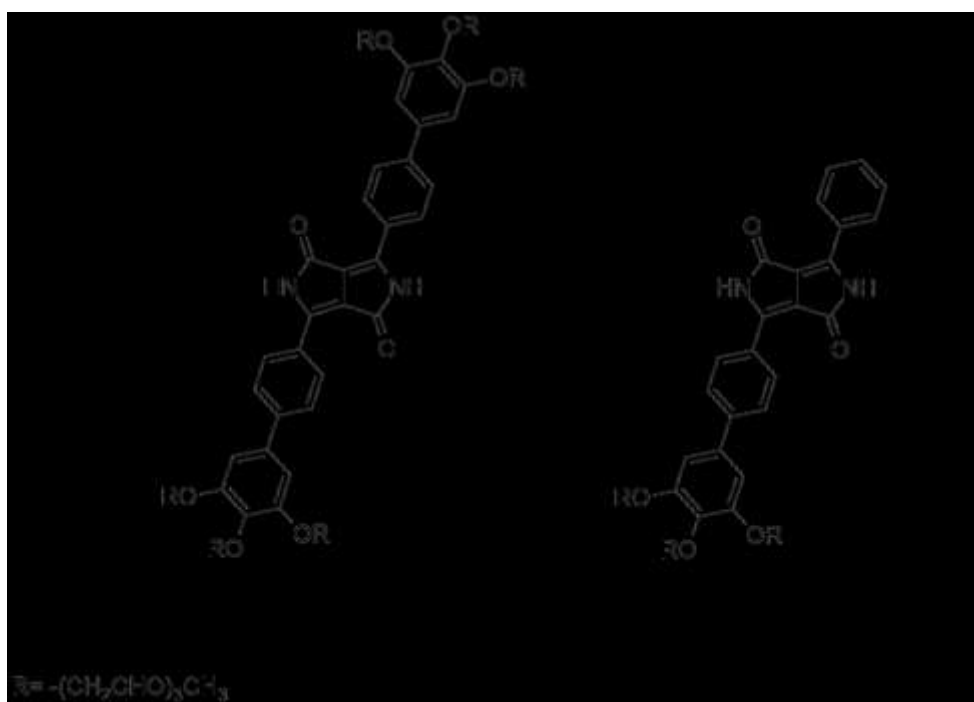


Figure 1.36 Molecular targets.

The peculiarity of this work is in the use of DPP molecule: synthetic supramolecular polymers in aqueous solution based on an organic pigment are particularly attractive in the conservation and restoration field, due to their dynamic and responsive nature.

Working in water could increase the number of possible applications of DPP compounds and could open to innovative solutions for the development of self-healing materials to employ in the restoration and conservation of Contemporary Art. Moreover these smart materials could permit to synthesize a supramolecular polymer in which pigment and medium coexist in the same molecular structure, guaranteeing stability and efficiency to the system. Furthermore, to realize these new materials is important to understand the supramolecular behaviour of DPP derivatives in water, the chemical and mechanical properties of these structures and their potential applications.

It has also been considered that even if aqueous supramolecular systems have shown great promise, the design principles for supramolecular polymers in water seem to be complex: it is known from the literature that hydrogen bonding interactions in aqueous media are often very weak because of the competition from water molecules, but they can still have a decisive effect on self-assemblies when used in combination with π - π stacking.⁴³

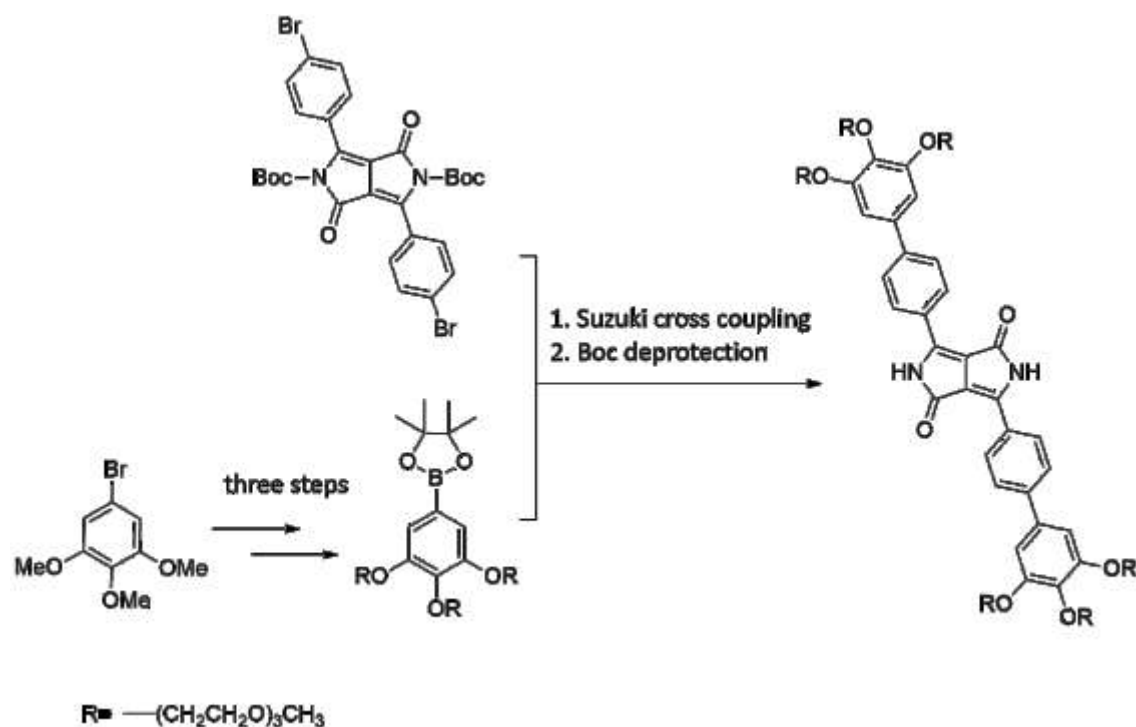
Two main features of supramolecular chemistry in aqueous media should be also analysed: how to gain high water solubility and how to control the supramolecular organizations. It is important to avoid, minimise or exploit the strong involvement of water in noncovalent processes.

In this chapter, an important focus will concern the stability of aggregates and the description of their mechanism of polymerization. The aggregates will be characterised using UV-Vis, DLS and ¹H-NMR spectroscopy and their morphology will be examined in depth using atomic force and scanning electron microscopy.

1.8 Synthesis of water soluble DPPs

1.8.1 Synthesis of TEG-DPP

TEG-DPP was synthesized with a Suzuki cross coupling involving a pinacol boronic ester and **BrDPP-Boc**, as shown in the Scheme 1.2.

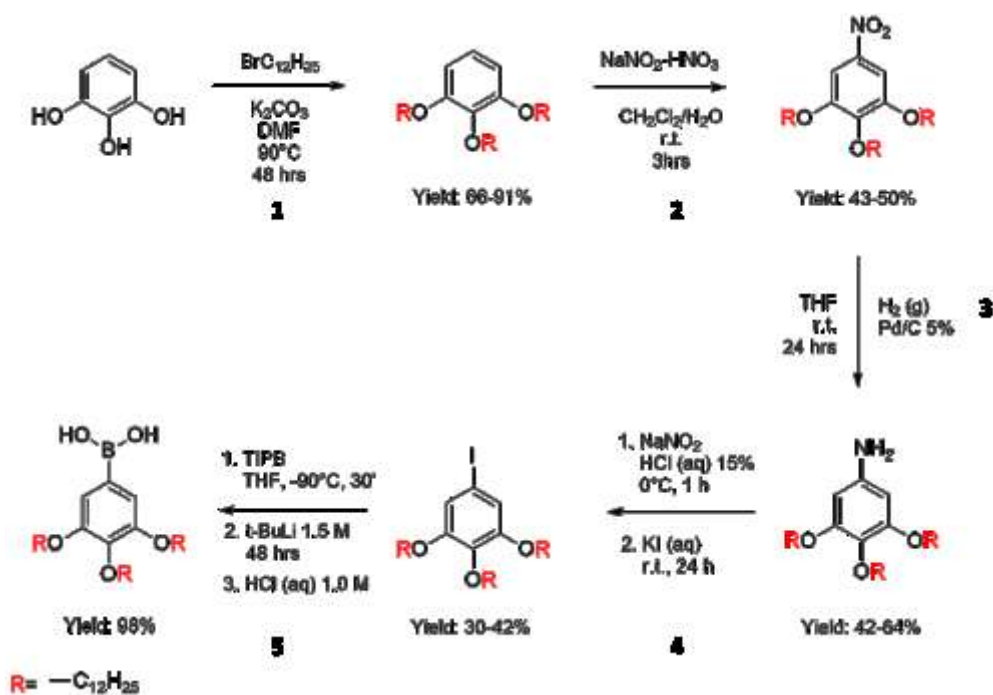


Scheme 1.2 Synthetic strategy to obtain TEG-DPP.

To obtain this molecule, our studies started considering the synthesis of *longchain-DPP*, described in Paragraph 1.6. *Longchain-DPP* was prepared through Suzuki cross-coupling between an organoboronic acid, in particular the (3,4,5-tris(dodecyloxy)phenyl)boronic acid, and a halide, the **BrDPP-Boc**, as shown at page 36.

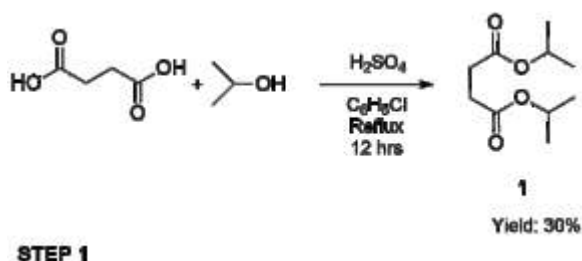
In this work the synthetic strategy studied for *longchain-DPP* is improved obtaining the molecular target with a reduced number of synthetic steps, in particular a pinacol boronic ester takes place of the boronic acid in the Suzuki cross-coupling with the **BrDPP-Boc**, as shown in Scheme 1.2.

The new strategy allows to obtain the pinacol boronic ester just in three synthetic steps, while the original procedure included 5 steps, as shown in Scheme 1.3.



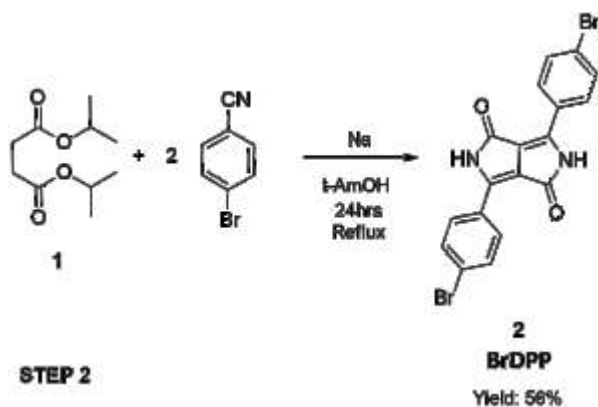
Scheme 1.3 Synthetic strategy used to obtain (3,4,5-tris(dodecyloxy)phenyl) boronic acid.

The starting point of this work was the synthesis of **BrDPP-Boc**. This molecule was prepared through three synthetic steps. The synthesis of diisopropyl succinate, shown in Scheme 1.4, was the first step to synthesize **BrDPP-Boc**. This precursor was obtained from the reaction between the succinic acid and isopropyl alcohol, using H_2SO_4 as catalyst and chlorobenzene as solvent. The yield was fair, but the final product was pure.



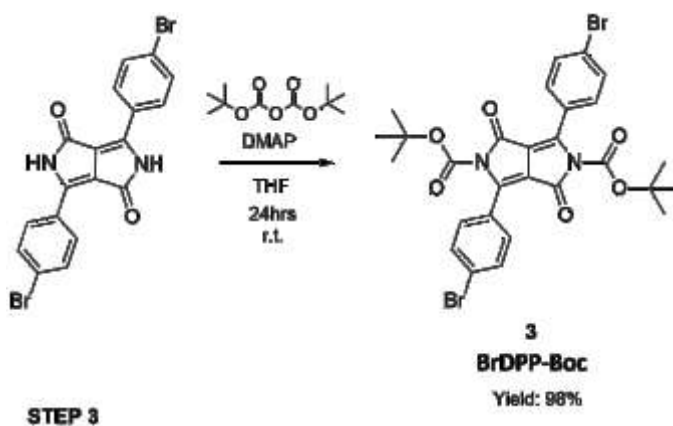
Scheme 1.4 Synthesis of diisopropyl succinate, 1.

In the second step the diisopropyl succinate reacted with 4-bromobenzonitrile through a pseudo-Stobbe condensation, according to the procedure described by Guo.⁴⁴ The reaction took place at 95° C, in presence of sodium and FeCl_3 , using *t*-AmOH as solvent. The diisopropyl succinate was added dropwise to avoid its self-condensation, as described in paragraph 1.2.2. After a night, the product was precipitated with water and acetic acid, then washed with hot methanol. In this way, the DPP was available as a dusty red solid (Scheme 1.5).



Scheme 1.5 Synthesis of BrDPP, 2.

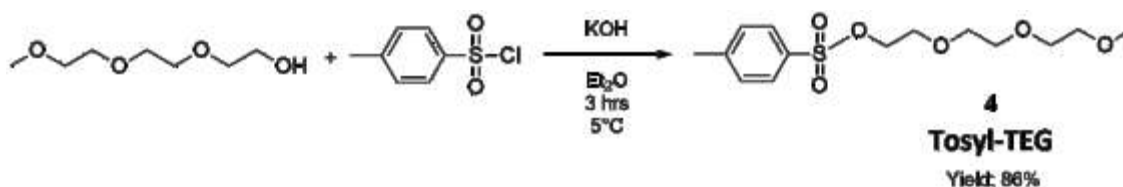
Product **2** was functionalized with *t*-Boc protecting group to obtain a system soluble in the most common solvents. Product **3** was prepared according to the procedure described in the literature⁴⁵ and it was obtained in good yields, as a yellow-orange solid, Scheme 1.6.



Scheme 1.6 Synthesis of BrDPP-Boc, 3.

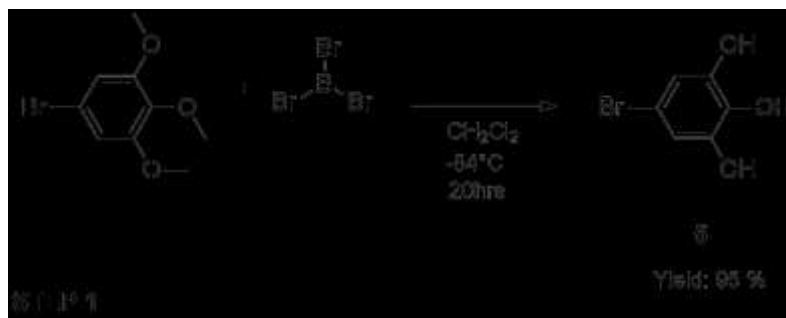
As said before, in this dissertation it is considered the synthesis of a pinacol boronic ester to obtain the molecular target, **TEG-DPP**, with a reduced number of synthetic steps.

The synthetic approach introduces the synthesis of **Tosyl-TEG**, according to the procedure described in literature⁴⁶ and shown in Scheme 1.7.



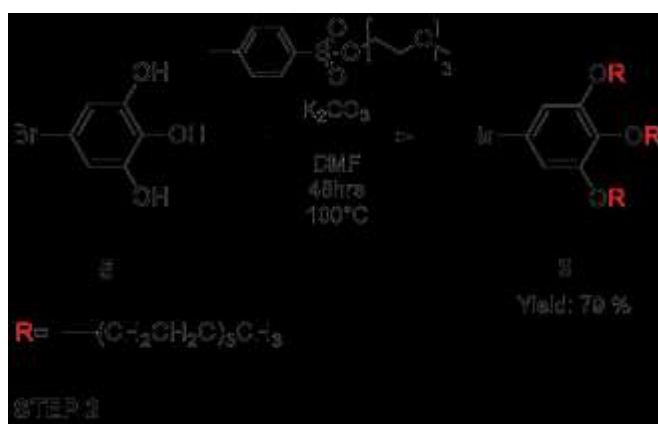
Scheme 1.7 Synthesis of Tosyl-TEG, 4.

The demethylation of 5-bromo-1,2,3-trimethoxybenzene with BBr_3 represents the first step of the synthetic route illustrated in Scheme 1.2. This procedure, described in the literature,⁴⁷ is reported in Scheme 1.8. Product **5** was obtained in good yields (95 %).



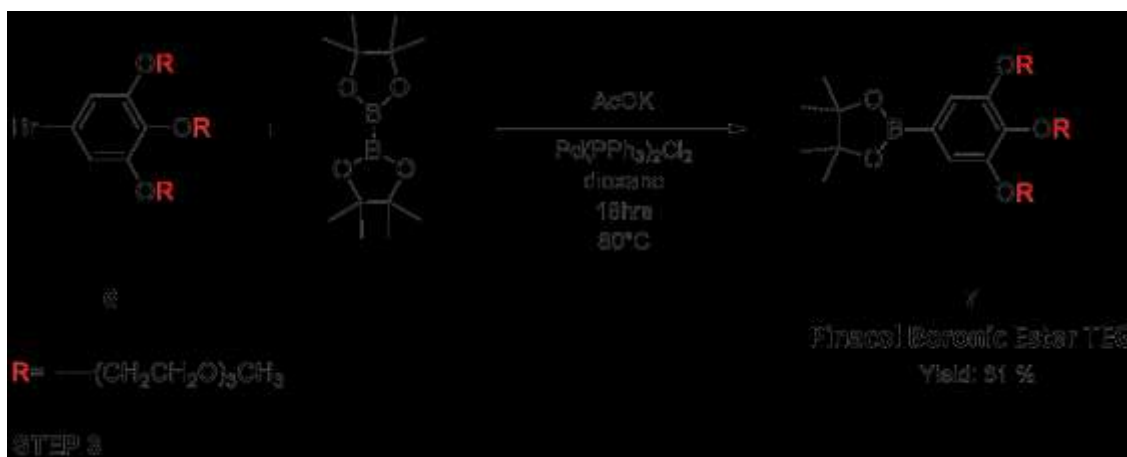
Scheme 1.8 Synthesis of 5-bromobenzene-1,2,3-triol, **5**.

The deprotected molecule (**5**) reacted through nucleophilic substitution with **4**, in dry DMF, using K_2CO_3 as base, as displayed in Scheme 1.9. The reaction occurred in good yield, the product **6** was not purified and it was obtained as a colourless oil.



Scheme 1.9 Synthesis of **6**.

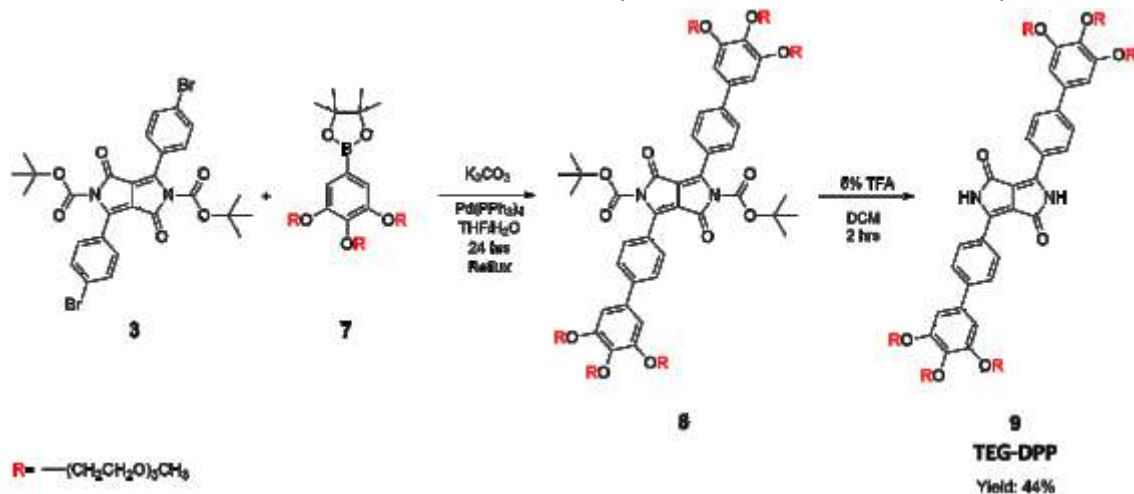
The Miyaura borylation⁴⁸ reaction enables the synthesis of boronates by cross-coupling of bis(pinacolato)diboron (B_2pin_2) with aryl halides, in this case with **6**. The reaction, described in Scheme 1.10, employs $\text{Pd}(\text{PPh}_3)_2\text{Cl}_2$, as catalyst, potassium acetate as base and dioxane as solvent. The product **7** was purified by column chromatography (9 AcOEt : 1 MeOH) to give a pale-yellow oil.



Scheme 1.10 Synthesis of TEG-pinacol boronic ester, **7**.

The Suzuki cross-coupling between the **BrDPP-Boc** and the **TEG-pinacol boronic ester (7)**, shown in Scheme 1.11 is the most important synthetic step. Pd(PPh₃)₄ is the catalyst, K₂CO₃ the base and toluene at reflux the solvent. The crude product was hydrolysed without any purification and the yield was calculated for the two steps. Our target, **TEG-DPP**, was purified by column chromatography (8 AcOEt : 2 MeOH).

Thanks to the TEG, the calculated **TEG-DPP** solubility in water is 10⁻² M at room temperature.

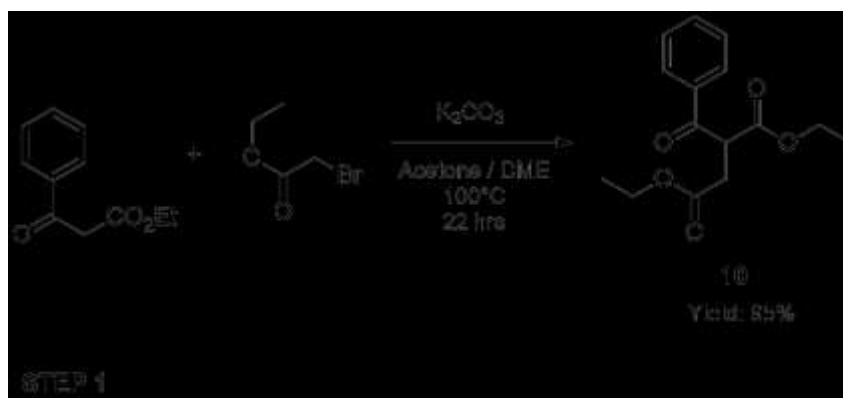


Scheme 1.11 Synthesis of **TEG-DPP** through Suzuki reaction and hydrolysis.

1.8.2 Synthesis of mono TEG-DPP

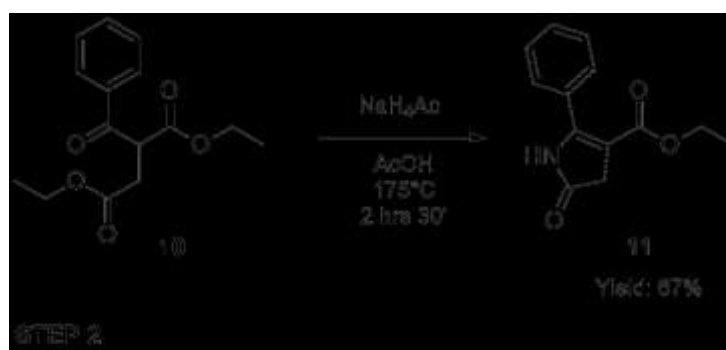
A non symmetric **TEG-DPP** was synthesized to study its supramolecular organization in water and to verify the types and dimensions of the supramolecular aggregates that could develop. The **mono TEG-DPP** was obtained with the same synthetic approach used for the symmetric molecule and shown in the general Scheme 1.2; the only difference was the use of **mono Br DPP** instead of **3**.

Mono Br DPP-Boc was obtained via four synthetic steps.⁴⁹ The first step was the reaction of ethyl-benzoacetate with the bromoacetic ester. The reaction was performed in acetone and DME, as shown in Scheme 1.12. The product was obtained in good yields (95 %).



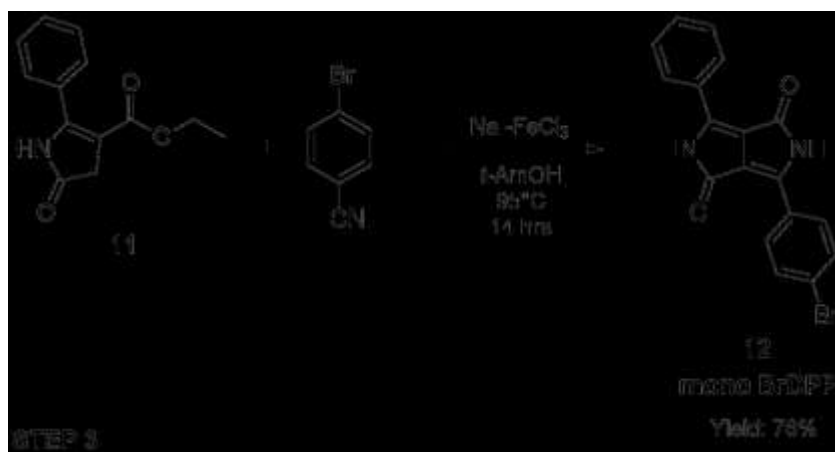
Scheme 1.12 Synthesis of diethyl benzoylsuccinate, **10**.

The second step, Scheme 1.13, involved the synthesis of the precursor **11** via cyclization: diethyl benzoylsuccinate reacted with ammonium acetate in acetic acid to give the pyrrolic ring.



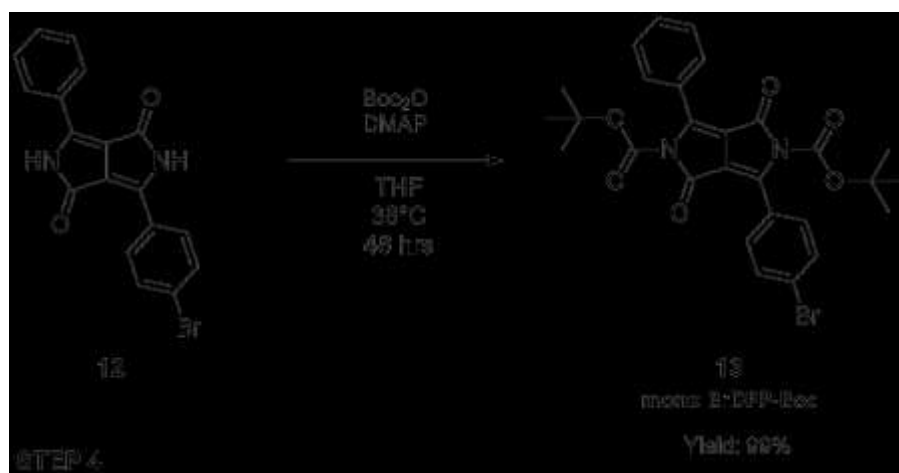
Scheme 1.13 Synthesis of pyrrolic ring, **11**.

The non symmetric pigment, called **mono BrDPP**, was prepared by the reaction between the pyrrolic ring and the p-bromobenzonitrile, following the procedure described in the literature⁷⁷ and shown in Scheme 1.14. The red dusty pigment obtained was practically insoluble.



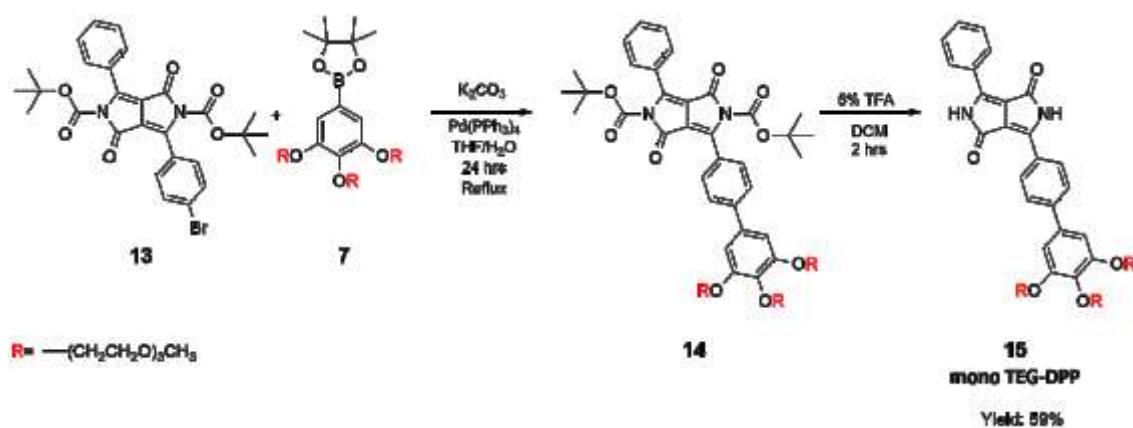
Scheme 1.14 Mono Br DPP synthesis.

The *t*-Boc protecting group was introduced, according to procedures⁷³ described in the literature, to solubilise the pigment. In this way the compound **13** (mono BrDPP-Boc) is soluble in the most common solvents, Scheme 1.15.



Scheme 1.15 Synthesis of mono Br DPP-Boc.

Mono BrDPP-Boc, 13, reacted with the pinacol boronic ester (**7**) via Suzuki cross coupling reaction, as shown in Scheme 1.16.



Scheme 1.16 Synthesis of mono TEG-DPP, **15**: Suzuki cross coupling reaction following by hydrolysis.

The crude product was hydrolysed without any purification and **mono TEG-DPP** was purified through column chromatography (8 AcOEt : 2 MeOH). **Mono TEG-DPP, 15**, was obtained with a yield of 59 % (calculated on the two steps: cross coupling and hydrolysis) and it appears as a red-violet solid.

1.8.3 TEG-DPP: supramolecular characterization in solution

a) UV-Vis spectroscopy

In the first instance, the **TEG-DPP** was characterized through UV-Vis spectroscopy at different concentration in AcOEt to calculate the molar extinction coefficient, ϵ (Figure 1.37). The angular coefficient of calibration line (with $R^2=0.999$) obtained at fixed λ (529 nm) gives ϵ , that is $44498 \text{ dm}^2 \text{ mol}^{-1}$.

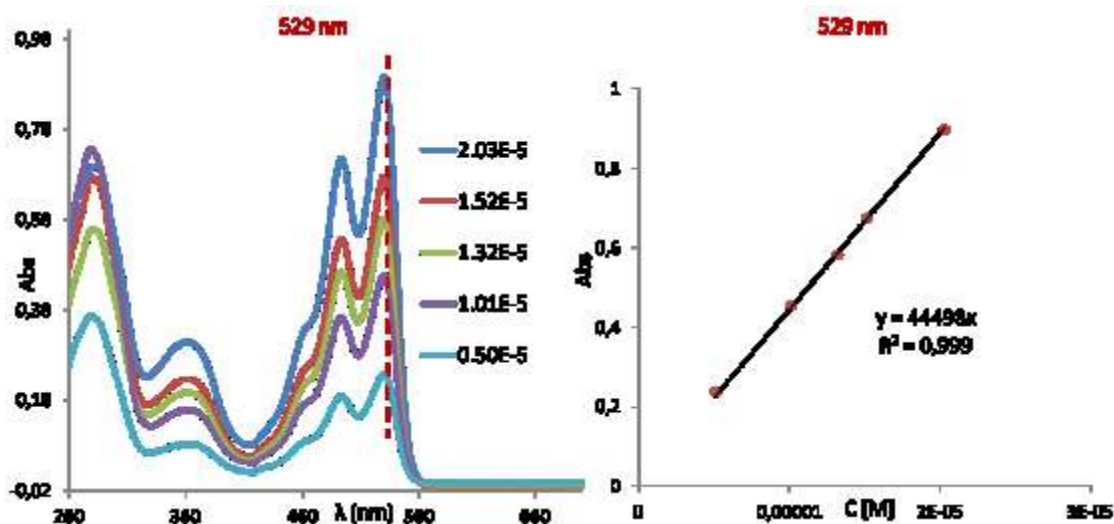


Figure 1.37 UV-Vis spectra in AcOEt for five concentrations of **TEG-DPP**.

A first observation of **TEG-DPP** solutions revealed that the compound is fluorescent at the monomeric state, whereas the fluorescence is quenched in the polymeric state. This behaviour can be due to the high compartmentalization of the chromophoric unit in the supramolecular aggregate.⁵⁰ Figure 1.38 reports two samples of **TEG-DPP** respectively in D_2O , where it is supposed to have the polymeric species, and in DMSO- d_6 , where it is known to have only the monomeric unit. This phenomenon, already described in the literature, does not concern the *longchain-DPP*, which is fluorescent in all kind of solvents and states.

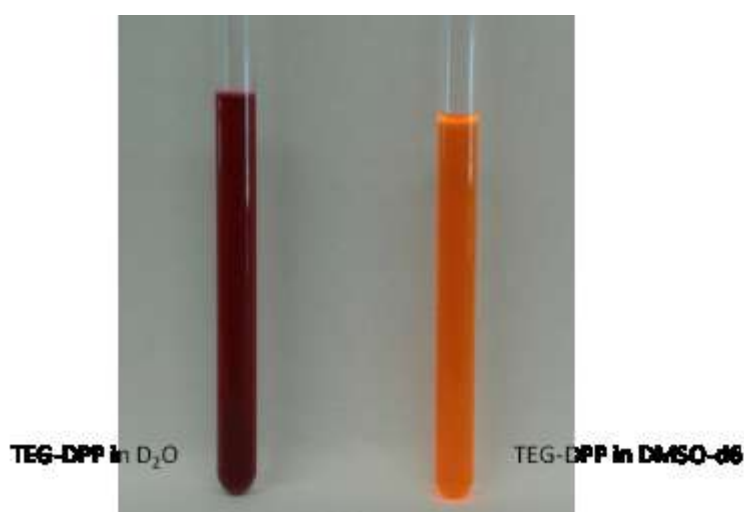


Figure 1.38 Samples of **TEG-DPP** respectively in D_2O and in DMSO- d_6 .

b) UV-Vis temperature-dependent analysis

UV-Vis temperature-dependent analysis in water

As described in the literature,⁷⁰ UV-Vis spectroscopy was used in order to investigate the self-assembly mechanism of **TEG-DPP**. With this technique the transition from monomeric to polymeric state could be visualised. Experiments were conducted at variable temperature and constant concentration in water. The general approach considered a first experiment in which spectra (from 750 nm, to 250 nm) were recorded in step of 5° C during the cooling process, from 363 K to 298 K. Then to gain insight into the self-assembly mechanism, the samples were analysed at fixed λ , where there was the maximum difference between the spectrum recorded at 363 K (monomeric state) and the spectrum recorded at 298 K (polymeric state).

The first experiment to analyse **TEG-DPP** was conducted for a solution $1.5 \cdot 10^{-5}$ M in H₂O. In Figure 1.39 temperature-dependent UV-Vis spectra, recorded in steps of 5° C, are reported.

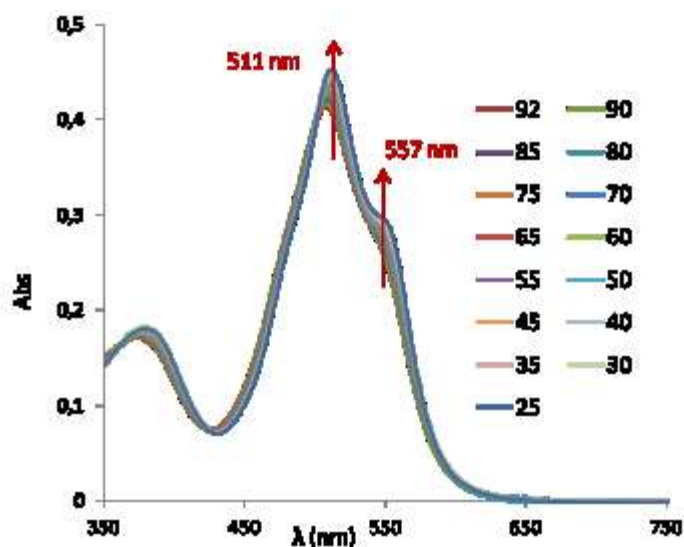


Figure 1.39 Temperature-dependent UV-Vis spectra of **TEG-DPP** ($c = 1.5 \cdot 10^{-5}$ M in H₂O).

The supramolecular organization of **TEG-DPP** was examined in depth comparing its behaviour with that already studied for **longchain-DPP**.

In Figure 1.40 the spectra of **longchain-DPP** in MCH at 90° C (blue line) and in DCM at 25° C (violet line) are reported. It is known that **longchain-DPP** develops a supramolecular polymer in MCH at room temperature and it is observed that the spectra recorded in MCH at 90° C has the same aspect of the spectrum recorded at 25° C in DCM, in which **longchain-DPP** is a monomer. This experiment demonstrates that a 90° C in MCH **longchain-DPP** is present only in the monomeric state.

In the same Figure, the spectra of **TEG-DPP** in water at 90° C (red line) and in AcOEt at 25° C (green line) are compared. It is known that **TEG-DPP** is present as monomer in AcOEt, while it organizes a supramolecular polymer in water at 25° C, thus increasing the temperature of the sample in water the presence of monomer should be ensured. Furthermore, the two recorded spectra (at 90° C in water and at 25° C in AcOEt) are very different and for this reason it is

possible to hypothesise that at 90° C in water **TEG-DPP** is present into a state of aggregation higher than monomeric unit.

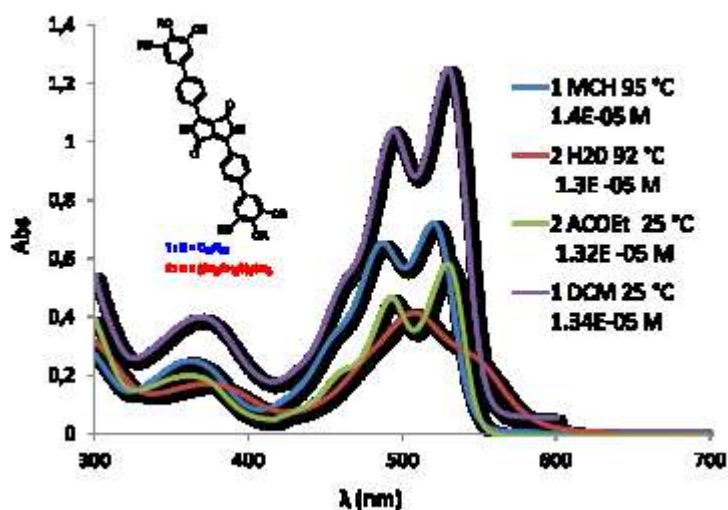


Figure 1.40 Comparison of UV-Vis spectra of *longchain-DPP* in MCH at 95° C (violet line), of *longchain-DPP* in DCM at 25° C (blue line), of *TEG-DPP* in AcOEt at 25° C (green line) and of *TEG-DPP* in water at 92° C (red line).

Moreover, it is observed in Figure 1.40 that the spectrum of **TEG-DPP** in water (red line) was hypsochromically shifted if compared with the absorption spectrum recorded in AcOEt (green line) at the same concentration. This displacement (about 22 nm) together with the minor absorption band of the spectrum in water can be attributed to the formation of H aggregates.⁵¹

In addition the spectra of *longchain-DPP* in MCH (blue line) and *TEG-DPP* in water (red line) are reported for comparison in Figure 1.41. At the same concentration *TEG-DPP* in water has a significant reduction in the maximum absorption band.

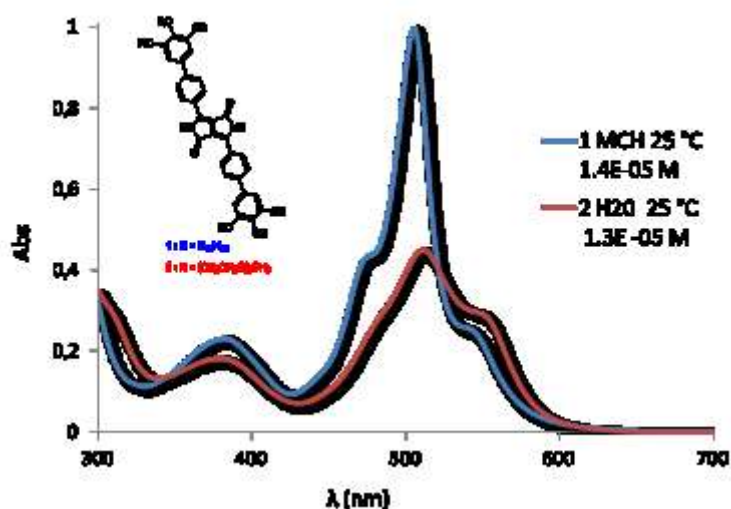


Figure 1.41 Comparison of UV-Vis spectra of *longchain-DPP* in MCH and of *TEG-DPP* in water.

After these considerations, **TEG-DPP** was analysed at fixed λ . From the spectra in Figure 1.64, the maximum spectral difference was calculated at 557 nm. Thus, the spectra at 557 nm for three concentrations were recorded, as shown in Figure 1.42.

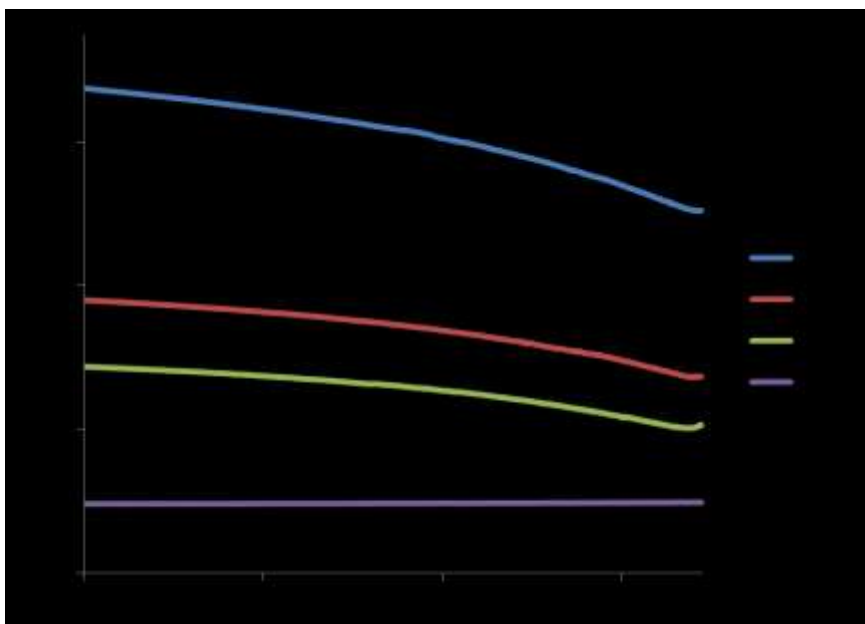


Figure 1.42 Spectra recorded at 557 nm for three concentrations of TEG-DPP in water and blank spectrum.

The spectra describe a cooperative mechanism of polymerization. Furthermore, only for concentration $4.0 \cdot 10^{-6}$ M it is possible to distinguish clearly the nucleation step.

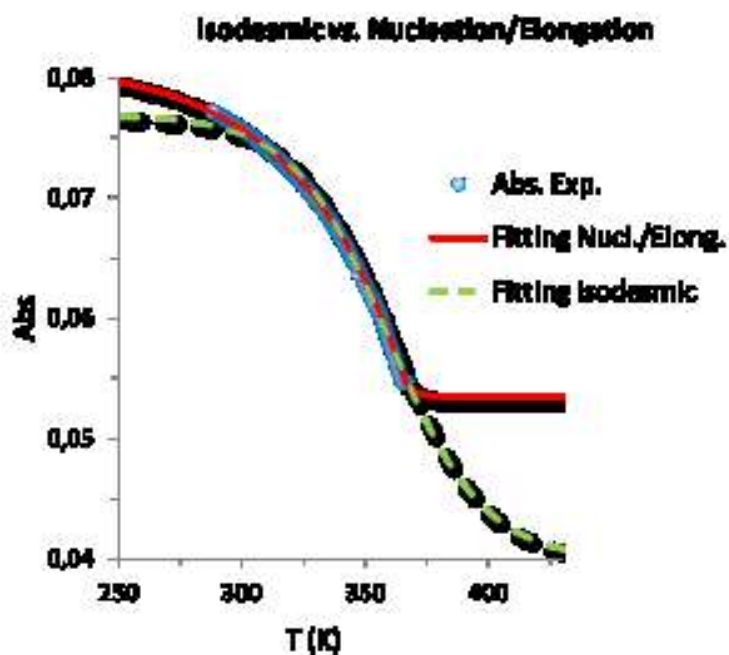


Figure 1.43 Comparison of TEG-DPP spectrum at 557 nm (blue line) with isodesmic fit (green line), elongation fit (red line) and nucleation fit (violet line).

As depicted in Figure 1.43, the experimental data, recorded for the solution $4.00 \cdot 10^{-6}$ M at 557 nm, was fitted with the isodesmic and with the cooperative model. The fitting procedure, using Scientist[®], confirms the hypothesis that TEG-DPP organizes a supramolecular polymerization via a cooperative mechanism.

In Figure 1.44, the fit of experimental data for the elongation and nucleation regimes for the solution $5.0 \cdot 10^{-6}$ M is reported. The experimental data were analysed through the van der Schoot's model described in paragraph A1.2, in Appendix A.

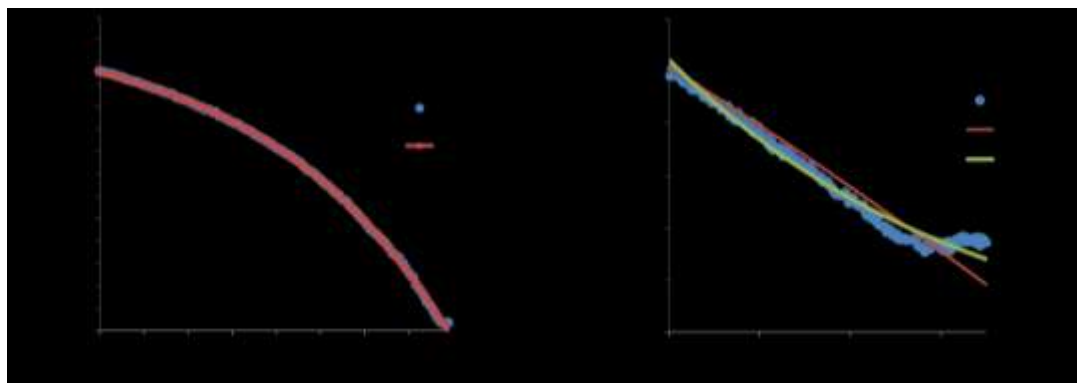


Figure 1.44 Fit of the experimental data for the elongation and the nucleation regimes, for clarity the number of absorbance values has been reduced at 100 units.

In the Table 1.3, the thermodynamic parameters calculated for the three concentrations are reported. The nucleation fit was effected only for the solution $5.0 \cdot 10^{-6}$ M. The apparent association constant K_{NE} , is on the order of $7.31 \cdot 10^{-4}$ M, while ΔH_e , obtained from the elongation fitting, has comperable values for the three concentrations. The Equation used to calculated the thermodynamic parameters are described in paragraph A1.2, in Appendix A.

Concentration [M]	Elongation				Nucleation	
	ΔH [kJ·mol ⁻¹]	Te	ϕ_{sat}	DP _n (298K)	DP _n (Te)	K_{NE}
8.0E-06	-26.14 ± 0.06	385.27 ± 0.04	1,060 ± 0.001			
5.0E-06	-26.14 ± 0.03	365.70 ± 0.01	1,060 ± 0.001	109.78	26.27	$(7.31 \pm 1.6) \cdot 10^{-4}$
4.0E-06	-35.49 ± 0.23	334,68 ± 0.23	1,320 ± 0.004	-		

Table 1.3 Thermodynamic parameters obtained from the fit of experimental data for three concentration of TEG-DPP in water.

Following Equation 9 in paragraph A1.2, in Appendix A. DP_n was calculated for all temperatures, as displayed in Figure 1.45.

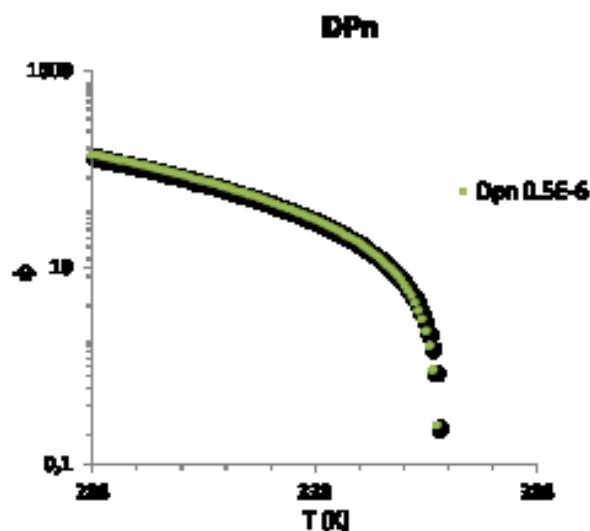


Figure 1.45 DP_n calculated for the solution $5.00 \cdot 10^{-6}$ M in H_2O .

The fitting procedure described above was verified with van't Hoff plot: a linear relationship between the logarithm of concentration versus reciprocal temperature for the three solutions in analysis is observed in Figure 1.46.⁵⁵ The enthalpy released was calculated by multiplying the slope by the gas constant: $\Delta H = 33.25 \cdot 8.31 = 27.52 \text{ KJ mol}^{-1}$ and this value is comparable to that obtained by the fitting of experimental data.

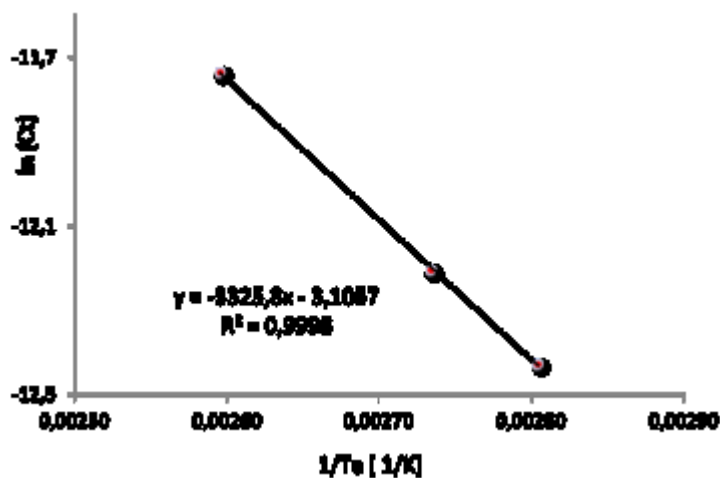


Figure 1.46 Van't Hoff plot.

To evaluate their reliability, these results will be compared with the results of DLS analysis at page 60.

UV-Vis temperature-dependent analysis in water and DMSO

In order to gain insight in the aggregation process, the monomeric state was investigated by adding a solvent able to break the initial aggregates not visible in pure water. Thus UV-Vis study was conducted using a solution of H_2O and DMSO, solvent able to break hydrogen bonding interactions.

At first, aliquots of DMSO were added at 363 K recording the spectra. After adding 500 μL (16.6 %) of DMSO, a significant change could be observed in the spectrum, as shown in Figure 1.47.

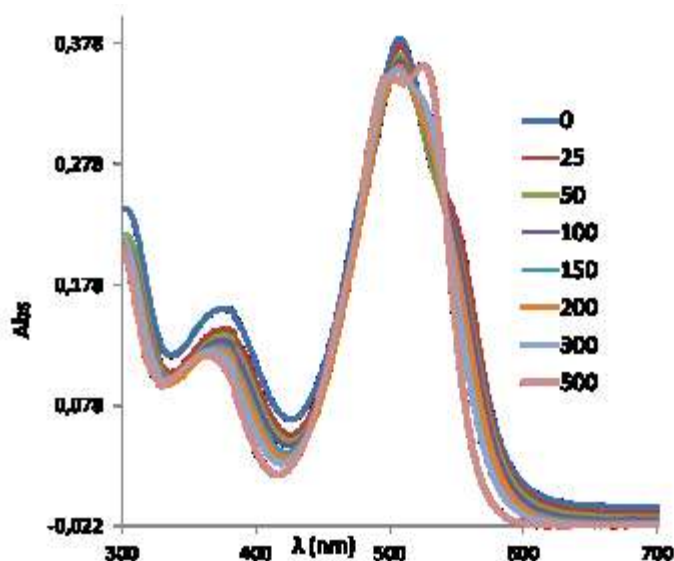


Figure 1.47 UV-Vis titrations of TEG-DPP with DMSO at high temperature.

The spectrum recorded for the solution $\text{H}_2\text{O}/16.6\%$ DMSO at 363 K appears a good compromise between the spectrum recorded in water (Figure 1.39) and that in AcOEt (Figure 1.37), where TEG-DPP is present in monomeric state. Observing the spectra it is possible to hypothesise that for the solution $\text{H}_2\text{O}/16.6\%$ DMSO monomeric units are present with a good percentage at 363 K. Thus, UV-Vis spectra were recorded for a solution $1.5 \cdot 10^{-5}$ M in $\text{H}_2\text{O}/15\%$ DMSO in step of 5°C from 365 K to 273 K.

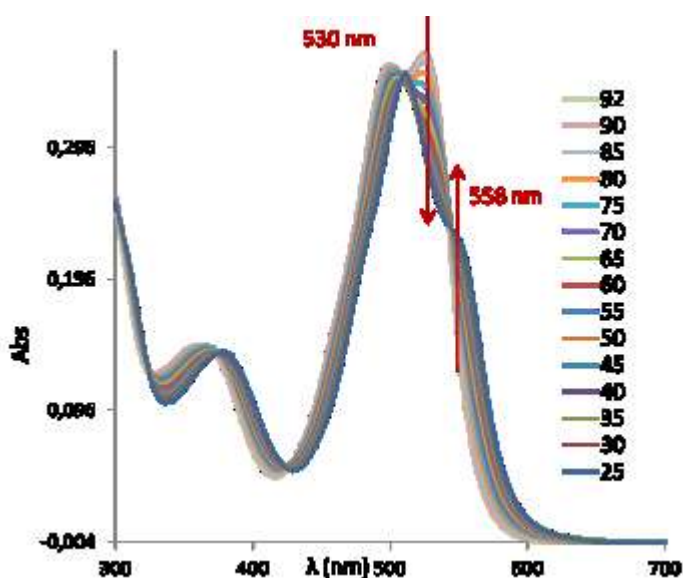


Figure 1.48 Temperature-dependent UV-Vis spectra of TEG-DPP ($c = 1.5 \cdot 10^{-5}$ M in $\text{H}_2\text{O}/15\%$ DMSO).

In the spectra reported in Figure 1.48 two transitions associated to two λ values are distinguished: the first transition, at 530 nm, is due to the disappearance of the monomer

that, during the cooling process, is converted in polymer and the second transition, at 558 nm, is due to the appearance of the polymeric species at lower temperature, as observed in pure water. Figure 1.49 displays this phenomenon.

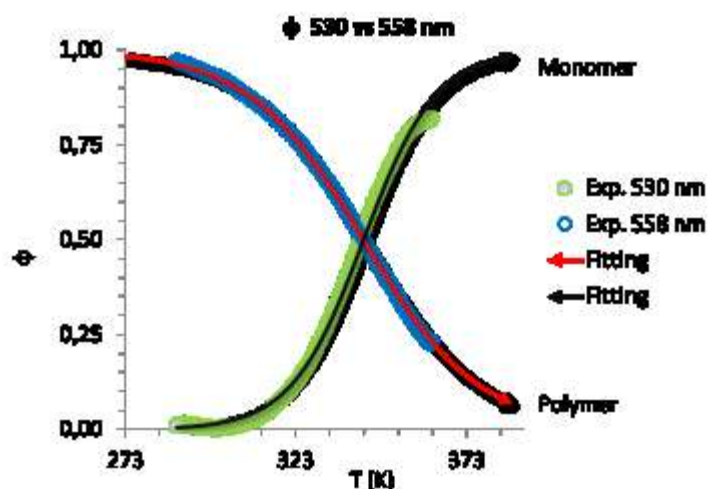


Figure 1.49 Comparison of fit experimental data for the two λ values (530 nm and 558 nm).

The temperature-dependent experiments were recorded for three concentration: $1.5 \cdot 10^{-5}$ M, $1.3 \cdot 10^{-5}$ M and $1.0 \cdot 10^{-5}$ M at 530 nm. The shape of the curves suggests an isodesmic mechanism in the self assembly of **TEG-DPP**, as shown in Figure 1.50.

Only the shape of the curves recorded at 530 nm was analysed, because the maximum spectral difference was found at this λ .

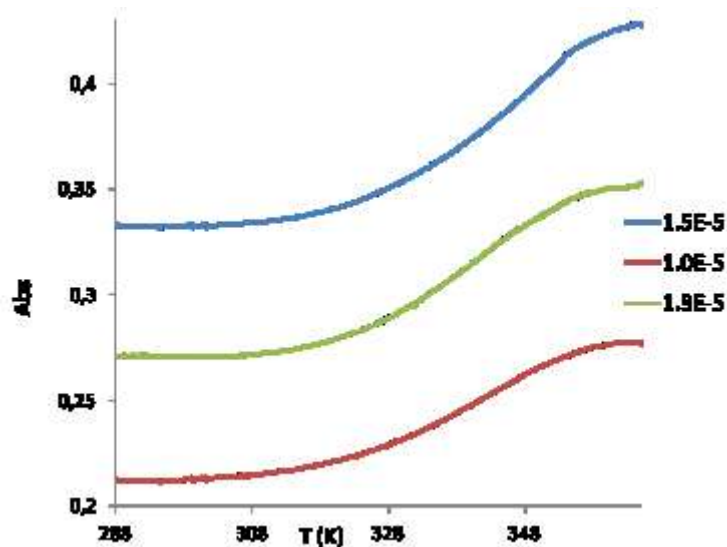


Figure 1.50 UV-Vis spectra at 530 nm for three concentration of **TEG-DPP** in $H_2O/15\%$ DMSO.

Using the model described in paragraph A1.1, in Appendix A, the experimental data were analysed and the thermodynamic parameters (ΔH , T_m and K_{is}) were obtained for each concentration. Figure 1.51 reports the graphic of ϕ in function of temperature and concentration for the three analysed solutions.

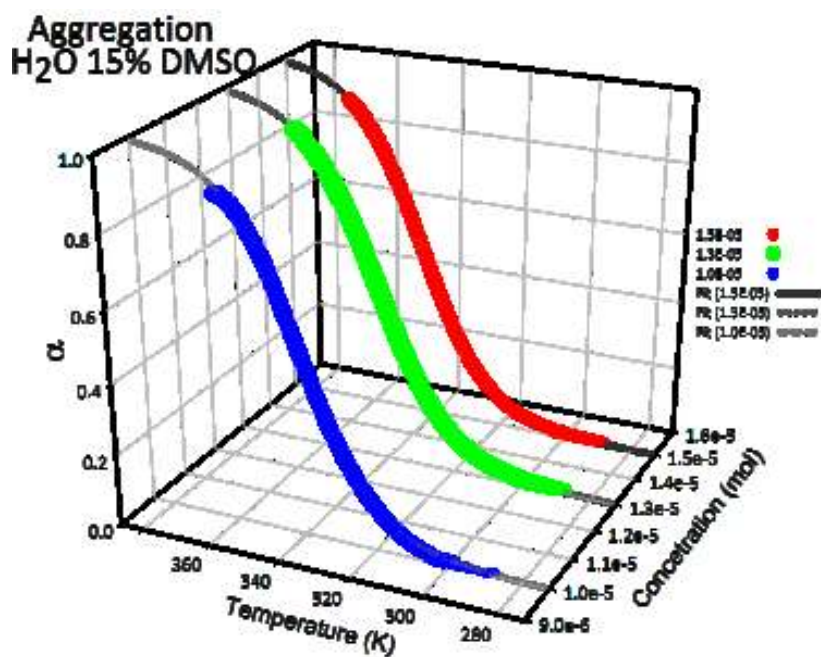


Figure 1.51 Aggregation of TEG-DPP in H₂O/15 % DMSO.

The DP_n was calculated using Equation 4, described in paragraph A1.1, in Appendix A. In Figure 1.52, DP_n is represented as function of temperature. The number of aggregates is limited, at room temperature is about of 8 molecules for the solution $1.3 \cdot 10^{-5}$ M.

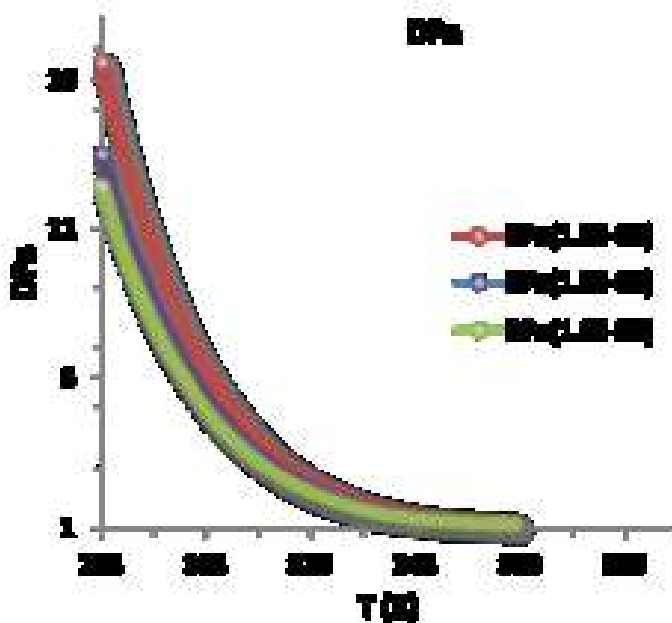


Figure 1.52 DP_n of TEG-DPP in H₂O/15 % DMSO.

Thermodynamic parameters for the three concentrations are shown in the Table 1.4. The apparent association constant, at 298 K is on the order of 10^{-5} M in a concentration range of $1.5 \cdot 10^{-5}$ M. ΔH has comparable values for the three concentrations.

Isodesmic Parameters

Concentration [M]	Wavelength [nm]	ΔH [KJ x mol ⁻¹]	Tm (K)	K_{is}^1 (298 K) [10^5 M ⁻¹]	DPn (298 K)
1.50E-05	530	-107.61 ± 0.20	344.56 ± 0.02	60.76	10.06
1.30E-05	530	-101.84 ± 0.33	342.80 ± 0.04	47.57	8.38
1.00E-05	530	-101.53 ± 0.22	340.48 ± 0.02	51.44	7.69

Table 1.4 Thermodynamic parameters obtained from the fit of experimental data for three concentrations of TEG-DPP in H₂O/15 % DMSO.

The melting temperature is proportional to the concentration: the temperature decreases with the dilution of the samples and van't Hoff plot reveals a linear relationship. In the Figure 1.53 it is observed the logarithm of concentration versus reciprocal temperature for the three solutions in analysis. The enthalpy released was calculated by multiplying the slope by the gas constant: $\Delta H = 11.76 \cdot 8.31 = 97.82$ KJ mol⁻¹ and this value is comparable to that obtained by the fitting.

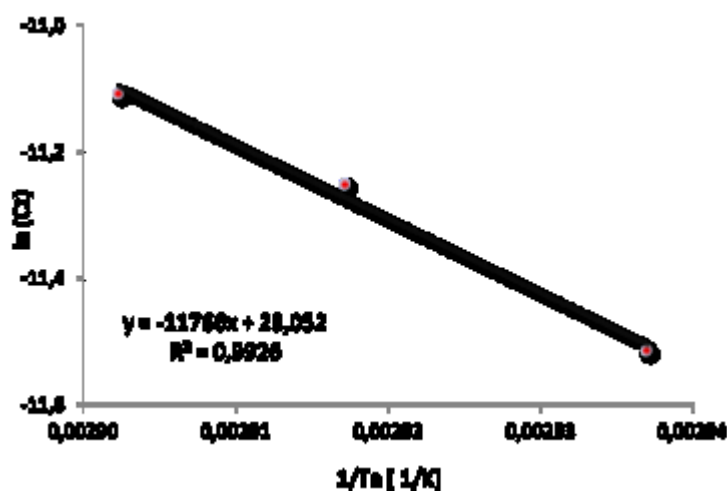


Figure 1.53 Van't Hoff plot.

¹ K_{is} is given by Equation 4 at page 95.

c) NMR temperature-dependent analysis

In order to confirm the UV-Vis data obtained, **TEG-DPP** was analysed by ^1H NMR temperature-dependent analysis.

The temperature-dependent ^1H NMR analysis was conducted for a solution of **TEG-DPP** ($c=2.3 \cdot 10^{-3}$ M, in D_2O) from 298 K to 363 K in steps of 10°C . In Figure 1.54 it is reported ^1H NMR spectra recorded at different temperatures in D_2O . The first spectrum reported in Figure 1.54 was recorded in DMSO-d_6 , where the molecule is in monomeric state.

During the heating process the number of aromatic peaks decreases, chemical shifts collapse and peaks resolution improves. This behaviour is due to the transition from polymeric state (at room temperature) to smaller species, as short oligomers or dimers at high temperature. This result confirms UV-Vis studies in water in which, at 363 K in diluted condition (10^{-6} M), only a oligomeric state instead of a monomeric one is distinguishable.

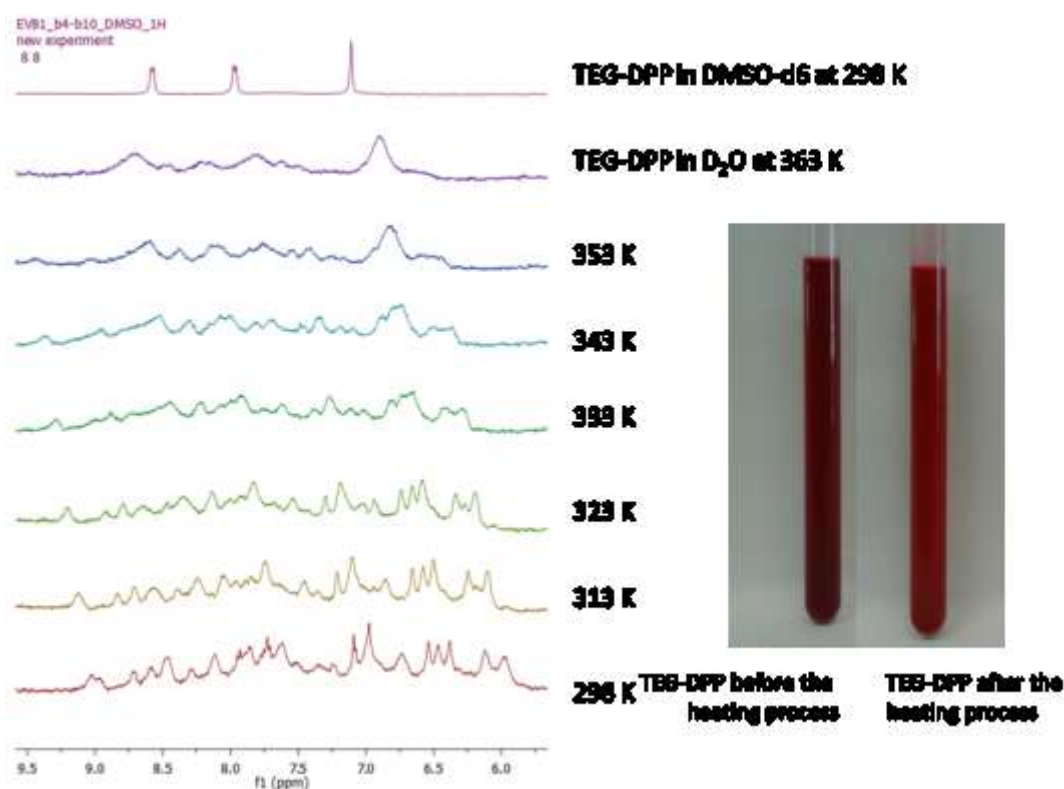


Figure 1.54 Temperature-dependent ^1H NMR spectra in D_2O , recorded between 298 K and 363 K and NMR tube of **TEG-DPP** in D_2O before and after the heating process.

The UV-VIS experiment was reproduced in ^1H NMR analysis: small aliquots of DMSO were added to **TEG-DPP** solution ($c=2.3 \cdot 10^{-3}$ M, in D_2O) at 363 K. The spectra in Figure 1.55 show the DMSO titration of **TEG-DPP**, where it is possible to appreciate the reduction of the number of aromatic peaks into three broad signals attributable to monomeric state, in equilibrium with the other oligomer species.

This result confirms the hypothesis formulated during UV-Vis analysis: in the previous paragraph it was supposed to arrive at monomeric level by adding the 15 % of DMSO to a

solution $1.5 \cdot 10^{-5}$ M of **TEG-DPP**. In NMR conditions (higher concentration) higher percentage of DMSO are required in order to observe this transition.

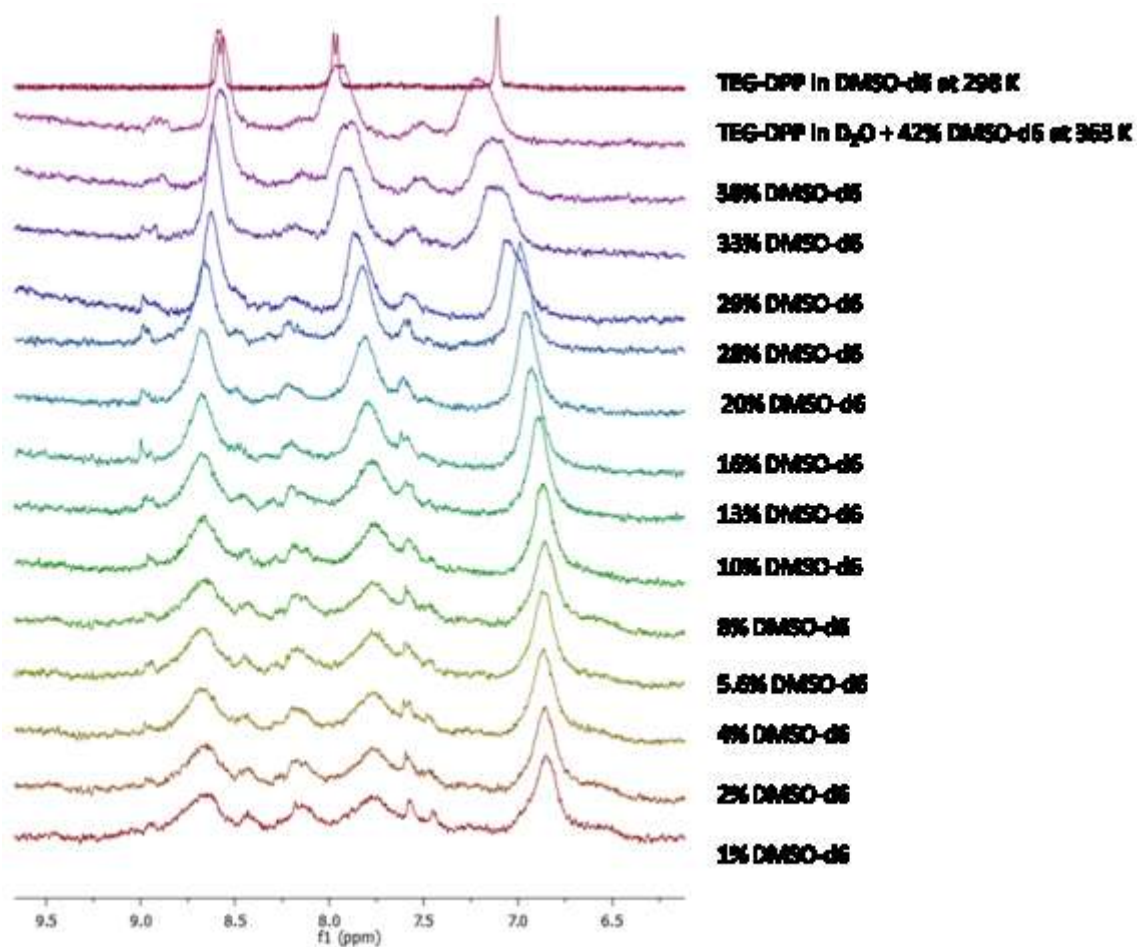


Figure 1.55 ^1H NMR spectra of TEG-DPP in D_2O and DMSO- d_6 recorded at 263 K.

d) Dynamic Light Scattering Analysis

DLS analysis was conducted to evaluate the real dimensions of aggregates in solution. The same solutions used in UV-Vis characterizations were tested to establish the range of sample concentrations for optimal measurements. Furthermore, at this concentrations the signal value of the light scattered was too low.

Thus, the size of the associates of **TEG-DPP** was investigated at a concentration of $7.5 \cdot 10^{-4}$ M in water and a variable distribution of particle sizes, ranging from 150 to 870 nm, was found, as shown in Figure 1.56.

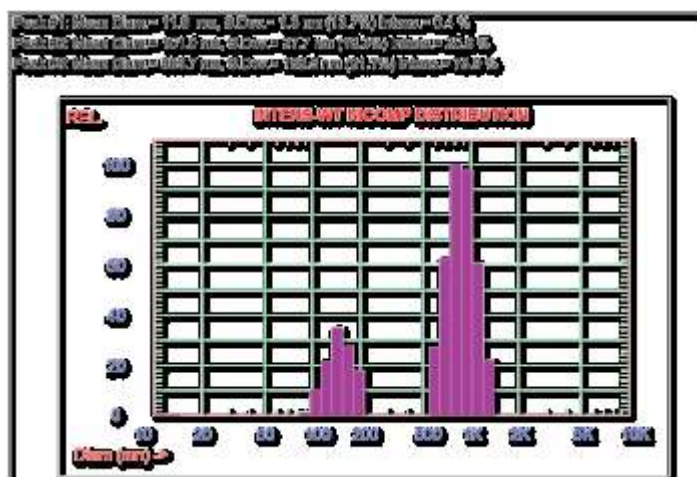


Figure 1.56 Distribution of particle sizes.

However this result can be compared with UV-Vis measurements. It is important to mention that, according to van der Shoot model, T_e is the only concentration-dependent value. Thus, it was possible to extrapolate T_e using the van't Hoff plot at page 57 for the solution $7.5 \cdot 10^{-4}$ M. As shown in Figure 1.57 “virtual DP_n ” can be estimated using the Equation at page 99, supposing that K_{NE} as well as ϕ_{SAT} and ΔH , does not change with the concentration.⁴⁵ This value is equal at 233 molecules for the solution used in DLS experiment at room temperature.

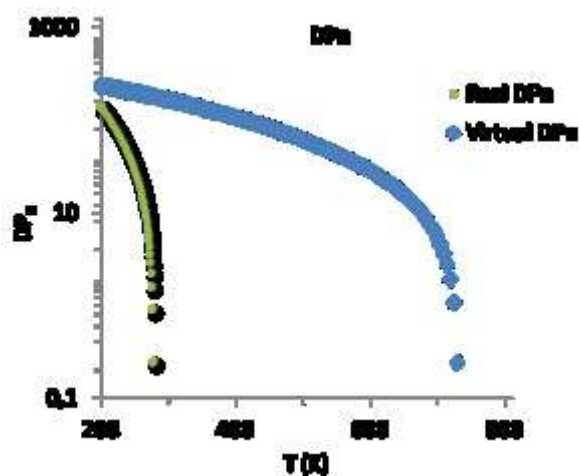


Figure 1.57 Comparison between the virtual DP_n calculated for $7.5 \cdot 10^{-4}$ M and the DP_n obtained for $5.0 \cdot 10^{-6}$ M.

Moreover the result of a geometry optimization, using PM3 semi empirical method, allows to estimate the length of **TEG-DPP** molecule approximately equal at 3.1 nm, as displayed in Figure 1.58.

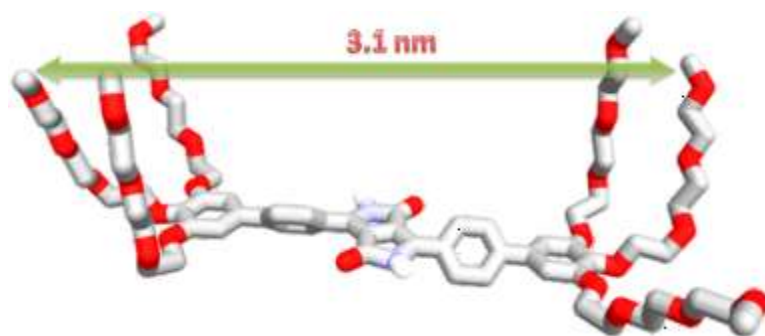


Figure 1.58 Molecular model realised using PM3.

Summarizing at room temperature, the length of **TEG-DPP**, at the given concentration, was determined to be about of 233 molecules, taking into consideration that the length of monomer by molecular model was approximately 3.1 nm. The calculated length of the aggregate would be 722 nm, which was in good agreement with DLS results.⁶²

The DLS analysis of **TEG-DPP** solutions in H₂O/15 % DMSO at different temperatures and also the direct estimation of the hydrodynamic radius of **TEG-DPP** in monomeric state are still in progress.

1.8.4 TEG-DPP: supramolecular characterizations in the solid state

a) Differential Scanning Calorimetry Analysis

DSC was used to measure the characteristic properties of **TEG-DPP**: using this technique, it is possible to establish the fusion and crystallization events and the presence of a mesomorphic phase. Analysis was made on 3.34 mg of sample, from 0° C to 175° C.

The procedure considered three cycles of heating and three cycles of cooling at the speed of 10° C at minute. The peaks in the spectra, Figure 1.59, show a reversible behaviour of the system. In the heating process three peaks are observed: melting point at 143° C, a phase transition at 107° C and another transition at 38° C. On the contrary in the cooling process only two peaks are observed: it is possible that the mesophase and the melting point combine into only one peak. The mesophase is in a defined range of temperature and time.

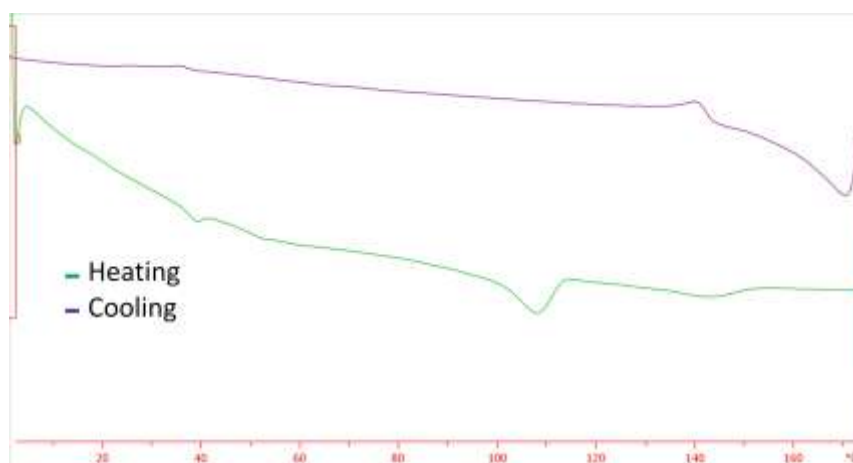


Figure 1.59 DSC spectra of TEG-DPP.

The enthalpy value can be obtained by the value of peaks integration. It is reported in the Table 1.5 the parameters calculated from DSC.

	1 st	2 nd	3 rd
Peak (° C)	38.79	107.93	143.42
Onset (° C)	35.45	99.86	132.57
ΔH (kJ·mol ⁻¹)	0.314	2.378	0.86

Table 1.5 Parameters derived from DSC.

b) Polarised Optical Microscopy Analysis

Polarised optical microscopy (POM) allows to establish the real presence of a mesomorphic phase for **TEG-DPP** and the observation of the molecule confirms the hypothesis elaborated with DSC experiment. The substrate was heated starting from 0° C just to reach the melting point. Upon heating the sample returns slowly to room temperature to give the molecules time to organize themselves.

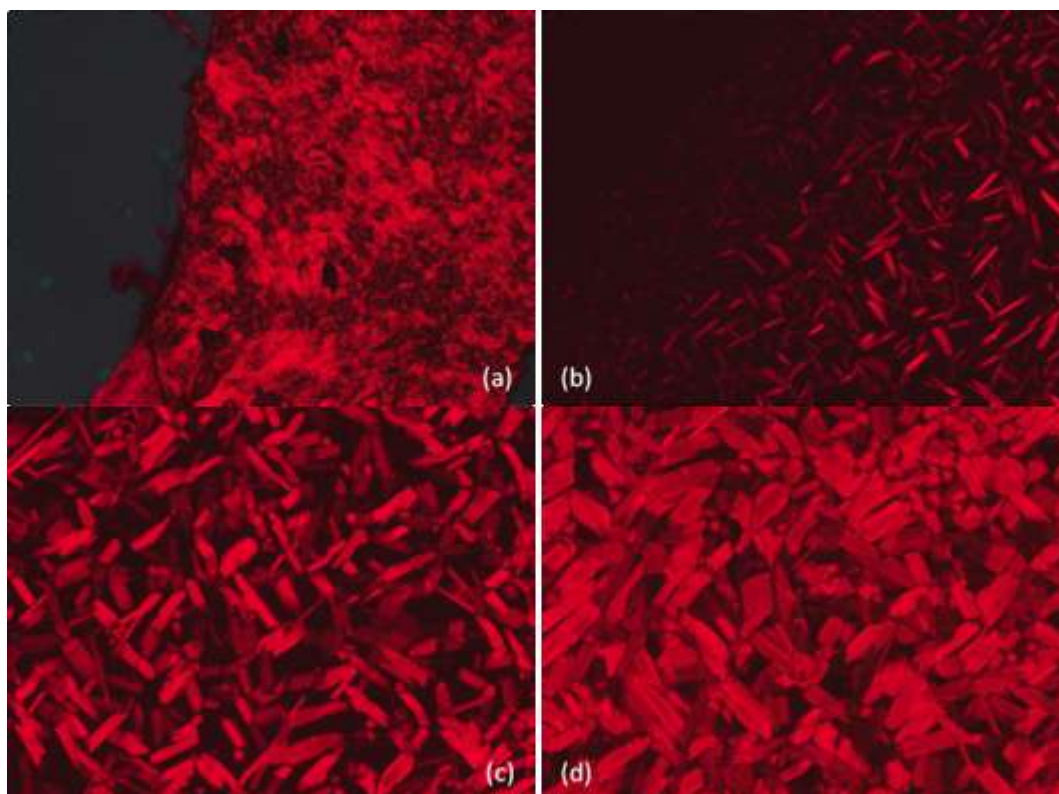


Figure 1.60 POM observation: **(a)** at 35° C; **(b)** 136° C; **(c)** at 125° C and **(d)** at 85° C.

At 35° C (temperature near to the temperature of the first peak in DSC) the substrate presents a viscous and birefringent aspect, as shown in Figure 1.60, **(a)**. Birefringence at POM is a good signal to suppose a mesomorphic phase. At 156° C the isotropization takes place (143° C at DSC). The sample is cooled slowly and at 136° C the first liquid-crystals begin to organize themselves, Figure 1.60, **(b)**.

It seems that a part of structures crystallises and another part is able to develop a mesophase (125° C), Figure 1.60, **(c)**.

The texture becomes bigger at lower temperature (85° C), as shown in Figure 1.60, **(d)**. The observed texture seems to describe a columnar phase: the segments are thin and elongated, in a sort of fern-like structure.

c) Atomic Force Microscopy Analysis

Atomic force microscopy analysis let us acquire a complete picture of the morphology of the compound and allow us to describe the kind of supramolecular organization of the sample in the solid state. The sample was deposited at room temperature using spin-coating technique. The concentration of solution was $1.0 \cdot 10^{-3}$ M (0.1 % m/m) in chloroform.

Sample distribution is homogeneous, it is possible to identify the silicon background. The aspect is clearly fibrous and the sample presents elongated structures, as shown in Figure 1.61.

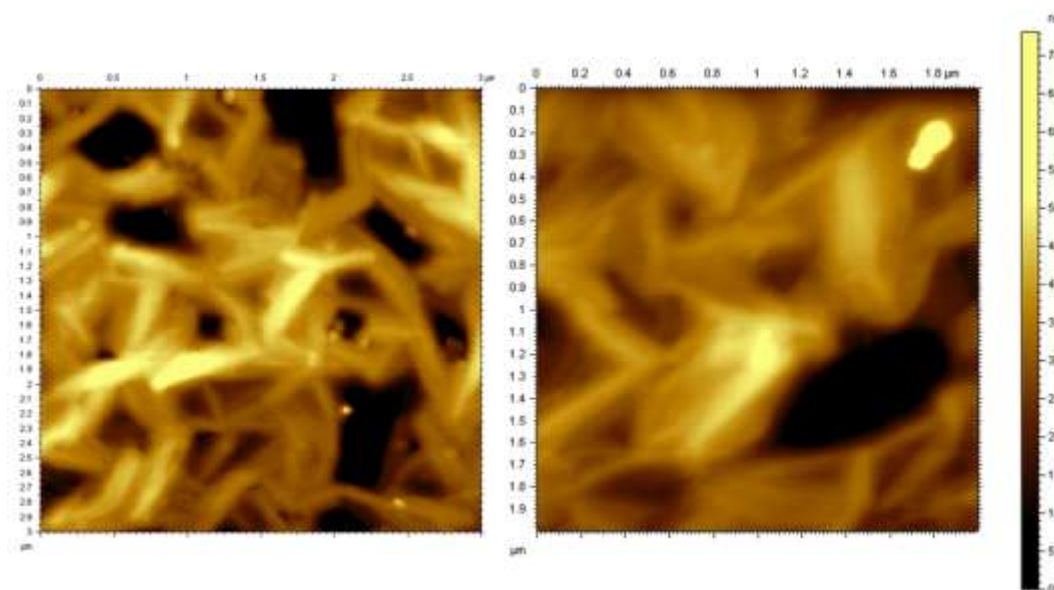


Figure 1.61 Fibrous structures observed with AFM.

In addition to presenting a surface image, a quantitative measurements of feature sizes, such as heights and width, were realized. The width is in a range of 120-150 nm and the height is comprised between 4-8 nm, as displayed in Figure 1.62.

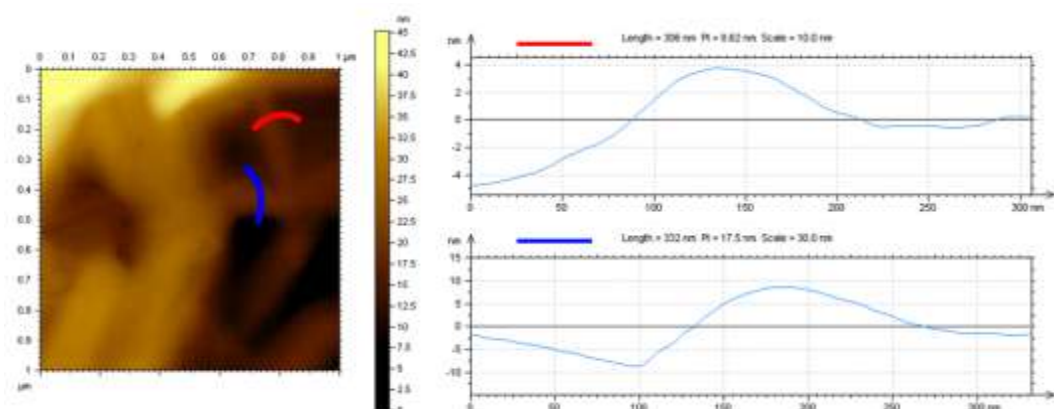


Figure 1.62 AFM observation and qualitative measurements of particles' size.

d) Scanning Electron Microscopy Analysis

The scanning electron microscope (SEM) reveals information about the sample including external morphology (texture), chemical composition and crystalline structure and orientation of materials. A sample deposited at room temperature using spin-coating technique was analysed. The concentration of solution was $1.0 \cdot 10^{-3}$ M (0.1 % m/m) in chloroform.

From the SEM observation, it is possible to distinguish elongated fibers with some interferences. As shown in Figure 1.63 the wire-like structures are similar to those observed at AFM and also in this case the dimension of the fibers can be estimated.

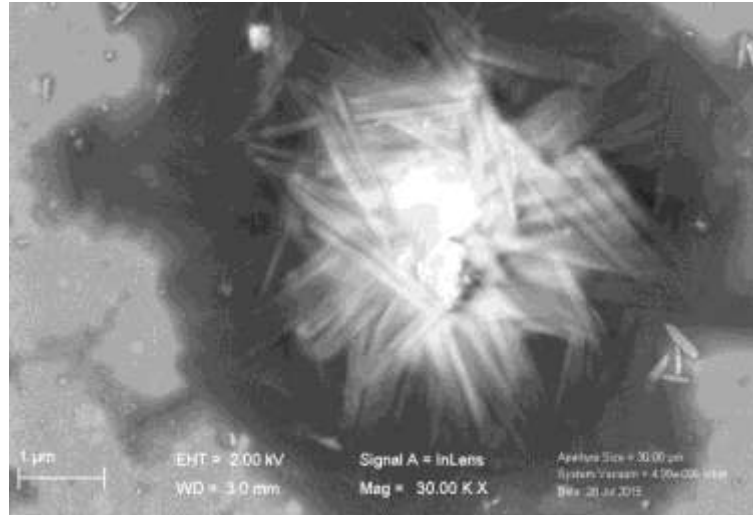


Figure 1.63 Elongated fibers observed at SEM.

Width is comparable to the result obtained with AFM: this value is comprised between 110-200 nm. The length of the structures was measured, but in this case it is difficult to distinguish the beginning and the end of a fiber (Figure 1.64). An indicative value could be 1 μm.

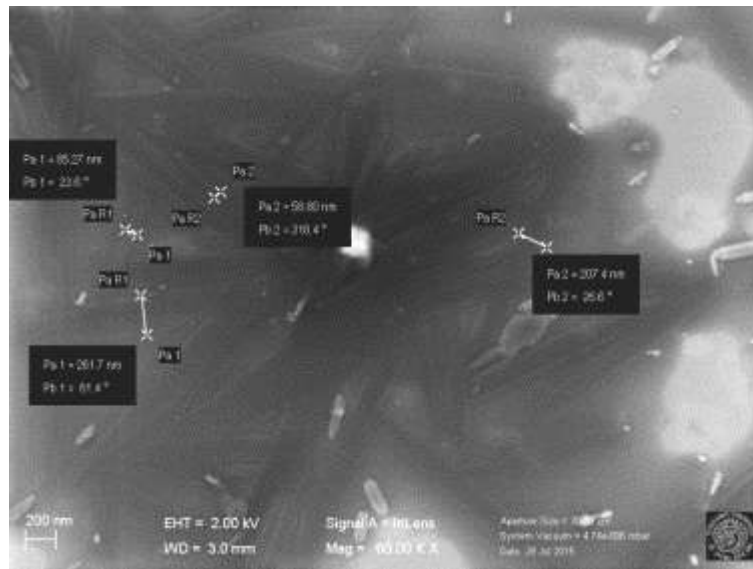


Figure 1.64 Measurements of fibers at POM.

1.8.5 Mono TEG-DPP: supramolecular characterization in solution

a) UV-Vis spectroscopy

In the first instance the **mono TEG-DPP** was characterized by UV-Vis spectroscopy. In Figure 1.65 UV-Vis spectra at different concentration of **mono TEG-DPP** in AcOEt are reported, to calculate the molar extinction coefficient, ϵ .

The angular coefficient of calibration line (with $R^2=0.996$) obtained at fixed λ (529 nm) gives the value of ϵ , that is $19634 \text{ dm}^2 \text{ mol}^{-1}$.

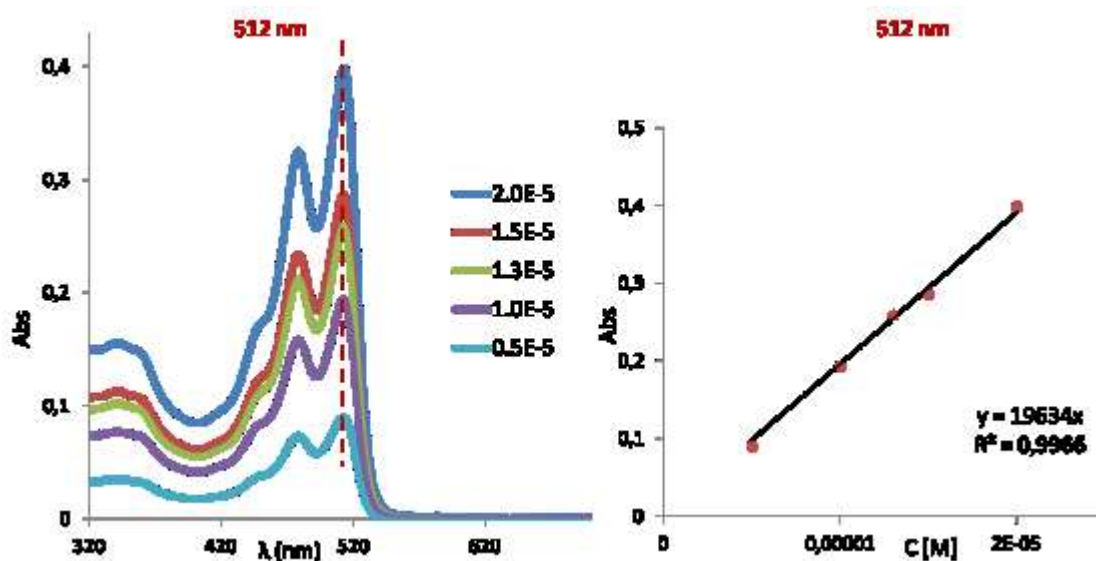


Figure 1.65 UV-Vis spectra in AcOEt for five concentrations of **mono TEG-DPP**.

An important detail is shown in Figure 1.66. As for **TEG-DPP**, the fluorescence of **mono TEG-DPP** is quenched in water, in which it is supposed to have only the polymeric species. This feature could be a consequence of the kind and dimension of aggregated species in solution.

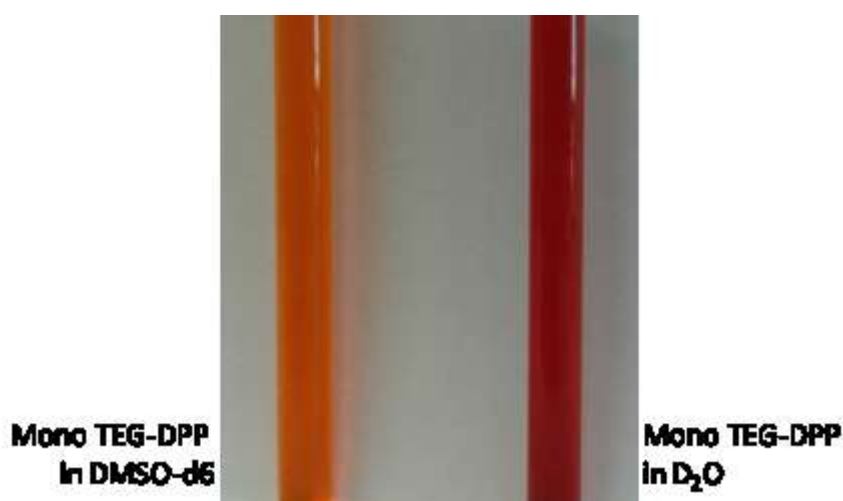


Figure 1.66 Samples of **mono TEG-DPP** respectively in DMSO-d6 and in D₂O.

b) UV-Vis temperature-dependent analysis

UV-Vis temperature-dependent analysis in water

The method described in paragraph 1.8.3 for the characterization of **TEG-DPP** was also used to analyse **mono TEG-DPP** behaviour. Temperature-dependent UV-Vis spectra were recorded for **mono TEG-DPP** in H₂O ($c=8.00 \cdot 10^{-6}$ M) from 363 K to 298 K in steps of 10° C. The arrows in Figure 1.67 indicate spectral changes upon decreasing temperature.

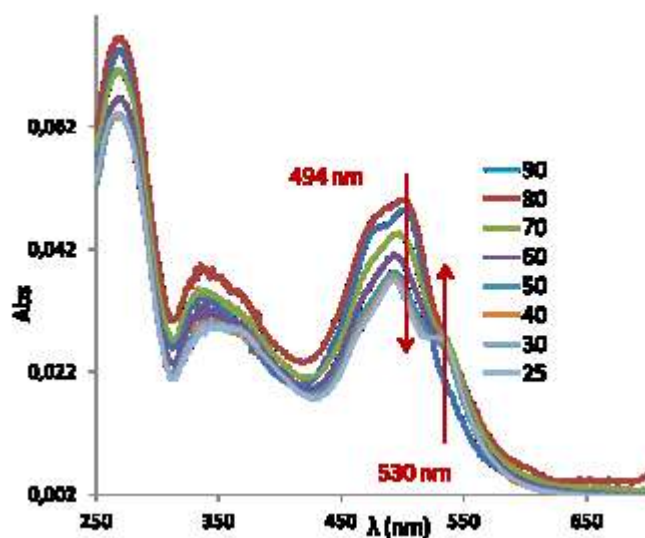


Figure 1.67 Temperature-depend UV-Vis spectra of **mono TEG-DPP** ($c=8.0 \cdot 10^{-6}$ M in H₂O).

The spectra in Figure 1.67 show two maximum transitions for **mono TEG-DPP** in water: the first transition, at 494 nm, and the second transition, at 530 nm.

In Figure 1.68 it is reported the experimental data of **mono TEG-DPP** ($c=8 \cdot 10^{-6}$ M, in H₂O) obtained in temperature-dependent experiment at a wavelength of 530 nm.

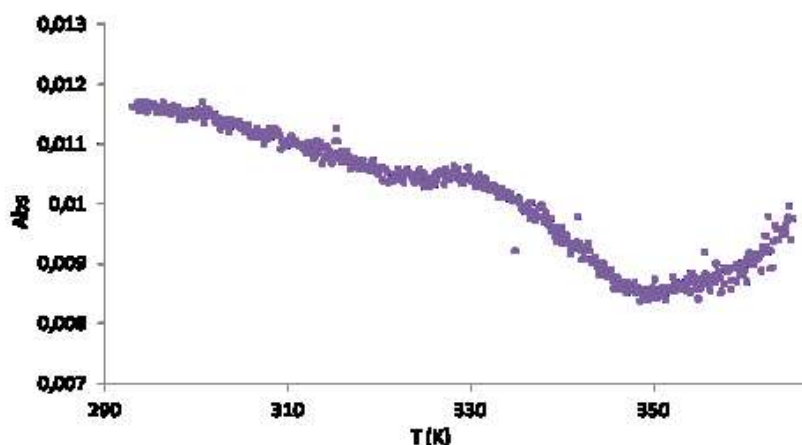


Figure 1.68 UV-Vis analysis at 530 nm for the solution $8.0 \cdot 10^{-6}$ M in H₂O of **mono TEG-DPP**.

This study reveals a complex mechanism of polymerization that we cannot associate neither to the isodesmic model nor to a cooperative model. This phenomenon appears clear observing a

concentrated solution prepared for $^1\text{H-NMR}$ analysis: when the NMR tube is heated a red ribbon structure begins to form, as shown in Figure 1.69. The phase separation of **mono TEG-DPP** with water could represent the formation of a new supramolecular aggregate. The study of this phenomenon (the precipitation of a solid state at high temperature) is in progress.

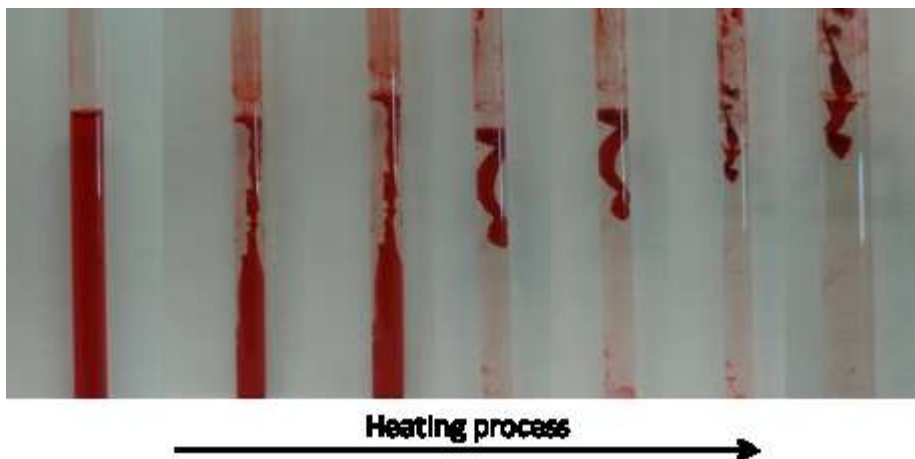


Figure 1.69 Phenomenon observed for a solution of **mono TEG-DPP** ($c = 3.5 \cdot 10^{-3}$ M, in H_2O) during the heating process.

UV-Vis temperature-dependent analysis in water and DMSO

To better understand **mono TEG-DPP** supramolecular organization, the same approach, described for the characterization of **TEG-DPP**, was used. The UV-Vis instrument was set up at 363 K and small aliquots of DMSO (50 μL at time) were added to the sample. The spectrum after every addition was recorded and significant change in its features was observed. The spectrum recorded for **mono TEG-DPP** at 363 K, with the 9 % of DMSO in H_2O , shows an important variation in its order, as displayed in Figure 1.70.

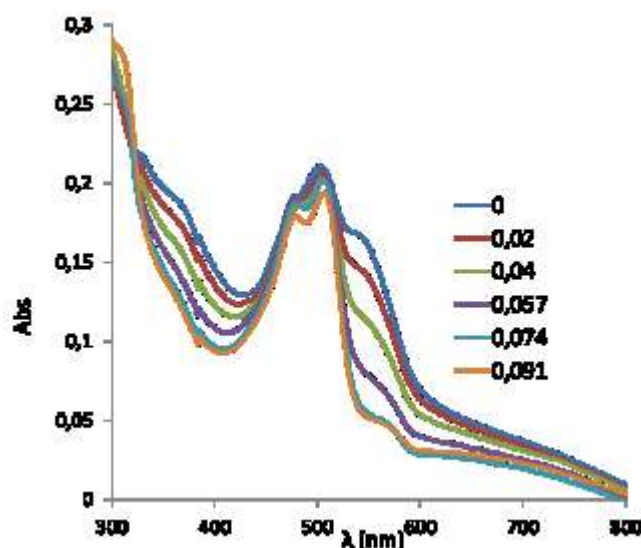


Figure 1.70 UV-Vis spectra at 363 K and with different concentrations of DMSO.

The self-assembly mechanism was studied recording spectra for **mono TEG-DPP** in H₂O/9 % DMSO ($c=1.6 \cdot 10^{-5}$ M) between 363 K and 293 K in steps of 5° C. The arrows in Figure 1.71 indicate spectral changes upon decreasing temperature.

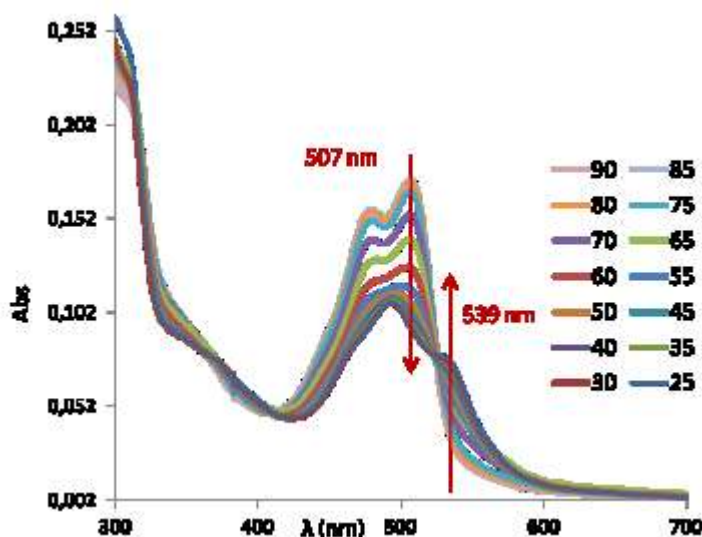


Figure 1.71 Temperature-dependent UV-Vis spectra of **mono TEG-DPP** ($c= 1.6 \cdot 10^{-5}$ M in H₂O/9 % DMSO).

The spectral changes, observed in Figure 1.72, were investigated and temperature-dependent experiments were conducted at the wavelengths of 539 nm and 507 nm, for three different concentrations: $1.5 \cdot 10^{-5}$ M, $1.25 \cdot 10^{-5}$ M and $1.0 \cdot 10^{-5}$ M. The solutions were slowly cooled automatically (from 365 K to 295 K), at a cooling rate of about 0.6 K min^{-1} and the values of absorbance were recorded in steps of 5 seconds.

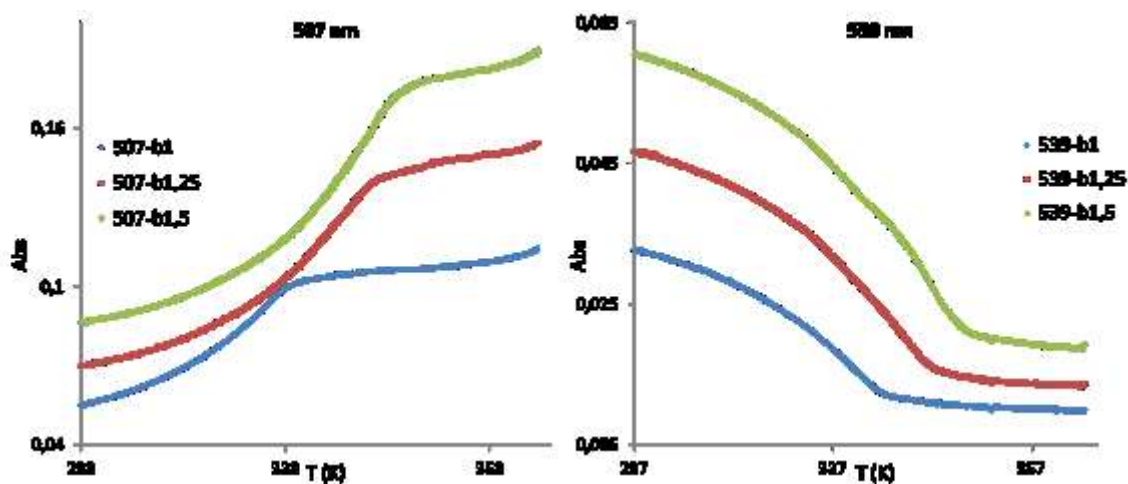


Figure 1.72 UV-Vis spectra recorded for **mono TEG-DPP** at 507 nm (on the left) and at 539 nm (on the right).

The fitting data, reported in Figure 1.73, shows as the cooperative model better describes the supramolecular polymerization of **mono TEG-DPP**. The fitting was conducted with Origin[®] Software, using the Van der Schoot model described in Appendix A.

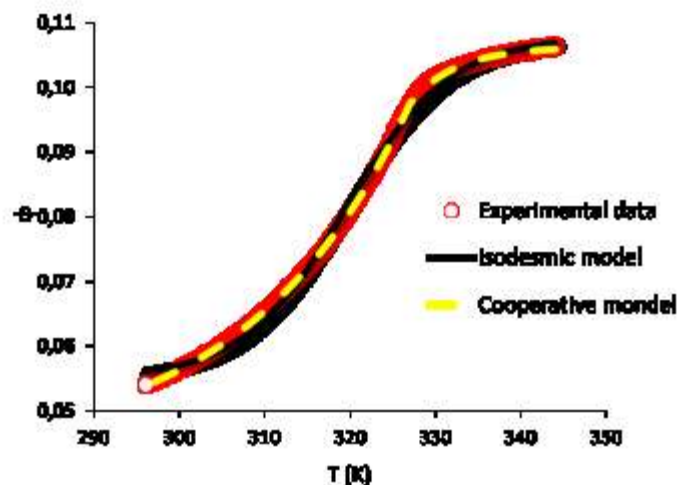


Figure 1.73 Experimental data fit following the cooperative and the isodesmic model.

As shown in Figure 1.73 the cooperative model involves a cooperative chain growth (elongation) that can only take place after that an initial critical-size of aggregated species is formed (nucleation). Once these species overcome an initial energetic barrier the polymer chains drastically develop.

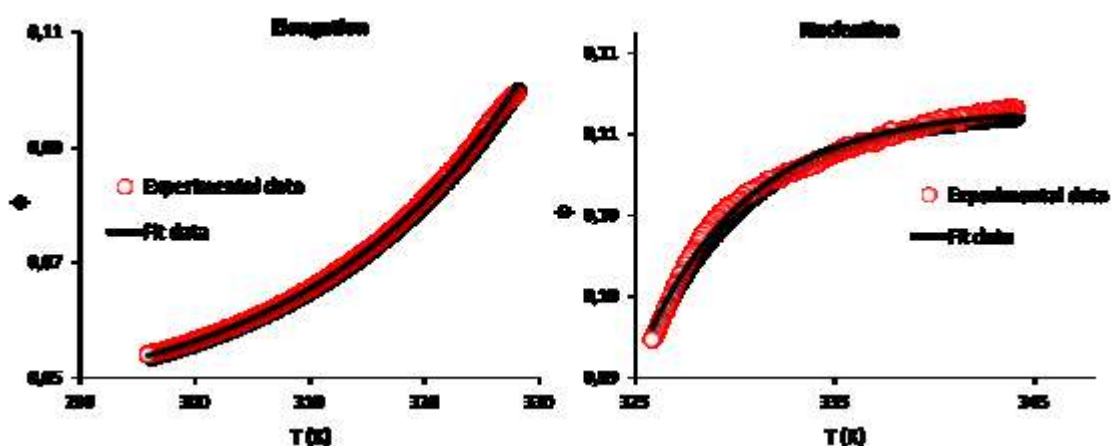


Figure 1.74 Fit of the experimental data for the elongation and the nucleation regimes.

In Figure 1.74 the elongation and the nucleation regimes are displayed for $1.0 \cdot 10^{-5}$ M solution at 507 nm.

The experimental data for temperatures below the elongation temperature were fitted using Equation 7, described in Appendix A, paragraph A1.2. For a concentration of $1.0 \cdot 10^{-5}$ M the enthalpy released (ΔH_e) during the self-assembly of **mono TEG-DPP** in the elongation process is -47.52 ± 0.12 kJ mol⁻¹ and the elongation temperature (T_e) is 330.00 ± 0.01 K.

The dimensionless activation constant, K_{NE} , was obtained using Equation 8 at page 99, in which the thermodynamic parameters (ΔH_e and ϕ_{SAT}) optimised in the elongation fitting were introduced. Fitting the experimental data for temperatures above the T_e , K_{NE} value is $(3.0 \pm 0.1) \cdot 10^{-3}$.^{52a}

In Figure 1.75 an example of the fitting of ϕ against T/T_e in the framework of the nucleation and elongation model for the solution $1.25 \cdot 10^{-5}$ M in H₂O/9 % DMSO at 507 nm is reported.

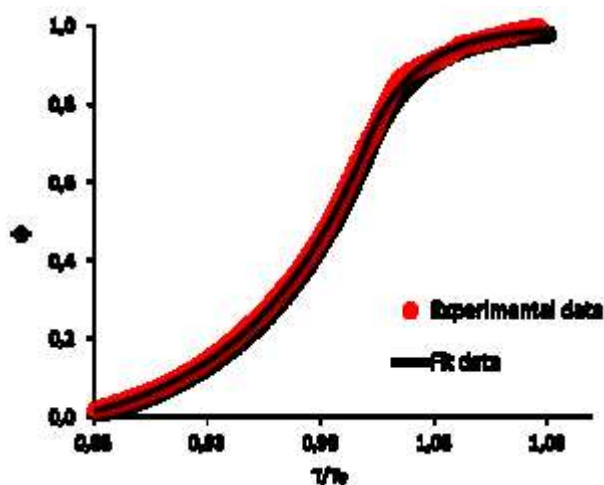


Figure 1.75 UV-Vis at 507 nm for the solution $1.25 \cdot 10^{-5}$ M of mono TEG-DPP in H₂O/9 % DMSO.

In Figure 1.76 the DP_n for all temperatures is shown. The number-averaged degree of polymerization in elongation regime is described by Equation 9 at page 99.

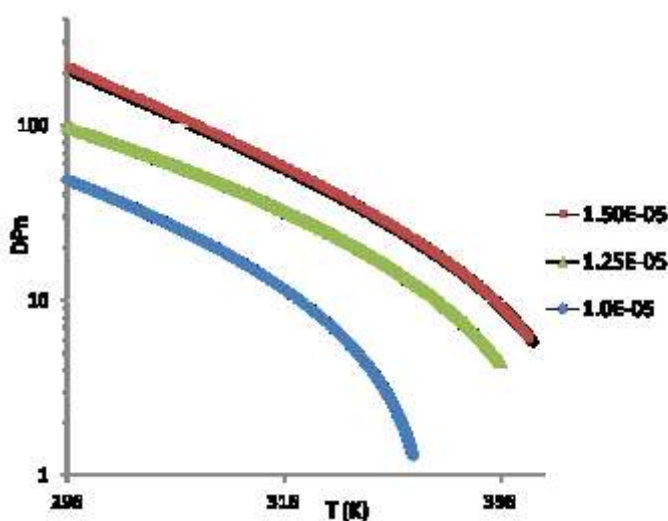


Figure 1.76 DP_n of mono TEG-DPP in H₂O/9 % DMSO.

The thermodynamic parameters K_{NE} , T_e , ΔH_e and ϕ_{SAT} obtained from the fitting of the experimental data are presented in the Table 1.6.

Concentration [M]	Elongation				Nucleation	
	ΔH [kJ·mol ⁻¹]	T_e	ϕ_{sat}	DP_n (298K)	K_{NE}	$DP_n(T_e)$
1.50E-05	-55.34 ± 0.01	339.79 ± 0.01	1.000 ± 0.001	190.66	$(5.0 \pm 0.1) \cdot 10^{-3}$	5.60
1.25E-05	-50.93 ± 0.01	335.97 ± 0.01	1.100 ± 0.001	88.63	$(7.0 \pm 0.18) \cdot 10^{-3}$	5.15
1.00E-05	-47.52 ± 0.12	330.00 ± 0.01	1.000 ± 0.001	77.3	$(3.0 \pm 0.1) \cdot 10^{-3}$	6,86

Table 1.6 Thermodynamic parameters obtained from the fit of experimental data at 507 nm.

Figure 1.77 reports the van't Hoff equation: a linear relationship, between the logarithm of concentration versus the reciprocal temperature, for the three solutions in analysis, is observed. The enthalpy released was calculated by multiplying the slope by the gas constant: $\Delta H = 45.97 \cdot 8.31 = 38.22 \text{ kJ mol}^{-1}$ that is in agreement to the fitting procedure.

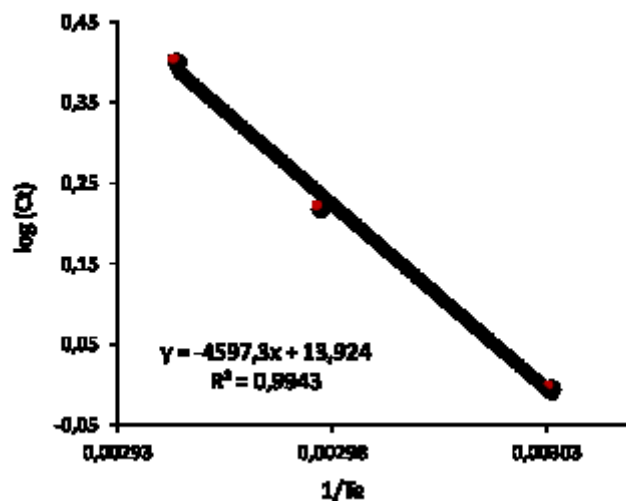


Figure 1.77 Van't Hoff plot.

The experimental data, obtained at 539 nm, were analysed to complete the UV-Vis characterization of **mono TEG-DPP**, as depicted in Figure 1.78.

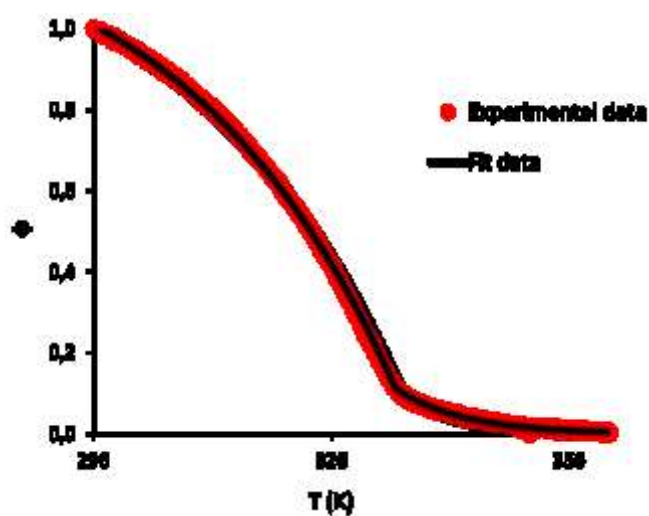


Figure 1.78 Fit of the experimental data for the elongation and the nucleation regimes.

In Figure 1.79 the elongation and the nucleation steps of solution $1.0 \cdot 10^{-5} \text{ M}$ at 539 nm are shown. The enthalpy released during the self-assembly of **mono TEG-DPP** and the elongation temperature were calculated, according to Equation 7 at page 98. The two values are respectively: $\Delta H_e = -35.4 \pm 0.2 \text{ kJ mol}^{-1}$ and $T_e = 334.6 \pm 0.2 \text{ K}$. The value of K_{NE} for this sample is $4.3 \pm 0.1 \cdot 10^{-3}$.

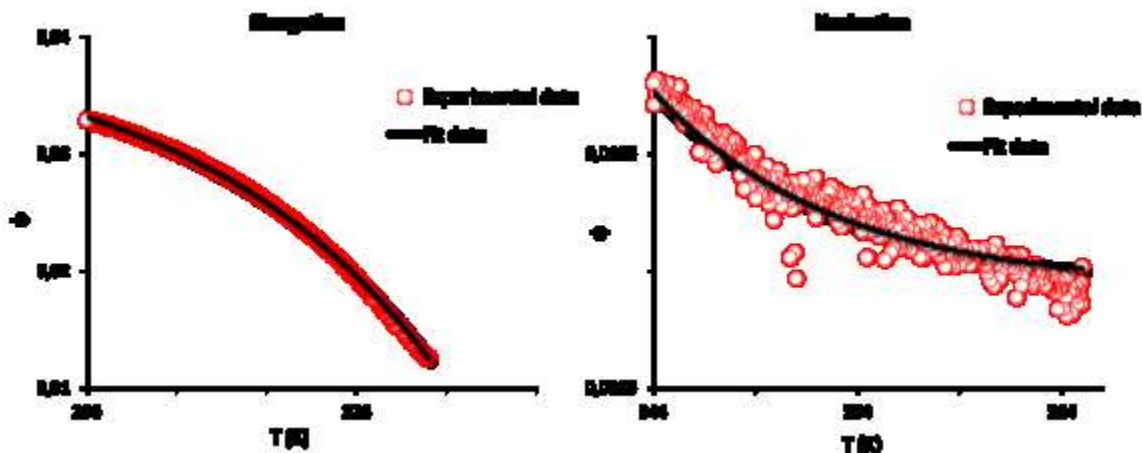


Figure 1.79 Fit of the experimental data for the elongation and the nucleation regimes.

DP_n was calculated according to Equation 9 at page 99 and it is shown in Figure 1.80.

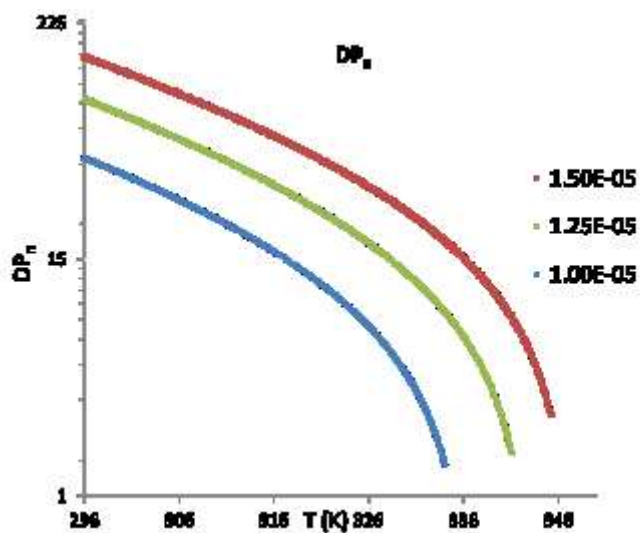


Figure 1.80 DP_n of mono TEG-DPP in H₂O/9 % DMSO.

The thermodynamic parameters K_{NE} , T_e , ΔH_e and ϕ_{SAT} obtained by the fitting of the experimental data for the three concentrations are presented in the Table 1.7. The values obtained at 539 nm are comparable at those obtained at 507 nm.

Concentration [M]	Elongation				Nucleation	
	ΔH [kJ·mol ⁻¹]	T_e	ϕ_{sat}	DP_n (298K)	K_{NE}	$DP_n(T_e)$
1.50E-05	-34.43 ± 0.12	345,49 ± 0.02	1,21 ± 0.02	141.37	$(1.0 \pm 0.05) \cdot 10^{-3}$	9,81
1.25E-05	-35.40 ± 0.20	341,74 ± 0.03	1,24 ± 0.03	86.88	$(2.2 \pm 0.07) \cdot 10^{-5}$	7,68
1.00E-05	-35.49 ± 0.23	334,68 ± 0.23	1,33 ± 0.01	44.07	$(4.3 \pm 0.12) \cdot 10^{-3}$	6,14

Table 1.7 Thermodynamic parameters obtained from the fit of experimental data at 539 nm.

In the Figure 1.81 van't Hoff equation was verified. The enthalpy released was calculated by multiplying the slope by the gas constant: $\Delta H = 42.385 \cdot 8.31447 = 35.24 \text{ J mol}^{-1}$. The theoretical value is comparable with the values obtained by Van der Schoot model.

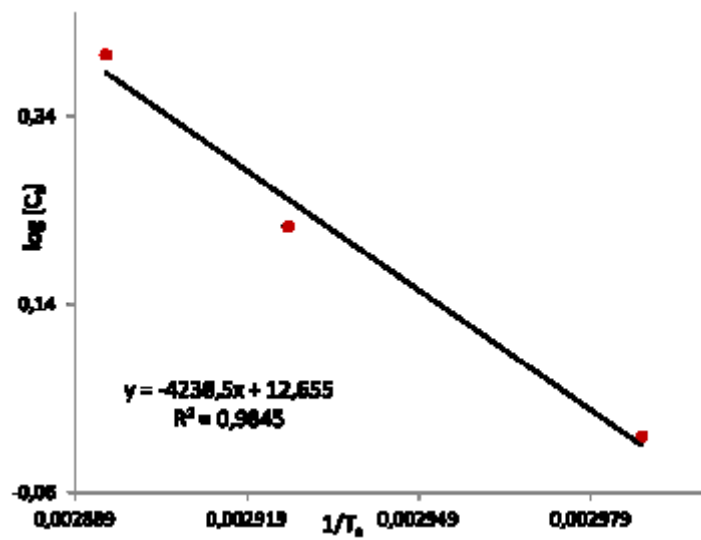


Figure 1.81 Van't Hoff plot.

1.8.6 Mono TEG-DPP: supramolecular characterization in the solid state

a) Differential Scanning Calorimetry Analysis

DSC was conducted to investigate a possible mesomorphic phase for **mono TEG-DPP**, as already studied for **TEG-DPP**. Analysis was made on 3.00 mg of sample, from 0° C to 320° C.

The procedure considered three cycles of heating and three cycles of cooling at the speed of 10° C at minute. The peaks in the spectra show an irreversible behaviour of the system: during the first heating three different peaks were present, whereas it was not possible to record any peaks during the cooling process. Probably the system collapses before of the melting point; this hypothesis will be confirmed by POM observation.

b) Polarised Optical Microscopy Analysis

POM observation shows a stable supramolecular organization even at high temperature. At 76° C (Figure 1.82, **(a)**) as well as at 182° C the system has a viscous and birefringent aspect (Figure 1.82 **(b)**). These features allow to hypothesize a mesomorphic phase.

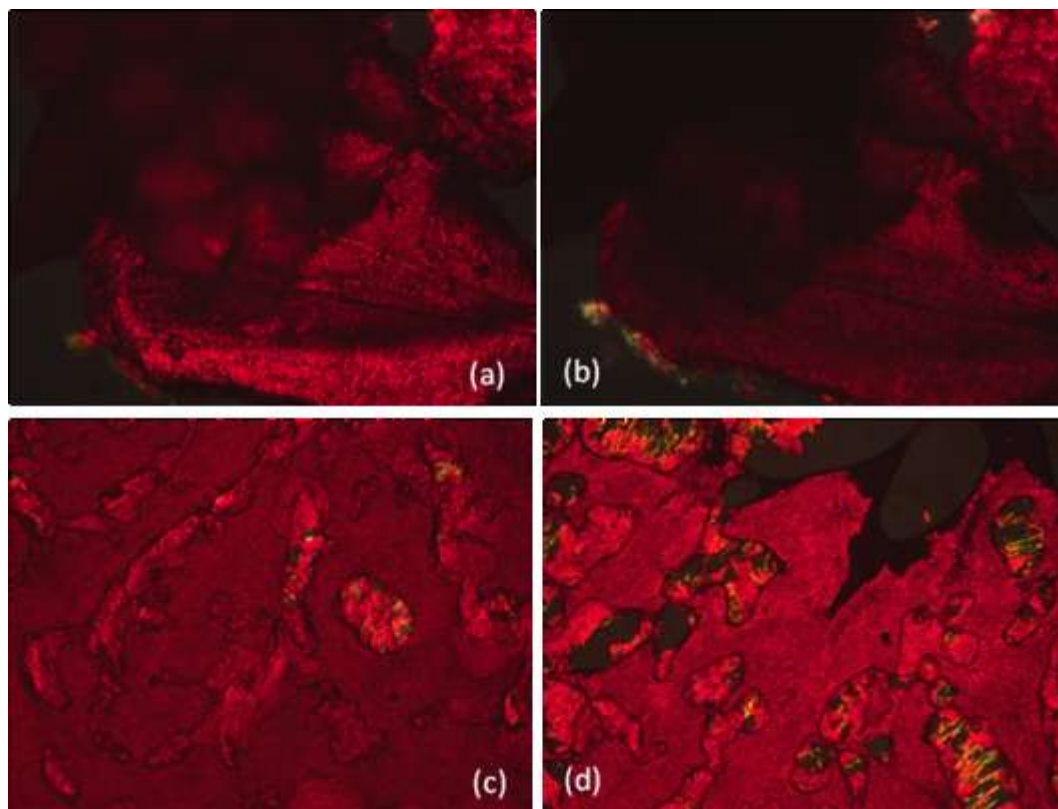


Figure 1.82 POM observations: **(a)** at 76° C; **(b)** at 182° C; **(c)** at 273° C and **(d)** at 289° C.

At 273° C (Figure 1.82, **(c)**) a sort of transition can be distinguished: a solid portion floats in a liquid system, while at 289° C the system begins to degrade, as shown in Figure 1.82, **(d)**.

At 291° C the liquid phase is not still reached, furthermore the molecular system collapses, as shown in Figure 1.83. In these conditions the mesomorphic phase can only be supposed.

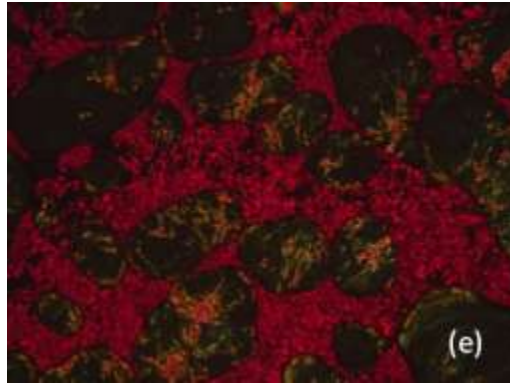


Figure 1.83 POM observation: (e) at 291° C.

c) Atomic Force Microscopy Analysis

As for **TEG-DPP**, AFM was used to describe the morphology of the compound and to better understand the supramolecular organization of **mono TEG-DPP** at the solid state. The sample was deposited using spin-coating technique at room temperature for a concentration of $1.7 \cdot 10^{-3}$ M (0.1 % m/m) in chloroform.

The system presents a thick stratification: the substrate is distributed over the whole silicon area and it is not possible to distinguish the initial surface.

The sample forms some thick multilayer structures that let us image a strong interaction first with the silicon plane and then with single portions of sample. This behaviour is shown in Figure 1.84.

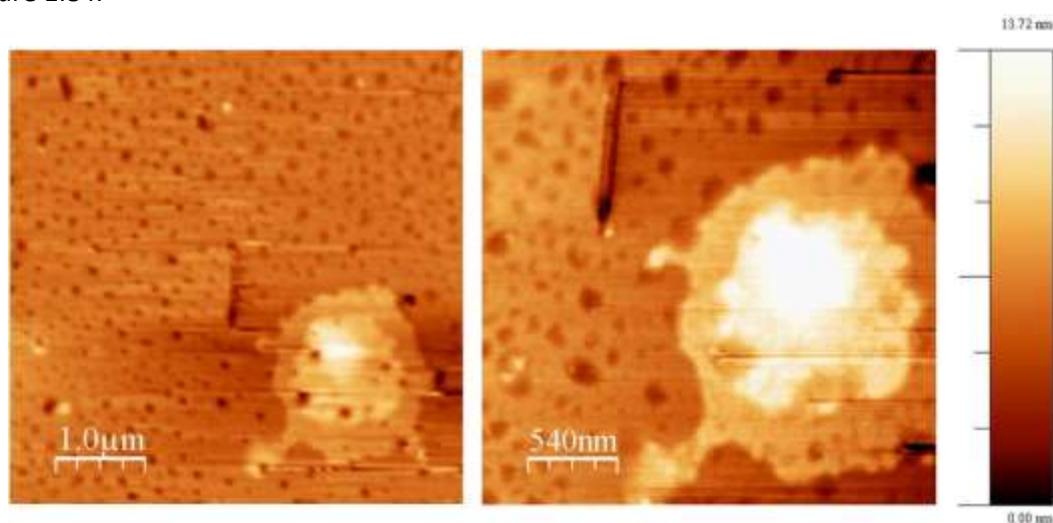


Figure 1.84 Thick multilayer of **mono TEG-DPP**, on the left and particular of multilayer on the right.

The analysis was conducted also with a more diluted solution ($2.0 \cdot 10^{-6}$ M) to evaluate the morphology of the supramolecular organization. However, it was not possible to determine the geometrical structure of the system: for diluted solutions the distribution of the compound on the silicon surface was observed, but no texture could be noticed.

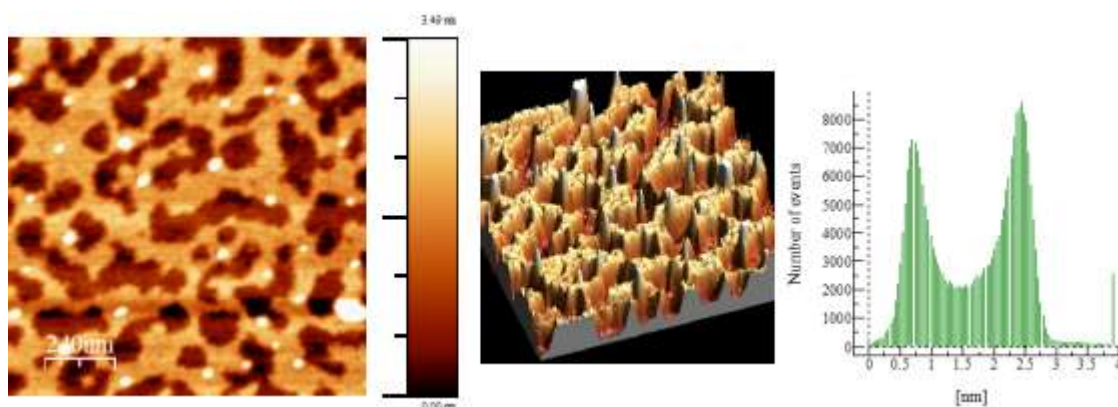


Figure 1.85 AFM observation and covered surface.

Figure 1.85 reports the sample distribution. The covered surface is 56 % , its height about 2 nm and its width measures about 50 nm.

d) Scanning Electron Microscopy Analysis

SEM observation revealed an irregular structure. A thin layer of sample covers the whole surface and small portions of sample, in which molecules seem to aggregate and stratify, can be observed. This result is in agreement with the AFM analysis.

Moreover, the structures present a ribbon texture on the borders; this detail is shown in Figure 1.86.

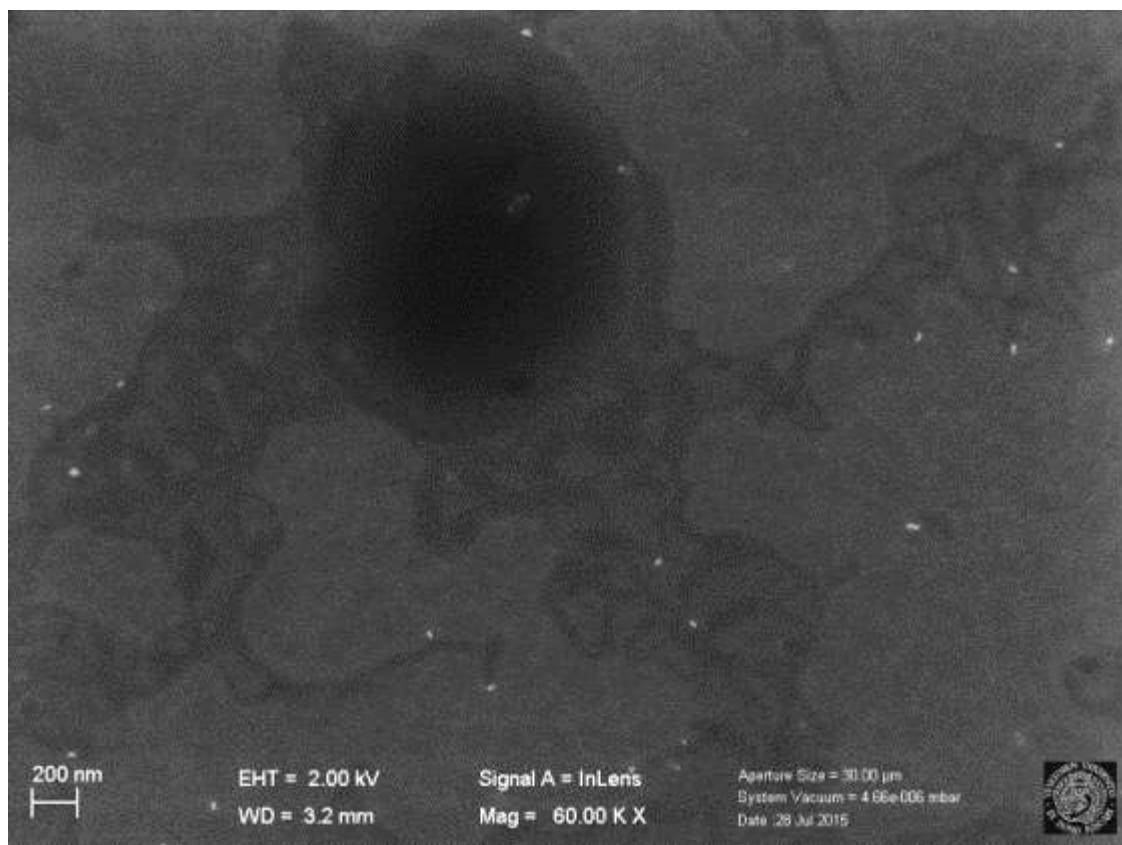


Figure 1.86 Ribbon texture of mono TEG-DPP at SEM.

1.9 Conclusions

In summary in this chapter we have presented two water soluble derivatives of DPP: **TEG-DPP** and **mono TEG-DPP**. TEG chains present in these molecules give a good water solubility. Using hydrogen bonding and π - π stacking interactions, these molecules develop supramolecular polymers able to self-assemble organising themselves in H aggregates. UV-Vis spectroscopy is used to describe the supramolecular polymerization and from a fit, calculated according to a suitable geometrical model, all the thermodynamic parameters have been deduced. Then UV-Vis measurements have been verified through DLS analysis. The structures of the aggregates have been also investigated through $^1\text{H-NMR}$ at different temperatures. In the solid state the two supramolecular organizations have been characterized through AFM and SEM.

The supramolecular polymer of **TEG-DPP** in water has been characterized through UV-Vis spectroscopy. The polymer self-assembles through a cooperative mechanism and the thermodynamic parameters have been calculated according to model proposed by van der Schoot. The average values of ΔH_e and K_{NE} are respectively $-26.14 \pm 0.04 \text{ kJ}\cdot\text{mol}^{-1}$ and $7.3\cdot 10^{-4} \pm 8.00\cdot 10^{-4}$. Van't Hoff plot confirms the values obtained from the fitting. The dimensions of aggregates have been confirmed through DLS analysis. The structure of the aggregate has been studied with $^1\text{H-NMR}$ temperature-dependent analysis for a solution $2.3\cdot 10^{-3} \text{ M}$ in D_2O . The spectra show that increasing temperature the number of signals decreases. Furthermore, at 363 K the signals of the monomeric species together with other species, such as small oligomers or dimmers, were observed.

In order to gain insight in the aggregation process, DMSO has been added at high temperature to promote the monomeric state. UV-Vis experiments show that with the 15 % of DMSO in water, **TEG-DPP** polymerizes through the isodesmic mechanism. From the fitting data carried out for three concentration comprised between $1.5\cdot 10^{-5}$ - $1.0\cdot 10^{-5} \text{ M}$, the values of thermodynamic parameters were obtained: ΔH_e and K_{IS} average values are respectively $-103.66 \pm 0.25 \text{ kJ}\cdot\text{mol}^{-1}$ and $53.25\cdot 10^5$.

$^1\text{H-NMR}$ experiments at 367 K adding aliquots of DMSO have been conducted: the peaks of the monomeric state are observed adding 42 % of DMSO to **TEG-DPP** solution in D_2O

At the solid state, supramolecular aggregates of **TEG-DPP** have been observed through AFM. The analysis reveals a fibrous structure that is confirmed by SEM analysis. Moreover, the presence of a mesomorphic phase can be hypothesized from DSC and confirmed by POM observation. We could not distinguish the geometry of the liquid-crystal phase.

The supramolecular polymer developed by **mono TEG-DPP** has been studied using the same analytical technique used for **TEG-DPP**. In this case, the supramolecular organization in water reveals a complex mechanism of polymerization that it is impossible to associate neither to the isodesmic model nor to a cooperative model. This phenomenon is observed even in $^1\text{H-NMR}$ analysis: heating the NMR tube it is noticed the phase separation between **mono TEG-DPP** and water.

In order to better understand the aggregation process, UV-Vis experiments have been performed adding aliquots of DMSO. With the 9 % of DMSO in water, **mono TEG-DPP** develops a supramolecular polymer through the cooperative mechanism. Van der Schoot nucleation-elongation model has been used to conduct the fitting data and to calculate the

thermodynamic parameters: the average values of ΔH_e and K_{NE} at 539 nm are respectively -35.10 kJ \pm 0.18mol⁻¹ and $2.5\cdot 10^{-3}\pm 8.1\cdot 10^{-5}$, whereas the average values of ΔH_e and K_{NE} at 507 nm measure $51.26 \pm 4.2\cdot 10^{-3}$ and $5\cdot 10^{-3} \pm 0.1\cdot 10^{-3}$.

At the solid state the supramolecular aggregates of **mono TEG-DPP** have been studied through AFM. This analysis reveals a complex structure and a thick stratification that is confirmed by SEM analysis in which ribbon structures can be distinguished. The melting point of the compound is too high to allow its characterization with DSC. The presence of a mesomorphic phase at room temperature can be supposed through POM observation: the substrate has a viscous and birefringent aspect.

1.10 Experimental Section

1.10.1 General

Solvents and reagents were used as purchased. Column chromatography was performed on silica gel MERK 60, 0.04-0.063 mm/230-400 mesh and thin layer chromatography (TLC) was conducted on Alugram silica gel UV₂₅₄ (Macherey-Nagel). Solvents for UV-Vis absorption, AFM studies were of spectroscopic grade and were used as received.

¹H-NMR spectra were recorded on a Varian Unity 400 MHz spectrometer using TMS (δ :0 ppm), CDCl₃ (δ :7.26 ppm), (CD₃)₂SO (δ :2.55 ppm) and CD₂Cl₂ (δ :5.3 ppm) as internal standards. Coupling constants (J) were denoted in Hz and chemical shifts (δ) in ppm. Multiplicities were denoted as follows: s= singolet, d= doublet, m= multiplet.

UV-Vis absorption spectra were recorded on a Perkin Elmer lambda 35 UV/Vis spectrometer with Perkin Elmer PTP 6 Peltier temperature programme.

POM studies were conducted through an Axio Scope Zeiss with THMS600 based on Linkam 93 system. Photos are taken with a AxioCam MRc (Zeiss) and visualised with Axio Vision Rel 4.8.

DSC analysis were recorded on a METTLER DSC 822 or METTLER DSC 1. The instrument is calibrate with a sample of indium ($F_{in} = 156.6^\circ \text{C}$, $\Delta_f(\text{In}) = 28.45 \text{ J/g}$) and zinc ($F_{zn} = 419.6^\circ \text{C}$, $\Delta_f(\text{Zn}) = 28.45 \text{ J/g}$). Samples were analysed in aluminium capsules (40 μl) under nitrogen atmosphere. Samples were analysed with a cooling and heating speed of 10°C/min . Transition temperatures were extrapolated by onset values and enthalpies were calculates by the area of peaks.

Elementar Analysis was conducted in collaboration with the Swiss Federal Institute of Technology of Zurich.

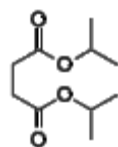
Mass spectra were carried out with a *Finnigan LCQ* ion trap mass *spectrometer* equipped with an *electrospray ionization (ESI)* source.

AFM experiments were performed on an Agilent Technologies 5500 scanning probe microscope, operating in acoustic AC AFM mode (tapping mode) with a silicon Asylum Research high frequency cantilever displaying a resonance frequency of 305 kHz. The samples for AFM observations were prepared by depositing several drops of the onto the silicon surface and after excess solution was removed with spin coater.

DLS measurements were recorded with a standard Nicomp 380, equipped with a 12 mW laser diode and PMT detector with an optical fiber set to 90° . Samples were introduced with drop-in cells.

1.10.2 Synthetic procedures

Synthesis of diisopropyl succinate, 1

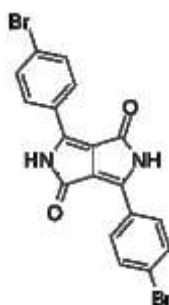


1

A mixture of succinic acid (30 g, 254.04 mmol), isopropyl alcohol (57 mL, 745.45 mmol), and concentrated sulphuric acid (1 mL, 18.75 mmol) in chlorobenzene (120 mL) was refluxed for 12 hours. It was then poured into excess of water, the chlorobenzene layer separated and washed successively with water. The organic phase was washed with brine and dried with MgSO_4 , the solvent was evaporated to give di-iso-propyl succinate (16 g, yield: 30 %).

^1H NMR (400 MHz, CDCl_3) δ (ppm): 5.08-4.90 (m, 2H, OCH), 2.56 (s, 4H, CH_2), 1.23 (d, $J = 6.2$ Hz, 12H, CH_3). PM ($\text{C}_{10}\text{H}_{18}\text{O}_4$): 202,25 u.

Synthesis of 3,6-bis(4-bromophenyl)pyrrolo[3,4-c]pyrrole-1,4(2H,5H)-dione, 2, BrDPP



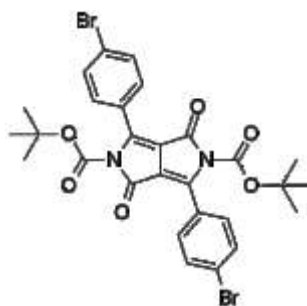
2

BrDPP

Under argon atmosphere sodium (2.9 g, 126.33 mmol), a spatula tip anhydrous FeCl_3 and tert-amylalcohol (60mL) were heated to reflux until all the sodium had reacted. 4-bromobenzonitrile (10 g, 54.93 mmol) were added in one portion. Then di-iso-propyl succinate (5.55 g, 27.46 mmol) was added over 7 hours with a syringe pump. Then the mixture was heated to reflux for a night. The mixture was added to a solution of water (100 mL) and acetic acid (7 mL). The red precipitate was filtered and washed with water and boiling methanol. This procedure was repeated until the filtrate was clear. The red solid was dried in vacuum (7 g, yield: 57 %).

^1H NMR (400 MHz, $(\text{CD}_3)_2\text{SO}$) δ (ppm): 8.40 (d, $J = 8.7$ Hz, 4H, H_{arom}), 7.82 (d, $J = 8.6$ Hz, 4H, H_{arom}). PM ($\text{C}_{18}\text{H}_{10}\text{Br}_2\text{N}_2\text{O}_2$): 446,09 u.

Synthesis of di-tert-butyl 3,6-bis(4-bromophenyl)-1,4-dioxopyrrolo[3,4-c]pyrrole-2,5(1H,4H)-dicarboxylate, 3, BrDPP-Boc



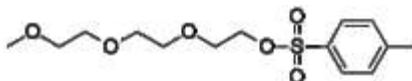
3

BrDPP-Boc

Compound **2** (2.5 g, 5.60 mmol) and DMAP (0.068 g, 0.56 mmol) were dissolved in dry THF (240 mL). After an hour di tert-butyl carbonate (4.24 mL, 18.49 mmol) was added. The mixture was stirred for a night at room temperature and then the solvent was evaporated. The orange solid was extracted with DCM. The combined extracts were dried over anhydrous MgSO_4 and evaporated. The product did not need any other purification (orange solid, 3.5 g, 97 %).

^1H NMR (400 MHz, CDCl_3) δ (ppm): 7.61 (m, 8H, H_{arom}), (s, 18H, $\text{C}(\text{CH}_3)_6$). PM ($\text{C}_{28}\text{H}_{26}\text{Br}_2\text{N}_2\text{O}_6$): 646,32 u.

Synthesis of 2-(2-(2-methoxyethoxy)ethoxy)ethyl 4-methylbenzenesulfonate, 4, Tosyl-TEG



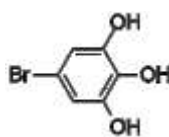
4

Tosyl-TEG

Triethylene glycol monomethyl ether (3.0 mL, 19.12 mmol) and p-toluenesulfonyl chloride (3.8 g, 21.04 mmol) were dissolved in diethyl ether (9.13 mL). Freshly ground KOH (4.18 g, 74.56 mmol) was added in several portions to the ice-cooled solution, keeping temperature below 5° C. After three hours of reaction ice and water were added, the organic phase was extracted three times with diethyl ether. The combined organic fractions were dried on MgSO_4 , filtered and the solvent was evaporated under reduced pressure to give the desired compound as a colorless oil (5.19 g, yield: 85 %).

^1H NMR (400 MHz, CDCl_3) δ (ppm): 7.80 (d, $J = 8.1$ Hz, 2H, H_{arom}), 7.34 (d, $J = 8.0$ Hz, 2H, H_{arom}), 4.26- 4.07 (t, $J = 6.2$, 2H, OCH_2), 3.70 (t, $J = 6.0$ Hz, 2H, OCH_2CH_2), 3.64-3.11 (m, 6H, H_{TEG}), 3.53 (t, $J = 50.1$ Hz, 2H, H_{TEG}), 3.38 (s, 3H OCH_3), 2.45 (s, 3H, CH_3Ph). PM ($\text{C}_{14}\text{H}_{22}\text{O}_6\text{S}$): 318,39 u.

Synthesis of 5-bromo-1,2,3-triol, **5**

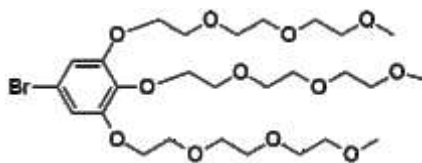


5

A solution of BBr_3 (35.41 mL) was added dropwise to a solution of 5-bromo-1,2,3-trimethoxybenzene (2.5 g, 10.11 mmol) in dry DCM (15 mL) at -84°C . The reaction mixture was allowed to warm to room temperature and stirred for 16 hours under argon. The reaction mixture was allowed to warm to room temperature and stirred for 12 hours. After ice-cold water was added. The mixture was stirred at room temperature for 2 hours and then extracted with ethyl acetate. The organic solution was dried over anhydrous MgSO_4 , filtered, and evaporated under reduced pressure to give compound **9** as a white solid (1.96 g, yield: 95 %).

^1H NMR (400 MHz, $(\text{CD}_3)_2\text{SO}$), δ (ppm): 9.26 (s, 2H, $(\text{OH})_2$), 8.29 (s, 1H, OH), 6.39 (s, 2H, H_{arom}).
PM ($\text{C}_6\text{H}_5\text{BrO}_3$): 205,01 u.

Synthesis of 5-bromo-1,2,3-tris(2-(2-(2-methoxyethoxy)ethoxy)ethoxy)benzene, **6**

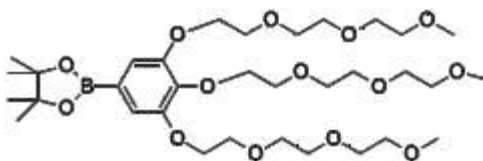


6

A solution of 5-bromo-1,2,3-triol (0.3 g, 1.46 mmol), K_2CO_3 (1.40 g, 10.74 mmol) in dry DMF (4.0 mL) was stirred for 45 minutes at room temperature under argon. A solution of **8** (1.63 g, 5.12 mmol) in dry DMF (2 mL) was added. The reaction mixture was heated at reflux over night. The reaction mixture was diluted with water and the solution was extracted with AcOEt. The organic phase was washed with brine, dried with MgSO_4 and evaporated under reduced pressure. The product **8** was obtained as a colourless oil (0.750 g, yield: 79 %).

^1H NMR (400 MHz, CDCl_3), δ (ppm): 6.72 (s, 2H, H_{arom}), 4.11 (m, 6H, OCH_2), 3.82 (t, $J = 10.0$ Hz, 4H, OCH_2CH_2), 3.76 (t, $J = 10$ Hz, 2H, OCH_2CH_2), 3.72-3.68 (m, 6H, H_{TEG}), 3.66-3.61 (m, 12H, H_{TEG}), 3.54-3.52 (m, 6H, H_{TEG}), 3.36 (s, 9H, $\text{O}(\text{CH}_3)_3$). ^{13}C NMR (100 MHz, CDCl_3), δ (ppm): 152.88, 137.44, 115.33, 111.05, 71.98, 71.59, 70.50, 70.34, 70.24, 70.17, 69.28, 68.75, 58.67.
PM ($\text{C}_{27}\text{H}_{47}\text{BrO}_{12}$): 643,56 u.

Synthesis of 4,4,5,5-tetramethyl-2-(3,4,5-tris(2-(2-methoxyethoxy)ethoxy)ethoxy)phenyl)-1,3,2-dioxaborolane, 7, TEG pinacol boronic ester



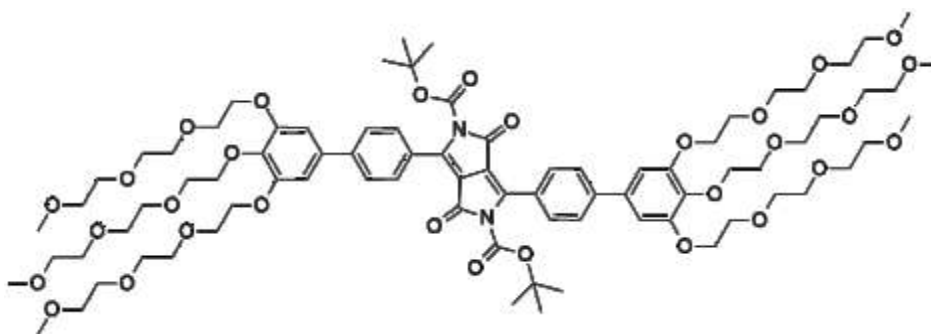
7

TEG pinacol boronic ester

Compound **10** (1.5 g, 2.33 mmol), dichlorobis(triphenylphosphine)palladium (0.054 g, 0.076 mmol), bis(pinacolato)diboron (0.887 g, 3.49 mmol), and potassium acetate (0.686 g, 6.99 mmol) were flushed with argon and charged with a mixture of degassed dioxane (29.0 mL). The mixture was heated at 80° C for 12 hrs, cooled, and then extracted with AcOEt. The combined extracts were dried over anhydrous MgSO₄ and evaporated. The crude product was purified by column chromatography (9AcOEt:1MeOH) to give compound **11** as a colourless oil (0.980 g, yield: 61 %).

¹H NMR (400 MHz, CDCl₃), δ (ppm): 7.01 (s, 2H, H_{arom}), 4.194.15 (m, 6H, OCH₂), 3.84 (t, *J* = 10.0 Hz, 4H, OCH₂CH₂), 3.78 (t, *J* = 10.4 Hz, 2H, OCH₂CH₂), 3.74-3.70 (m, 6H, H_{TEG}), 3.67-3.62 (m, 12H, H_{TEG}), 3.55-3.53 (m, 6H, H_{TEG}), 3.36 (s, 9H,), 1.34 (s, 12H, O(CH₃)₃). ¹³C NMR (100 MHz, CDCl₃) δ 151.99, 141.39, 113.95, 108.09, 83.52, 71.95, 71.51, 70.50, 70.36, 69.28, 68.54, 68.43, 59.07, 24.62. PM (C₃₃H₅₉BO₁₄): 690,62 u.

Synthesis of di-tert-butyl 1,4-dioxo-3,6-bis(3',4',5'-tris(2-(2-(2-methoxyethoxy)ethoxy)ethoxy)-[1,1'-biphenyl]-4-yl)pyrrolo[3,4-c]pyrrole-2,5(1H,4H)-dicarboxylate, 8



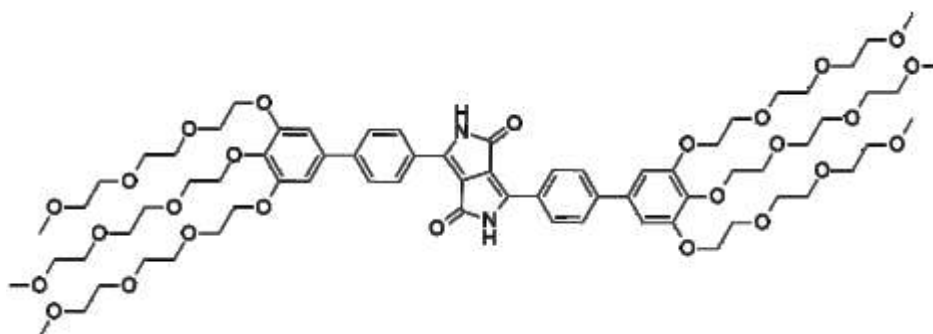
8

To a suspension of degassed toluene (61.0 mL) and K₂CO₃ (3.50 g of a 2 M aqueous solution) were added, under argon atmosphere, Br DPP-Boc (0.250 g, 0.38 mmol), product **11** (0.598 g, 0.96 mmol) and a catalytic amount (1 % m/m) of Pd(PPh₃)₄. The resulting mixture was heated at 80° C for 27 hours, cooled and then extracted with AcOEt. The combined extracts were

dried over anhydrous MgSO_4 and evaporated under reduced pressure. The crude product **10** was not purified. It was obtained as a violet solid (0.532 g, crude).

^1H NMR (400 MHz, CDCl_3), δ (ppm): 7.82 (d, $J = 8.4$ Hz, 4H, H_{arom}), 7.63 (d, $J = 4.8$ Hz, 4H, H_{arom}), 6.86 (s, 4H, H_{arom}), 4.25-4.19 (m, 12H, H_{TEG}), 3.88 (t, $J = 9.6$ Hz, 8H, H_{TEG}), 3.82 (t, $J = 10$ Hz, 4H, H_{TEG}), 3.76-3.63 (m, 36H, H_{TEG}), 3.36-3.53 (s, 12H, H_{TEG}), 3.37-3.35 (m, 18H, $\text{O}(\text{CH}_3)_6$), 1.25 (s, 18H, $\text{C}(\text{CH}_3)_6$). PM ($\text{C}_{82}\text{H}_{120}\text{N}_2\text{O}_{30}$): 1613,83 u.

Synthesis of 3,6-bis(3',4',5'-tris(2-(2-(2-methoxyethoxy)ethoxy)ethoxy)-[1,1'-biphenyl]-4-yl)pyrrolo[3,4-c]pyrrole-1,4(2H,5H)-dione, **9**, TEG-DPP

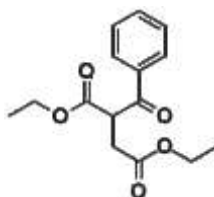


9
TEG-DPP

A solution of compound **14** (0.532 g, 0.347 mmol) in DCM (32 mL) was stirred at room temperature. TFA was added (1.6 mL). The mixture was stirred for one hour, thus it was evaporated under reduced pressure. The crude product was purified by column chromatography (8AcOEt:2MeOH). Product **15** was obtained as a violet solid (0.213 g, yield of two steps: 44 %).

^1H NMR (400 MHz, CDCl_3), δ (ppm): 8.55 (s, 2H, H_{arom}), 8.25 (d, $J = 8.2$ Hz, 4H, H_{arom}), 7.64 (d, $J = 8.3$ Hz, 4H, H_{arom}), 6.82 (s, 4H, H_{arom}), 4.20-4.14 (m, 12H, H_{TEG}), 3.85 (t, $J = 9.6$ Hz, 8H, H_{TEG}), 3.77 (t, $J = 10$ Hz, 4H, H_{TEG}), 3.73-3.60 (m, 36H, H_{TEG}), 3.53-3.51 (m, 12H, H_{TEG}), 3.33 (s, 18H, $\text{O}(\text{CH}_3)_6$). ^{13}C NMR (100 MHz, CDCl_3), δ (ppm): 163.20, 154.22, 151.07, 139.49, 138.72, 133.32, 132.58, 128.86, 127.40, 125.59, 109.12, 109.12, 73.66, 70.24, 70.15, 69.94, 69.52, 57.81, 57.81. PM ($\text{C}_{72}\text{H}_{104}\text{N}_2\text{O}_{26}$): 1413,59 u. MS (ESI) m/z : 1435 ($\text{M}^+ + \text{Na}^+$, 100 %).

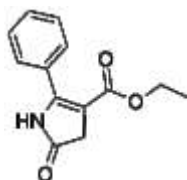
Synthesis of diethyl 2-benzoylsuccinate, **10**



10

A mixture of ethyl-benzoacetate (4.6 mL, 26.56 mmol), acetone (12 mL, 163.43 mmol), DME (8.8 mL, 84.74 mmol), bromoacetic ester (3.2 mL, 29.22 mmol) and K_2CO_3 (4.0 g, 29.22 mmol) was stirred at reflux for 22 hours. After cooling the reaction mixture was diluted with hexane, filtered and the solvent was evaporated to give compound **4** as a brown oil (7.06 g, yield: 95 %). PM ($C_{15}H_{18}O_5$): 278.30u.

Synthesis of ethyl 5-oxo-2-phenyl-4,5-dihydro-1H-pyrrole-3-carboxylate, **11**

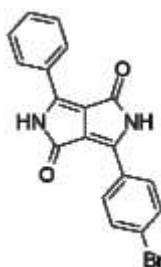


11

A mixture of diethyl benzoylsuccinate (7.06 g, 25.37 mmol), acetic acid (21 mL) and ammonium acetate (19.58 g, 254 mmol) was stirred at reflux for 3 hours. After cooling the reaction mixture was diluted with ice and water. The crude product was first filtered and the dissolved in DCM. The solution was extracted. The organic phase was washed with brine, dried with $MgSO_4$ and evaporated under reduced pressure. The product was obtained as a green solid (3.94 g, yield: 67 %).

1H NMR (400 MHz, $CDCl_3$) δ (ppm): 7.89 (s, 1H, H_{arom}), 7.62-7.57 (m, 2H, H_{arom}), 7.49-7.42 (m, 3H, H_{arom}), 4.12 (q, $J = 7.1$ Hz, 2H, H_{arom}), 3.51 (s, 2H, CH_2), 1.19 (t, $J = 7.1$ Hz, 3H, CH_3). ^{13}C NMR (100 MHz, $CDCl_3$) δ (ppm): 163.3, 151.4, 130.8, 129.5, 128.8, 128.4, 104.6, 60.2, 38.9, 14.3. PM ($C_{13}H_{13}NO_3$): 231.25 u. MS (EI, 70 eV) m/z : 231 (M^+ , 39); 202 (20); 158 (100 %).

Synthesis of 3-(4-bromophenyl)-6-phenylpyrrolo[3,4-c]pyrrole-1,4(2H,5H)-dione, **12**, mono BrDPP



12

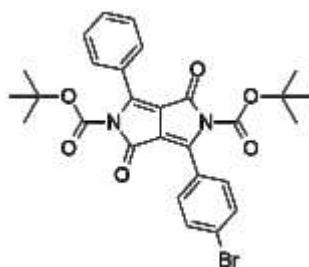
Mono BrDPP

Under argon atmosphere sodium (0.59 g, 25.95 mmol), a spatula tip anhydrous $FeCl_3$ and tert-amylalcohol (56.8 mL, 518.92 mmol) were heated to reflux until all the sodium had reacted. Then the solution was cooled at 60° C and 4-bromobenzonitrile (2.05 g, 11.24 mmol) was added in one portion. The mixture was heated at 95° C and compound **5** (2.0 g, 8.65 mmol)

was added. The reaction was stirred for 14 hours. Then the mixture was cooled at 60° C and it was added to a solution of water (300mL) and HCl (1M, 10mL). The red precipitate was filtered and washed with iPrOH and Et₂O. This procedure was repeated until the filtrate was clear. The red solid was dried in vacuum (2.44 g, resa: 76 %).

¹H NMR (400 MHz, (CD₃)₂SO) δ (ppm): 11.38 (s, 2H, H_{arom}), 8.55-8.44 (m, 2H, H_{arom}), 8.40 (d, *J* = 8.5 Hz, 2H, H_{arom}), 7.81 (d, *J* = 8.5 Hz, 2H, H_{arom}), 7.67-7.52 (m, 3H, H_{arom}). IR (KBr), cm⁻¹: 3450 (m, b), 3137 (w), 1641 (vs), 1602 (s), 1560 (m), 1490 (w), 1454 (m), 1432 (w), 1384 (w), 1323 (w), 1314 (w), 1194 (w), 1141 (w), 1071 (w), 1006 (w), 830 (w), 813 (m), 699 (w), 682 (w), 660 (w), 626 (w), 455 (w). UV-Vis (DCM), λ_{max} (nm): 502, 547. PM (C₁₈H₁₁BrN₂O₂): 367.20 u.

Synthesis of di-tert-butyl 3-(4-bromophenyl)-1,4-dioxo-6-phenylpyrrolo[3,4-c]pyrrole-2,5(1H,4H)-dicarboxylate, 13, mono BrDPP-Boc



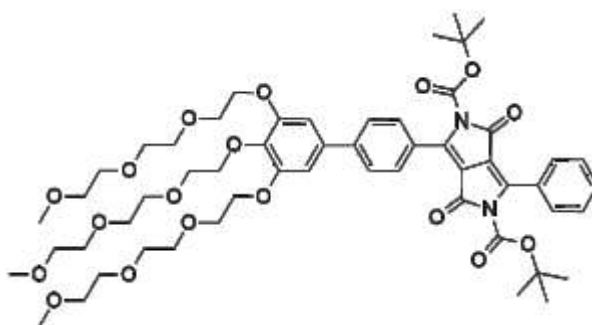
13

Mono BrDPP-Boc

Compound **6** (1.0 g, 2.72 mmol) and DMAP (68mg, 0.56mmol) were dissolved in dry THF (120mL). After an hour di tert-butyl carbonate (1.50 mL, 6.54 mmol) was added. The mixture was stirred for a night at room temperature and then the solvent was evaporated. The orange solid was extracted with DCM. The combined extracts were dried over anhydrous MgSO₄ and evaporated. The product did not need any other purification (orange solid, 1.53 g, yield: 99 %).

¹H NMR (400 MHz, CDCl₃), δ (ppm): 7.77-7.70 (m, 2H, H_{arom}), 7.62 (s, 4H, H_{arom}), 7.54-7.45 (m, 3H, H_{arom}), 1.44 (s, 9H, C(CH₃)₃), 1.40 (s, 9H, C(CH₃)₃). ¹³C NMR (100 MHz, CDCl₃), δ (ppm): 159.5, 159.3, 148.3, 148.1, 146.9, 145.0, 131.8, 130.0, 128.6, 128.6, 128.3, 127.2, 126.2, 112.9, 112.2, 110.3, 85.7, 85.6, 27.7, 27.6. IR (KBr), cm⁻¹: 3434 (w, b), 2980 (w), 2924 (w), 1751 (vs), 1709 (vs), 1622 (s), 1488 (m), 1446 (w), 1395 (w), 1370 (m), 1331 (m), 1289 (vs), 1261 (s), 1208 (m), 1146 (vs), 1104 (s), 1057 (vs), 1006 (m), 895 (vw), 875 (w), 830 (m), 805 (w), 772 (w), 752 (w), 735 (w), 721 (w), 688 (w). UV-Vis (DCM), λ_{max} (nm): 435. PM (C₂₈H₂₇BrN₂O₆): 567.43 u.

Synthesis of di-tert-butyl 1,4-dioxo-3-phenyl-6-(3',4',5'-tris(2-(2-(2-methoxyethoxy)ethoxy)ethoxy)-[1,1'-biphenyl]-4-yl)pyrrolo[3,4-c]pyrrole-2,5(1H,4H)-dicarboxylate, 14

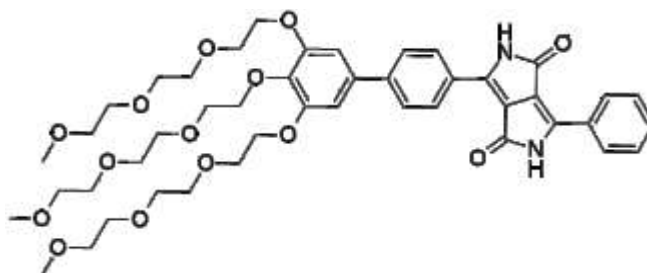


14

To a suspension of degassed toluene (55 mL) and K_2CO_3 (2.82 g of a 2 M aqueous solution) were added, under argon atmosphere, monoBr DPP-Boc (0.220 g, 0.340 mmol), product **11** (0.588 g, 0.850 mmol) and a catalytic amount (1 % m/m) of $Pd(PPh_3)_4$. The resulting mixture was heated at 80° C for 27 hours, cooled and then extracted with AcOEt. The combined extracts were dried over anhydrous $MgSO_4$ and evaporated under reduced pressure. The product **10** was obtained as a red solid (0.320 g, crude).

PM ($C_{55}H_{74}N_2O_{18}$): 1051,18 u

Synthesis of 3-phenyl-6-(3',4',5'-tris(2-(2-(2-methoxyethoxy)ethoxy)ethoxy)-[1,1'-biphenyl]-4-yl)pyrrolo[3,4-c]pyrrole-1,4(2H,5H)-dione, 15, mono TEG-DPP



15

Mono TEG-DPP

A solution of compound **12** (0.320 g, 0.304 mmol) in DCM (24 mL) was stirred at room temperature. TFA (1.2 mL) was added. The mixture was stirred for one hour. After the mixture was evaporated under reduced pressure. The crude product was purified by column chromatography (AcOEt:MeOH, 8:2). Product **11** was obtained as a red solid (0.200 g, yield of two steps: 59 %)

1H NMR (400 MHz, $(CD_3)_2SO$), δ (ppm): 8.56 (d, $J = 8.6$ Hz, 2H, H_{arom}), 8.47 (m, 2H, H_{arom}), 7.95 (d, $J = 8.6$ Hz, 2H, H_{arom}), 7.57 (m, 3H, H_{arom}), 7.09 (s, 2H, H_{arom}), 4.24 (t, $J = 9.6$ Hz, 4H, OCH_2), 4.06 (t, $J = 9.6$ Hz, 2H, OCH_2), 3.78 (t, $J = 8.6$ Hz, 4H, OCH_2CH_2), 3.69 (t, $J = 9.6$ Hz, 2H, OCH_2CH_2),

3.62- 3.57 (m, 6H, H_{TEG}), 3.54-3.49 (m, 12H, H_{TEG}), 3.42-3.39 (m, 6H, H_{TEG}), 3.22-3.24 (m, 9H, O(CH₃)₃). ¹³C NMR was not recorded because of the low solubility of the compound.

Appendix A

A1 Supramolecular polymerizations

The mechanism of chain growth for conventional polymers always involves three principles: step-growth, addition chain and living chain. As mentioned in paragraph 1.3, the formation of a covalent polymer occurs under kinetic control: the potential barrier for back reaction is often much larger than for the forward reaction barrier. It means that dilution or heating cannot modify these macromolecules.⁵² On the contrary the polymerisation process in supramolecular polymers is dynamic, reversible and proceeds to thermodynamic equilibrium, thus it depends on temperature, concentration, pressure and pH. During a supramolecular polymerisation the physical nature of noncovalent forces, the type of monomers used and the evolution of the Gibbs free energy of the polymer are three important principles to consider. The structure of supramolecular polymers is constantly moving and at the equilibrium, both polymerisation and de-polymerisation take place. In particular conditions, polymerisation is spontaneous and thermodynamically stable.

To better understand the behaviour of a supramolecular polymer and its properties, it is important to describe its mechanism of polymerization and to know approximately its degree of polymerization (DP). Three major mechanisms of supramolecular polymerisations, reported in Figure A1, are described in the literature:

1. Isodesmic model
2. Cooperative growth
3. Ring-Chain equilibrium

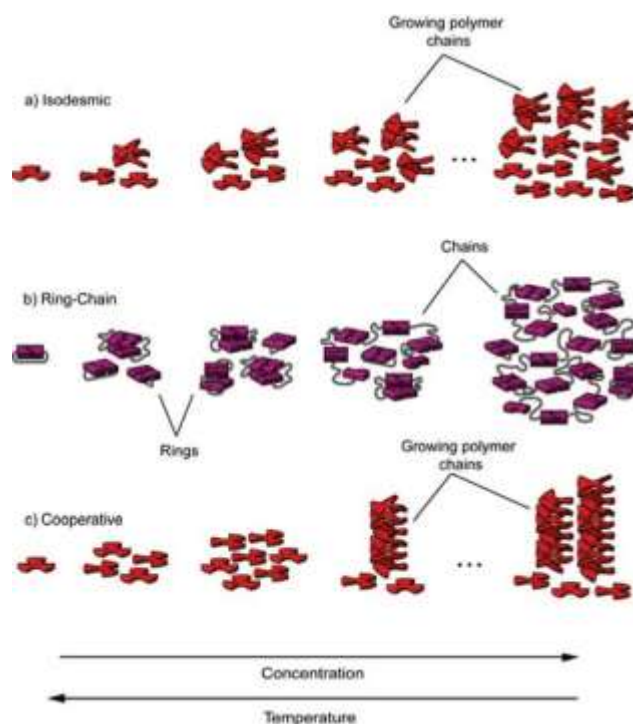


Figure A1 Types of supramolecular polymerisations.

Self-assembly allows the development of complex, big and functional systems starting from small and simple molecular structures. However, the dynamic nature of supramolecular polymers makes difficult their characterization and requires the combination of different characterization methods.

In the next paragraphs, the isodesmic and cooperative models are examined.

A1.1 Isodesmic model

The word isodesmic comes from Greek: *isos* means equal and *desmos*, bond.

The isodesmic polymerisation is characterized by high polydispersity and the degree of polymerisation depends on the association constant of the linking supramolecular units. Every monomer addition to the growing chain is identical at all steps of polymerisation process and it is governed by a single equilibrium constant, K_s . It means that there is a gradual increase in the number and length of the aggregated species and that the responsiveness of the end groups does not change during the polymerisation. In this polymerisation the successive addition of monomers to the growing chain leads to a constant decrease in the free energy, due to the affinity of a subunit for the polymer end.⁵³

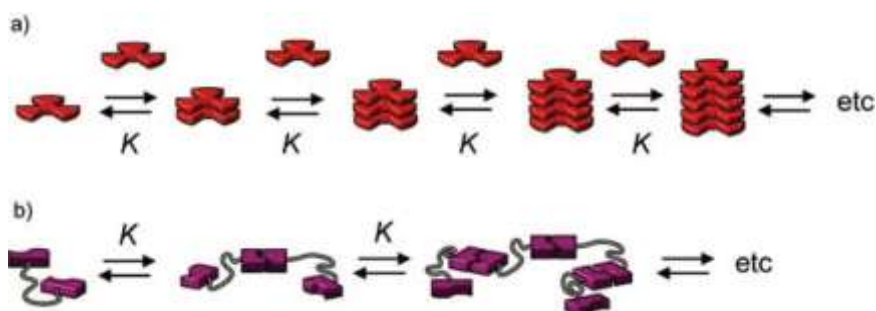


Figure A2 Schematic representation of the isodesmic polymerisation.

The Figure A2 displays the isodesmic polymerisation of a rigid disc molecule into a linear supramolecular polymer **(a)** and the isodesmic polymerisation of a bifunctional monomer, in which the two units are connected via a flexible spacer **(b)**. K is the intermolecular equilibrium constant and is independent of the chain length.

Concentration dependent model

An isodesmic supramolecular polymerisation can be also described as shown in Figure A3, in which M_1 represents the monomer and K_s the molar equilibrium constant.

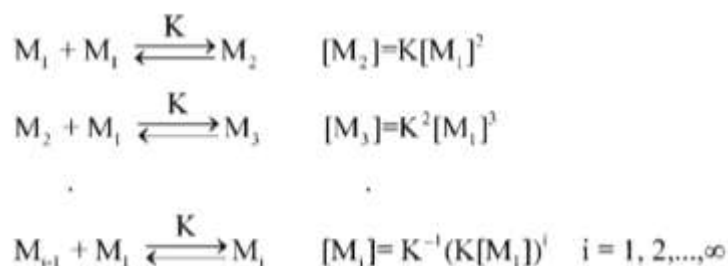


Figure A3 Addition of monomeric units during isodesmic polymerisation.

This polymerisation is characterized by the absence of a critical concentration or a critical temperature. To demonstrate the absence of a critical concentration in the isodesmic polymerisation, a large number of concentration dependent properties have been calculated through Zhao and Moore model.

Equation 1 and 2 permit to calculate the fraction of converted monomer (ϕ) to supramolecular polymer and the degree of polymerization (DP_n) through Zhao and Moore model.⁵²ⁱ

$$\phi = \frac{2 K_{Is} C_T + 1 - \sqrt{4 K_{Is} C_T + 1}}{2 K_{Is}^2 C_T^2} \quad \text{Equation 1}$$

$$DP_n = \frac{1}{1 - K_{Is} [C_t]} \quad \text{Equation 2}$$

The Figure A4 shows the fraction of converted monomer to supramolecular polymer ϕ , as function of dimensionless concentration $K_{Is} C_t$.

The fraction of monomer converted to polymeric species rises gradually as the concentration of ditopic monomer in dilute solution is increased. This transition appears gradual even if the weight- and number-averaged degrees of polymerisation (DP_w and DP_n , respectively) are plotted as a function of the dimensionless concentration.

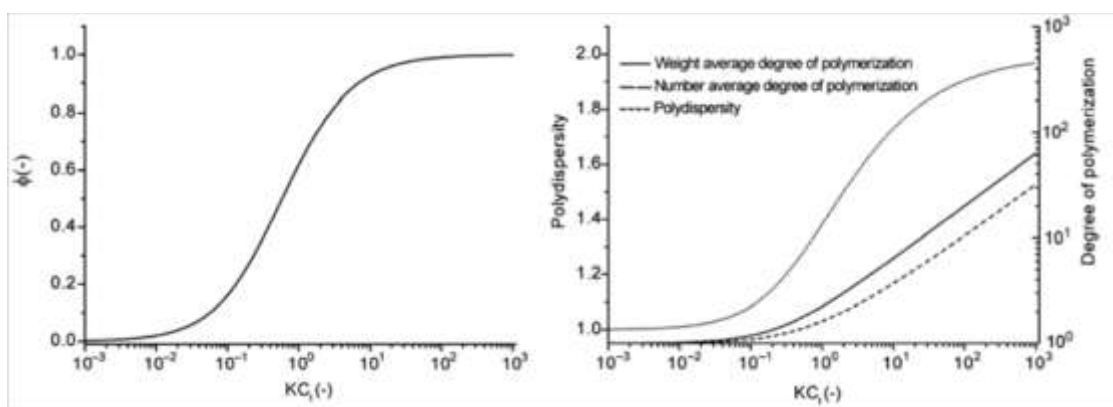


Figure A4 Concentration dependent properties in isodesmic polymerisation.

Furthermore the graphs reveal a drawback of isodesmic supramolecular polymerisation: supramolecular polymers with high DP_n are obtained only at very high values of $K_{Is} C_t$. Thus, to obtain supramolecular polymer with high DP_n in dilute solution a high value of the equilibrium constant K is necessary ($K_{Is} > 10^6 \text{ M}^{-1}$).

The isodesmic equilibrium constant can be obtained by concentration dependent spectroscopic analysis (UV-Vis,⁵⁴ IR,⁵⁵ fluorescence,⁵⁶ NMR,⁵⁷ CD⁵⁸). The changes in the measured signal are usually considered to be proportional with the concentration or fraction of the aggregated material. Therefore, the quality of fits cannot be used to distinguish dimerization and isodesmic association. For this reason, the fits must be associated to other analysis that prove the degree of polymerisation as function of concentration (DOSY⁵⁹, DLS⁶⁰ or VPO).

Temperature dependent model

The concentration-dependent isodesmic self-assembly models have been developed using chemical equilibrium considerations, on the contrary temperature-dependent models have been constructed using the framework of statistical mechanics. Van der Schoot^{52d} has elaborated the first model to study this phenomenon. In this model, there are two parameters: the concentration-dependent melting temperature (T_m , defined as the temperature at which the fraction of monomer present in supramolecular polymers equals 0.5) and a temperature-independent polymerisation enthalpy (ΔH , kJ·mol⁻¹).

In the isodesmic model, described by Van der Schoot, the degree of aggregation can be related to the temperature via a sigmoidal relation and it can be described with the Equation 3:

$$\phi \cong \frac{1}{1 + \exp\left[-0.908\Delta H \frac{T - T_m}{RT_m^2}\right]} \quad \text{Equation 3}$$

From the degree of aggregation, the number-averaged degree of polymerisation, DP_n , can be calculated directly, via Equation 4:

$$DP_n(T) = \frac{1}{\sqrt{1-\phi(T)}} = \frac{1}{2} + \frac{1}{2} \sqrt{4 K_{IS}(T)c_T + 1} \quad \text{Equation 4}$$

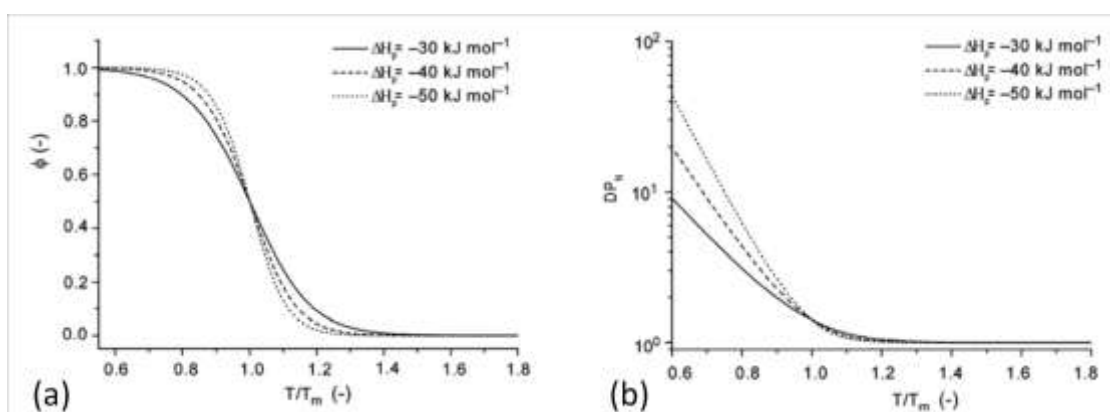


Figure A5 Temperature-dependent properties in isodesmic polymerisation.

Figure A5 **(a)** displays ϕ as function of the dimensionless temperature (T/T_m) for different realistic values of ΔH_p for a supramolecular polymer that aggregates upon cooling. The shape of the curve is sigmoidal. The graph **(b)** in Figure A5 shows the number-averaged degree of polymerisation (DP_n) as a function of dimensionless temperature (T/T_m) according to the same model: when the temperature is lowered DP_n gradually increases.

3,3'-diamino-2,2'-bipyridine and bifunctional derivatives of ureido-pyrimidinone, shown in Figure A6, are two important examples of monomeric units that polymerize via isodesmic mechanism and show all the characteristic features of such a mechanism.

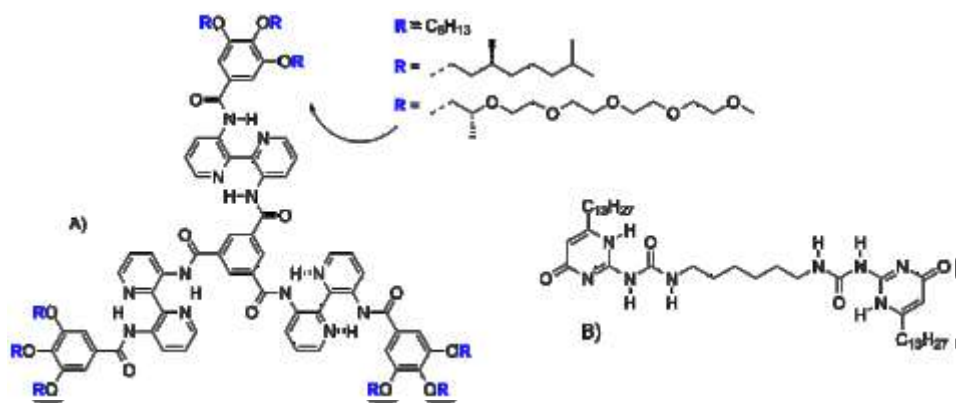


Figure A6 Examples of molecules that polymerize via isodesmic model.

A1.2 Cooperative model

The cooperative supramolecular polymerisation is characterized by non-linear growth and comprises two stages: nucleation and elongation. The first step is a linear isodesmic polymerisation with a binding constant K_n equals for the addition of each monomer. In this phase, a nucleus of degree of polymerisation is formed. The second step involves another linear isodesmic elongation process, and due to the cooperative effect, the supramolecular polymerisation proceeds by a binding constant K_e higher than K_n .

A schematic representation of cooperative model is reported in Figure A7.

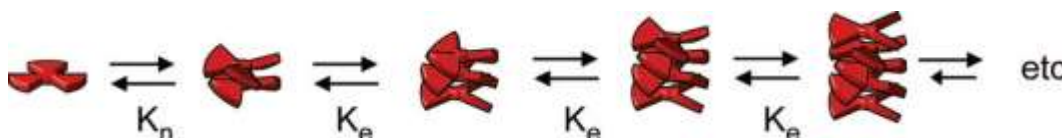


Figure A7 Schematic representation of cooperative polymerisation.

Concentration dependent properties

This model is characterized by at least two different association constants and a critical concentration or temperature at which the supramolecular polymer starts growing, as shown in Figure A8:

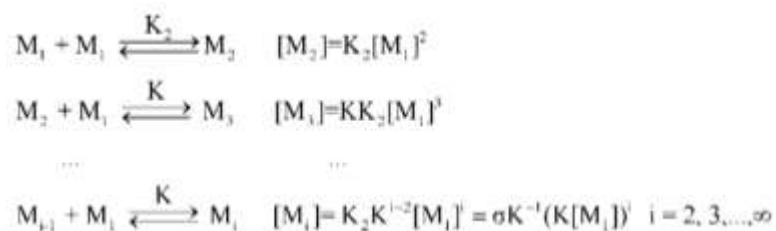


Figure A8 Addition of monomeric units and polymer constitution.

This kind of supramolecular polymerisation can be described using the mean-field chemical equilibrium model by Zhao and Moore. This model is a modification of isodesmic model. In this process, it is introduced σ , a parameter that defines the degree of polymerisation as K_n/K_e . For a cooperative process σ is smaller than unity. The graph in Figure A9 shows the mole fraction of self-assembled material, ϕ , as a function of the dimensionless concentration $K C_t$ for three different values of σ and Equation 5 permits to define ϕ value and Equation 6 allow to estimate the DP_n :

$$\phi = \frac{1}{2} \frac{2K C_t + \sigma - \sqrt{4\sigma K C_t + \sigma^2}}{K^2 C_t^2} \quad \text{Equation 5}$$

$$DP_n = \frac{\sigma + (1-\sigma)(1-K[\phi \cdot C_t])^2}{\sigma(1-K[\phi \cdot C_t]) + (1-\sigma)(1-K[\phi \cdot C_t])^2} \quad \text{Equation 6}$$

Moreover the cooperativity influences the growth profile of the polymeric species: increasing the cooperativity ($\sigma \ll 1$) nucleation/elongation become clearer.⁶¹

Whereas for the isodesmic growth ($\sigma=1$) a gradual increase in polymeric species is observed with increasing concentration, for the cooperative systems, below a critical dimensionless concentration of 1, any polymeric species can be formed. Only when the concentration is raised above the critical concentration does chain growth occur and all monomers are converted into high molecular weight polymers over a relatively small concentration range. Higher DP_n values are obtained increasing K_e and decreasing σ .

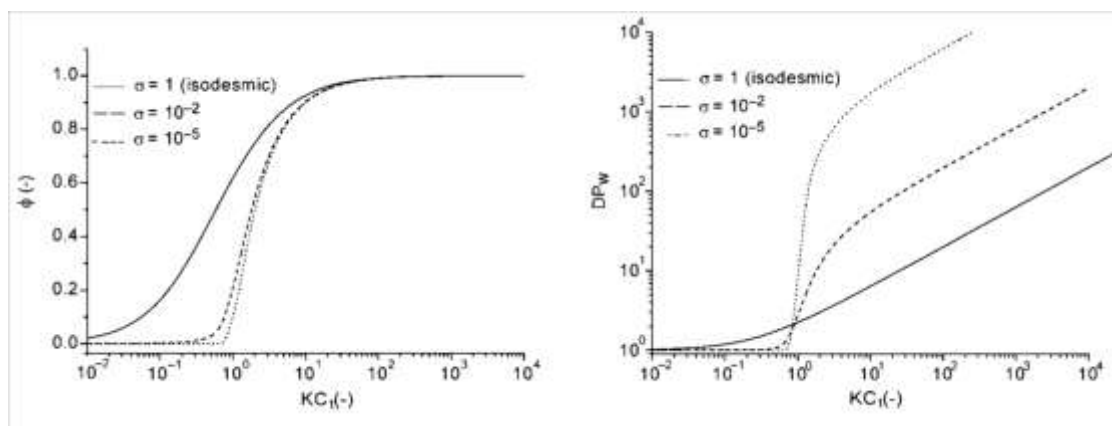


Figure A9 Concentration dependent properties in cooperative polymerisation.

Temperature dependent properties

In the model described by Van der Schoot, K_{NE} is a dimensionless activation constant that describes the monomeric activation step; ΔH_e represents temperature-dependent elongation enthalpy and T_e is the concentration dependent elongation temperature. For polymers that aggregate upon cooling, the elongation enthalpy is negative.

The critical elongation temperature, T_e separates two polymerization regimes. Above the critical elongation temperature molecules are in an inactive state, called nucleation regime. At the critical elongation temperature activation occurs and the small fraction of active monomers can elongate to form supramolecular polymers with high DP_n . For low value of K_{NE} any polymeric species are present at temperature above the critical temperature T_e . Below the critical temperature T_e the fraction of polymerised material increases quickly and the transition becomes clearer as K_{NE} becomes smaller, as shown in Figure A10, **(a)**. High degree of polymerization can be reached when cooperativity increases (Figure A10 **(b)**). Hence, the dimensionless activation constant K_{NE} in this model has a role identical to that of the cooperativity parameter σ in the model described by Zhao and Moore.⁵²

The elongation regime can be described with the Equation 7:

$$\phi = \phi_{SAT} \left(1 - \exp \left[\frac{-\Delta H_e}{RT_e^2} (T - T_e) \right] \right) \quad \text{Equation 7}$$

where, ΔH_e is the enthalpy corresponding to the aggregation process, T the absolute temperature, T_e the elongation temperature, R the ideal gas constant and ϕ_{SAT} is a parameter introduced to assure that ϕ_{agg}/ϕ_{SAT} does not exceed unity.

Whereas Equation 8 describes the nucleation regime:

$$\phi_{agg} = \phi_{SAT} \left[\sqrt[3]{K_{NE}} \exp \left[\left(\frac{2}{\sqrt[3]{K_{NE}}} - 1 \right) \frac{\Delta H_e}{RT_e^2} (T - T_e) \right] \right] \quad \text{Equation 8}$$

where, K_{NE} is the dimensionless equilibrium constant of the activation step at the elongation temperature.

The number-averaged degree of polymerization in elongation regime is described by Equation 9. We obtain DP_n introducing in the Equation 9 K_{NE} , calculated in the nucleation regime, ϕ_{agg} and ϕ_{SAT} obtained from elongation regime.

$$DP_n = \frac{1}{\sqrt[3]{K_{NE}}} \frac{\phi_{agg}}{\phi_{SAT} - \phi_{agg}} \quad \text{Equation 9}$$

In contrast to isodesmic polymerization the curves that describe the fraction of aggregated material are non-sigmoidal.

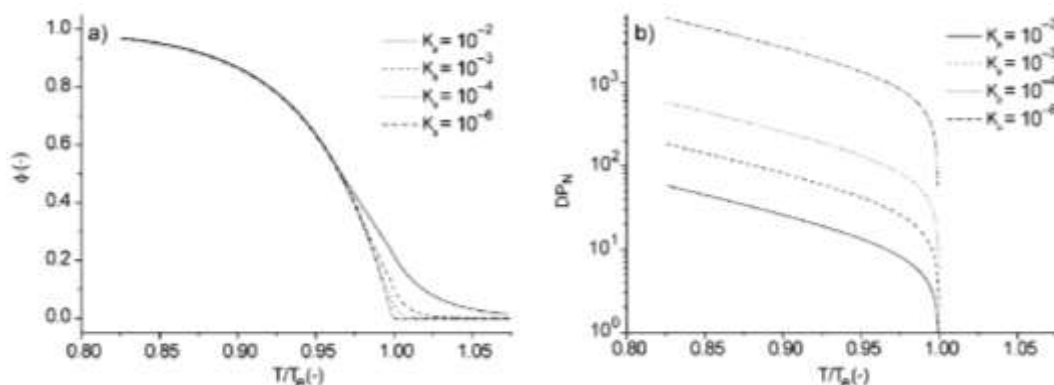


Figure A10 Temperature dependent properties in cooperative model.

Trialkylbenzene-1,3,5-tricarboxamides (BTAs) is an example of monomeric unit that shows a cooperative supramolecular polymerisation (Figure A11). These molecules self-assemble by means of strong, threefold α -helix-type intermolecular hydrogen bonding into well-defined, helical, one-dimensional columnar aggregates.

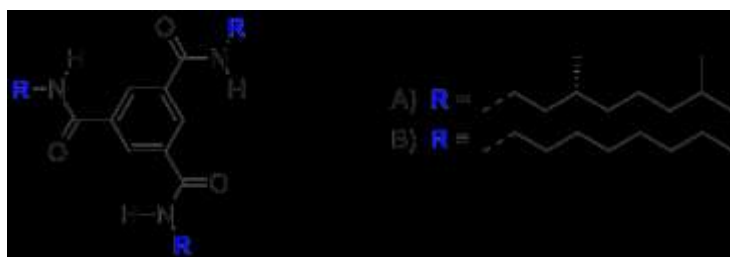


Figure A11 BTAs monomeric unit.

Oligo(*p*-phenylene vinylenes) (OPV) is another example of cooperative supramolecular polymerization synthesized by Mejer et al.⁶². This molecule, shown in Figure A12 reflects a high level of cooperativity thanks to hydrogen bonding and π - π stacking interactions. Thermal treatment of these lamellae at high temperatures induces columnar liquid-crystalline

mesophases as a result of microsegregation between the rigid OPV parts and the molten aliphatic wedges.

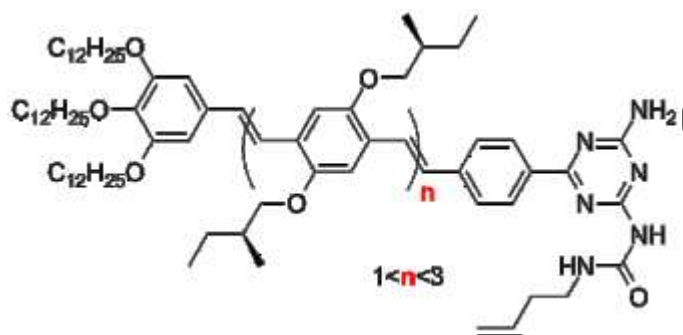


Figure A12 OPV, monomeric unit.

-
- ¹ Hao, Z.; Iqbal A. *Chem. Soc. Rev.* **1997**, *26*, 203-213.
- ² a) Iqbal, A.; Kirchmayr, R.; Pfenninger, J.; Rochat, A. C.; Wallquist, O. *Bull. Soc. Chim. Belg.* **1988**, *97*, 615-643. (b) Mizuguchi, J.; Wooden, G. *Ber. Bunsenges. Phys. Chem.* **1991**, *95*, 1264-1274. (c) Mizuguchi, J.; *J. Phys. Chem. A.* **2000**, *104*, 1817-1821.
- ³ Wallquist, O.; Lenz, R. in *High Performance Pigments*, ed. E. B. Faulkner and R. J. Schwartz, Wiley-VCH Verlag, **2009**, 165-194.
- ⁴ (a) Potrawa, T.; Langhals, H. *Chem. Ber.* **1987**, *120*, 1075-1078. (b) Langhals, H.; Grundei, Th.; Potrawa, Th.; Polbom, K. *Liebigs Ann.* **1996**, 679-682.
- ⁵ Lenz, R.; Wallquist, O. *Surface Coatings Int. B: Coatings Trans.* **2002**, *85*, 19.
- ⁶ (a) Mizuguchi, J.; Rihs, G. *Acta Crystallogr. Sect. C: Cryst. Struct. Commun.* **1992**, *C48(7)*, 1279-1283. (b) Mizuguchi, J.; Rochat, A. C.; Rihs, G.; *Ber. Bunsen-Ges. Phys. Chem.* **1992**, *96(4)*, 597-606. (c) Mizuguchi, J.; Grubenmann, A.; Wooden, G.; Rihs, G. *Acta Crystallogr. Sect. C: Cryst. Struct. Commun.* **1992**, *B48(5)*, 696-700. (d) Kirchmayr, R.; Iqbal, A.; Pfenninger, J.; Rochat, A.; Wallquist, O. *Polym. Paint Colour J.* **1988**, *179(4238)*, 370-372.
- ⁷ Farnum, D. G.; Mehta, G.; Moore, G. G. I.; Siegal, F. P. *Tetrahedron Lett.* **1974**, *29*, 2549.
- ⁸ Rochat, A. C.; Cassar, L.; Iqbal, A. (Ciba-Geigy AG), *Eur. Pat. Appl.* 94911, **1983**.
- ⁹ Semyonov, A. N. "Design Synthesis and Characterization of Fluorescent Dyes and Liquid Crystal Semiconductors", Kent State University, **2006**, 1-115.
- ¹⁰ Potrawa, T.; Langhals, H. *Chem. Ber.* **1987**, *120*, 1075.
- ¹¹ Glowacki, E. G.; Mihai Irimia-Vladu, M.; Bauer, S.; Sariciftci, N. S. *J. Mater. Chem. B*, **2013**, *1*, 3742-3753.
- ¹² Otsuka, H. *Polymer Journal*, **2013**, *45*, 879-891.
- ¹³ Stryer, L. *Biochemistry*; Fourth Edition ed.; W. H. Freeman and Company: New York, **1995**.
- ¹⁴ Petrucci, R. H. *General Chemistry: Principles and Modern Applications*; Fifth Edition ed.; Macmillan Publishing Company: New York, **1989**.
- ¹⁵ Brunsveld, L.; Folmer, B. J. B.; Meijer, E. W.; Sijbesma, R. P. *Chem. Rev.* **2001**, *101*, 4071-4097.
- ¹⁶ (a) Jorgenson, W. L.; Pranata, J. *J. Am. Chem. Soc.* **1990**, *112*, 2008-2010. (b) Pranata, J.; Wierschke, S. G.; Jorgenson, W. L. *J. Am. Chem. Soc.* **1991**, *113*, 2810-2819. (c) Yang, L.; Tan, X.; Wang, Z.; Zhang, X. *Chem. Rev.* **2015**, *115* (15), 7196-7239.
- ¹⁷ (a) Murray, T. J.; Zimmerman, S. C. *J. Am. Chem. Soc.* **1992**, *114*, 4010-4011. (b) Zimmerman, S. C.; Murray, T. J. *Tetrahedron Lett.* **1994**, *35*, 4077-4080. (c) Murray, T. J.; Zimmerman, S. C.; Kolotuchin, S. V. *Tetrahedron* **1995**, *51*, 635-648. (d) Quinn, J. R.; Zimmerman, S. C.; Del Bene, J. E.; Shavitt, I. *J. Am. Chem. Soc.* **2007**, *129*, 934-941.
- ¹⁸ (a) Fouquey, C.; Lehn, J.-M.; Levelut, A.-M. *Adv. Mater.* **1990**, *2*, 254-257. (b) Lehn, J.-M. *Makromol. Chem., Macromol. Symp.* **1993**, *69*, 1-17.
- ¹⁹ Gulik-Krczywicki, T.; Fouquey, C.; Lehn, J.-M. *Adv. Mater.* **1990**, *2*, 254-257.
- ²⁰ (a) Kotera, M.; Lehn, J.-M.; Vigneron, J.-P. *J. Chem. Soc. Chem. Commun.* **1994**, 197-199. (b) Kotera, M.; Lehn, J.-M.; Vigneron, J.-P. *Tetrahedron* **1995**, *51*, 1953-1972.
- ²¹ (a) Sijbesma, R. P.; Beijer, F. H.; Brunsveld, L.; Folmer, B. J. B.; Hirschberg, J. H. K. K.; Lange, R. F. M.; Lowe, J. K. L.; Meijer, E. W. *Science* **1997**, *278*, 1601-1604. (b) Folmer, B. J. B.; Sijbesma, R. P.; Meijer, E. W. *Polym. Mater. Sci. Eng.* **1999**, *217*, 39.
- ²² Palmans, A. R. A.; Vekemans, J. A. J. M.; Havinga, E. E.; Meijer, E. W. *Angew. Chem., Int. Ed. Engl.* **1997**, *36*, 2648-2651.
- ²³ Green, M. M.; Peterson, N. C.; Sato, T.; Teramoto, A.; Lifson, S. *Science* **1995**, *268*, 1860-1866.
- ²⁴ Anderson, T.; Sanders, J. K. M.; Pantos, G. D. *Org. Biomol. Chem.* **2010**, *8*, 4274-4280
- ²⁵ (a) Burattini, S.; Greenland, B. W.; Merino, D. H.; Weng, W.; Seppala, J.; Colquhoun, H. M.; Hayes, W.; Mackay, M. E.; Hamley, I.E.; Rowan, S.J. *J. Am. Chem. Soc.* **2010**, *132*, 12051-12058. (b) Grimme, S. *Angew. Chem. Int. Ed.* **2008**, *47*, 3430 - 3434. (c) Roesky, H. W.; Andruh, M. *Coordination Chemistry Reviews* **2003**, *236*, 91-119. (d) Khlobystov, A. N.; Blake, A. J.; Champness, N. R.; Lemenovskii, D. A.; Majouga, A. G.; Zyk, N. V.; Schröder, M. *Coordination Chemistry Reviews* **2001**, *222*, 155-192.

- ²⁶ Meyer, E. A.; Castellano, R. K.; Diederich, F. *Angew. Chem. Int. Ed.* **2003**, *42*, 1210-1250.
- ²⁷ (a) Edwards, R. G.; Henderson, J. R.; Pinning, R. L. *Mol. Phys.* **1995**, *86*, 567-598. (b) Henderson, J. R. *J. Chem. Phys.* **2000**, *133*, 5965-5970.
- ²⁸ van Nostrum, C. F.; Nolte, R. J. M. *Chem. Commun.* **1996**, 2385-2392.
- ²⁹ (a) Sielcken, O. E.; van Tilborg, M. M.; Roks, M. F. M.; Hendriks, R.; Drenth, W.; Nolte, R. J. M. *J. Am. Chem. Soc.* **1987**, *109*, 4261-4265. (b) Kobayashi, N.; Lever, A. B. P. *J. Am. Chem. Soc.* **1987**, *109*, 7433-7441.
- ³⁰ Michelsen, U.; Hunter, C. A. *Angew. Chem., Int. Ed.* **2000**, *29*, 764-767.
- ³¹ Besenius, P.; de Feijter, I.; Sommerdijk, N. A.; Bomans, P. H.; Palmans, A. R. *J. Vis. Exp.* **2012**, *66*, 3975.
- ³² (a) Oshovsky, G. V.; Reinhoudt, D. N.; Verboom, W. *Angew. Chem. Int. Ed.* **2007**, *46*, 2366-2393. (b) Terao, J.; Konoshima, Y.; Matono, A.; Masai, H.; Fujihara, T.; Tsuji, Y. *Beilstein J. Org. Chem.* **2014**, *10*, 2800-2808. (c) Brunsveld, L.; Zhang, H.; Glasbeek, M.; Vekemans, J. A. J. M.; Meijer, E. W. *J. Am. Chem. Soc.* **2000**, *122*, 6175-6182.
- ³³ (a) Arnaud, A.; Belleny, J.; Boué, F.; Bouteiller, L.; Carrot, G.; Wintgens, V. *Angew. Chem. Int. Ed.* **2004**, *43*, 1718-1721.
- ³⁴ Obert, E.; Bellot, M.; Bouteiller, L.; Andrioletti, F.; Lehen-Ferrenbach, C.; Boué, F. *J. Am. Chem. Soc.* **2007**, *129*(50), 15601-15605.
- ³⁵ (a) Beijer, F. H.; Kooijman, H.; Spek, A. L.; Sijbesma, R. P. & Meijer, E. W. *Angew. Chem. Int. Ed.* **1998**, *37*, 75-78; (b) L Brunsveld, L.; Vekemans, J.; Hirschberg, J.; Sijbesma, R. P.; Meijer, E. W., *Proc. Natl. Acad. Sci.* **2002**, *99*, 4977-4982.
- ³⁶ (a) Brunsveld, L.; Vekemans, J. A. J. M.; Hirschberg, J. H. K. K.; Sijbesma, R. P.; Meijer, E. W. *Pnas* **2002**, *99*(8), 4977-4982. (b) Gaylord, B. S.; Wang, S.; Heeger, A. J.; Bazan, G. C. *J. Am. Chem. Soc.* **2001**, *123*, 6417-6418.
- ³⁷ Wool, R. P., *Soft Matter*, **2008**, *4*, 400-418.
- ³⁸ Fan, F.; Szpunar, J., *J. Appl. Polym. Sci.* **2015**, *132*, 42135
- ³⁹ Burnworth, M.; Tang, L.; Kumpfer, J. R.; Duncan, A. J.; Beyer, F. L.; Fiore, G. L.; Rowan, S. J.; Weder, C., *Nature*, **2011**, *472*, 334-338.
- ⁴⁰ Cordier, P.; Tournilhac, F.; Soulie-Ziakovic, C.; Leibler, L. *Nature*, **2008**, *451*, 977-980.
- ⁴¹ Sordo, F.; Mougner, S. J.; Loureiro, N.; Tournilhac, F.; Michaud, V. *Macromolecules*, **2015**, *48*, 4394-4402.
- ⁴² Obert, E.; Bellot, M.; Bouteiller, L.; Andrioletti, F.; Lehen-Ferrenbach, C.; Boué, F. *J. Am. Chem. Soc.* **2007**, *129*, 15601-15605.
- ⁴³ Baker, M. B.; Albertazzi, L.; Voets, I. K.; Leenders, C. M. A.; Palmans, A. R. A.; Pavan, G. M.; Meijer, E. W. *Nature Communications* **2015**, *6*, 6234.
- ⁴⁴ Guo, E. Q.; Ren, P. H.; Zhang, Y. L.; Zhang, H. C.; Yang, W. J. *Chem. Commun.* **2009**, 5859-5861.
- ⁴⁵ Zambounis, J. S.; Hao, Z.; Iqbal, A. *Nature* **1997**, *388*, 131.
- ⁴⁶ Michel Rosso, M.; Nguyen, A. T.; de Jong, E.; Baggerman, J.; Paulusse, J. M. J.; Giesbers, M.; Fokkink, R. G.; Norde, W.; Schröen, K.; van Rijn, C. J. M.; Zuilhof, H. *ACS Appl. Mater. Interfaces* **2011**, *3*, 697-704.
- ⁴⁷ An, Z.; Yu, J.; Domercq, B.; Jones, S. C.; Barlow, S.; Kippelen, B.; Marder, S. R. *J. Mater. Chem.*, **2009**, *19*, 6688-6698.
- ⁴⁸ Haketa, Y.; Sakamoto, S.; Chigusa, K.; Nakanishi, T.; Maeda, H. *J. Org. Chem.* **2011**, *76*, 5177-5184.
- ⁴⁹ (a) Riggs, R. L.; Morton, C. J. H.; Slawin, A. M. Z.; Smith, D. M.; Westwood, N. J.; Austen, W. S. D.; Stuart, K. E., *Tetrahedron* **2005**, *61*, 11230; (b) Morton, C. J. H.; Riggs, R. L.; Smith, D. M.; Westwood, N. J.; Lightfoot, P.; Slawin, A. M. Z., *Tetrahedron* **2005**, *61*, 727; (c) Morton, C. J. H.; Gilmour, R.; Smith, D. M.; Lightfoot, P.; Slawin, A. M. Z.; MacLean, E. J., *Tetrahedron* **2002**, *58*, 5547.
- ⁵⁰ G. Fernández, M. Stolte, V. Stepanenko, F. Würthner, *Chem. Eur. J.* **2012**, *19*, 206-217.
- ⁵¹ Würthner, F.; Kaiser, T. E.; Saha-Moller, C. R., *Angew. Chem. Int. Ed.* **2011**, *50*, 3376.
- ⁵² De Greef, T. F. A.; Smulders, M. M. J.; Wolfs, M.; Schenning, A. P. H. J.; Sijbesma, R. P.; Meijer, E. W. *Chem. Rev.* **2009**, *109*, 5687-5754.
- ⁵³ (a) Ciferri, A. *Macromol. Rapid Commun.* **2002**, *23*, 511. (b) Dudowicz, J.; Freed, K. F.; Douglas, J. F. *J. Chem. Phys.* **2003**, *119*, 12645. (c) Martin, R. B. *Chem. Rev.* **1996**, *96*, 3043. (d) van der Schoot, P. "Theory of Supramolecular Polymerization" in *Supramolecular Polymers – 2nd edition*, Ciferri, A. ed., Taylor & Francis: London (U.K.), **2005**. (e) Henderson, J. R. *Phys. Rev. E* **1997**, *55*, 5731. (f) Douglas, J. F.; Dudowicz, J.; Freed, K. F. *J. Chem. Phys.* **2008**, *128*, 224901. (g) Mukerjee, P.; Ghosh, A. K. *J. Am. Chem.*

-
- Soc. **1970**, *92*, 6408. (h) Connors, K. A. *Binding Constants: The Measurement of Molecular Complex Stability*; Wiley: New York, **1987**. (i) Zhao, D.; Moore, J. S. *Org. Biomol. Chem.* **2003**, *1*, 3471.
- ⁵⁴ Braswell, E. H. *J. Phys. Chem.* **1984**, *88*, 3653.
- ⁵⁵ Coggeshall, N. D.; Saier, E. L. *J. Am. Chem. Soc.* **1951**, *73*, 5414.
- ⁵⁶ Bierzynski, A.; Kozłowska, H.; Wierzchowski, K. L. *Biophys. Chem.* **1977**, *6*, 213. (b) Gajewska, J.; Bierzynski, A.; Bolewska, K.; Wierzchowski, K. L.; Petrov, A. I.; Sukhorukov, B. I. *Biophys. Chem.* **1982**, *15*, 191.
- ⁵⁷ Broom, A. D.; Schweizer, M. P.; Ts'o, P. O. P. *J. Am. Chem. Soc.* **1967**, *89*, 3612.
- ⁵⁸ Gilligan, T. J.; Schwarz, G. *Biophys. Chem.* **1976**, *4*, 55.
- ⁵⁹ Price, W. S.; Tsuchiya, F.; Arata, Y. *J. Am. Chem. Soc.* **1999**, *121*, 11503.
- ⁶⁰ Tojo, H.; Horiike, K.; Shiga, K.; Nishina, Y.; Watari, H.; Yamano, T. *J. Biol. Chem.* **1985**, *260*, 12607.
- ⁶¹ Smulders, M. M. J.; Nieuwenhuizen, M. M. L.; de Greef, T. F. A.; van der Schoot, P.; Schenning, A. P. H. J.; Meijer, E. W. *Chem. Eur. J.* **2010**, *16*, 362-367.
- ⁶² Smulders, M. M. J.; Schenning, A. P. H. J.; Meijer, E. W. *J. Am. Chem. Soc.* **2008**, *130* (2), 606-611.

2 DOSY characterization of *longchain*-DPP and TEG- DPP

2.1 Introduction: measuring High-Resolution Diffusion by NMR Spectroscopy

Diffusion-ordered spectroscopy (DOSY) seeks to separate the NMR signals of different species according to their diffusion coefficient.¹ The diffusion coefficient of a certain molecular species under given conditions (for example, solvent and temperature) depends on its “effective” molecular weight, size, and shape. For these reasons diffusion NMR measurements can be used in many different fields ranging from the medical sciences to material sciences,² especially this technique plays an important role in the characterization of supramolecular systems in solution. Moreover this technique permits to include the estimation of association constants and mapping the intermolecular interactions in multicomponent systems as well as investigating aggregation, ion pairing, encapsulation, and the size and structure of labile systems.³

2.1.1 Concepts of Molecular Diffusion in Isotropic Systems

Translational diffusion is one of the most important modes of molecular transport.⁴ In an isotropic homogeneous system the conditional probability $P(r_0, r, t_d)$ of finding a molecule, which was initially at position r_0 , at position r after a time t_d is given by Equation 1, where D is the self-diffusion coefficient.

$$P(r_0, r, t_d) = (4\pi D t_d)^{-\frac{3}{2}} \exp\left(-\frac{(r-r_0)^2}{4 D t_d}\right) \quad \text{Equation 1}$$

This equation shows that the volume occupied by a molecule, originally at position r_0 relative to an arbitrary reference position, in a non restricted system is a Gaussian distribution that broadens with the increase in the diffusion time t_d , as shown in Figure 2.1.

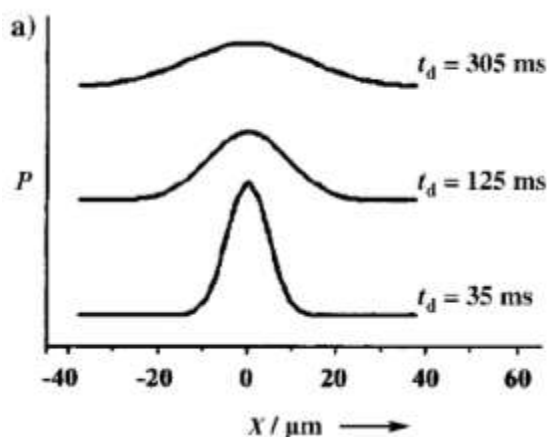


Figure 2.1 Free diffusion in a solution of *tert*-butanol.

However, the self-diffusion root-mean-square displacement $(X^2)^{1/2}$ in such systems is given by the Einstein equation (2), where n is 2, 4, or 6 for the cases of one-, two- and three-dimensional diffusion.

$$\sqrt{(X^2)} = \sqrt{(n D t_d)} \quad \text{Equation 2}$$

From this equation it follows that the mean displacement for free diffusion increases linearly with the square root of the diffusion time.⁵

In addition, it is well known that diffusion is closely related to molecular size, as seen from the Einstein–Smoluchowski Equation (3), where k_b is the Boltzmann constant, T is the absolute temperature, f is the hydrodynamic frictional coefficient, N is Avogadro's number, and R is the gas constant.

$$D = \frac{k_b T}{f} = \frac{R T}{N f} \quad \text{Equation 3}$$

For a sphere in a continuous medium of viscosity η , f is given by the Stokes Equation (4). In this equation, r_s is the hydrodynamic radius.

$$f = 6 \pi \eta r_s \quad \text{Equation 4}$$

Combining Equations (3) and (4) leads to the familiar Stokes–Einstein equation (5).

$$D = \frac{k_b T}{6 \pi \eta r_s} \quad \text{Equation 5}$$

Equation 5 confirms that we can obtain information about the effective size or weight of species in solution by measuring the self-diffusion coefficient of a given molecular species under controlled conditions. Therefore, we can also estimate the specific interactions of the species with its molecular environment. Thus, the diffusion coefficients are sensitive to structural properties of the observed molecular species such as weight, size, and shape, as well as binding phenomena, aggregation, and molecular interactions.⁶

2.1.2 The 2D DOSY Technique

The diffusion experiments can be processed and displayed as a 2D matrix with chemical shifts plotted along one axis and diffusion coefficients plotted along the perpendicular axis, as shown in Figure 2.2 **(a)**. While the chemical shift information is obtained by fast Fourier transformation (FFT) of the time domain data, the diffusion information is obtained by an inverse Laplace transformation (ILT) of the signal decay data (Figure 2.2, **b**). The goal of the DOSY experiment is to separate species spectroscopically (not physically) present in a mixture of compounds. In this sense, the use of the DOSY experiment is reminiscent of the physical separation of compounds by chromatography.⁷

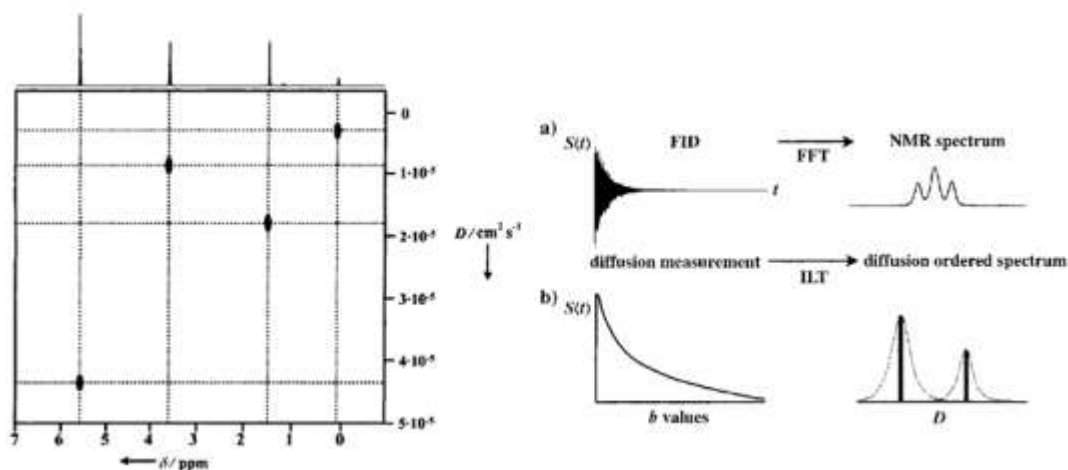


Figure 2.2 (a) 2D DOSY spectrum showing four different species characterised by four different diffusion coefficients; (b) comparison of FFT and ILT transformations, in contrast the FT for the inverse Laplace transform (ILT).⁸

2.1.3 Applications of NMR Diffusion Measurements in Supramolecular Chemistry

Diffusion NMR spectroscopy seems to have a great potential in assisting the characterization of molecular interactions.

An important example of diffusion NMR spectroscopy study applied to supramolecular polymers concerns the formation of head-to-tail assemblies derived from endo-cavity inclusion of alkylammonium moiety. Purrello et al.⁹ optimise a method for enhancing the degree of polymerization of ionizable AB-type supramolecular monomers. They incorporate an ancillary anion-binding site into calix[5]arene C₅-NH₂ with the aim of facilitating salt dissociation and making polymer formation more efficient.¹⁰ The molecular target was synthesized through four synthetic steps, as shown in Figure 2.3.

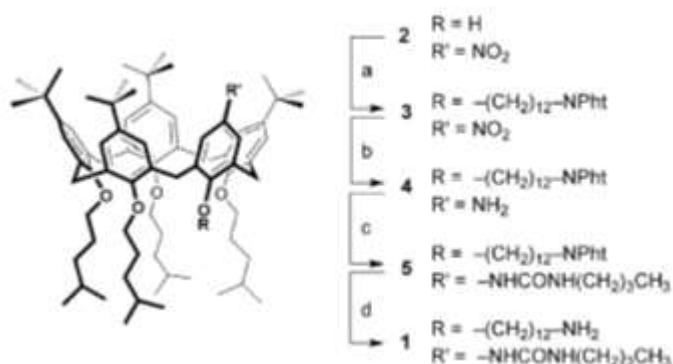


Figure 2.3 Synthesis of calix[5]arene.

As expected, exposure of the amino-calixarene precursor 1 to an aqueous 1M HCl solution triggered the self-assembly of monomer 1-HCl and, as a result we observe the formation of a polymer in which the dodecylammonium moiety of one calixarene monomer enters into the cavity of another, as display in Figure 2.4.

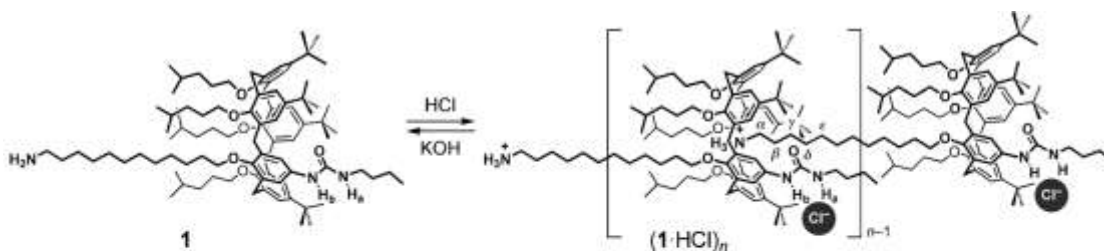


Figure 2.4 Supramolecular polymer organized by amino-calixarene precursor 1.

Conversion of the amino precursor 1 into polymer $(1 \cdot \text{HCl})_n$ caused a substantial broadening of the ^1H NMR spectrum, as shown in Figure 2.5. In particular in the high-field region ($\delta = 2.0$ to 1.0 ppm) a series of diagnostic signals consistent with the intermolecular endo-cavity inclusion of the five methylene groups closest to the ammonium moiety appears.¹¹

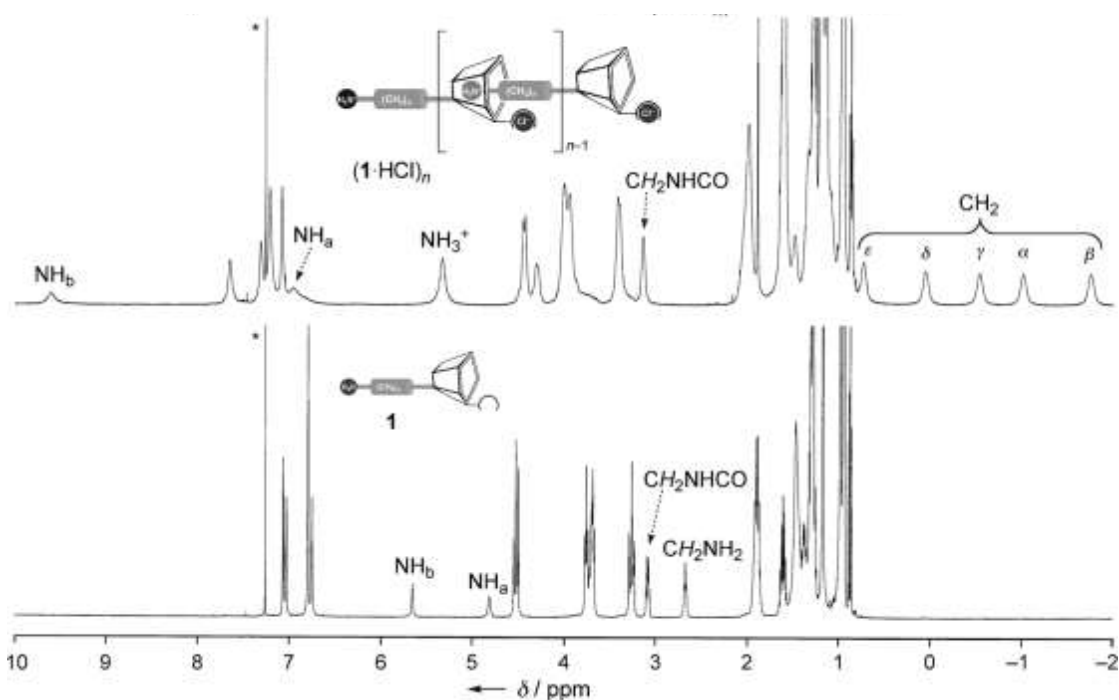


Figure 2.5 ^1H -NMR spectra of 1 and $(1 \cdot \text{HCl})_n$.

Furthermore the concentration-dependent diffusion NMR studies are used to estimate the number-average degree of polymerization (X_n) of monomer $1 \cdot \text{HCl}$ in CD_2Cl_2 solutions. Upon increase of the $1 \cdot \text{HCl}$ monomer concentration from 2 to 25 mM, the average diffusion coefficients (D), extracted from the signal decay of two representative signals (i.e. $\beta\text{-CH}_2$ and ArCH_2Ar), decreased from $(3.4 \pm 0.1) \cdot 10^{-6} \text{ cm}^2 \text{ s}^{-1}$ to $(1.1 \pm 0.1) \cdot 10^{-6} \text{ cm}^2 \text{ s}^{-1}$, hence indicating the formation of larger aggregates, as shown in Figure 2.6.

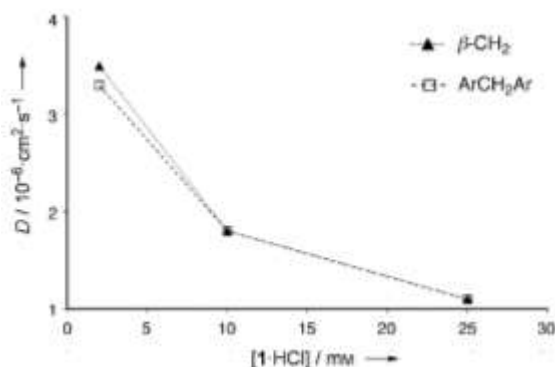


Figure 2.6 Diffusion coefficient (D) of two representative signals of $(1\text{HCl})_n$ at different concentrations in CD_2Cl_2 at 298 K.

With these analysis they demonstrate that this kind of molecule permits to control oligomer formation by means of simple acid/base treatment and that oligomerization is influenced by ion-pairing effects between the cationic monomer and its counterion. Furthermore the oligomer size can be tuned, to some extent, via the formation of a variety of monomeric salt species.

Another important example is described by Haino et al.¹²: they report the construction of a supramolecular polymer by molecular recognition between bisporphyrin and trinitrofluorenone.

The electron deficient guest moiety at the head, 4,5,7-trinitrofluorenone-2-carboxylate (TNF), can bind within the bisporphyrin cleft at the tail through a charge transfer interaction, and the head-to-tail style complexation leads to supramolecular polymerization (Figure 2.7 a).

The monomer and its analogue, which is without the TNF moiety, has been tested by DOSY. As shown in Figure 2.7 b, the diffusion coefficient of the analogue $D_{\text{avg}} = 3.02 \cdot 10^{-10} \text{ m}^2 \text{ s}^{-1}$ is not significantly influenced by concentration and this result demonstrates the independence of the diffusion coefficient from concentration and thus that there is no supramolecular polymerization.

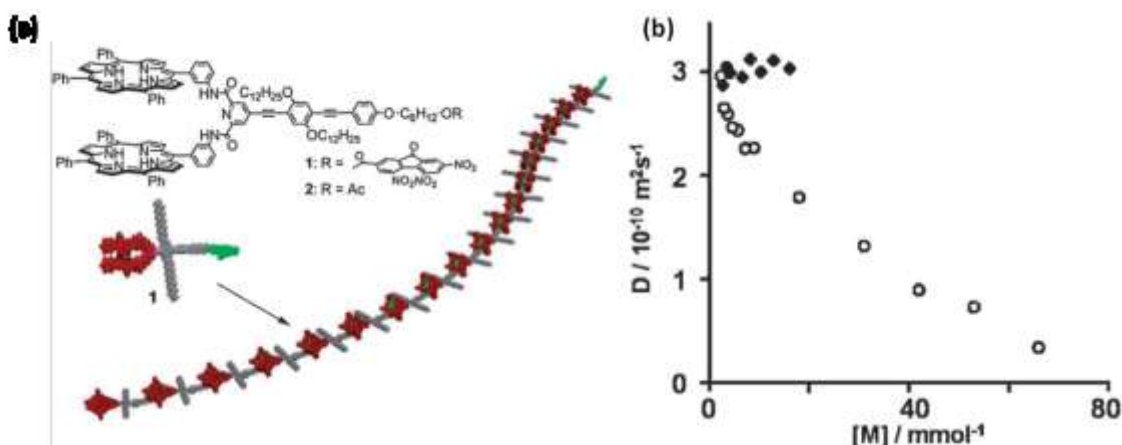


Figure 2.7 (a) Molecular structures of the heteroditopic monomer and a schematic representation of the supramolecular polymers; **(b)** diffusion coefficients of the monomer (cycle) and its analogue (rhombus) under different concentrations.

In contrast, the diffusion coefficient of the monomer is significantly dependent on concentration, showing a diffusion constant of $2.96 \cdot 10^{-10} \text{ m}^2 \text{ s}^{-1}$ at 2.34 mM, and $3.4 \cdot 10^{-10} \text{ m}^2 \text{ s}^{-1}$ at 66 mM, respectively (Figure 2.7 b). The decrease of D implies that large polymeric aggregates are formed at the higher concentration. Assuming that all the aggregations are hydrodynamically spherical,¹³ the Stokes–Einstein equation can be applied to calculate the average size of the supramolecular polymer, that results approximately 660 times the monomeric form.

We report another example described by Wang's group¹⁴: they synthesize a quadruple hydrogen bonded linear supramolecular polymer and then cross-linked it into networks via bisparaquat molecules.

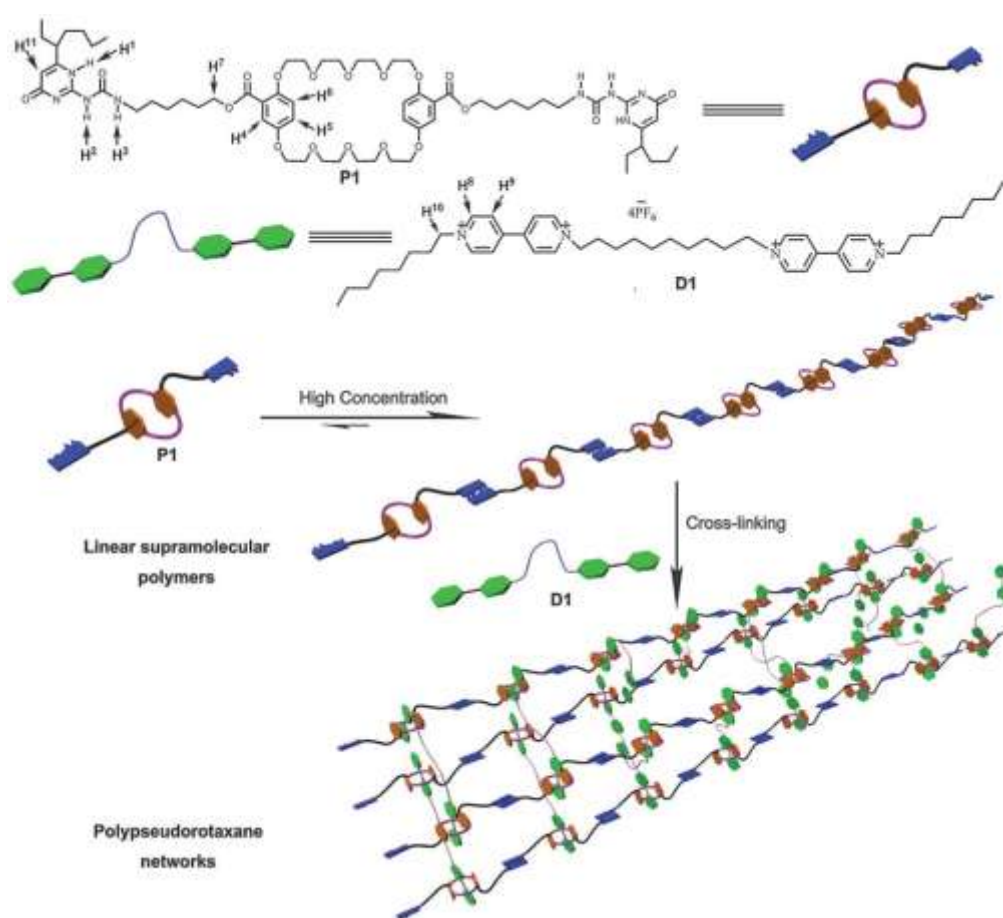


Figure 2.8 Representation of the construction of polypseudorotaxane networks from monomers P1 and D1.

The DOSY results show that as the monomer concentration increased, the diffusion coefficient decreases gradually and this suggests that longer supramolecular polymers are formed. After cross-linking, the diffusion coefficient becomes much smaller than those of linear supramolecular polymers.¹⁵

The last example that we illustrate is the self-assembly of perylene bismide B described by Würthner's group. The molecular structures are shown in Figure 2.9.

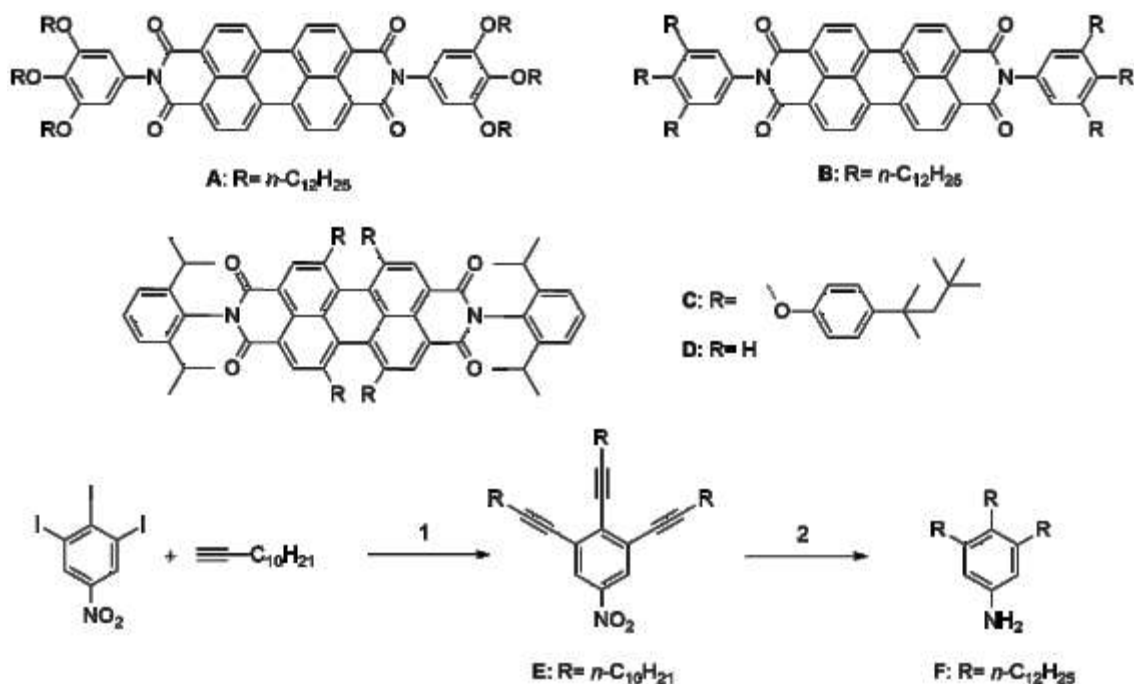


Figure 2.9 Chemical structures of the trialkoxyphenyl-containing PBI dye (**A**) and trialkylphenyl-functionalized PBI (**B**) and the two reference PBIs (**C**) and (**D**).

In this case they optimize a method to determine the aggregate size using DOSY NMR experiments obtaining a result in perfect agreement with that obtained for the concentration and temperature-dependent UV/Vis spectral data by employing the isodesmic model.

According to the Stokes-Einstein, Equation 5, the size of species could be compared based on their diffusion coefficients when the other parameters are identical.

For PBI (in Figure 2.9, **B**), only a single apparent diffusion coefficient is observed at different concentrations for all the aggregated species. If only monomer–dimer equilibrium exists, the D values for both monomer and dimer species should be nearly identical, whereas, for highly aggregated species which have much larger R values than monomers, obviously, a change of D values should be observable on DOSY NMR spectra.

As the monomeric form of (**B**) can only be obtained at very low concentrations, a reference PBI (**C**), which has a nearly identical molecular mass ($1528 \text{ g}\cdot\text{mol}^{-1}$) as (**B**) ($1552 \text{ g}\cdot\text{mol}^{-1}$) and does not aggregate owing to its extremely bulky substituents.

For all the aromatic signals of (**B**), D value of $1.57\cdot 10^{-10} \text{ m}^2 \text{ s}^{-1}$ is observed at a concentration of $1.1\cdot 10^{-3} \text{ M}$ while the reference compound (**C**) showed diffusion coefficient of $3.40\cdot 10^{-10} \text{ m}^2 \text{ s}^{-1}$ at $1.3\cdot 10^{-3} \text{ M}$ (see Figure 2.10). The large difference between the D values of (**B**) and monomeric (**C**) indicates that the hydrodynamic radius of the present species of (**B**) is much higher than that of the reference compound. These data indicate formation of extended aggregates of dye (**B**) in MCH.

They can calculate the average aggregate size of (**B**) applying the Equation 6:

$$N_{DOSY} = \left(\frac{D_{REF}}{D} \right)^3 \quad \text{Equation 6}$$

Where D_{REF} and D are the translational diffusion coefficients obtained from DOSY NMR. The average numbers of aggregated dye (**B**) are estimated at three different concentrations and are given in Table 2.1.

T (°C)	C_T (mol L ⁻¹)	N_{DOSY}
25	$1.1 \cdot 10^{-3}$	10
25	$2.2 \cdot 10^{-2}$	20
25	$1.1 \cdot 10^{-1}$	99

Table 2.1 Average number of aggregated molecules N of PBI (**B**) at different concentration.

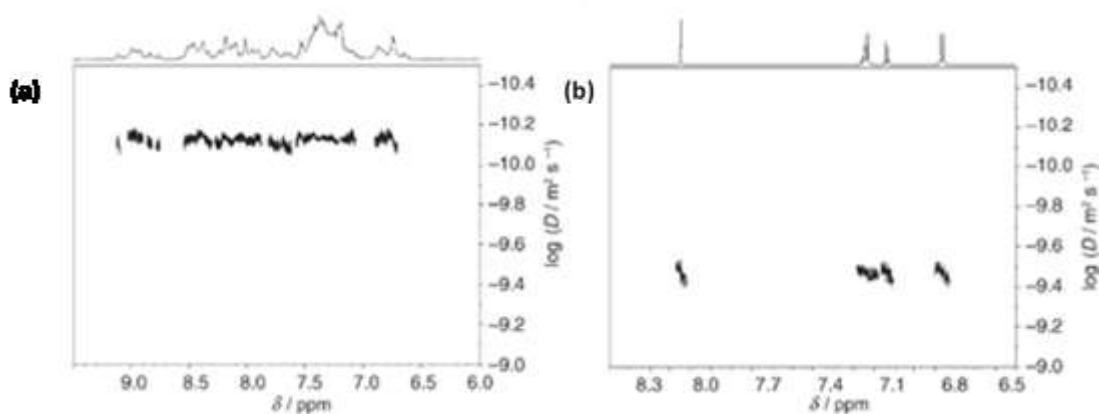


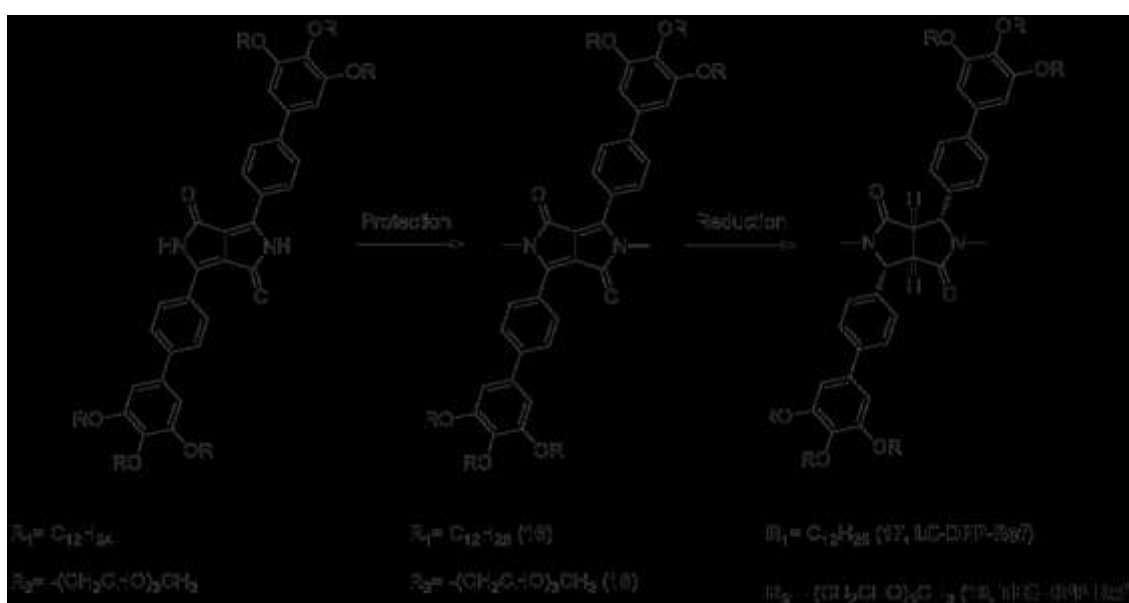
Figure 2.10 DOSY NMR spectra of (a) PBI (**B**) at $c=0.11$ M and (b) the reference compound **C** at $c=1.3 \cdot 10^{-3}$ M in MCH. The diffusion coefficients D [$\text{m}^2 \text{s}^{-1}$] are plotted in a logarithmic scale against chemical shift δ [ppm].

2.2 Aim

Our aim is to realize a measurement of the average aggregates size obtained from **longchain-DPP** and from **TEG-DPP** using DOSY NMR experiments, in order to compare this result with those obtained for the temperature-dependent UV-Vis spectral data and with that of the NMR titration described in a previous dissertation for **longchain-DPP**.

Following the DOSY-NMR study realized by Würthner's group and described in the last paragraph we synthesize two molecular references which have a nearly identical molecular mass (32 u.m.a of difference) and shape as **longchain-DPP** (described in paragraph 1.8) and **TEG-DPP** (described in paragraph 1.9) and not able to aggregate.

As molecular references **LC-DPP-Ref** and **TEGDPP-Ref** have been synthesized following the synthetic approach shown in Scheme 2.1.



Scheme 2.1 Synthetic strategy to obtain DOSY references.

The two references are unable to develop supramolecular polymers in solution because the N-methylation followed by hydrogenation prevent the monomer polymerization via hydrogen bonding and by π - π stacking. In this way, two molecules to carry out DOSY experiments and to complete the characterization of **longchain-DPP** and **TEG-DPP** are obtained.

2.3 Synthesis of DOSY references

Longchain-DPP protected with methyl groups was synthesized to obtain a molecule unable to interact by means hydrogen bonds. The molecule was prepared through a nucleophilic substitution between **longchain-DPP** and methyl iodide, using dry DMF and NaH, as base. The **methyl longchain-DPP** was obtained in good yields as a red oil, (Scheme 2.1, **16**). The **methyl longchain-DPP** was reduced in AcOEt with H₂ using Pd/C 5% to avoid π - π interactions. In this way **LC-DPP-Ref** was synthesized in good yields as a colourless oil (Scheme 2.1, **17**).

The same synthetic strategy was used to synthesize **TEG-DPP-Ref**: a nucleophilic substitution between **TEG-DPP** and methyl iodide in dry THF, using NaH as base, was performed, as shown in the Scheme 2.1. The crude product was purified by column chromatography, its spectrum is reported in Figure 2.11.

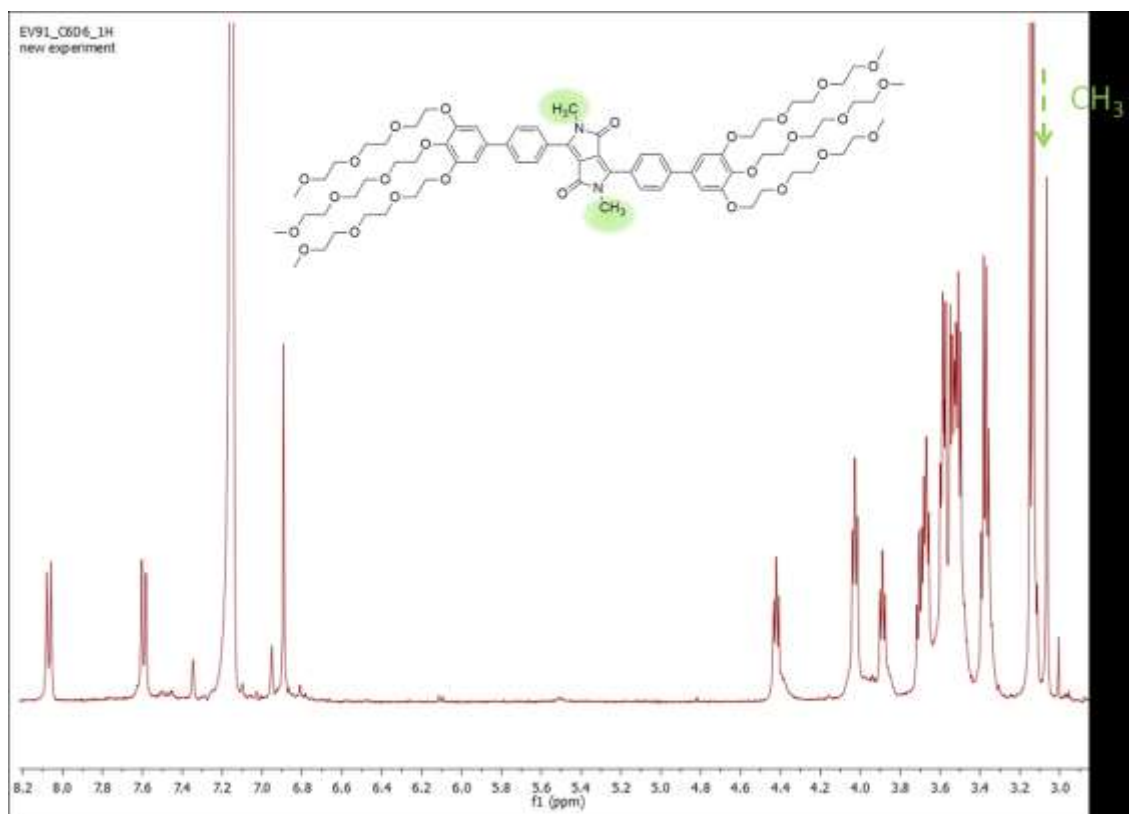


Figure 2.11 ¹H NMR spectrum recorded for **18** in CDCl₃.

Methyl TEG-DPP in MeOH was reduced using H₂ and Pd/C 5% as catalyst. The reduction of DPP core is an important step to avoid the formation of π - π interactions. Unfortunately we noticed that **TEG-DPP-Ref** is not enough soluble in water and for this reason we cannot use it to perform DOSY experiment.

2.3.1 Dosy characterization

According to Stoke Einstein Equation described in paragraph 2.1.1, the diffusion coefficient D of a molecular species is function of its shape and size, assuming a spherical size of the molecule. Thus, the size of two species could be compared through their diffusion coefficients, provided that the other parameters are identical.

The diffusion coefficients for **LC-DPP-Ref** and **longchain-DPP** are measured in CDCl_3 at a concentration of 1.21×10^{-2} M at 293 K, as shown in Figure 2.12. The values of diffusion coefficient found for **LC-DPP-Ref** and **longchain-DPP** are $D = 4.2 \times 10^{-9} \text{ m}^2 \text{ s}^{-1}$ and $D = 2.1 \times 10^{-9} \text{ m}^2 \text{ s}^{-1}$, respectively. The average size of the supramolecular polymers can be obtained by taking into account that the cube root of the molecular weight is proportional to D^{-1} .

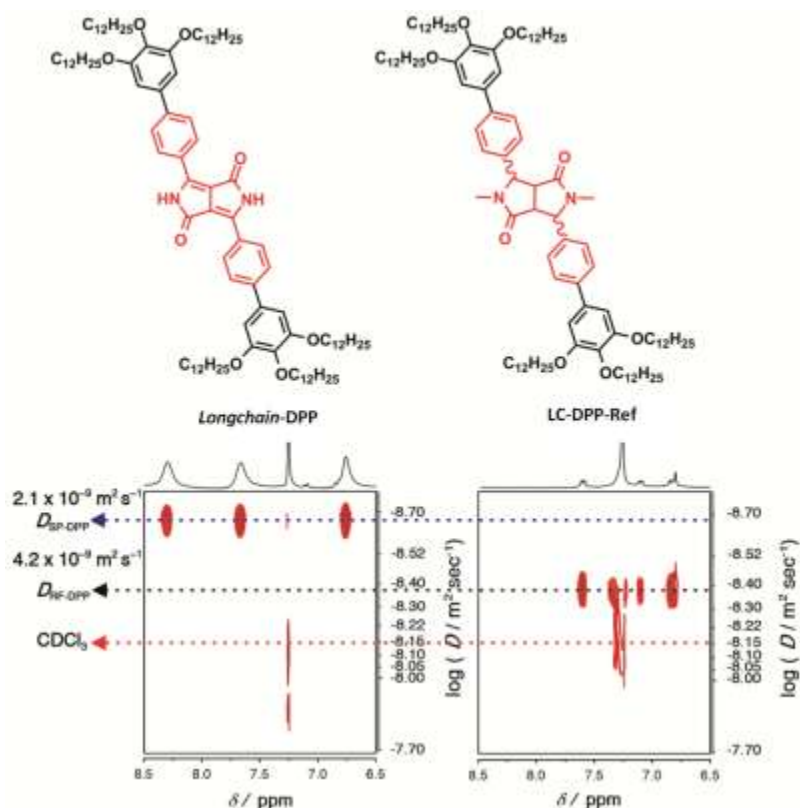


Figure 2.12 DOSY NMR spectra of **longchain-DPP** and **LC-DPP-REF** in CDCl_3 .

The result of the formula $DP_{\text{DOSY}} \approx [D(\text{LC-DPP-Ref}) / D(\text{longchain-DPP})]^3 = 8$ is in good agreement with previous NMR titrations experiments in the same solvent, as shown in Figure 2.13. The above formula holds true assuming that both size and molecular weight are approximately the same for **LC-DPP-Ref** ($\text{MW} = 1577.31 \text{ g mol}^{-1}$) and **longchain-DPP** ($\text{MW} = 1545.25 \text{ g mol}^{-1}$).

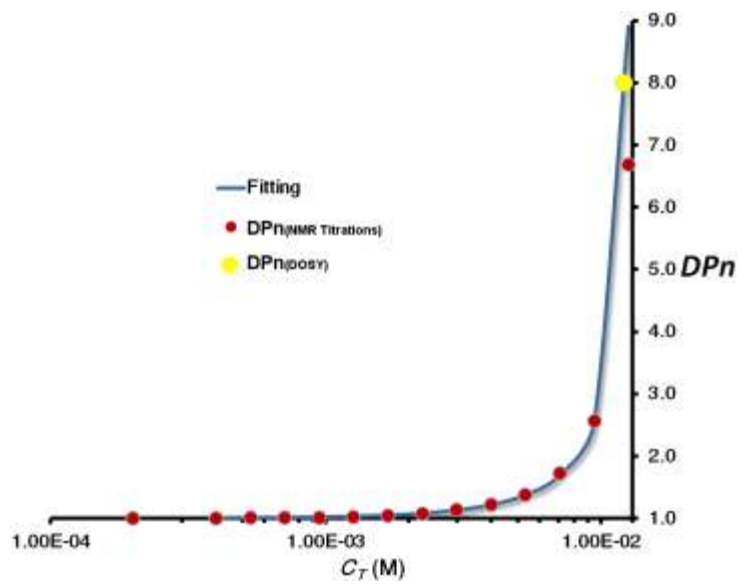


Figure 2.13 Comparison between NMR titrations experiments and DOSY result.

2.4 Conclusions

In summary in this chapter we have synthesized a **LC-DPP-Ref** unable to develop supramolecular interactions in solution and we have shown that DOSY NMR technique is a useful and reliable non-invasive spectroscopic method for the analysis of supramolecular species in solution.

This method can really discriminate among the differential diffusion of species having various hydrodynamic radii, even when there is only very small variations in their structures, thus potentially affording valuable information on constitutional dynamic systems.

As illustrated in paragraph 2.3.1 the value of $DP_{(DOSY)}$ for **longchain-DPP** appears comparable to the values obtained with other techniques, such as 1H -NMR and UV-Vis methods.

Unfortunately DOSY NMR technique has not been useful for the characterization of **TEG-DPP** because of the low solubility of **TEG-DPP-Ref** in water and consequently we could not obtain significant information about the shape and size of our aggregated species in solution.

2.5 Experimental Section

2.5.1 General

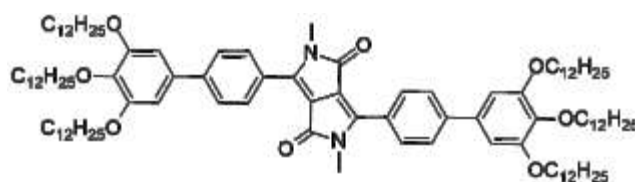
Solvents and reagents were used as purchased. Column chromatography was performed on silica gel MERK 60, 0.04-0.063 mm/230-400 mesh and thin layer chromatography (TLC) was conducted on Alugram silica gel UV₂₅₄ (Macherey-Nagel).

The 2D-DOSY spectrum was recorded with a Bruker AMX 300 spectrometer (1H = 300.15 MHz) equipped with a PABBO BB-1H Z GRD probe head. The pulse sequence used was ledbpgp2s 2D sequence for diffusion measurements using stimulated echo and LED using bipolar gradient pulses with two spoil gradients. The duration of the magnetic field pulse gradients (δ) and diffusion time (Δ) were 1 and 75 ms, respectively. The pulsed field gradients were incremented from 1 to 32 Gcm¹. A series of 32 spectra on 16000 data points were collected with 32 transients; the total measuring time was approximately 1 h. After Fourier transformation and baseline correction, the diffusion dimension was processed with the Bruker Xwin-NMR software package and MestreNova[®] software. In the experiments, gradients were calibrated against the HOD diffusion constant at 258C (D₂O (99.9% D) 19.0·10⁻¹⁰ m² s⁻¹). Spectra were measured at 258C with a 908 pulse duration of 8.3 ms and a relaxation delay of 5 s.

Maldi-TOF mass spectra was conducted in collaboration with the University of Namur.

2.5.2 Synthetic procedures

Synthesis of 2,5-dimethyl-3,6-bis(3',4',5'-tris(dodecyloxy)-[1,1'-biphenyl]-4-yl)pyrrolo[3,4-c]pyrrole-1,4(2H,5H)-dione, **16**, methyl *longchain*-DPP



16

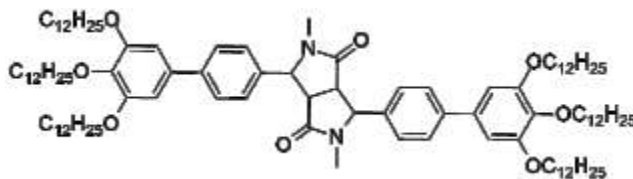
methyl *longchain*-DPP

A mixture of NaH (5 mg, 0.11 mmol) and compound **4** (50 mg, 0.03 mmol) in dry THF (10 mL) was stirred for 45 minutes at 35° C. Then methyl iodide (20 μ L, 0.32 mmol) was added. The reaction was stirred for a night at 35° C. After the solution was evaporated under vacuum, the crude was extracted with DCM. The combined extracts were dried over anhydrous MgSO₄ and evaporated under reduced pressure. The product **5** was obtained as a red solid (0.049 g, yield: 97 %).

¹H NMR (300 MHz, CDCl₃), δ (ppm): 8.00 (d, J = 8.5 Hz, 4H, H_{arom}), 7.74 (d, J = 9.0 Hz, 4H, H_{arom}), 6.83 (s, 4H, H_{arom}), 4.09-4.01 (m, 12H, OCH₂), 3.43 (s, 6H, OCH₂CH₂), 1.93-1.73 (m, 12H,

OCH₂CH₂), 1.55-1.19 (m, 108H, H_{aliph}), 0.89 (m, 18H, CH₂CH₃). ¹³C NMR (100 MHz, CDCl₃), δ (ppm): 199.15, 187.81, 181.38, 176.74, 165.69, 158.98, 155.87, 130.08, 90.81, 85.01, 48.16, 39.72, 37.85, 37.15, 36.96, 36.69, 36.57, 36.10, 32.46, 28.80, 18.08, 14.41. PM (C₁₀₄H₁₆₈N₂O₈): 1574,46 u.

Synthesis of 2,5-dimethyl-3,6-bis(3',4',5'-tris(dodecyloxy)-[1,1'-biphenyl]-4-yl)tetrahydropyrrolo[3,4-c]pyrrole-1,4(2H,5H)-dione, 17, LC-DPP-Ref

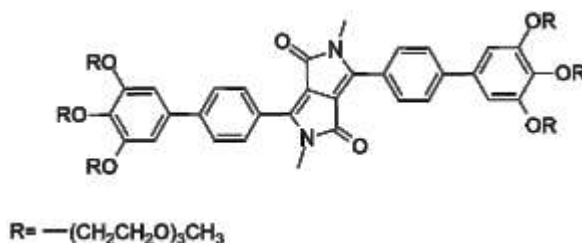


17
LC-DPP-Ref

A mixture of compound **5** (50 mg, 0.031 mmol) and a catalytic amount of Pd/C in AcOEt (10mL) was stirred under hydrogen for a night at room temperature. The solution was filtered and evaporated under reduced pressure. The pure product was obtained as a colourless oil (48 mg, yield: 97 %).

¹H NMR (CDCl₃, 400 MHz), δ(ppm): 7.61 (d, *J* = 8.5 Hz, 4H, H_{arom}), 7.29 (d, *J* = 8.5 Hz, 4H, H_{arom}), 6.81 (s, 4H, H_{arom}), 4.95-4.87 (m, 2H, OCCH), 4.09-3.98 (m, 12H, OCH₂), 3.73-3.78 (m, 2H, NCH), 2.62 (s, 6H, NCH₃), 1.89-1.55 (m, 12H, H_{aliph}), 1.74-1.45 (m, 18H, H_{aliph}), 1.40-1.18 (m, 90 H, H_{aliph}), 0.92-0.86 (m, 18H, CH₂CH₃). ¹³C NMR (100 MHz, CDCl₃), δ (ppm): 172.06, 153.83, 142.18, 136.46, 134.76, 131.36, 127.59, 106.57, 74.05, 69.87, 68.69, 65.21, 45.00, 32.38, 30.77, 30.09, 29.84, 29.75, 26.54, 23.23, 14.50, 11.40. PM (C₁₀₄H₁₇₂N₂O₈): 1578.49 u.

Synthesis of 2,5-dimethyl-3,6-bis(3',4',5'-tris(2-(2-(2-methoxyethoxy)ethoxy)ethoxy)-[1,1'-biphenyl]-4-yl)pyrrolo[3,4-c]pyrrole-1,4(2H,5H)-dione, 18, methyl TEG-DPP



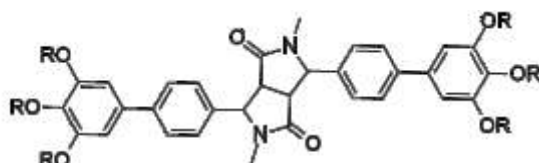
18
methyl TEG-DPP

A mixture of NaH (5 mg, 0.12 mmol), compound **TEG-DPP** (50 mg, 0.03 mmol) in dry THF (11 mL) was stirred for 45 minutes at 35° C. Then methyl iodide (23 μL, 0.37 mmol) was added.

The reaction was stirred for a night at 35° C. After the solution was evaporated under vacuum, the crude was extracted with DCM. The combined extracts were dried over anhydrous MgSO₄ and evaporated under reduced pressure. The crude was purified by column chromatography (DCM:MeOH, 9:1). The product **7** was obtained as a red solid (0.043 g, yield: 86 %).

¹H NMR (400 MHz, D₆C₆), δ (ppm): 8.07 (d, *J* = 8.4 Hz, 4H, H_{arom}), 7.59 (d, *J* = 8.4 Hz, 4H, H_{arom}), 6.95 (s, 4H, H_{arom}), 4.42 (t, *J* = 7.5 Hz, 12H, OCH₂), 4.03 (t, *J* = 7.2 Hz, 8H, OCH₂CH₂), 3.89 (t, *J* = 7.5 Hz, 4H, OCH₂CH₂), 3.71-3.47 (m, 36H, H_{TEG}), 3.41-3.35 (m, 12H, H_{TEG}), 3.15-3.11 (s+s, 18H, H_{TEG}), 3.06 (s, 6H, NCH₃). PM (C₇₄H₁₀₈N₂O₂₆): 1441,65 u.

Synthesis of 2,5-dimethyl-3,6-bis(3',4',5'-tris(2-(2-(2-methoxyethoxy)ethoxy)ethoxy)-[1,1'-biphenyl]-4-yl)tetrahydropyrrolo[3,4-c]pyrrole-1,4(2H,5H)-dione, 19, TEG-DPP-Ref



19

TEG-DPP-Ref

A mixture of compound **7** (50 mg, 0.034 mmol) and a catalytic amount of Pd/C in AcOEt (10mL) was stirred under hydrogen for a night at room temperature. The solution was filtered and evaporated under reduced pressure. The pure product was obtained as a colourless oil (45 mg, yield: 93 %). PM (C₁₀₄H₁₇₂N₂O₈): 1578.49 u.

¹H NMR (400 MHz, CDCl₃), δ (ppm): 7.60 (d, *J* = 8.3 Hz, 4H, H_{arom}), 7.28 (d, *J* = 8.4 Hz, 4H, H_{arom}), 6.86 (s, 4H, H_{arom}), 4.90-4.88 (m, 2H, CCHC), 4.30-4.17 (m, 14H, OCH₂+ CCHN), 3.89 (t, *J* = 4.5 Hz, 8H, OCH₂CH₂), 3.81 (d, *J* = 4.6 Hz, 4H, OCH₂CH₂), 3.76-3.64 (m, 36H, H_{TEG}), 3.56-3.53 (m, 12, H_{TEG}), 3.38-3.37 (s+s, 18H, CH₂CH₃), 2.61 (s, 6H, NCH₃). PM (C₇₄H₁₁₂N₂O₂₆): 1445,68 u.

¹ <http://nmr.chemistry.manchester.ac.uk/>

² (a) Bardley, W. G., *Magnetic Resonance Imaging*, 2nd ed., Mosby Company, St. Louis, **1992**; (b) *Methods of Magnetic Resonance Imaging and Spectroscopy* (Ed.: I. R. Young), Wiley, Chichester, **2000**; (c) *Perfusion and Diffusion Magnetic Resonance Imaging: Applications to functional MRI* (Ed.: D. Le Bihan), Raven Press, New York, **1995**; (d) Moseley, M. E., Cohen, Y., Mintorovitch, J., Chileuitt, L., Shimizu, H., Kucharczyk, J., Wendland, M. F., Weinstein, P. R., *Magn. Reson. Med.* **1990**, *16*, 330 – 346; (e) Basser, P. J., *NMR Biomed.* **1995**, *8*, 333 – 344; Basser, P. J., Mattiello, J., Le Bihan, D., *Biophys. J.* **1994**, *66*, 259 – 267.

³ C.S. Johnson / *Progress in Nuclear Magnetic Resonance Spectroscopy*, **1999**, *34*, 203–256

⁴ (a) Crank, J., *The Mathematics of Diffusion*, 2nd ed., Clarendon Press, Oxford, 1975; (b) Cussler, E. L., *Diffusion: Mass Transfer in Fluid Systems*, Cambridge University Press, Cambridge, **1984**.

⁵ Einstein, A., *Ann. Phys.* **1906**, *19*, 289 – 306.

⁶ Cohen, Y., Avram, L., Frish, L. *Angew. Chem. Int. Ed.* **2005**, *44*, 520 – 554

⁷ Gounarides, J. S., Chen, A., Shapiro, M. J., *J. Chromatogr. B* **1999**, *725*, 79 – 90.

⁸ Johnson, C. S., Jr., *Prog. Nucl. Magn. Reson. Spectrosc.* **1999**, *34*, 203 – 256.

⁹ Garozzo, D., Gattuso, G., Notti, A., Pappalardo, A., Pappalardo, S., Parisi, M. F., Perez, M., Pisagatti, I., *Angew. Chem.* **2005**, *117*, 4970 – 4974; *Angew. Chem. Int. Ed.* **2005**, *44*, 4892 – 4896.

¹⁰ Pappalardo, S., Villari, V., Slovak, S., Cohen, Y., Gattuso, G., Notti, A., Pappalardo, A., Pisagatti, I., Parisi, M. F., *Chem. Eur. J.* **2007**, *13*, 8164 – 8173.

¹¹ Capici, C., Cohen, Y., D'Urso, A., Gattuso, G., Notti, A., Pappalardo, A., Pappalardo, S., Parisi, M. F., Purrello, R., Slovak, S., Villari, V., *Angew. Chem. Int. Ed.* **2011**, *50*, 11956 – 11961.

¹² Haino, T., Watanabe, A., Hirao, T., Ikeda, T., *Angew. Chem., Int. Ed.*, **2012**, *51*, 1473.

¹³ Schmidt, R., Stolte, M., Grüne, M., Würthner, F., *Macromolecules*, **2011**, *44*, 3766 – 3776.

¹⁴ Li, S., Xiao, T., Hu, B., Zhang, Y., Zhao, F., Ji, Y., Yu, Y., Lin, C., Wang, L., *Chem. Commun.*, 2011, *47*, 10755.

¹⁵ (a) Yan, X., Zhou, M., Chen, J., Chi, X., Dong, S., Zhang, M., Ding, X., Yu, Y., Shao, S., Huang, F., *Chem. Commun.*, **2011**, *47*, 7086–7088; (b) Ohkawa, H., Takayama, A., Nakajima, S., Nishide, H., *Org. Lett.*, **2006**, *8*, 2225–2228; (c) Keizer, H.M., Gonzalez, J. J., Segura, M., Prados, P., Sijbesma, R. P., Meijer, E. W., Mendoza J. D., *Chem.–Eur. J.*, **2005**, *11*, 4602–4608; (d) Folmer, B. J. B., Sijbesma, R. P., Meijer, E. W., *J. Am. Chem. Soc.*, **2001**, *123*, 2093–2094.

3 Liquid Crystals based on DPPs

3.1 Dendritic architecture

Dendritic architecture is one of the most common topologies observed in nature at the macro- and micro-dimensional length scales.¹ At the nanoscale (nm) the most notable dendritic molecules in biological system are glycogen and amylopectin (Figure 3.1), hyperbranched structures that nature uses for energy storage.

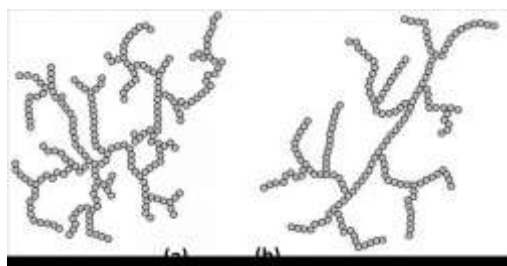


Figure 3.1 Glycogen (a) and amylopectin (b).

At the macro scale we can observe trees (metres), fungi (millimeters/centimeters) and neurons (microns), as illustrated in Figure 3.2.

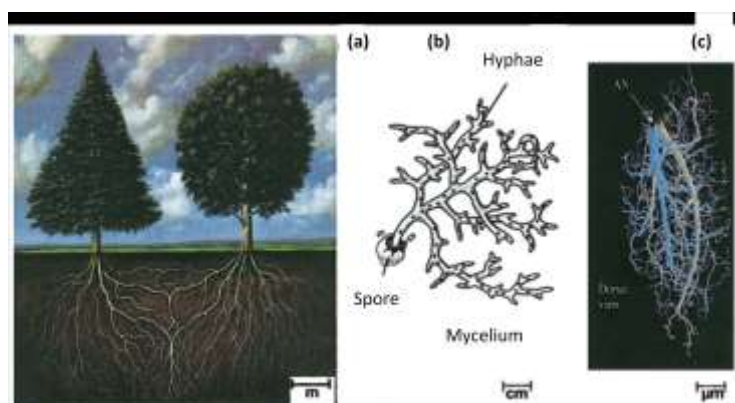


Figure 3.2 Coniferous trees with root systems (a), fungal anatomy (b) and root's detail (c).

The first inspiration for synthesizing such molecular level tree-like structures evolved from a lifetime hobby of the chemist D. A. Tomalia and he also used for the first time the word dendrimer associated with a molecular structure.²

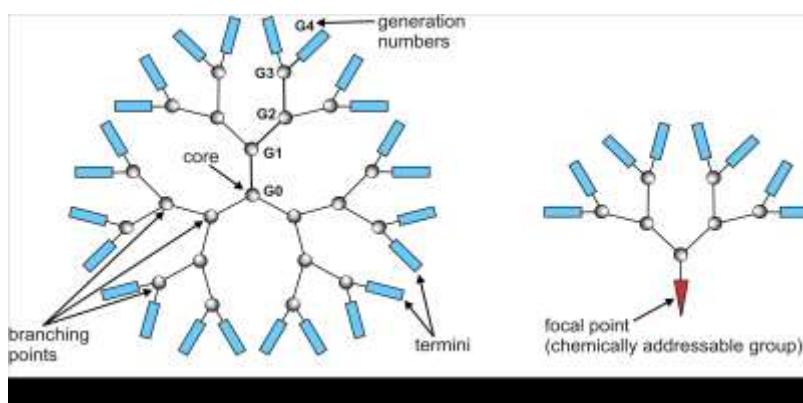


Figure 3.3 Dendrimer (a); dendron (b).

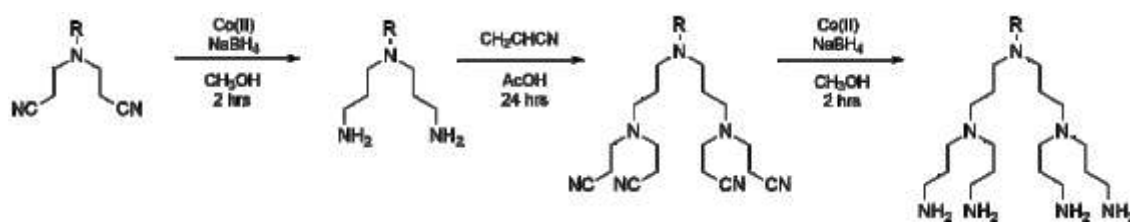
At the state of the art dendrimers stand for a new class of polymeric materials.³ Their structure, shown in Figure 3.3, comprises three major portions: a core or focal point, the branching points and chain ends. These three portions can have different functionalities able to control their physical and chemical properties, as solubility, thermal stability and reactivity. With the just synthetic approach is possible to control the size and the number of branches on the dendrimer, even if the growth of dendrimers is limited in the space for steric reasons.⁴

3.2 Dendrimers: design and synthesis

The first studies about branched structure start in the late 1860's, when these macromolecules are considered as being responsible for insoluble and intractable materials formed in polymerization reactions.

A century later, in 1950, Flory⁵ examined the potential role of branched units in macromolecular architectures, but at this stage branched structures are still considered primarily from a theoretical vantage point with initial attempts at preparation via classical, or single spot, polymerization of functionally differentiated monomers.

The modern era of dendrimer chemistry came to life when Vögtle, in 1978, published "Cascade and Nonskid-Chain-like Synthesis of Molecular Cavity Topologies".⁶ In this paper he described an iterative cascade method for the synthesis of low molecular weight branched amines, shown in Scheme 3.1.



Scheme 3.1 First dendrimer synthesized by Vögtle.

'Cascade' synthesis means reaction sequences whereby a functional group is made to react in such a way as to appear twice in the subsequent molecule. In particular, Vögtle described a sequence comprising two procedures: alkylation and reduction. Therefore, treatment of a diamine with acrylonitrile afforded tetranitrile. Cobalt-mediated nitrile reduction gave tetraamine. Further amine alkylation provided the second generation octanitrile. Again another reduction gave the second generation octaamine.⁷

Few years later, in 1984, Tomalia and his group managed to synthesize and characterize the first family of dendrimers. The synthesis initiated by Michael addition of a "core" molecule of ammonia to three molecules of methyl acrylate, followed by exhaustive amidation of the trimer adduct using a large excess of ethylenediamine, a process that generates a molecule with six terminal amine groups. Iterative growth is then continued using alternating Michael addition and amidation steps with the appropriate excess of reagents. With this method is possible to synthesize poly(amidoamine) dendrimers (PAMAM) with molecular weight well above 25000 and moreover this PAMAM core-shell architecture grows linearly in diameter as a function of added generations.⁸ In Figure 3.4, the first PAMAM synthesized by Tomalia is reported.

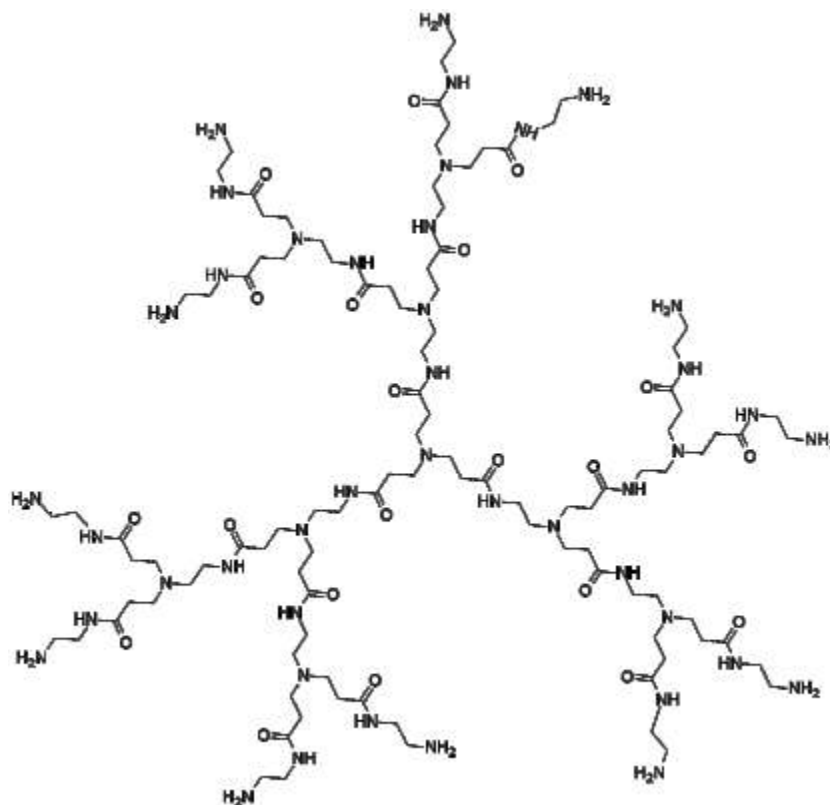


Figure 3.4 First PAMAM with ammonium core synthesized by Tomalia et al.

In 1985, Newkome synthesized a new family of trisbranched polyamide dendrimers,⁹ and in 1993 Meijer and Mulhaupt improved Vögtle original synthesis to obtain poly(propylene imine) dendrimers (PPI), an example is reported in Figure 3.5.

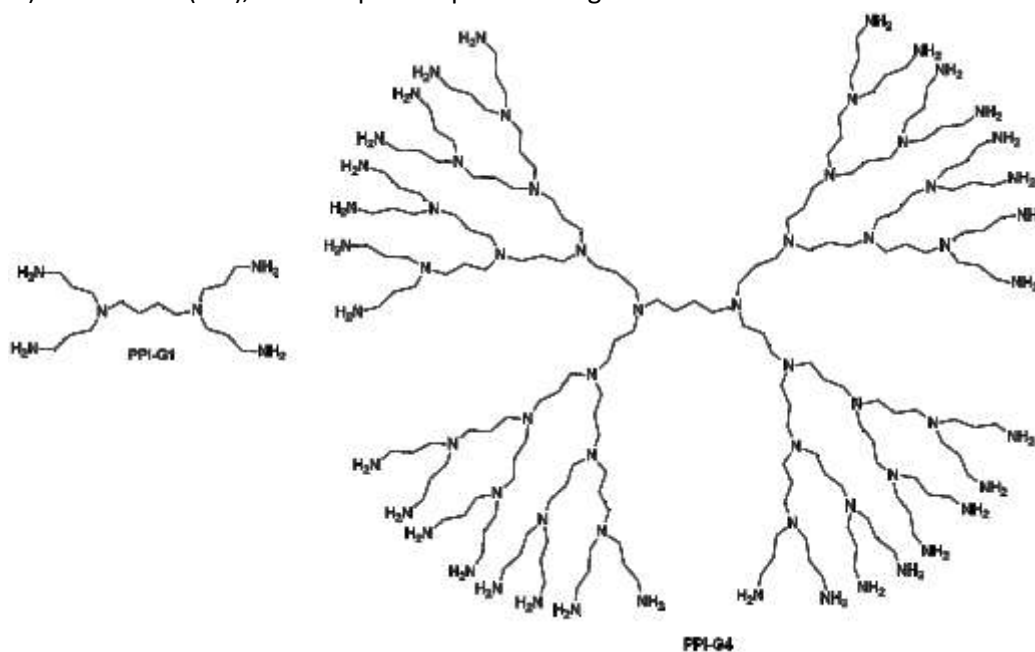


Figure 3.5 Poly(propylene)imines (PPI) structure.

In 1989-1990, Hawker and Fréchet introduced the convergent growth approach to dendrimers, the second general route to dendritic structures.¹⁰

Actually poly(amido)amines (PAMAM) and poly(propylene)imines (PPI) are the most common classes of synthesized dendrimers. These classes are available until the fifth generations and they are characterized by primary amines and azotetes branches.

The important properties of dendrimers, such as their high degree of branching, multivalency, monodispersity, globular architecture and well-defined molecular weight, make them promising in different technical fields, as shown in Figure 3.6. The most popular studies are about controlled drug delivery,¹¹ magnetic resonance imaging,¹² catalysis,¹³ sensors¹⁴ coatings,¹⁵ anthrax detection agent,¹⁶ gene therapy or gene transfection.¹⁷

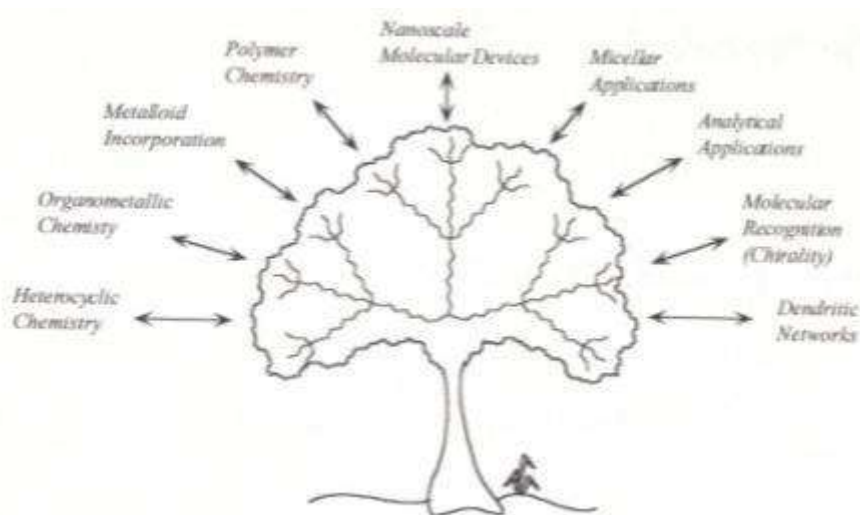


Figure 3.6 Areas of material science that have benefited from dendritic chemistry.

3.2.1 Synthetic Methodologies

Dendrimers can be synthesized by two complementary synthetic approaches: the convergent and the divergent method.¹⁸

a. Divergent Method

Divergent growth¹⁹ starts with the multifunctional core molecule and then by the repetition of coupling and activation steps the dendrimer is assembled, as displayed in Figure 3.7. This method allows to synthesize big molecules quickly, but the correct growth of the dendrimer at each step must be verified to prevent mistakes in the final structure.

Vögtle synthesized the first dendrimer with this approach in 1978.

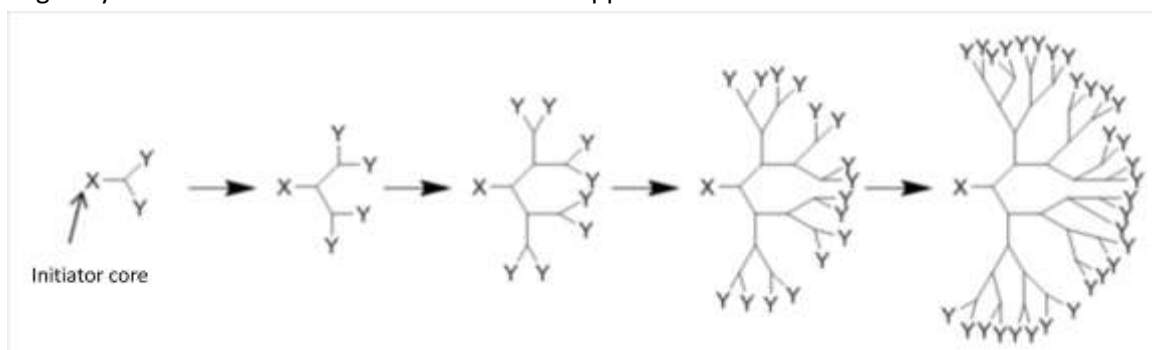


Figure 3.7 Divergent synthesis scheme.

b. Convergent Procedures

Convergent growth starts with what will become the eventual periphery of the macromolecule and proceeds inward through the core, as shown in Figure 3.8. With this approach the reactions need only a slight excess of reagent to completion and product purification is facilitated by the small number of components in the reaction mixture. Moreover, the convergent growth allows a best control over functionality at the specified positions of the growing molecules and it provides access to a lot of innovative architectures through the reactions of dendron with other molecules.

This innovative method was introduced by Fréchet and Hawker in 1990 when they synthesized the first dendrimer of sixth generations.

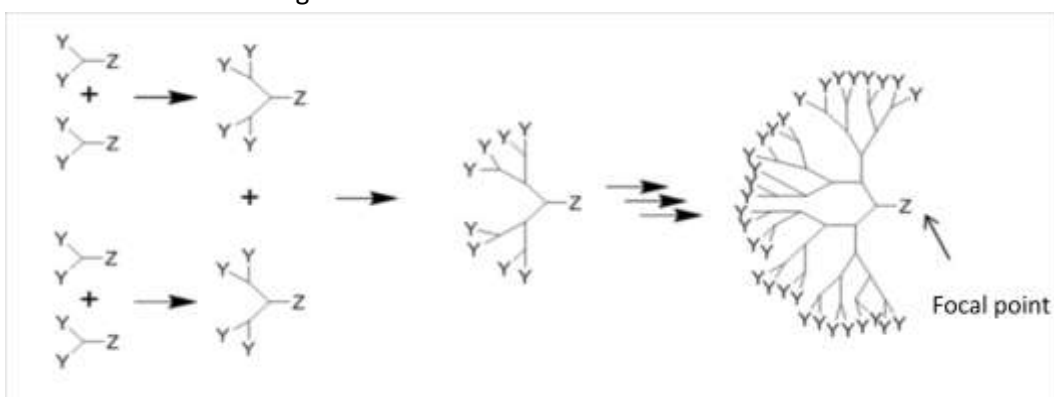


Figure 3.8 Convergent synthesis scheme.

However, the convergent procedure has also its weakness: steric hindrance affects the convergent synthesis more than divergent method. The highest generation ever obtained using the convergent strategy rises to the sixth generation, whereas with the divergent method Tomalia goes up to the ninth generation of polyamide.²⁰

3.3 Liquid Crystals

In the last decade the structural organization of different types of dendritic systems that form liquid crystalline mesophases have been analysed with special emphasis. As described below PAMAM and PPI develop calamitic mesophases.

The liquid crystal state is a special state of matter comprised between the solid state and the liquid state, as shown in Figure 3.9. In this phase we observe different degree of orientation, anisotropy (like crystal) and fluid properties, like liquids. The order of liquid crystals can be manipulated with mechanical, magnetic or electric forces.

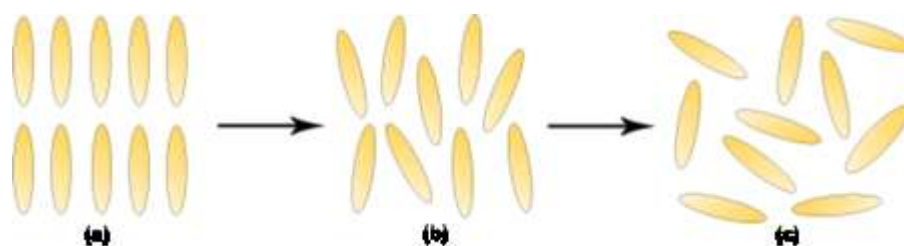


Figure 3.9 State of matter: crystal (a); liquid-crystalline phase (b) and liquid (c).

Molecules that can generate liquid crystal are called mesogens, while the liquid crystal phase is called mesophase or mesomorphic phase (mesos, gr: middle; morphe: shape).

The mesophase can be induced by temperature (thermotropic LCs) or by solvation (lyotropic LCs).²¹

The thermotropic LCs are usually constituted by anisotropic molecules, either elongated or disk-like. These molecules usually have high molecular weights and comprise two parts: a rigid central core (generally an aromatic system) and a flexible tail (often an aliphatic group). The elongated or rod-like molecules form calamitic LCs, as shown in Figure 3.10, (a), while disk-like molecules form discotic LCs, as displayed in Figure 3.10, (b).

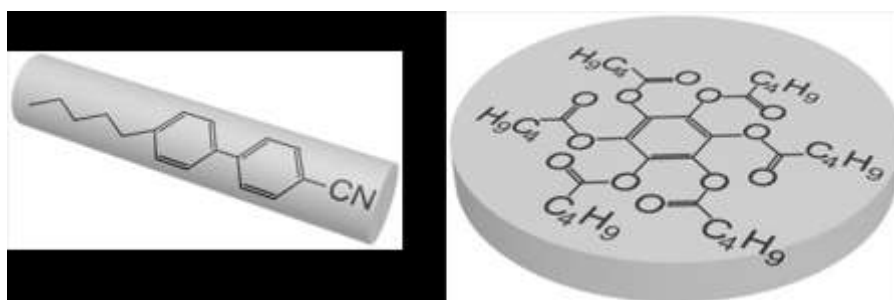


Figure 3.10 Thermotropic LCs: calamitic structure (a) and discotic structure, (b).

The lyotropic LCs feature more complex systems in which an amphiphilic compound is dissolved in a solvent. In particular the amphiphilic compound comprises two distinct parts: a hydrophilic polar head and a hydrophobic non polar tail, as displayed in Figure 3.11.

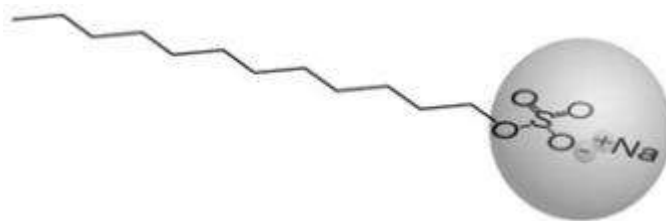


Figure 3.11 Lyotropic LC.

Three methods are mainly used for the investigations and characterization of LC materials²²:

1. differential scanning calorimetry (DSC), that provides the phase-transition temperatures and associated enthalpy values;
2. polarizing optic microscopy (POM);
3. X-ray diffraction (XRD) analysis, to obtain information about the kind of order in the mesophase.

In the next paragraphs we will describe the mesophase formed by calamitic and discotic mesogens.²³

3.3.1 Mesophase of calamitic mesogens

Calamitic mesogens show nematic, cholesteric and smectic mesophases.

In the nematic phase (the word nematic comes from Greek, *nema-nemata* that means thread) LCs have one directional order (1D): they exhibit parallel molecular axes but molecular centres are not oriented, as show in Figure 3.12, **(b)**. This phase has a relatively low viscosity and they can be deformed by weak external forces.

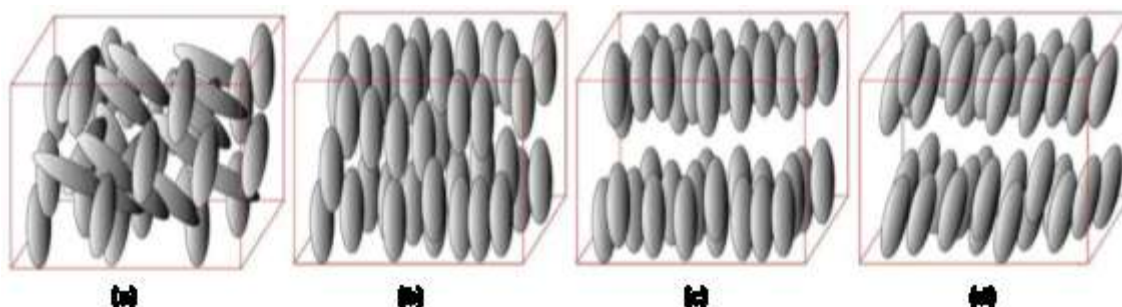


Figure 3.12 Thermotropic LC phase: **(a)** isotropic liquid phase, **(b)** nematic phase, **(c)** smA phase, **(d)** smC phase.

In the smectic phase (from Greek *smektos*, that means smeared) the LCs have two directional orders (2D): they show parallel molecular axes and molecule centres are oriented in the layers. In particular in *smectic A* (SmA) phases, the molecules are parallel to one another and are arranged in layers, with the long axes perpendicular to the layer plane, as shown in Figure 3.12, **(c)**. In contrast, in smectic C (SmC) phases the molecules are always arranged in layers, but the long axes of the molecules are tilted to the layers planes, as displayed in Figure 3.12, **(d)**. Usually, mesogenic molecules with terminal alkyl or alkoxy chains tend to give smectic phases.

In the nematic chiral phase or *cholesteric* phase, N^* , chiral molecules cause a twist in the nematic structure. In this phase individual directors are turned by a fixed angle on proceeding from one layer to the next, as shown in Figure 3.13.

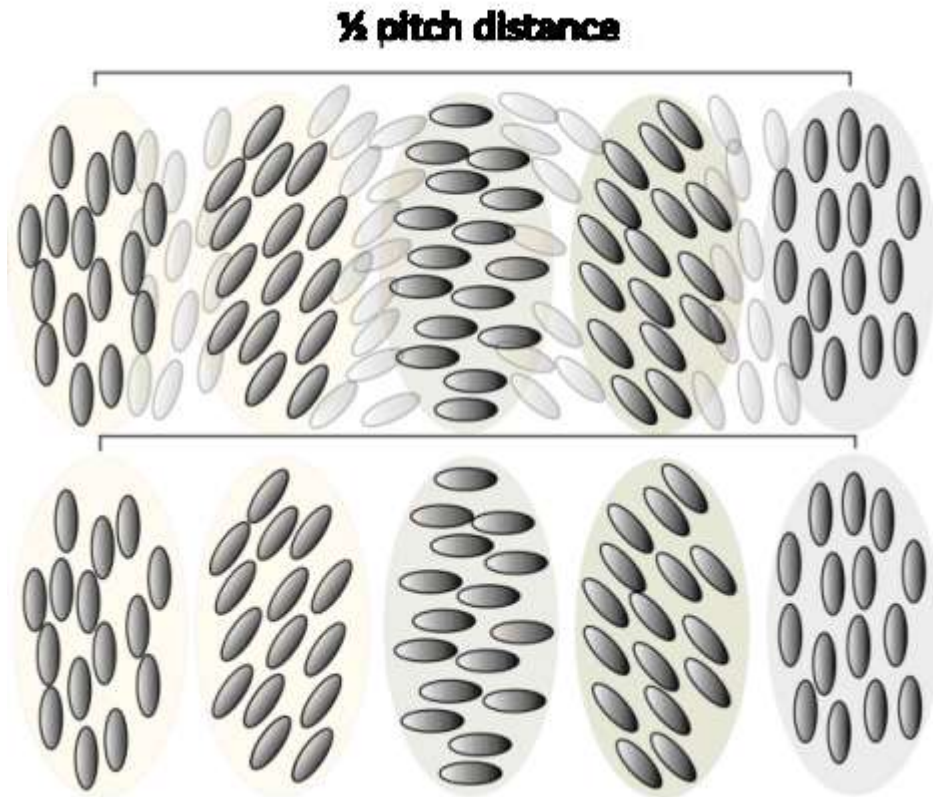


Figure 3.13 Schematic representation of a cholesteric phase, N^* .

In particular in the SmC^* phase, chiral molecules develop a helicoidal structure that is perpendicular to the layers, as shown in Figure 3.14. In contrast for the SmA^* phase the bend and twist deformations of the director field in the structure are prohibited.

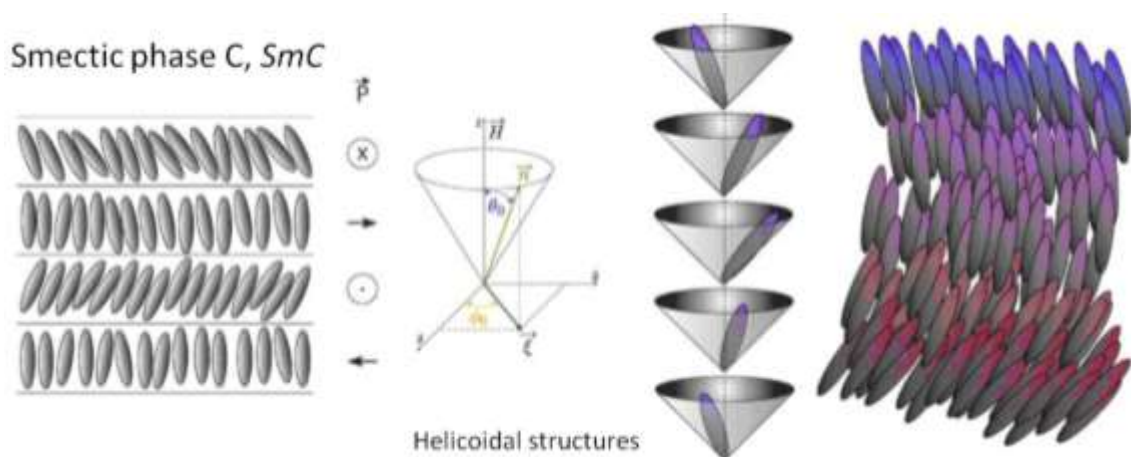


Figure 3.14 Schematic representation of a SmC^* phase and of the helicoidal structure that these mesogens can develop.

Figure 3.15 displays the typical textures of calamitic phase described before: **(a)** nematic phase, **(b)** SmA phase, **(c)** SmC phase and **(d)** N^* phase.

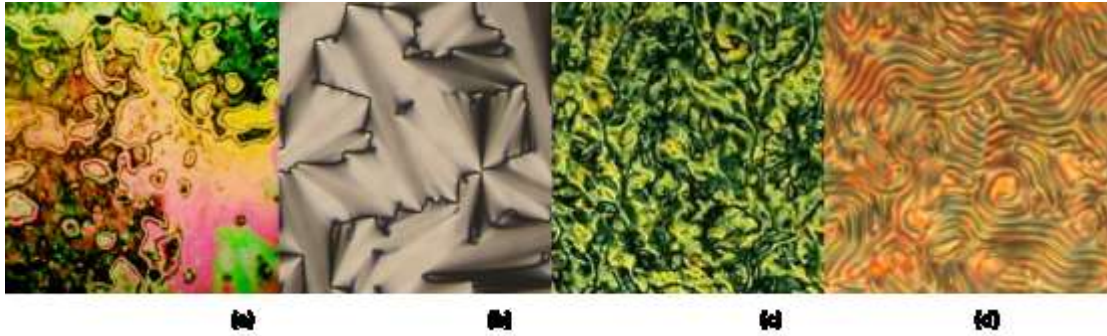


Figure 3.15 Calamitic mesophase observed at POM: (a) nematic phase, (b) SmA phase, (c) SmC phase and (d) N* phase.

3.3.2 Mesophase of Discotic mesogens

Discotic mesogens show nematic, columnar and cubic phases.

The nematic phase, generated by discotic mesogens, consists of an arrangement of disk-like molecules but with no long-range translational order, as shown in Figure 3.16, (a). Differently, columnar phases are obtained by packing of disc like molecules into columns and they are characterized by the symmetry of the arrangement, for example hexagonal (Col_h), rectangular (Col_r), square (Col_s) or oblique (Col_o). In Figure 3.16, (b), we report an example of columnar hexagonal phase.

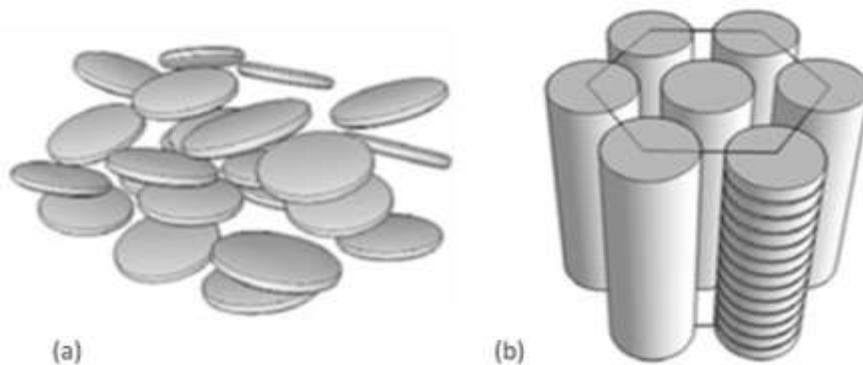


Figure 3.16 Discotic mesophase: (a) nematic phase and (b) hexagonal columnar phase.

The cubic phase stands for the most ordered systems. Different cubic phases are defined by the symmetry of the cubic mesh, as shown in Figure 3.17.

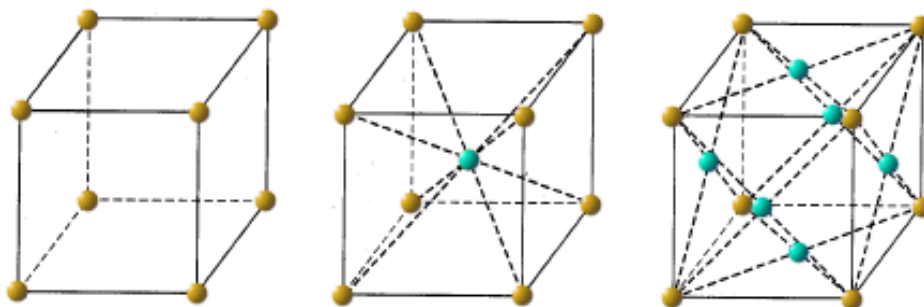


Figure 3.17 Cubic mesh.

Figure 3.18 reports the typical textures of discotic phase described before: **(a)** nematic phase and an example of hexagonal columnar phase **(b)**.

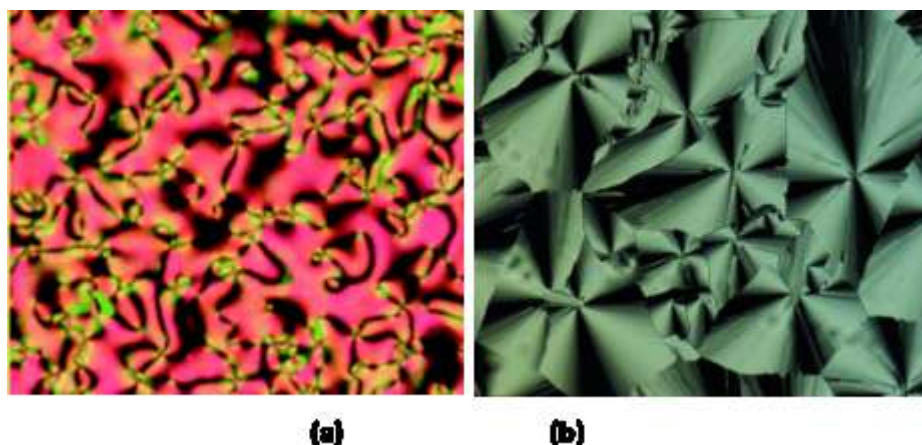


Figure 3.18 Discotic mesophase observed at POM: **(a)** nematic phase and **(b)** hexagonal columnar phase.

All the described LC systems are nowadays very common in everyday life. The most important use is in display devices (LCD). These are produced in huge numbers and used for various applications such as calculators, watches, mobile phones or computers and televisions displays. These common LCD's are usually built with calamitic liquid crystals.²⁴ The field of discotic mesogens and columnar LC phases has developed into a broad field.²⁵ Presently columnar phases formed by molecules with p-conjugated disc-like cores are a promising group of materials for organic semiconductors and photoconductors, field-effect transistors and for photovoltaic applications.²⁶

3.4 Liquid-Crystal dendrimers

Liquid-crystal dendrimers allow combining mesomorphic properties of LC materials, described in paragraph 3.3, to the particular structure of dendrimers, described in paragraph 3.2. LC dendrimers can be considered as block of molecules in which the dendritic core and the functionalised terminal groups will tend to microphase separation due to their incompatible chemical nature. For this reason the mesomorphic properties, such as phase type, transition temperature and thermodynamic stability are highly depend on the enthalpy/entropy balance, the degree of the chemical incompatibility and the size of the different building block. In general the terminal units determine the nature of the mesomorphism of the entire compound and the dendritic architecture is used only as the scaffold.²⁷

LC dendrimers are subdivided into three classes:

1. LC dendrimers with terminal mesogens;
2. Main chain LC dendrimers;
3. Intrinsic dendromesogens.

In the next paragraphs we will describe the principal features of these three classes.

3.4.1 LC dendrimers with terminal mesogens

In these systems mesogenic groups are found on the periphery of a dendritic molecule or laterally attached. Three structural elements can be distinguished in this kind of substrate, as shown in Figure 3.19: (1) mesogenic group; (2) aliphatic spacer and (3) polymer chain.²⁸

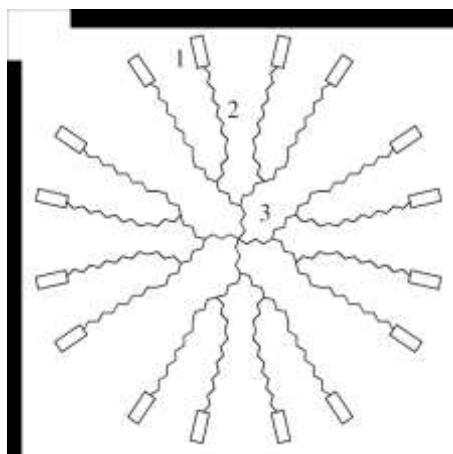


Figure 3.19 Schematic representation of LC dendrimers with terminal mesogens.

The mesophases formed from these structures are influenced by numerous factors, such as the kind of mesogens attached to the peripheral groups, the flexibility of dendritic network and its tendency to adopt a globular isotropic conformation. Moreover, the supramolecular organization of LC dendrimers is function of the dendrimer generation.

Poly(propyleneimine) (PPI) is an important example of LC dendrimers belonged to this subclass. Mejer et al.²⁹ described two series of PPI dendrimers functionalised with pentyloxy

and decyloxy cyanobiphenyl mesogens at the periphery, as shown in Figure 3.20. The dendrimer with the pentyl spacer showed liquid crystal phase between the glass transition temperature and the isotropic liquid. The dendrimer with decyloxy spacer also showed liquid crystalline behaviour, but with the presence of a crystalline or semi-crystalline state at low temperature and with higher transitions temperature, probably due to efficient hydrogen bonding network in the dendritic part. X-ray diffraction analysis showed that all the mesomorphes observed are SmA phase. In Figure 3.20, we report the schematic representation of PPI SmA phase.³⁰

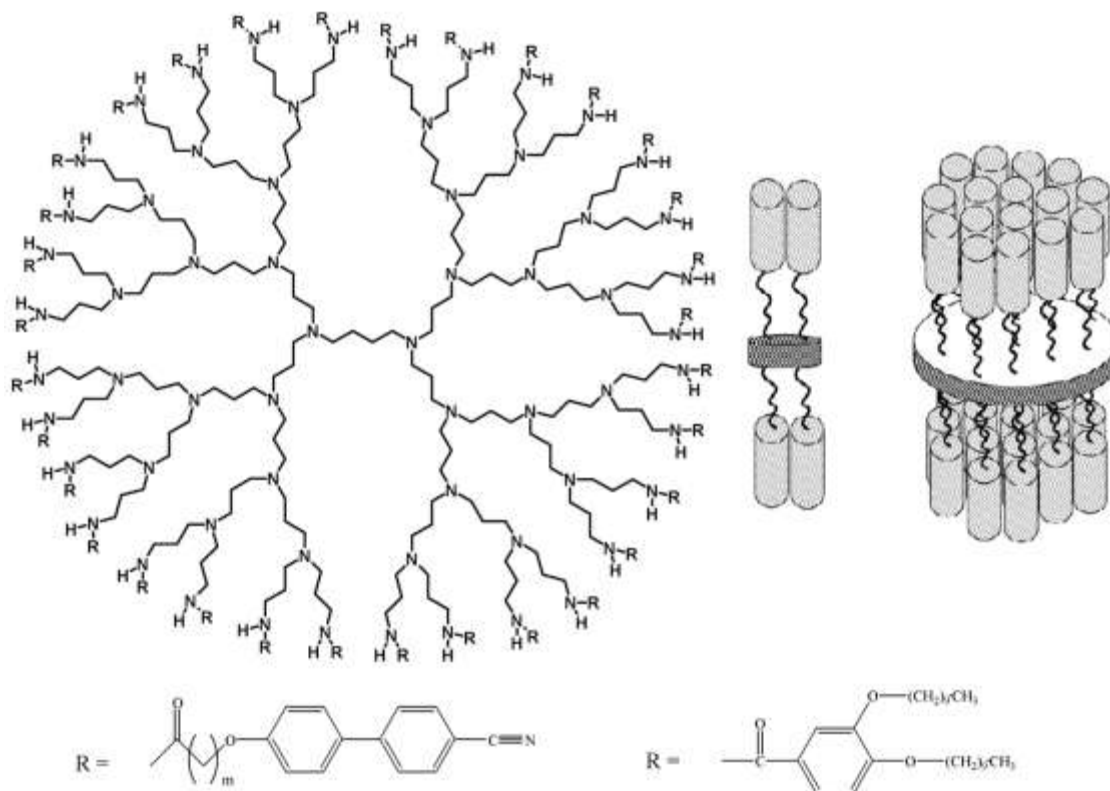


Figure 3.20 PPI dendrimers with a terminal mesogenic groups and PPI Smectic A phase. The disks stand for the dendritic part, the wavy lines for the aliphatic spacer and the cylinders for the mesogenic moieties.

Polyamidoamine (PAMAM) LC dendrimers³¹ is another important example: its dendritic motif, shown in Figure 3.20, is the same as that of PPI dendrimers. In this structure the microphase separation between the mesogenic rigid unit and flexible dendritic skeleton leads to formation of smectic phases.

3.4.2 Main chain liquid crystal dendrimers

In contrast to LC dendrimers with terminal mesogens, in which the junctions are consisting of single atoms, main chain liquid crystalline dendrimers contain anisotropic molecular moieties at every branching points. For this reason molecular architectures possess less conformational freedom and the presence of these anisotropic segments forces the dendrimer to adopt more extended conformation. Conformational restriction occurs due to squeezing of the dendritic part within the peripheral cell.

B. Donnio et al.³² have synthesized main chain LC dendrimers with homolithic systems containing building blocks of identical dendritic branches and heterolithic systems with different anisotropic cores. These blocks were formed by tolane and stilbene units, that have not mesomorphic properties; in Figure 3.21 we report two of the final structure that they have synthesized by convergent/divergent approach.

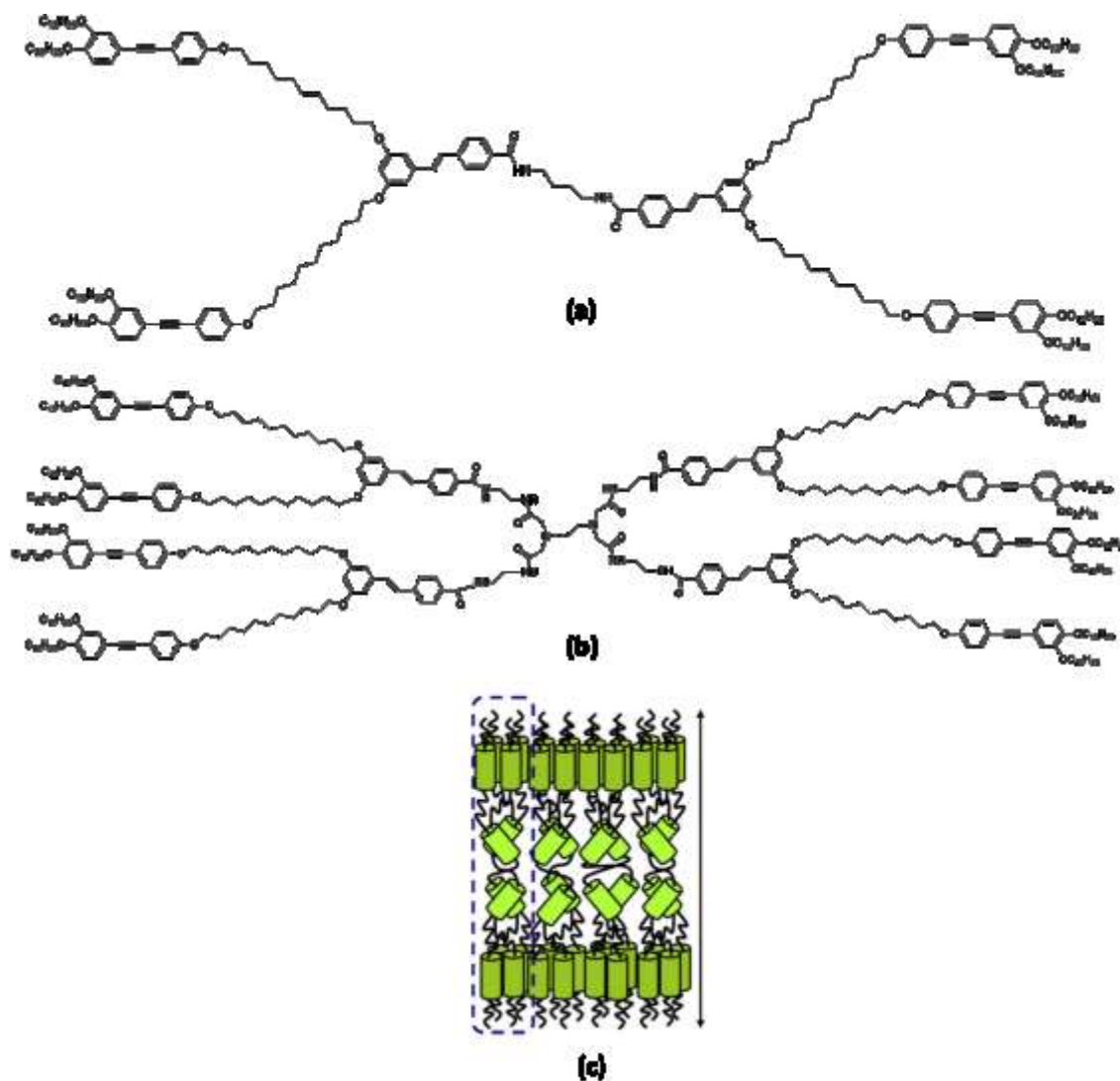


Figure 3.21 Main chain LC dendrimers: (a) homolithic structure, (b) alternate heterolithic system, (c) schematic representation of the multilayer formed by (b).

Main chain LC dendrimers with eight functional arms are also known as ‘octopus dendrimer’. Depending on the chain substitution pattern of the terminal units, octopus dendrimers with terminal mesogenic groups may feature smectic mesomorphism or columnar mesophase. The morphology of these main chain LC dendrimers include homolithic structures and heterolithic segments.

With these examples Donnio's group have demonstrated that mesomorphic properties can be induced towards the dendritic architecture and they verified the correlation between the stability of mesophase and the position of heterolithic blocks in the structure, as displayed in Figure 3.22.

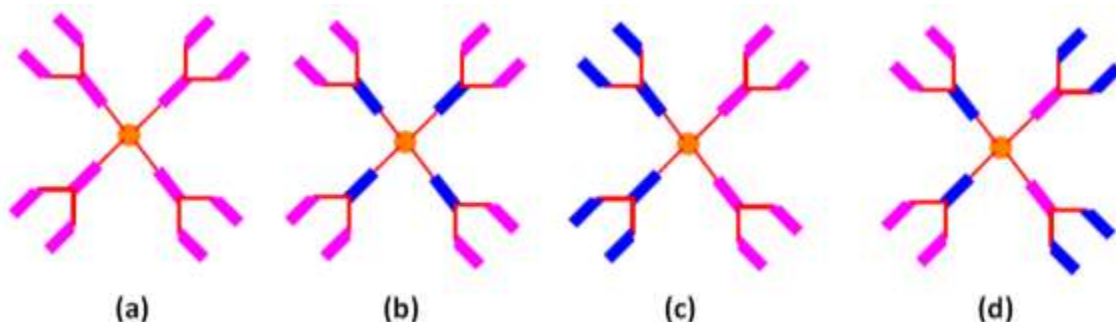


Figure 3.22 Schematic representation of a G1 octopus dendrimer: **(a)** homolithic; **(b)** heterolithic alternated; **(c)** segmented and **(d)** alternated segmented structure.

3.4.3 Intrinsic dendromesogens

In intrinsic dendromesogens, each component molecule can be considered as a single mesogen. These particular and complex structures were examined in depth for the first time in 1992 by Percec's group.³³ They apply the principles of self-assembly to cone-shaped monodendrons containing crown ether, oligo hydroxymethylene groups and polymer chains as endoreceptors and they demonstrated that such molecules are capable of spontaneously gathering into columnar supramolecular ensembles forming a hexagonal phase. In Figure 3.23 we report a schematic representation of the self-assembly of benzyl ether dendrons in columnar and cubic mesophases: a flat cone-shaped of poly (benzyl ether) units assemble into supramolecular cylindrical dendrimers subsequently forming a columnar hexagonal mesophase, as shown in Figure 3.23, **(a)** and at the same time a cone-shaped of poly (benzyl ether) units associate into supramolecular spherical dendrimers subsequently forming a cubic LC phase³⁴, as displayed in Figure 3.23, **(b)**.

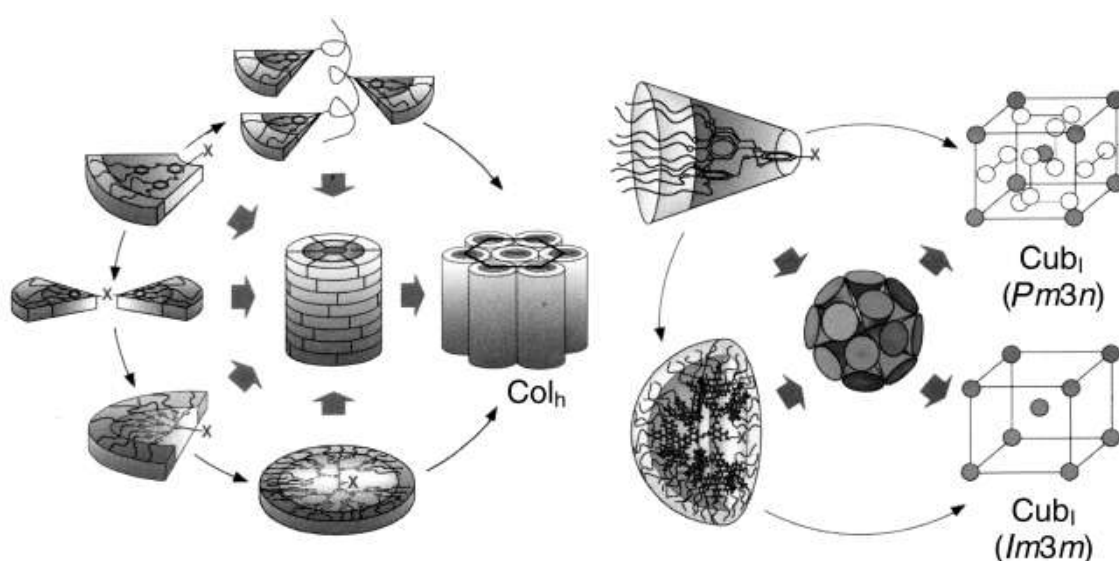


Figure 3.23 Self-assembly of benzyl ether dendrons in columnar and cubic mesophases.

All the described structures of dendrimers associated with a mesogenic behaviour are complex systems promising in the medical field, in particular for drug delivery and molecular targeting. Furthermore, self-assembled supramolecular organic liquid crystal structures at nanoscale have potential applications in molecular electronics, photonics, and porous nanomaterials.

3.5 Aim

Combination of DPP properties, such as fluorescence and thermal stability, with the interesting and unique properties of dendritic architecture is described in this chapter. In particular we wanted to exploit the properties of poly(benzylether) dendrimers to synthesize new and innovative DPP derivatives able to develop mesophases. This work has been made in collaboration with the macromolecular laboratory of the University of Neuchâtel, under the supervision of Prof. R. Deschenaux.

Our research group had already synthesized a derivative of DPP able to arrange in a discotic columnar phase. The **longchain-DPP**, displayed in Figure 3.24 (a), shows the typical fern structure of this mesophase, Figure 3.24, (b), (c), (d) and it has been characterized through POM and DSC.

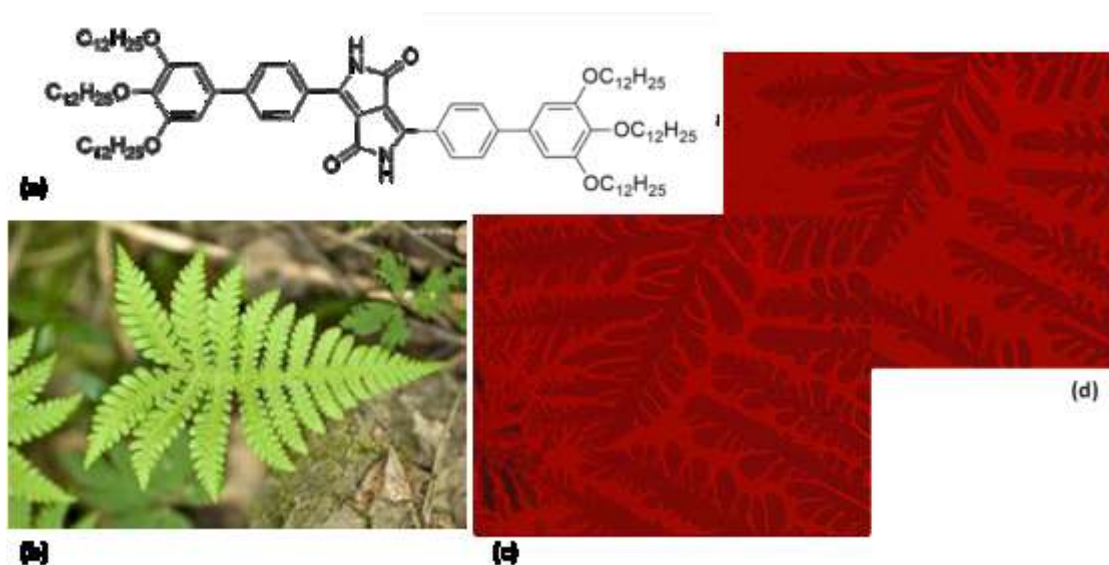


Figure 3.24 (a) Longchain-DPP; (b) fern structure and (c), (d) columnar phase observed at POM.

The DSC spectrum shows the high stability of the substrate: the melting point is about 280° C, the mesophase is comprised between 240-280° C and transition is reversible.

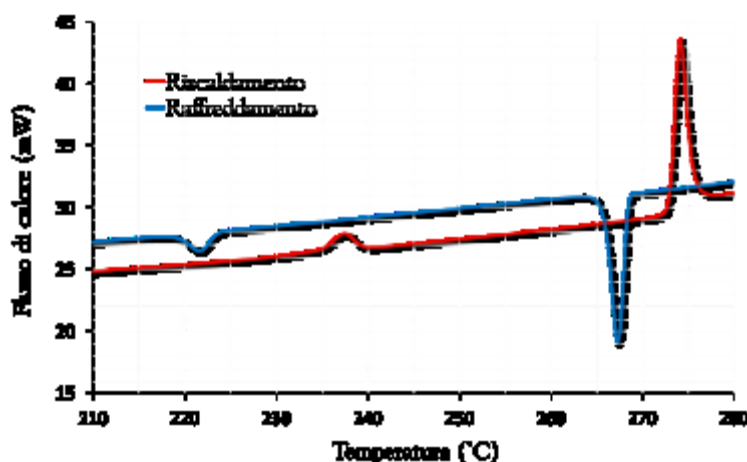


Figure 3.25 DSC of longchain-DPP.

In this chapter it is described the synthesis of poly(benzylether) dendrimers³⁵ of first (G1) and second generation (G2) using the synthetic approach proposed by Fréchet and described in paragraph 3.2.1. Then, these structures were combined with the DPP molecule to study the supramolecular organization of these new dendritic architectures. In Figure 3.26 one of the molecular target (**G1-pDPP dendrimer**) is displayed.

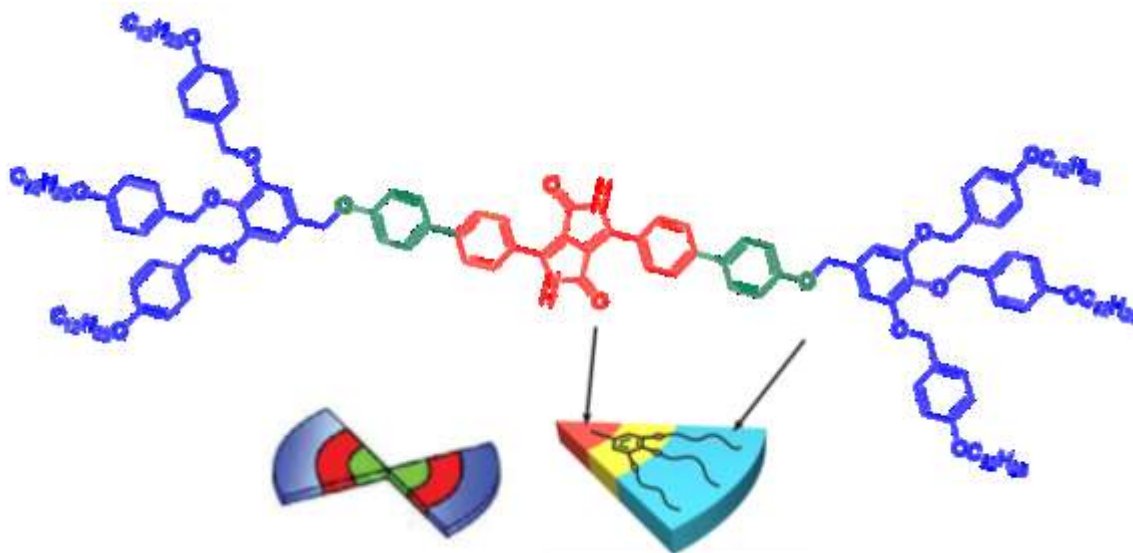


Figure 3.26 Example of dendrimer with DPP core.

Modifying the central dendrimeric core the structure-activity relationship in liquid crystals was examined in depth and the supramolecular contribution of hydrogen bonds to the final structures was tested. In particular, dendritic architectures based on not protected DPP (Figure 3.27, **a**) and protected DPP (Figure 3.27, **b**) were compared, focusing the attention on the study of phase stability and transition temperatures. In the last instance, we tried to synthesize a DPP where G1 and G2 dendrimers as linked to nitrogen atoms (Figure 3.27, **c**), to discover if the dendrimers' positions can influence and modify the supramolecular organization of mesophase and the stability of the DPP molecule.

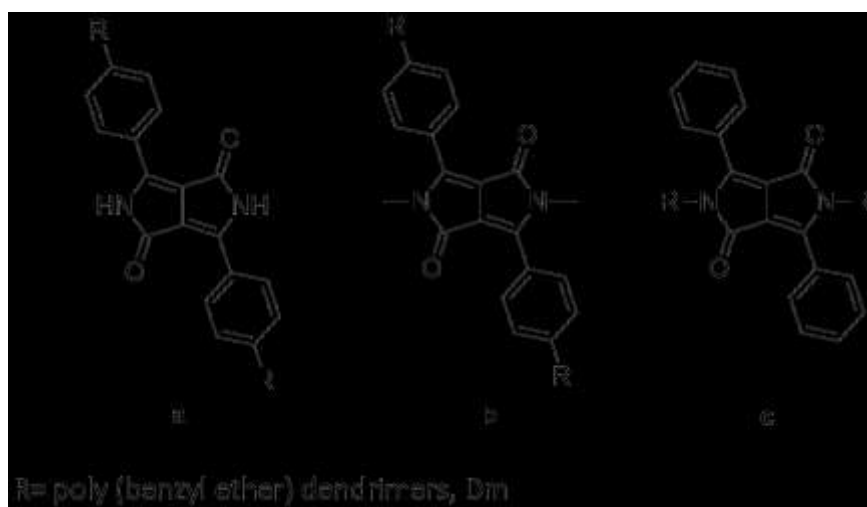


Figure 3.27 DPP cores of synthesized dendrimers.

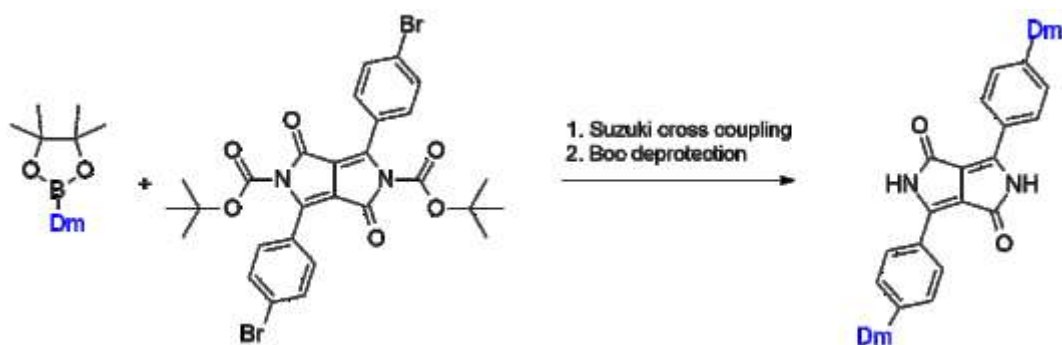
All the synthesized molecules have been characterized through elemental analysis (a good purity level is a fundamental requirement for the correct characterization of mesomorphic phase), ¹H-NMR and MALDI-TOF mass spectroscopy, DSC and POM.

The combination of the DPP features to the dendritic architectures enhances their prospect as potential candidates for developing functional materials.³⁶ These molecules could be promising substrates in the development of molecular wires in nanopore of inorganic templates;³⁷ their well conjugated structure with strong π - π interactions and electron-withdrawing effect could assure efficient charge transport in organic solar cells³⁸ and application in pharmacological field, such as polymers in drug delivery can also be advanced.³⁹

3.6 Synthetic strategy

The poly(benzylether) dendrimers, described in the next paragraphs, were synthesized following the convergent growth approach proposed by Fréchet⁴⁰ and illustrated in paragraph 3.2.1.

The synthetic approach, shown in Scheme 3.2 and used to obtain DPP derivatives, considers the Suzuki cross coupling between the **BrDPP-Boc** and an opportunely functionalized dendrimer.



Scheme 3.2 Synthetic strategy to obtain poly(benzylether) dendrimers with DPP core¹.

Poly(benzylether) dendrimers are largely described in the literature⁴¹, but none reports use of the borylation through Myaura reaction of the corresponding bromide dendrimers using bis(pinacolato)diboron (B_2pin_2) as borylating agent.⁴² In Figure 3.28 two pinacol boronic esters of first generation (G1), **A**, **B** and a pinacol boronic ester of second generation (G2), **C**, are shown.

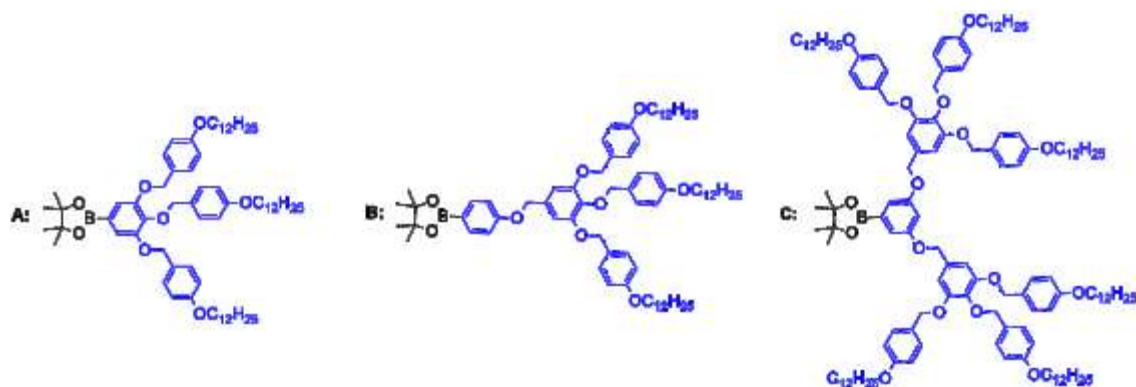


Figure 3.28 Pinacol esters of first generation (**A-B**) and of second generation (**C**).

The pinacol boronic esters and their precursors were characterized by elemental analysis, ESI and NMR spectroscopy, POM and DSC, as described in the experimental part.

¹ Dm, means dendrimers.

3.6.1 Synthesis of G1 pinacol boronic ester

The synthesis of pinacol boronic esters began with the synthesis of 1-(hydroxymethyl)-4 (dodecyloxy) benzene, represented in Figure 3.29.

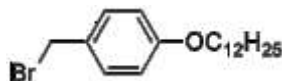
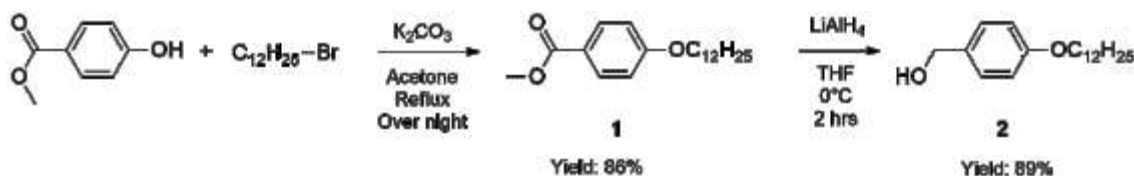


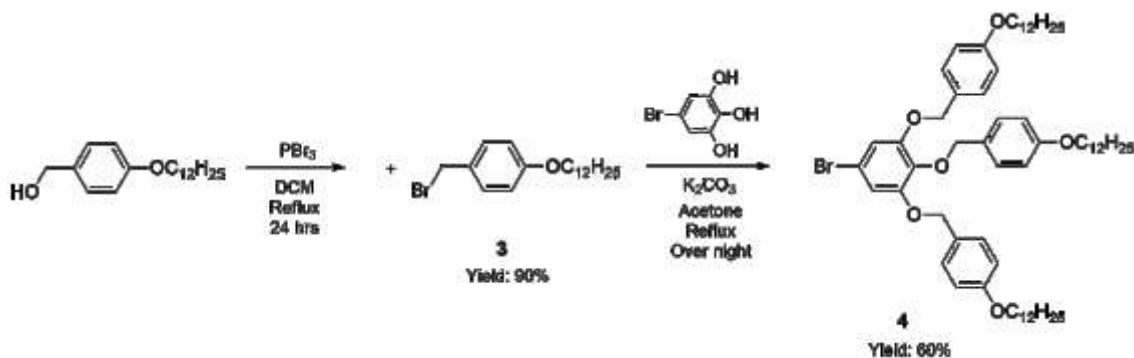
Figure 3.29 Mesogen.

G1 pinacol boronic ester was obtained through six synthetic steps. Williamson synthesis, as shown in Scheme 3.3, between methyl 4-hydroxybenzoate and bromo dodecane, in dry DMF and with K_2CO_3 , as base was the first step. Product **1** was obtained with a yield of 86 %. The second step considered the reduction of methyl 4-(dodecyloxy)benzoate with $LiAlH_4$ in dry THF. Product **2** was obtained as a colourless solid with a yield of 89 %.



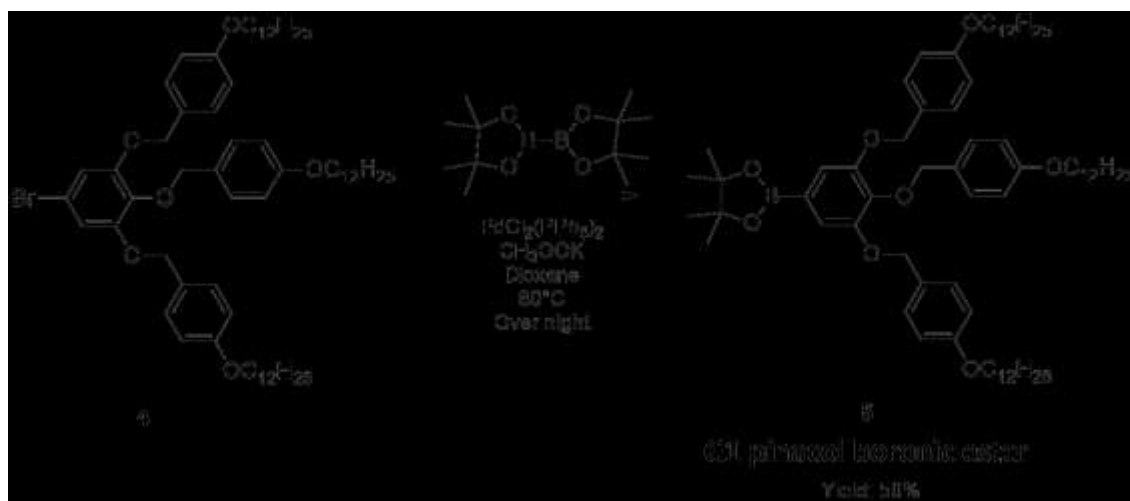
Scheme 3.3 Synthetic strategy to obtain **2**.

The third step comprised the bromination of **2** with PBr_3 in dry DCM, as shown in Scheme 3.4. The pure product **3** was obtained with a yield of 98 % without any purification. In the fourth step product **3** reacted with 5-bromobenzene-1,2,3-triol using K_2CO_3 , as base in a mixture of dry DMF and THF at 60° C. The product **4** was obtained with a good yield and any purification was necessary. The 5-bromobenzene-1,2,3-triol employed in this reaction was synthesized according to the literature,⁴³ using BBr_3 in DCM at -84° C.



Scheme 3.4 Synthetic strategy to obtain **4**.

The **G1 pinacol boronic ester (5)** was prepared through Miyaura borylation reaction, as shown in Figure 3.5. The reaction enables the synthesis of boronates by cross-coupling of bis(pinacolato)diboron (B_2pin_2) with aryl halides, in this case with compound **4**. The reaction entails the use of bis(triphenylphosphine) palladium(II) dichloride, as catalyst, potassium acetate, as base and degassed dioxane, as solvent. The product was purified by precipitation (solvent mixture: acetone/methanol) and it was obtained as a colourless solid with a yield of 50 %.



Scheme 3.5 Synthesis of G1 pinacol boronic ester.

Product **4** and product **5** are new molecules and they were characterized through POM and DSC: both analysis demonstrate that they are not mesomorphic. In Figure 3.30 it is reported the DSC spectrum of product **4** in which only the transition from solid to liquid state is observed.

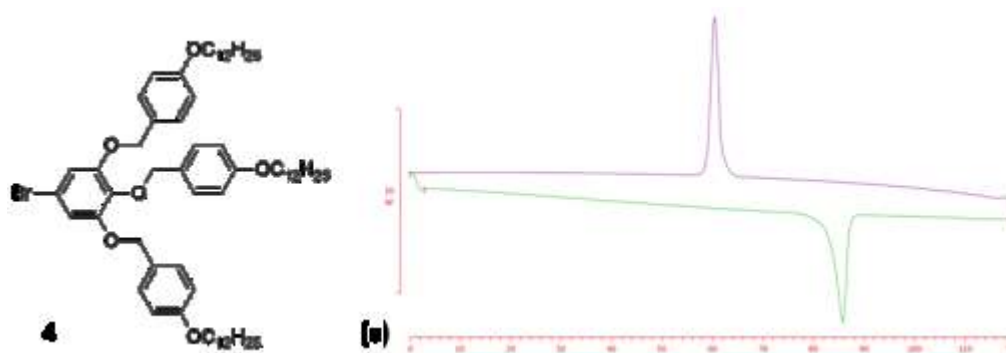


Figure 3.30 Substrate **4**; DSC of **4** (a).

POM observation confirms the absence of mesophases. In Figure 3.31 the transition from solid to liquid phase (a) and the constitution of crystalline phase (b) are displayed.

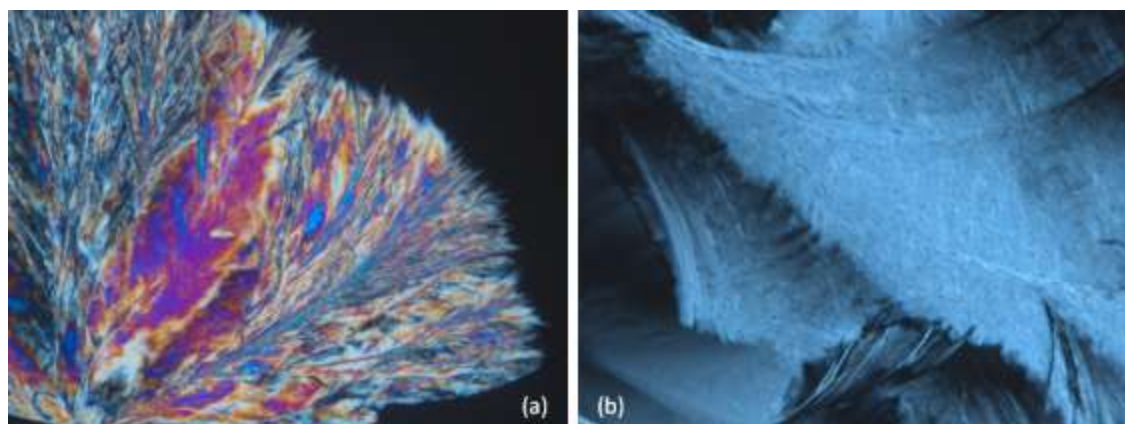


Figure 3.31 (a) Heating process at 70° C; (b) cooling process at 70° C.

Product **5** shows a particular behaviour that was observed for all the synthesized pinacol boronic esters: these structures present low melting point (about 45° C) and once in a liquid phase they require time to return at the initial viscous state. For this reason in DSC, reported in Figure 3.32, only a peak during the first heating process is observed. This behaviour is confirmed also by POM observation. Figure 3.33 displays substrate **5** at room temperature before the heating process **(a)** and at the end of the cooling process **(b)**.

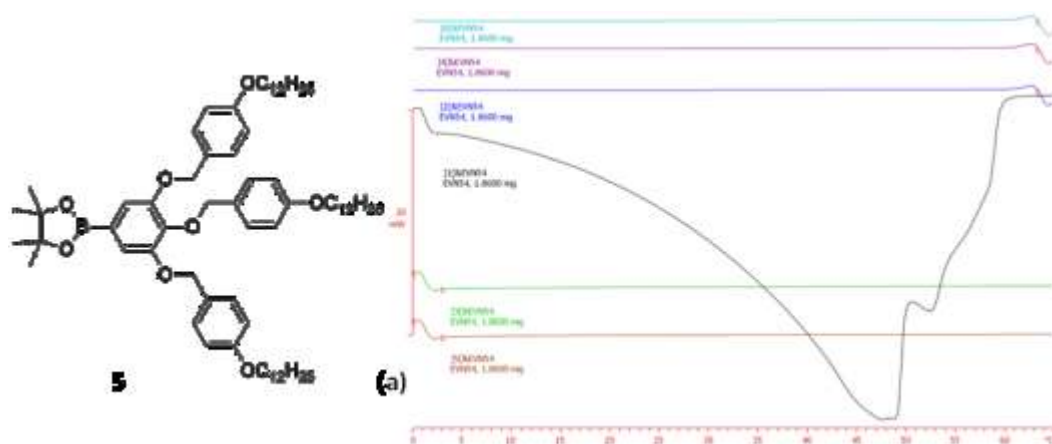


Figure 3.32 G1 Pinacol boronic ester, **5**, and DSC of **5** (a).

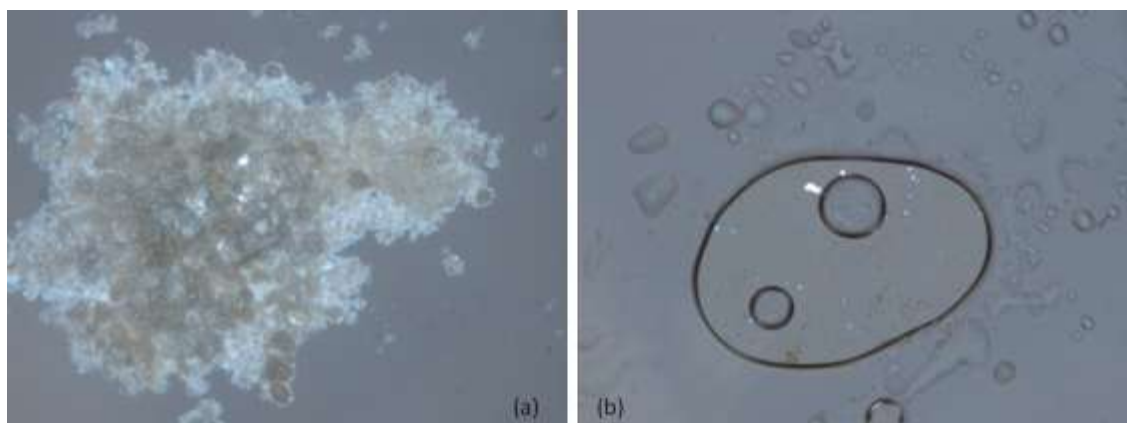
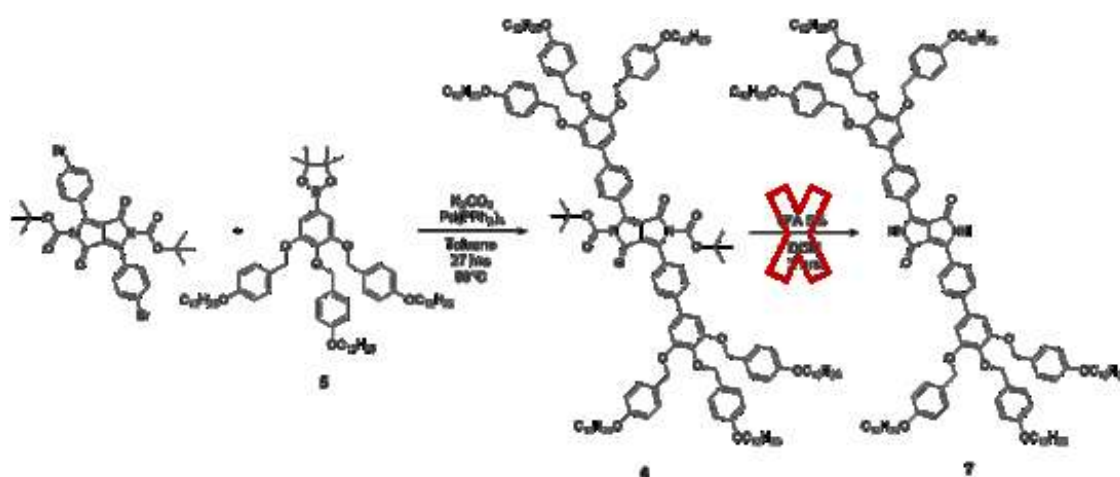


Figure 3.33 Images take at room temperature: before the heating process **(a)**; after the cooling process **(b)**.

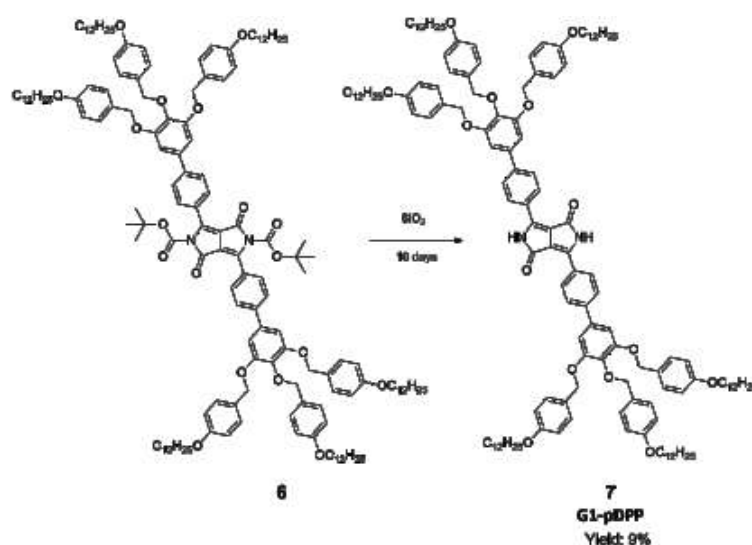
3.6.2 Synthesis and characterization of G1-pDPP

Once obtained the **G1 pinacol boronic ester**, the Suzuki cross coupling reaction was conducted, as shown in Figure 3.6. Tetrakis (triphenylphosphine) palladium(0) catalyses the reaction, K_2CO_3 is the base and toluene at reflux the solvent. The crude product was not isolated: precipitation is not an efficient method and FC cannot be used because the silica gel reacts with the Boc-groups deprotecting the molecule. Thus, the hydrolysis was conducted with 5 % of TFA in DCM, but the acid conditions, even if weak, decompose the dendritic structure. This behaviour depends on the presence of the benzyl group, that in acid conditions collapses.⁴⁴



Scheme 3.6 Synthesis and hydrolysis of **G1-pDPP**.

For this reason the compound was hydrolysed using silica gel, as described in the literature.⁴⁵ The substrate was left to be absorbed on silica gel and dried. This process was controlled with TLC and when the reagent's spot disappeared in TLC, the crude product was isolated through FC (DCM) obtaining **G1-pDPP**, **7**. This method pointed out two disadvantages: the long time of deprotection (more than a week) and the low yield (9 %) due to the decomposition of a part of the product on silica gel.



Scheme 3.7 Hydrolysis of 6.

G1-pDPP was characterized by DSC (Figure 3.34 (a)), showing no peaks in cooling as well as in heating. This result suggests that any kind of transitions takes place in the range of temperature comprised between 0 and 240° C and probably higher temperatures are necessary to observe a transition. The molecule's behaviour was investigated also with TGA and the spectrum shows a stable system until 250° C, while at higher temperature, the molecular structure collapses (Figure 3.34, (b)).

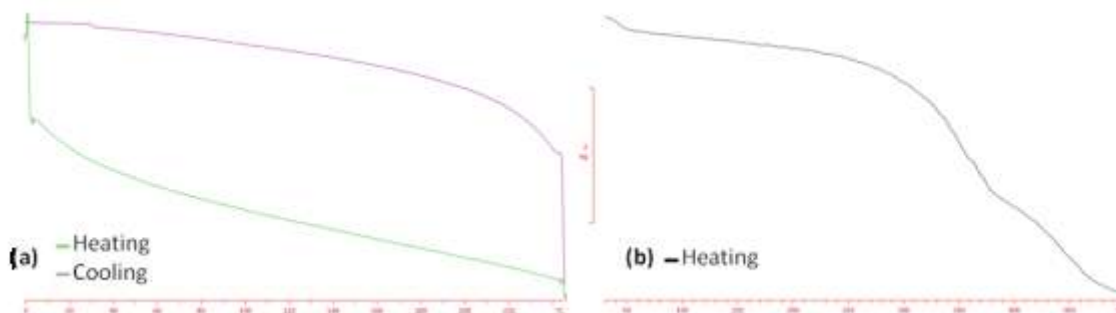


Figure 3.34 DSC (a) and TGA (b) of **G1-pDPP**.

Observing POM images, the molecule seems to be in a liquid-crystalline phase already at room temperature, as shown in Figure 3.35 (a), where the substrate has a viscous and birefringent aspect, while heating the substrate a solid in a liquid phase is noticed (Figure 3.35, (b)).

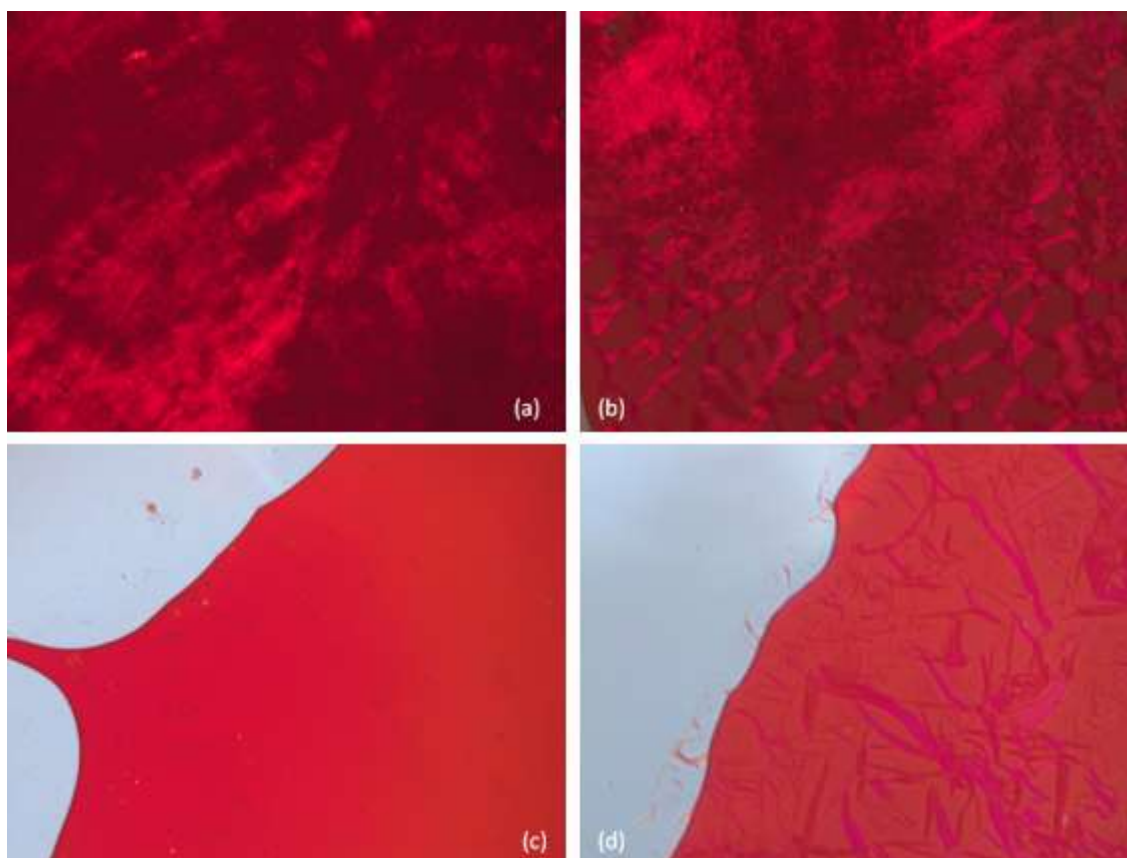
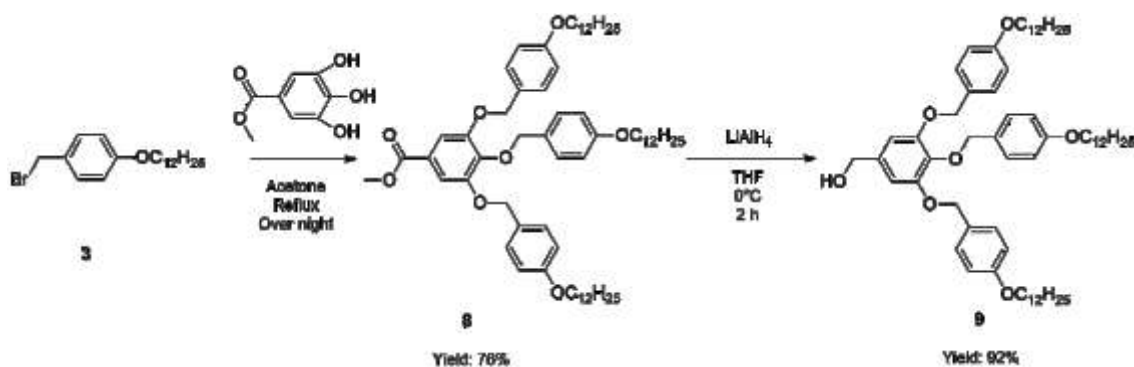


Figure 3.35 Heating process: (a) at room temperature; (b) at 141° C; (c) isotropization at 230° C and (d) small crystals begin to arrange, 185° C.

Reaching 230° C the molecule seems in a liquid state and isotropization takes place (Figure 3.35, **(c)**). Cooling slowly, at 185° C large crystals begin to form (Figure 3.35, **(d)**), but it is difficult to distinguish if they represent a mesophase or the beginning of the solid state.

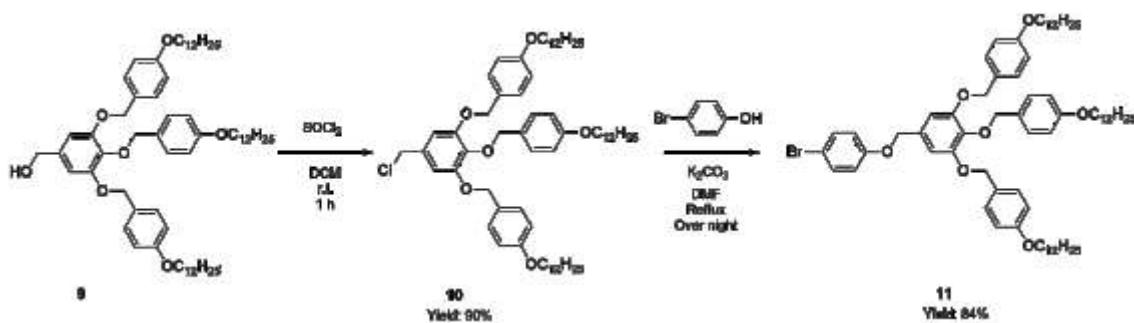
3.6.3 Synthesis of G1.1 pinacol boronic ester

The synthetic route to obtain **G1.1 pinacol boronic ester** started from molecule **3** described in paragraph 3.6.1. Product **3** reacted with methyl gallate through a Williamson etherification. K_2CO_3 is the base and the reaction takes place in acetone at $60^\circ C$. The product **8** was purified by crystallization in acetone to give a colourless solid in good yield, 75 %. Compound **8** was reduced with $LiAlH_4$ in dry THF to give **9**, with a yield of 92 %, as shown in Figure 3.8.



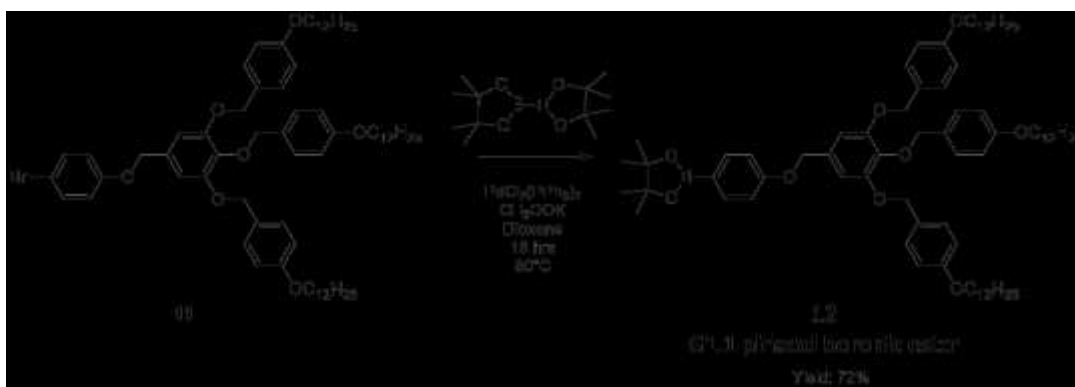
Scheme 3.8 Synthetic steps to synthesize 9.

The third step, displayed in Figure 3.9, comprised the chlorination of compound **9** with thionyl chloride in dry DCM. Product **10** was obtained as a pale yellow solid, with a yield of 90 %. Thus compound **10** reacted with 4-bromophenol through a Williamson etherification. K_2CO_3 is the base and the reaction takes place in DMF at $60^\circ C$. The crude product was purified by precipitation (Acetone/MeOH) to give compound **11** (84 % yield).



Scheme 3.9 Synthetic steps to synthesize 11.

The **G1.1 pinacol boronic ester (12)** was prepared through Miyaura borylation reaction. The reaction conditions were the same described in paragraph 3.6.1 for structure **5**. The product was purified by column chromatography (9 DCM : 1 heptane) to give a colourless solid with a yield of 72 %.



Scheme 3.10 G1.1 pinacol boronic ester, **12**.

Product **11** and product **12** are new molecular structures and for this reason they were investigated through DSC and POM. The two molecules do not give mesophases. DSC spectrum of compound **11**, displayed in Figure 3.36, shows a cold crystallization:⁴⁶ melting points and change of crystallinity with temperature are recorded and the exothermic peaks are not observed. During the heating process the spectrum shows the transition from solid to liquid only in the first cycle. For the second and third heating process the substrate displays consecutive and reversible transitions from solid to liquid.

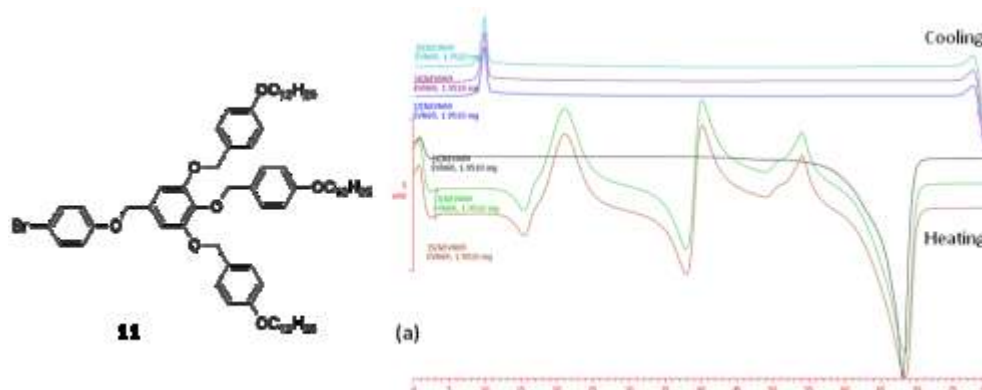


Figure 3.36 Compound **11** and its DSC (a).

POM observation is in good agreement with DSC result and it is possible to observe different forms of crystallization (polymorphism) for compound **11**. Two examples are reported in Figure 3.37.

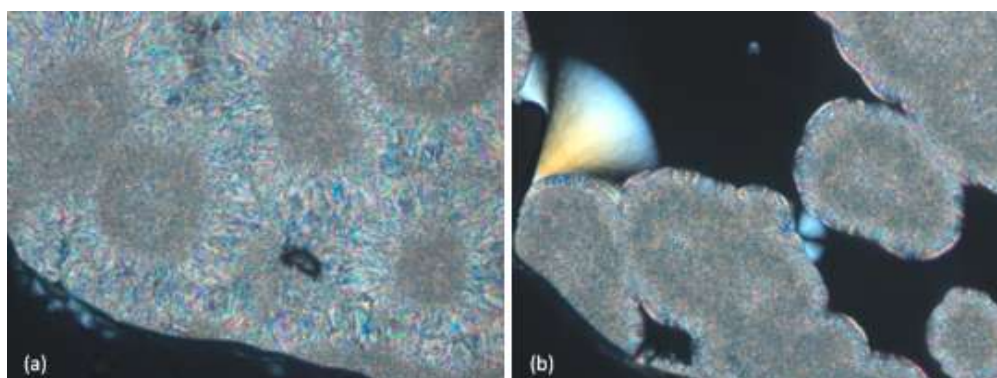


Figure 3.37 (a) First cooling, 47° C; (b) second cooling 30° C.

Compound **12**, as compound **5**, remains in the liquid state after the first heating process and for this reason no peaks during the second heating are observed as well as during the second cooling process. The DSC spectrum is reported in Figure 3.39.

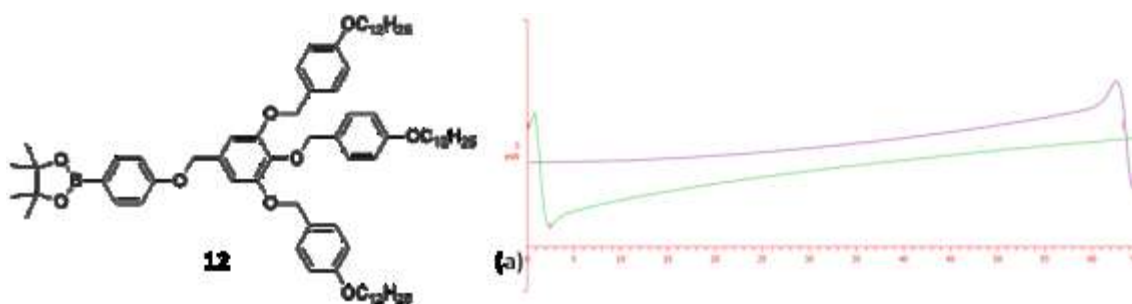


Figure 3.38 Compound **12** and its DSC (a).

This phenomenon is also observed with POM.

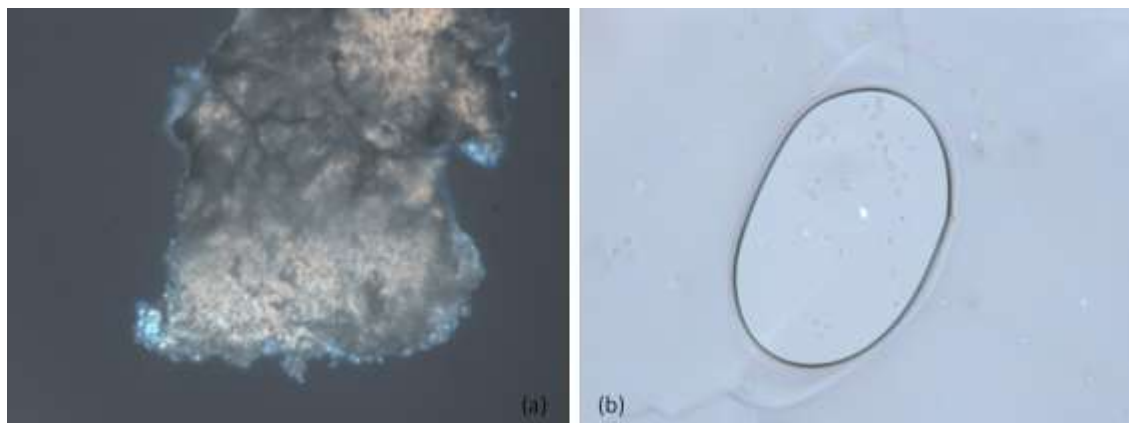
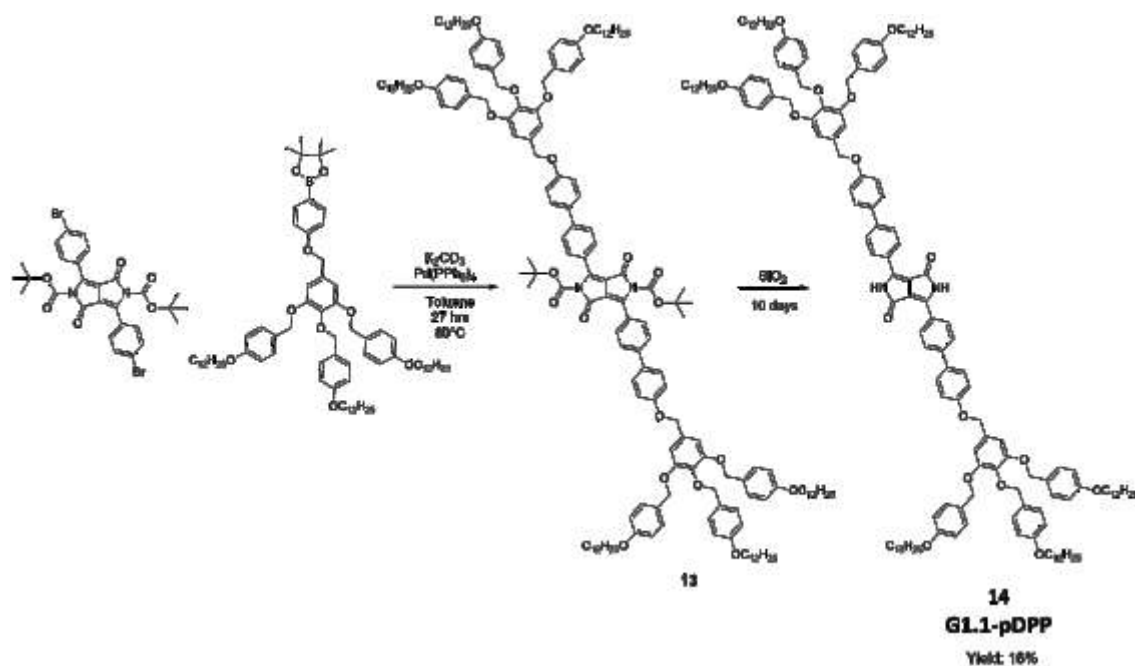


Figure 3.39 Substrate **12** at room temperature, before the heating process (a) and after the cooling process (b).

3.6.4 Synthesis and characterization of G1.1-pDPP

Once obtained the **G1.1 pinacol boronic ester** the Suzuki cross coupling reaction was carried out, Scheme 3.11. The reaction conditions were the same described for structure **7** in paragraph 3.6.2. The crude product **13** was not purified, but directly hydrolysed. It was left to be absorbed on silica gel and dried until in TLC, the reagent's spot disappeared. Finally, the molecular target **14** was isolated by column chromatography (DCM).



Scheme 3.11 Synthesis of **G1.1-pDPP**.

G1.1-pDPP was investigated through DSC and POM. The DSC spectrum, reported in Figure 3.40, does not give any information, as for structure **5** any transition cannot be observed. The structure decomposed at high temperature, probably before to be completely melt (melting point >260° C).

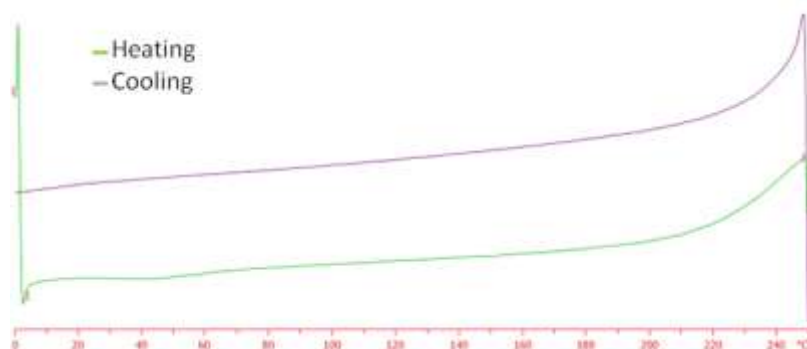


Figure 3.40 DSC of **14**.

POM images show a viscous and birefringent aspect even at room temperature as shown in Figure 3.41, (a). The compound assumes on heating a rubbery aspect when the mesophase is probably forming (103° C), Figure 3.41, (b).

At 210° C the substrate continues to have a rubbery and birefringent aspect, shown in Figure 3.41, (c). Heating at 240° C a solid in a liquid phase is observed, Figure 3.41, (d). Further heating at temperatures higher than 240° C decompose the system.

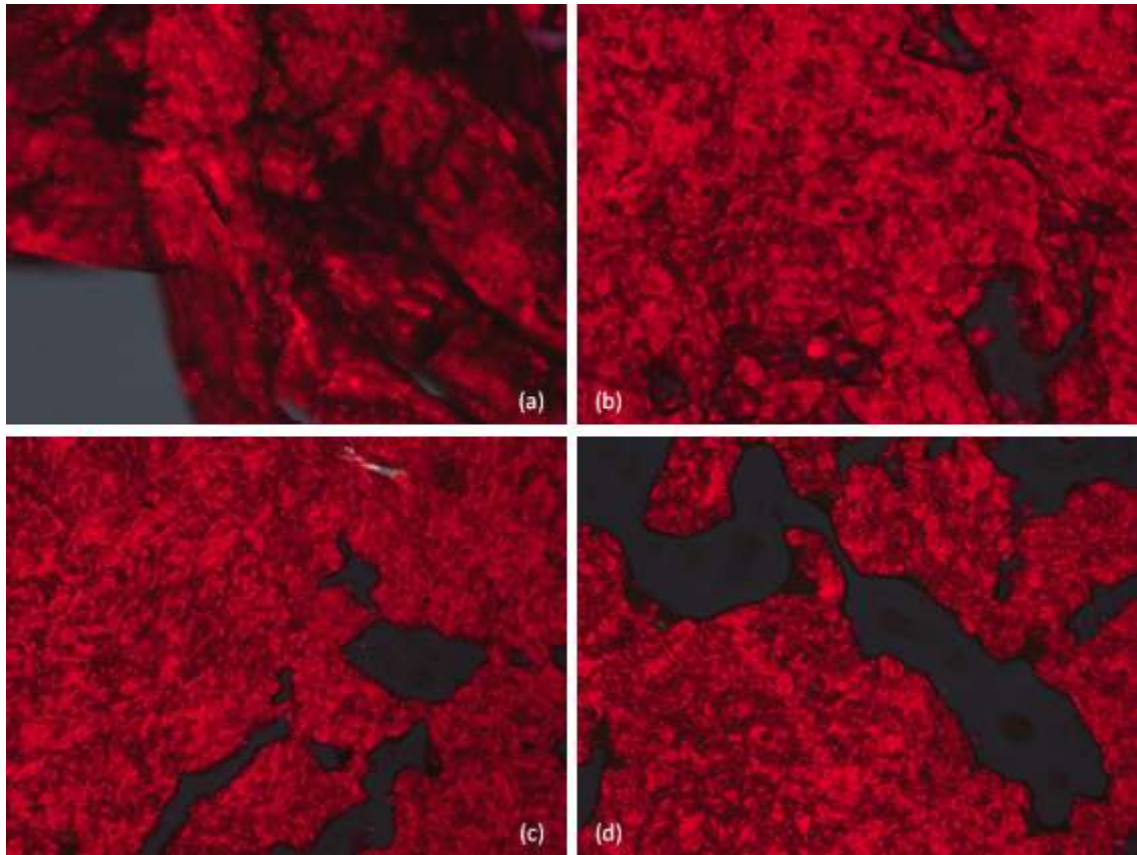
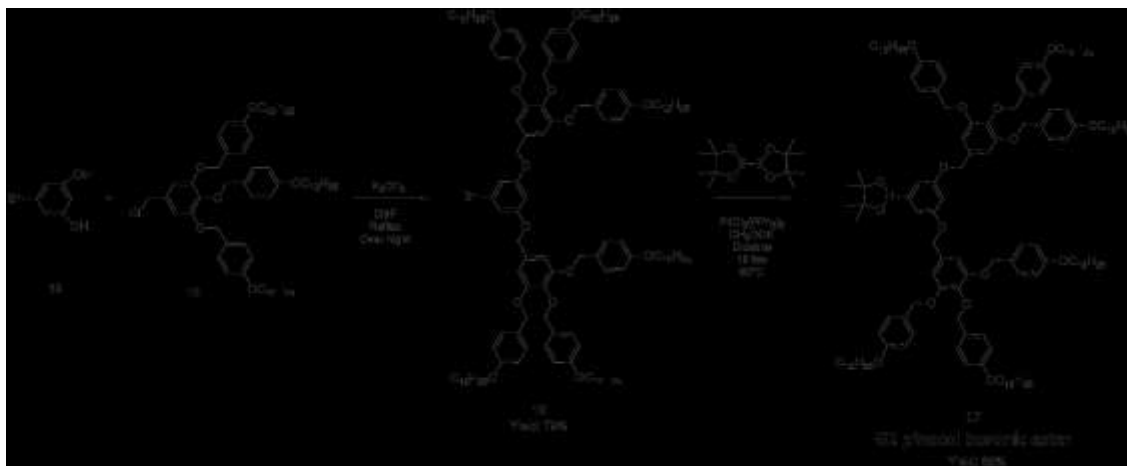


Figure 3.41 Heating process: ((a) at room temperature; (b) at 103° C; (c) at 146° C and (d) 240° C.

3.6.5 Synthesis of G2 pinacol boronic ester

G2 pinacol boronic ester was prepared starting from molecule **10**, described in paragraph 3.6.3. Product **10** reacted with **15**, through a Williamson etherification. Product **16** was purified by column chromatography (8 DCM : 2 Heptane) to give a colourless solid (yield 79 %).



Scheme 3.12 Synthesis of **G2 pinacol boronic ester**

The **G2 pinacol boronic ester**, **17**, was obtained through Miyaura borylation reaction, reported in Scheme 3.12. The reaction conditions are the same described in paragraph 3.6.1 for structure **5**. The crude product was purified by column chromatography (9 DCM : 1 Heptane) to give compound **17**, as a pale yellow solid.

Product **16** and **17** were characterized through POM and DSC. DSC spectrum (Figure 3.42, (b)) of compound **16** shows only a peak: it is broad and not well defined during the heating process while it becomes sharp and defined during the cooling process.

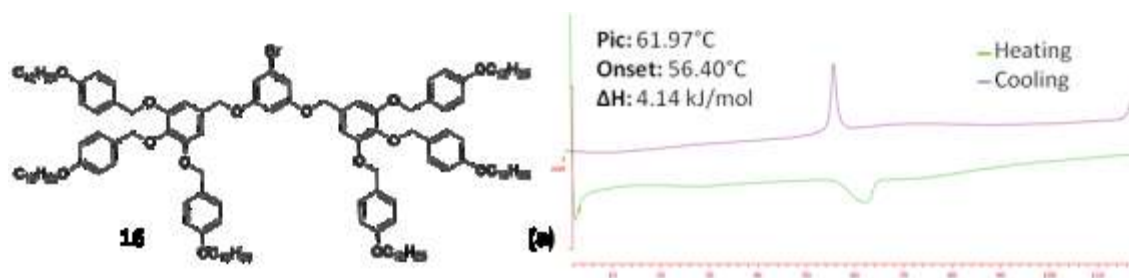


Figure 3.42 Substrate **16** and its DSC (a).

POM observation reveals the presence of a mesomorphic phase: small liquid-crystals start to organize during the cooling process. The discotic columnar phase, typical of poly(benzylether) dendrimers, can be distinguished, but it is not possible to recognise the geometry of the system. Two details of columnar phase during the heating process are reported in Figure 3.43 (a) and (b), while in Figure 3.43 (c) and (d) the cooling process is displayed.

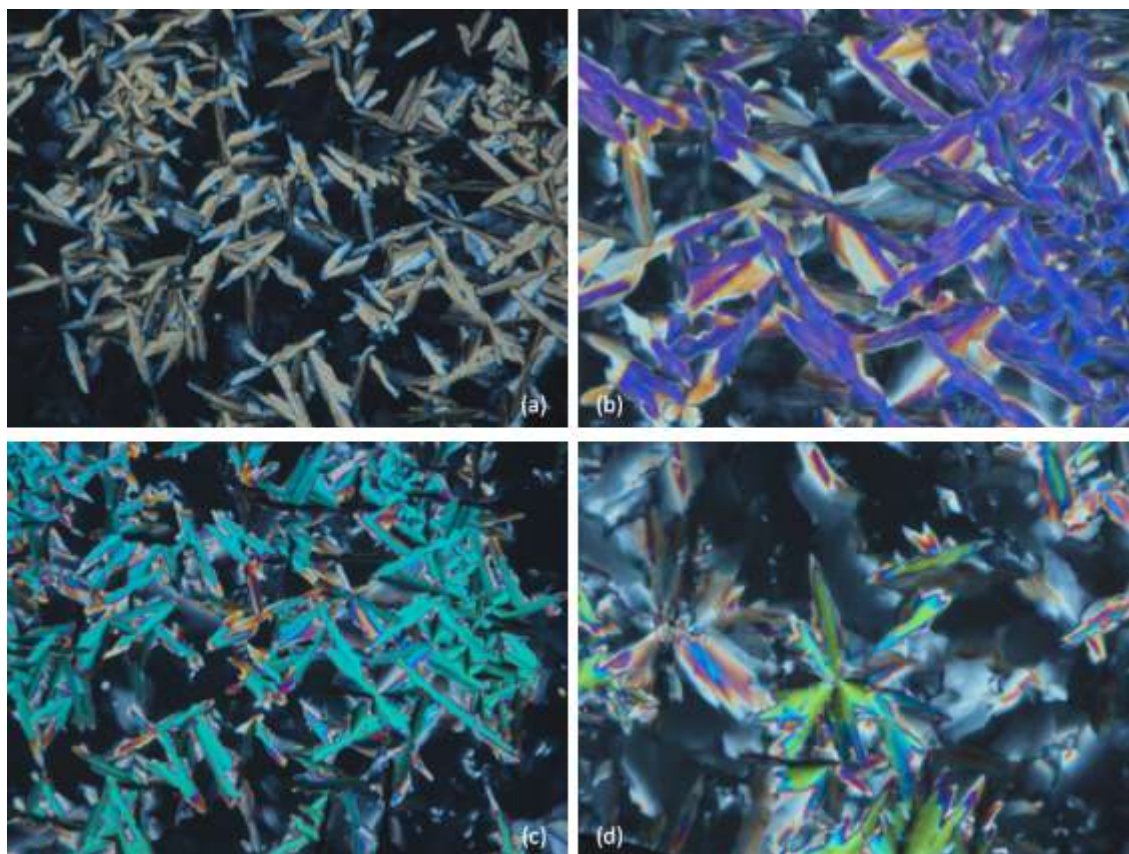


Figure 3.43 Cooling process: 70° C (a) and 58° C (b). Cooling process: 31° C (c) and 20° C (d).

In contrast compound **17** does not give mesophase. As the other synthesized pinacol boronic esters, compound **17**, upon cooling remains in the liquid state after the first process.

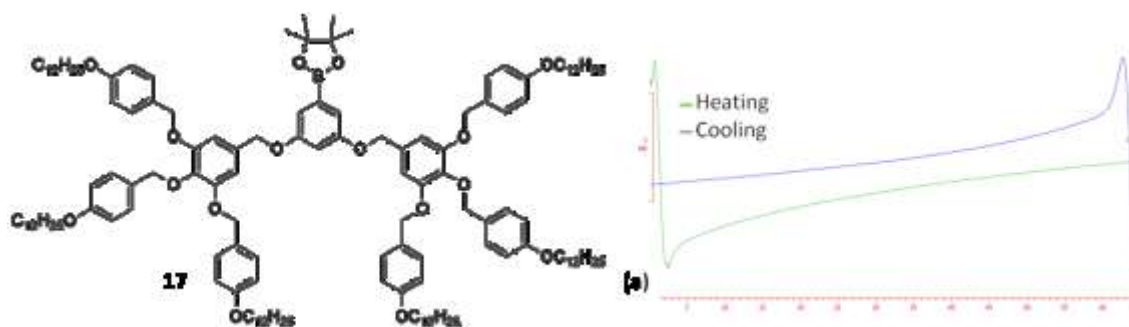


Figure 3.44 Substrate **17** and its DSC (a).

POM confirms the result shown in DSC spectrum. In Figure 3.45 the **G2 pinacol boronic ester** is reported before the heating process and after the cooling process.

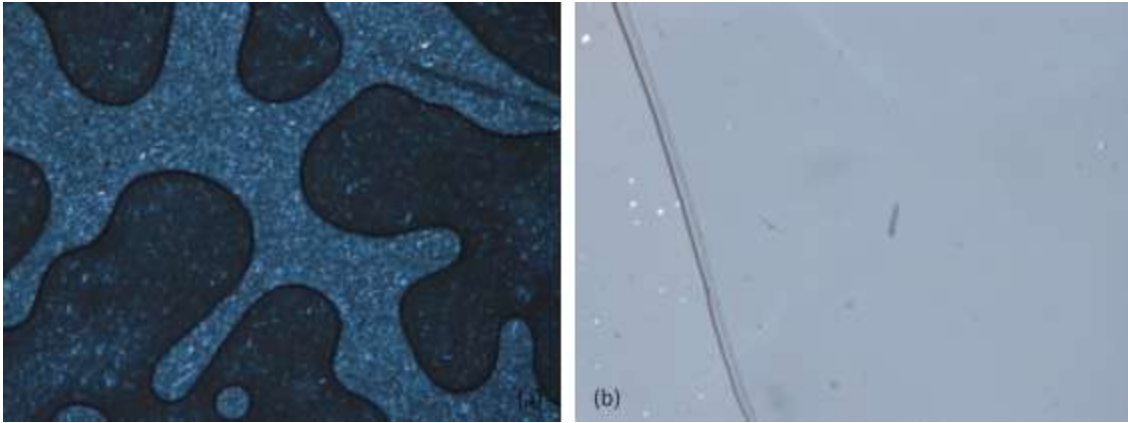
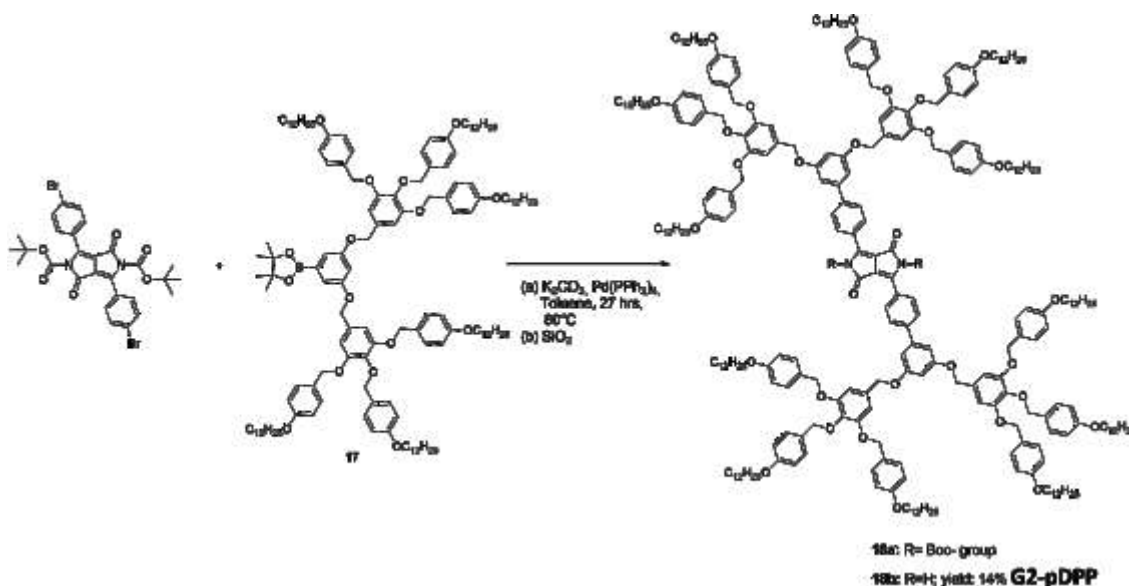


Figure 3.45 Substrate 17 at room temperature before heating process **(a)** and after cooling process **(b)**.

3.6.6 Synthesis and characterization of G2-pDPP

Once obtained the **G2 pinacol boronic ester** the Suzuki cross coupling reaction was performed, as shown in Scheme 3.13. The reaction conditions were the same described for **G1-pDPP**, in paragraph 3.6.2. The crude product was not purified, but directly hydrolysed. It was left to be absorbed on silica gel and dried until the reagent's spot disappeared in TLC. Later through a FC (DCM) the molecular target **18b** was isolated.



Scheme 3.13 Synthesis of **G2-pDPP**.

G2-pDPP was characterized through POM and DSC. As for substrate **7** and **14** DSC does not give any information. We cannot observe any peaks.

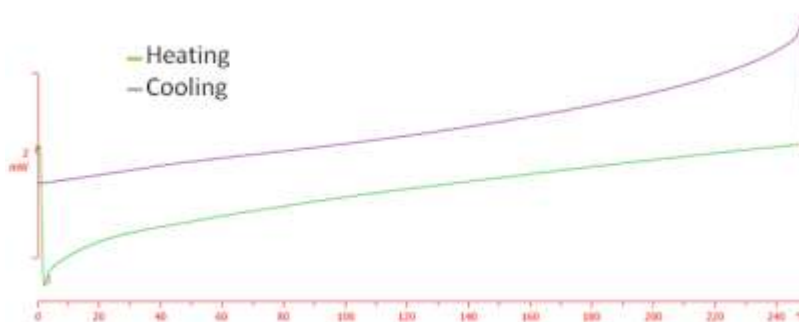


Figure 3.46 DSC of 18b.

POM images show the same behaviour described for substrate **7** and **14**. At room temperature compound **18b** has a viscous and birefringent aspect, Figure 3.47, (a); at 107° C it assumes a rubbery aspect, Figure 3.47, (b) and at higher temperature a solid in a liquid phase is observed, Figure 3.47, (c) and (d). During the cooling process the formation of small crystals occurs, but the texture is too thick to be distinguishable and to confirm the real presence of a mesomorphic state.

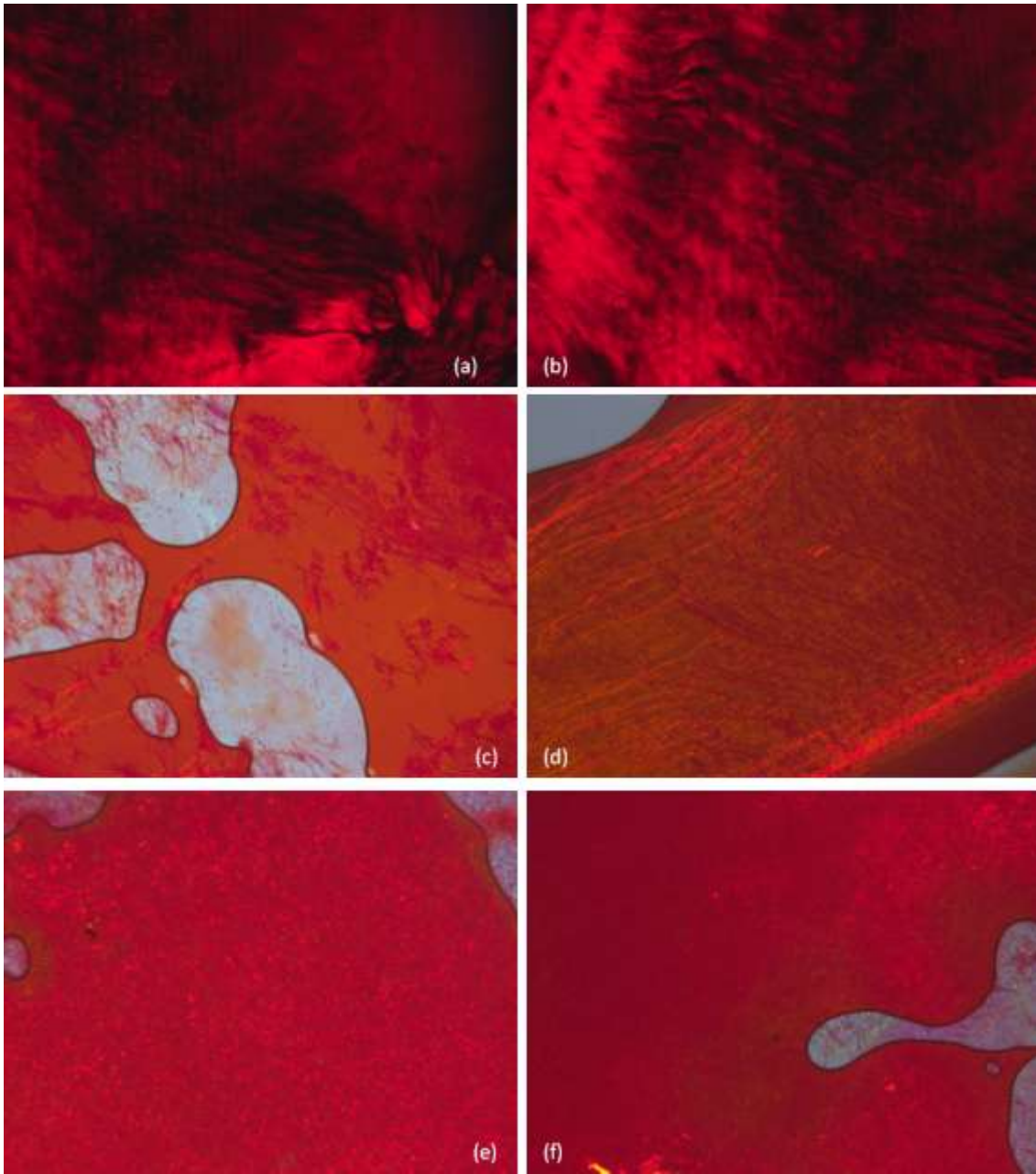


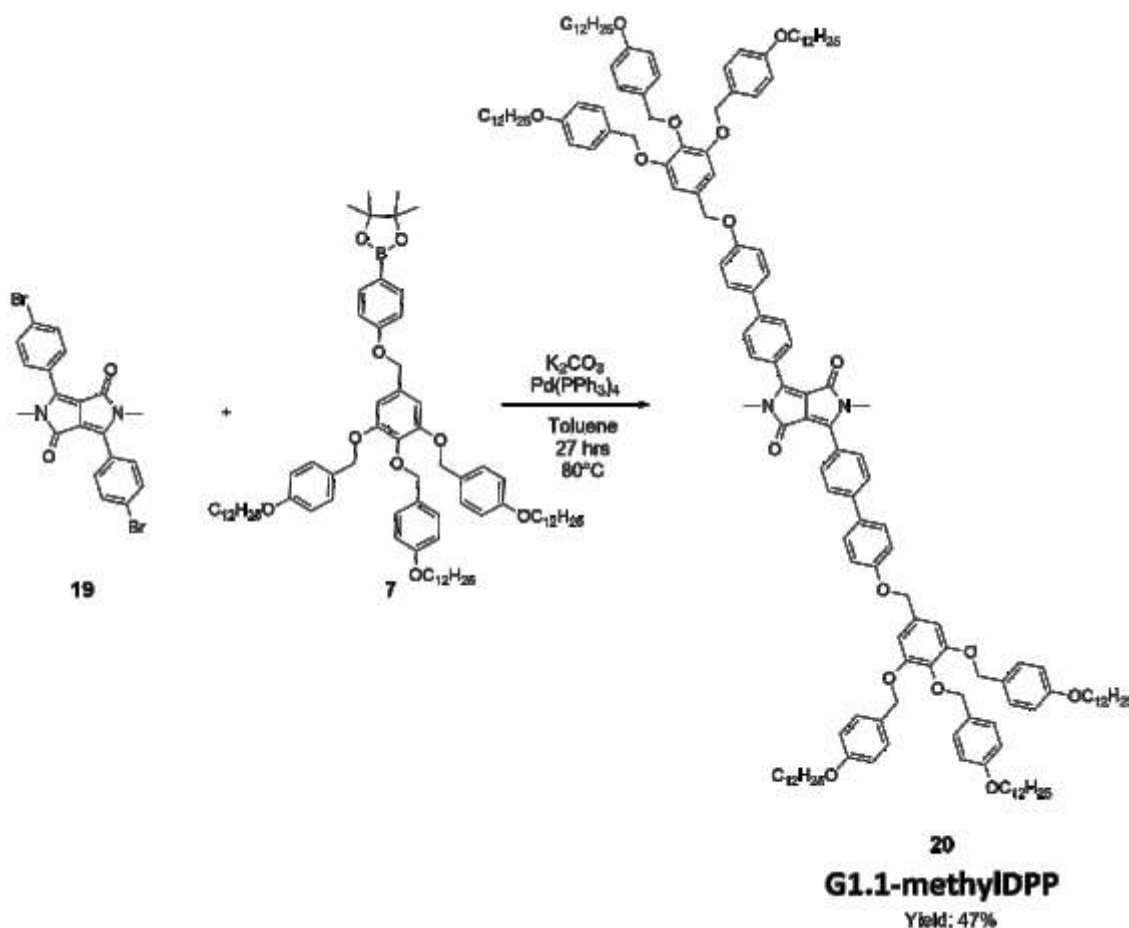
Figure 3.47 Heating process: **(a)** at room temperature; **(b)** at 107° C; **(c)** at 180° C and **(d)** at 204° C (d). Cooling process details: **(e)** 146° C and **(f)** 86° C.

3.6.7 Synthesis of methyl protected DPP dendrimers

Two dendrimers in which DPP core is protected with methyl groups were synthesized to better understand the behaviour of dendrimers with DPP core and to evaluate the effects that DPP induces in the dendrimetic architecture. In this way it can be possible to establish how the hydrogen bonds influence the molecular structures obtaining molecules easier to characterize with lower melting points.

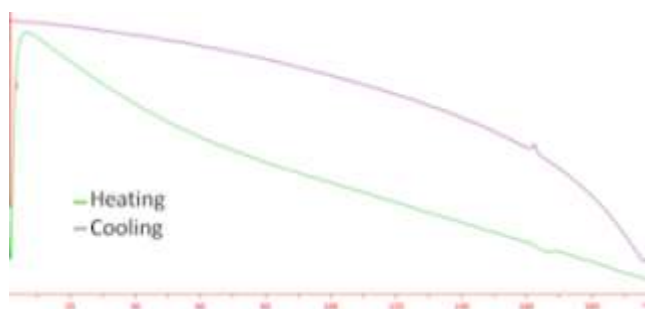
a) Synthesis and characterization of G1.1-methylDPP

The Suzuki cross coupling reaction between the **G1.1 pinacol boronic ester, 9**, and the **methyl BrDPP, 19**, was carried out to obtain **G1.1-methylDPP, 20**, as displayed in Scheme 3.14. The reaction conditions were the same described for structure **7** in paragraph 3.6.2. The crude product was purified by column chromatography (9.8 DCM : 0.2 AcOEt) to obtain the product **20**, as a red solid (yield: 47 %).



Scheme 3.14 Synthesis of 20.

Compound **20** was characterized through DSC and POM. DSC spectrum in Figure 3.48 shows the isotropization signal at $165^\circ C$ and this value appears significantly lower than that obtained for deprotected DPP.



1 st peak	
Onset (° C)	161.40
T (peak) (° C)	165.31
ΔH (kJ/mol)	2.79

Figure 3.48 DSC of 20.

POM observation confirms that at room temperature the substrate displays a viscous and birefringent aspect, Figure 3.49, **(a)**. These two features could indicate the presence of a mesomorphic phase at room temperature, whereas during the cooling process, at 150° C, small liquid-crystals begin to form, Figure 3.49, **(b)**.

At 143° C liquid-crystals seem to expand, as shown in Figure 3.49, **(c)**, but it could not be asserted if the geometry of the system changes. In Figure 3.49, **(d)** a detail of the columnar phase at 94° C is reported.

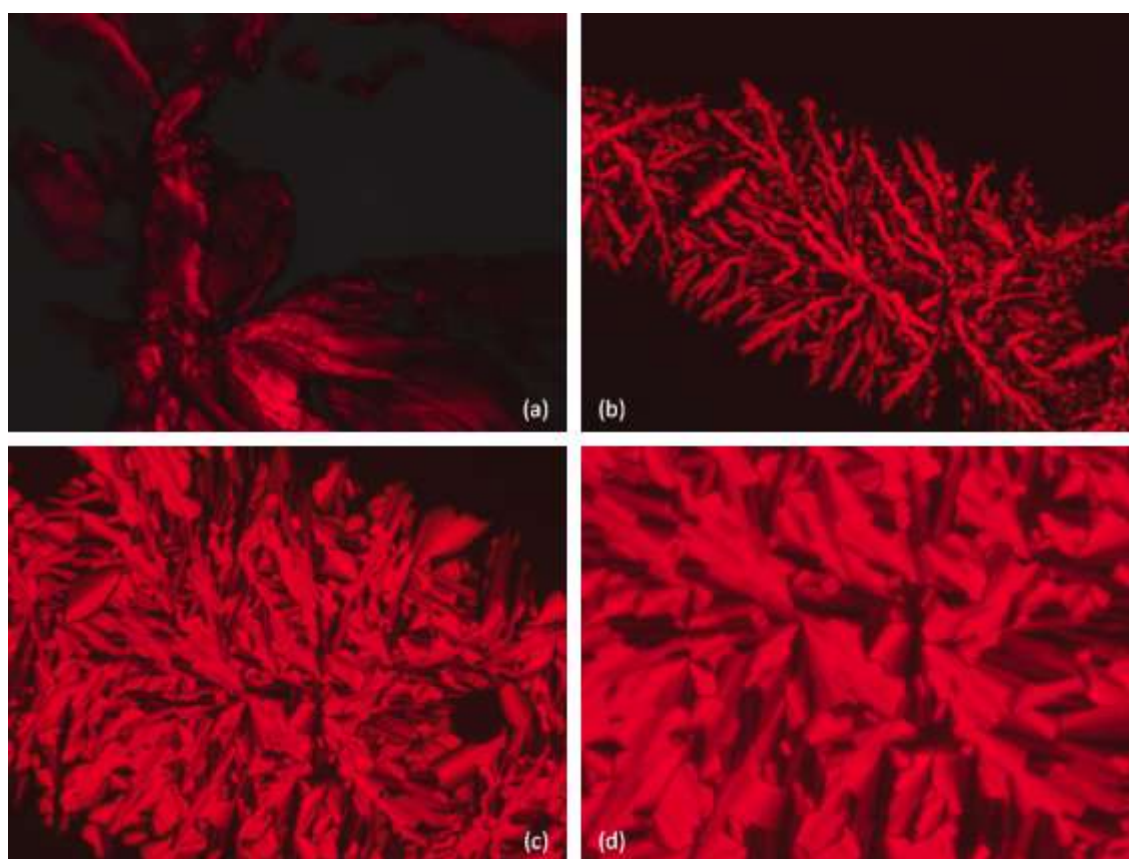
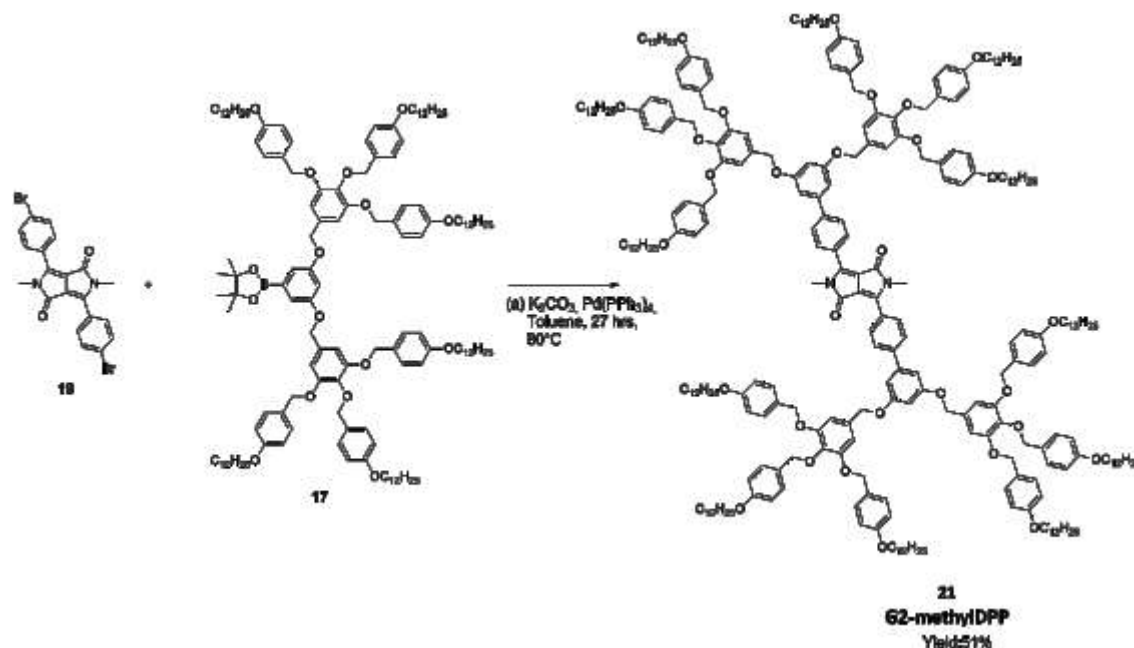


Figure 3.49 Heating process: **(a)** at room temperature. Cooling process: **(b)** at 150° C; **(c)** 143° C and **(d)** at 94° C.

b) Synthesis and characterization of G2-methylDPP

The Suzuki cross coupling reaction between the **G2 pinacol boronic ester** and the **methyl BrDPP, 19**, was performed to obtain **G2-methylDPP**, as shown in Scheme 3.15. The reaction conditions were the same described for structure **7** in paragraph 3.6.2. The crude product was purified by column chromatography (9.8 DCM : 0.2 AcOEt) to obtain the molecular target, **21**, as a red solid (yield: 51 %).



Scheme 3.15 Synthesis of G2-methylDPP, 21.

DSC spectrum displays a transition signal at $150^\circ C$ and this value appears significantly lower than those obtained for structure **7,14, 18b**, but also for compound **20**.

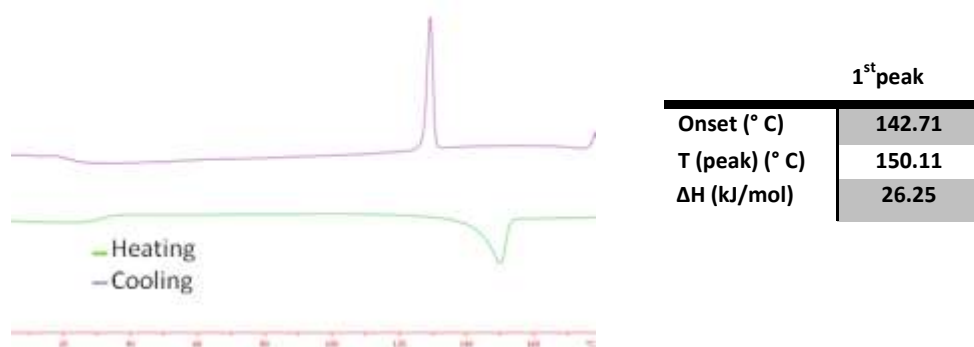


Figure 3.50 DSC of **22**.

POM observation confirms that at room temperature the substrate has a viscous and birefringent aspect, as shown in Figure 3.51, (a), so it could be possible to observe at room temperature a mesomorphic phase and in this case the transition, observed at $150^\circ C$ in DSC

spectrum, could be associated with the isotropization signal. At 66° C the substrate assumes a rubbery aspect and it could be confirmed the presence of a mesophase, Figure 3.51, **(b)**.

During the cooling process at 123° C small liquid-crystals seem to form, but the texture is too thick and not well-defined, as shown in Figure 3.51 **(c)**. In Figure 3.51 **(d)** a detail of the thin texture is reported.

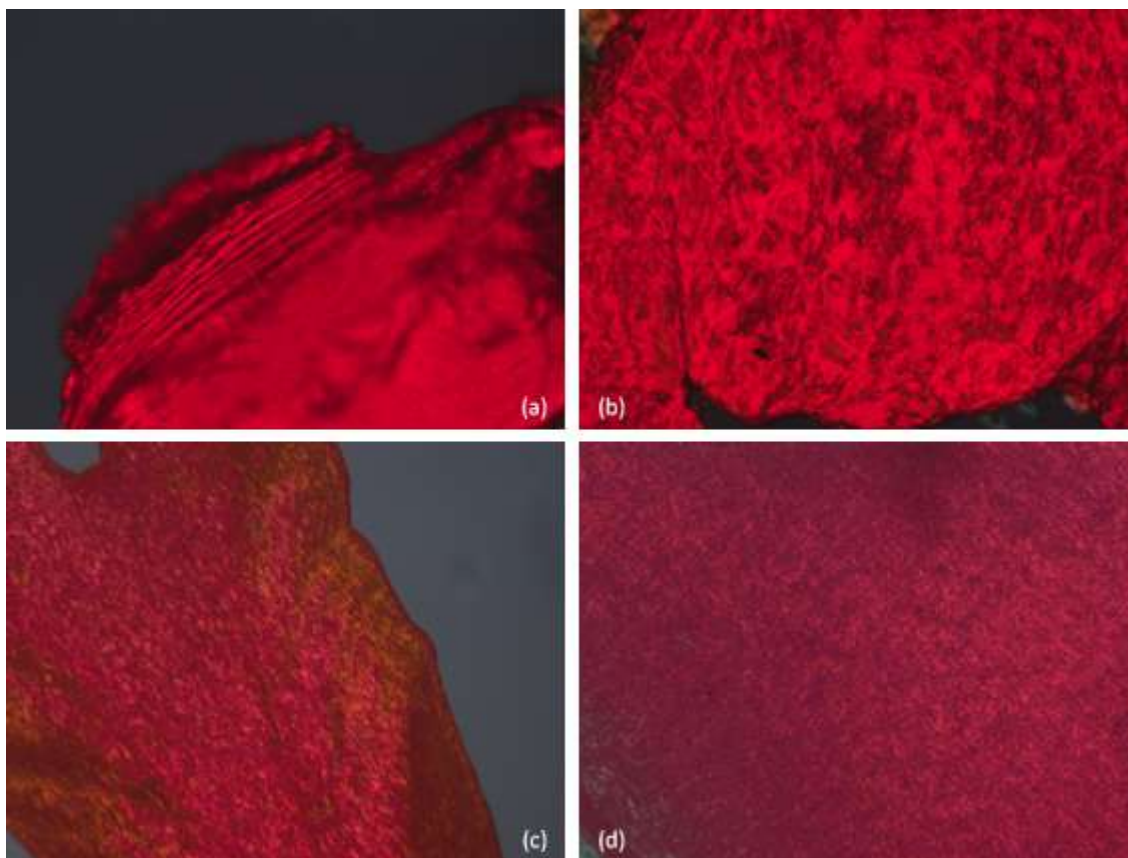


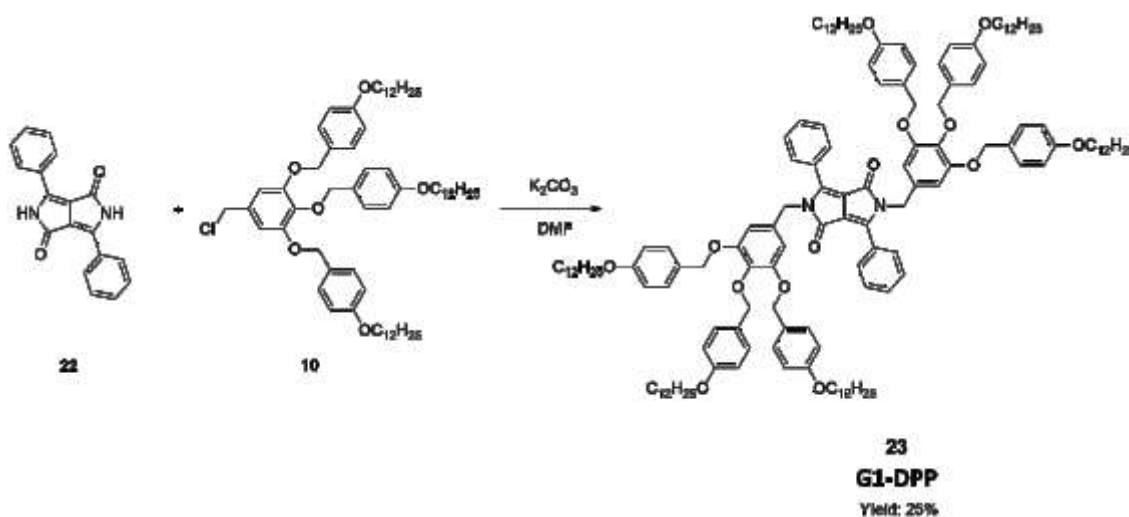
Figure 3.51 Heating process: **(a)** room temperature and **(b)** at 86° C. Cooling process details: **(c)** at 132° C and **(d)** at 87° C.

3.7 Synthesis of N-functionalized DPP

Other possible combinations between poly(benzylether) dendrimers and DPP were studied protecting the pigment with dendrimers of first and second generation. In this way we intended to evaluate and compare the behaviour of these new structures with that of the substrates already described.

3.7.1 Synthesis and characterization of G1-DPP

G1-DPP was synthesized through a nucleophilic substitution between DPP, **22**, and substrate **10**, as shown in Scheme 3.16. This reaction takes place in dry DMF and K_2CO_3 is the base. During the reaction several by-products were formed and for this reason FC was not useful to obtain the molecular target, **23**, with a good purity. Thus, the product was isolated through preparative HPLC (AcOEt : Hexane).



Scheme 3.16 Synthesis of **23**.

Product **23** was characterized through DSC and its spectrum in Figure 3.52 suggests the presence of a mesomorphic phase between 90 and 120° C, thus the temperature are significantly different from those presented for substrates **7**, **14** and **18b**.

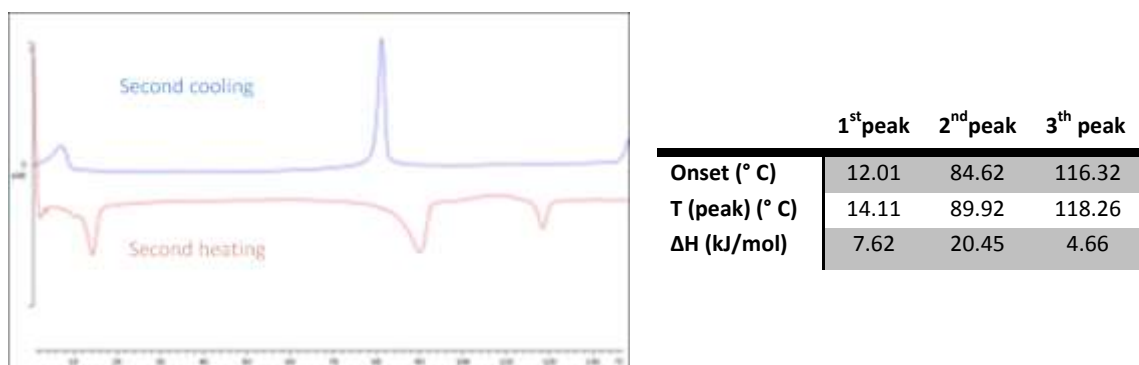


Figure 3.52 DSC of **24**.

Furthermore, even at lower temperature POM observation is not useful to distinguish the mesophase. A viscous substrate is observed below 96° C, while at around 106° C it assumes a rubbery aspect, as shown in Figure 53, **(a)** and **(b)** respectively.

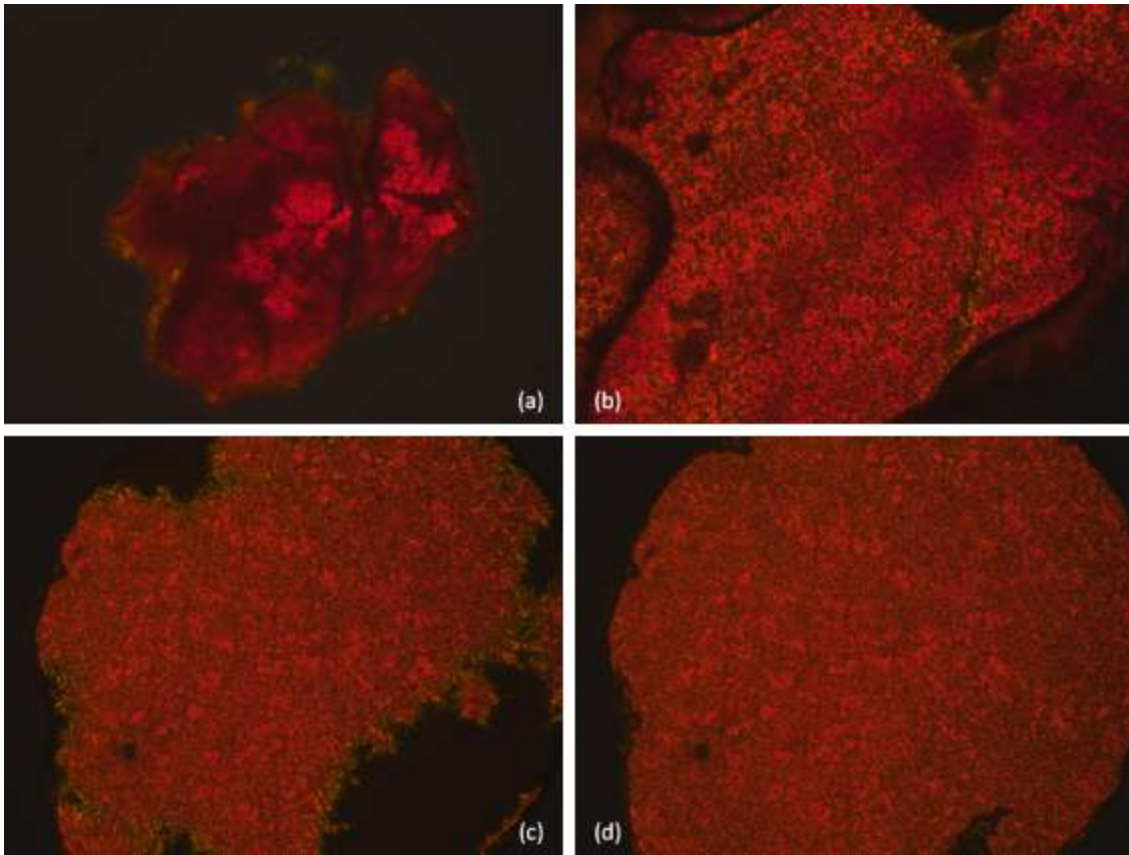
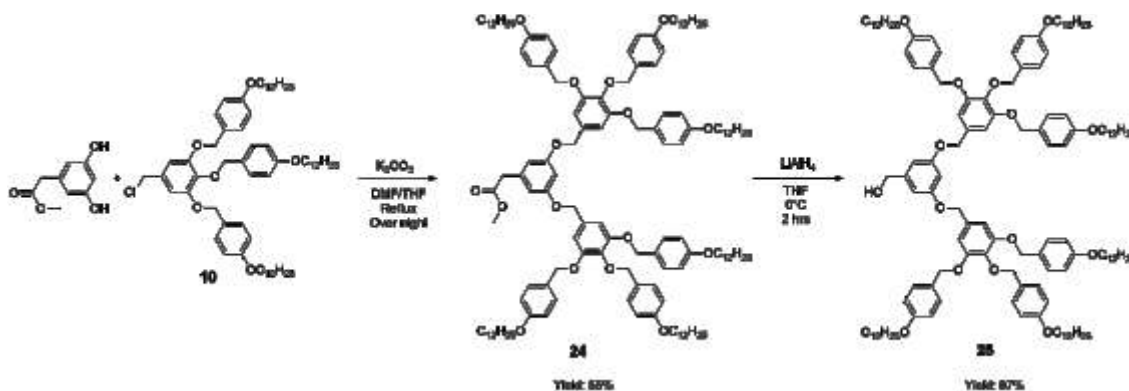


Figure 3.53 Heating process: **(a)** at 96° C and **(b)** at 106° C. Cooling process: **(c)** at 92° C and **(d)** at 85° C.

During the cooling process small crystals start to assemble, but the texture is too thick to demonstrate that it is a mesophase and to define its geometry. Thus from DSC a mesophase can be supposed, but POM does not produce any information.

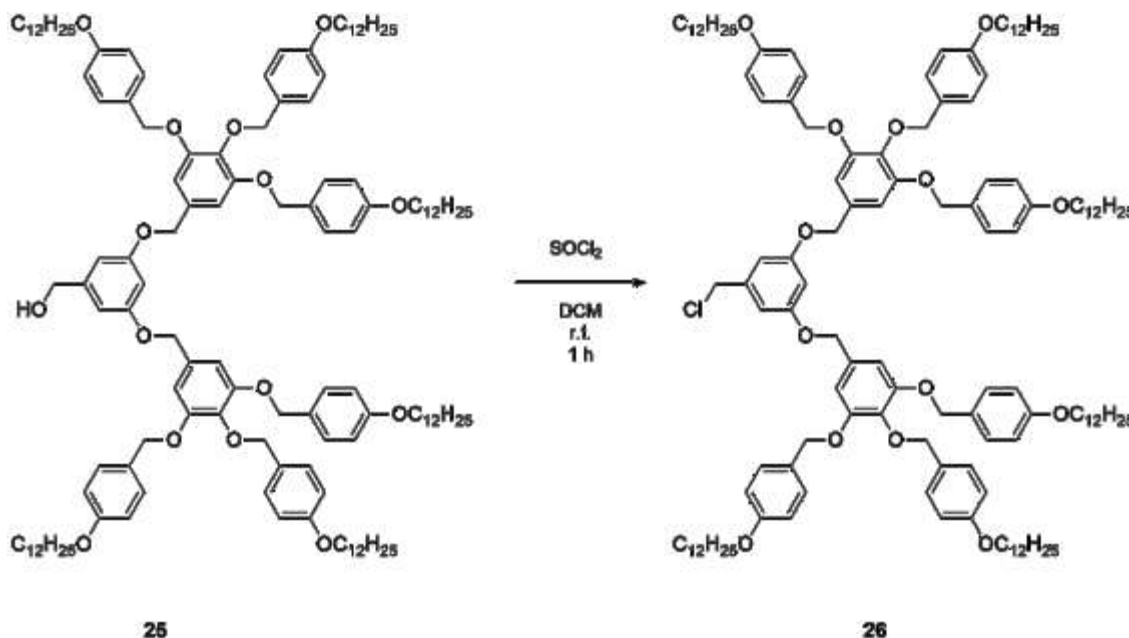
3.7.2 Synthesis of G2-DPP

In order to synthesize **G2-DPP** with the same procedure described for **23** a new dendrimer of second generation was synthesized. The synthesis of **G2** started from molecule **10**, as shown in Scheme 3.17. It reacted with methyl 2-(3,5-dihydroxyphenyl)acetate through a Williamson etherification using K_2CO_3 as base and a mixture of DMF/THF as solvents. The product **24** was obtained as a colourless solid after crystallization in MeOH (55 % yield). The compound **24** was reduced with $LiAlH_4$ and in dry THF to give **25**, with a yield of 97 %.



Scheme 3.17 Synthetic steps to obtain **25**.

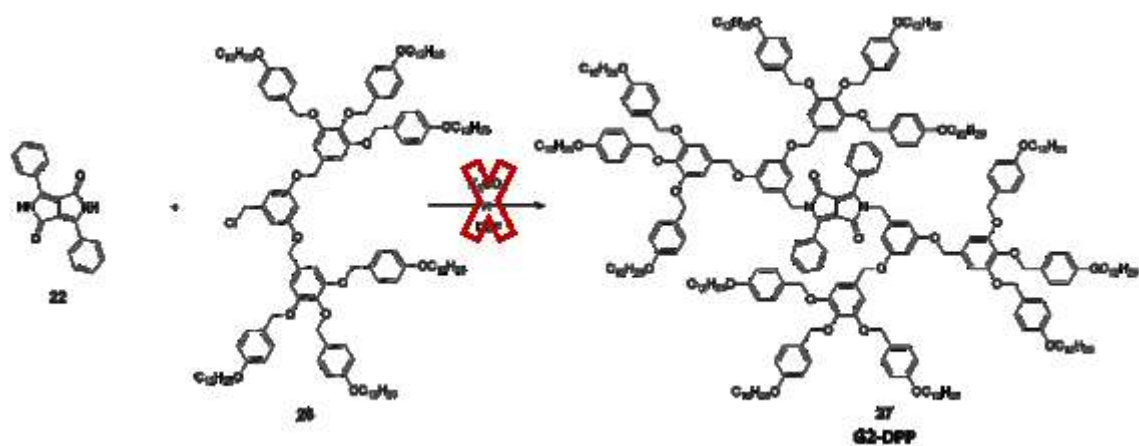
The chlorination of compound **25** with thionyl chloride in dry DCM, is displayed in Scheme 18. Product **26** was obtained as colourless solid, with a yield of 94 %.



Scheme 3.18 Synthesis of **26**.

Product **26** was subjected to nucleophilic substitution with DPP **23**. In this case product **27** could not be isolated with sufficient purity: the reaction's yield was too low and different by-products were formed. The reaction conditions (bases, solvents and temperature) were

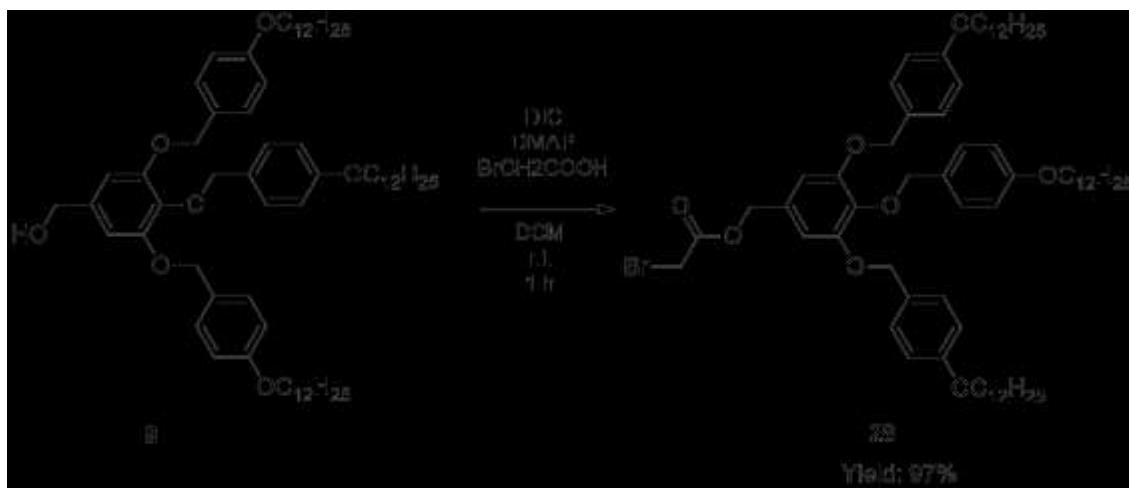
changed but with no success. This negative result could be due to steric factors or to the low reactivity of the system.



Scheme 3.19 Synthesis of 27.

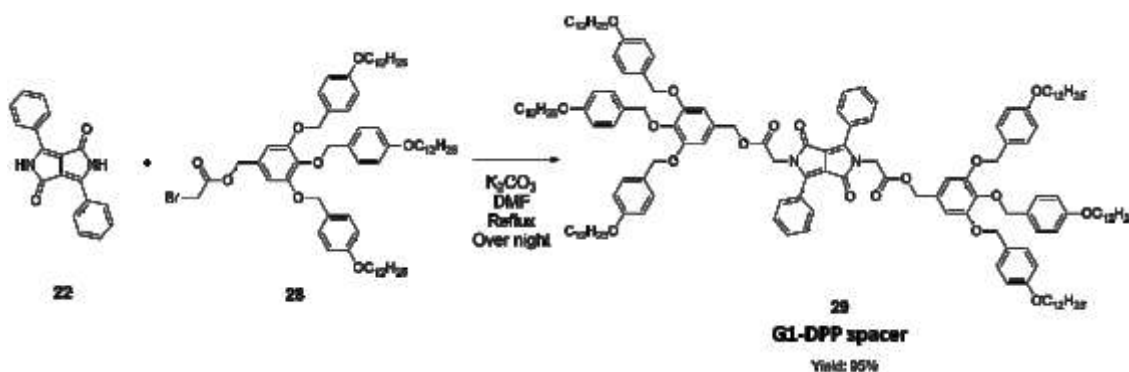
3.7.3 Synthesis and characterization of G1-DPP spacer

A small spacer was introduced in the molecule **9**, using a procedure described in the literature⁴⁷ to improve the synthesis of **G1-DPP**. In this way the steric hindrance of dendrimer was reduced and at the same time the dendrimer reactivity increased by using the more electrophilic bromo acetate group instead of the chloro benzyl one. The molecular target, **29**, was obtained via esterification reaction by bromoacetic acid and alcohol **9** using DIC as coupling agent, as describe in Scheme 3.20. The product was a colourless solid with a yield of 97 %.



Scheme 3.20 Synthesis of **28**.

G1-DPP spacer, **29**, was prepared using the same procedure described for **23**, through a nucleophilic substitution between DPP, **22**, and substrate **28**, as a brilliant orange solid with a yield of 95 %. The product was purified by crystallization in MeOH.



Scheme 3.21 Synthesis of **29**.

The substrate was characterized through DSC and POM. DSC spectrum, in Figure 3.54, let us suppose the presence of a mesophase between 80 and 145° C.

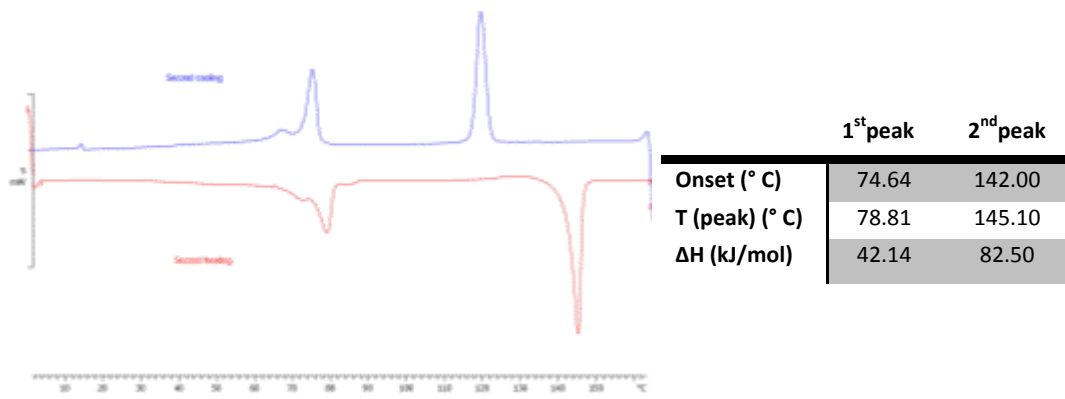


Figure 3.54 DSC of 29.

The POM experiments does not give any useful information. The substrate has a birefringent and rubbery aspect, but during the cooling process small crystals begin to form and any texture could not be distinguished.

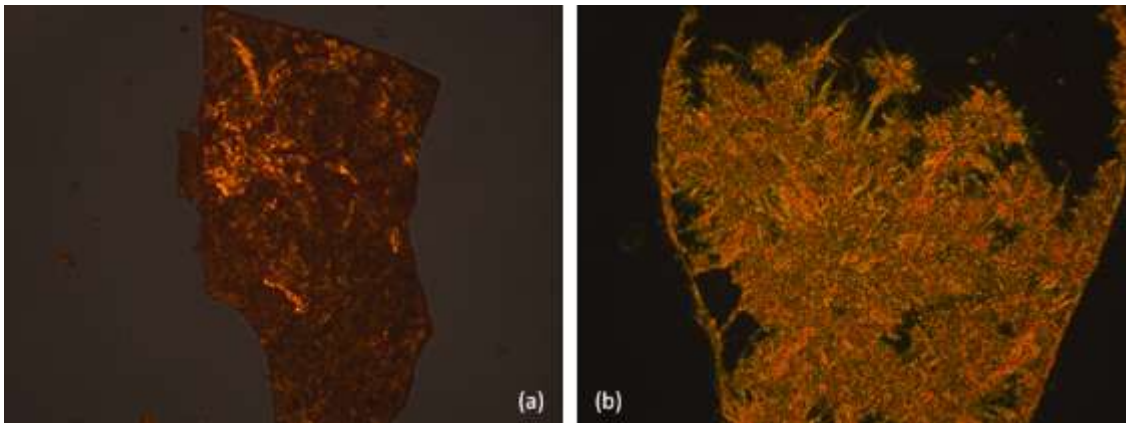


Figure 3.55 Heating process: (a) at 100° C and cooling process: (b) at 140° C.

3.7.4 Synthesis and characterization of G2-DPP spacer

The same procedure described for the synthesis of **29** was applied to synthesized **G2-DPP spacer**. Introducing in structure **25**, a small ligand, as shown in Scheme 3.56, the molecular target, **30**, was obtained as a colourless solid in 93 % yield.

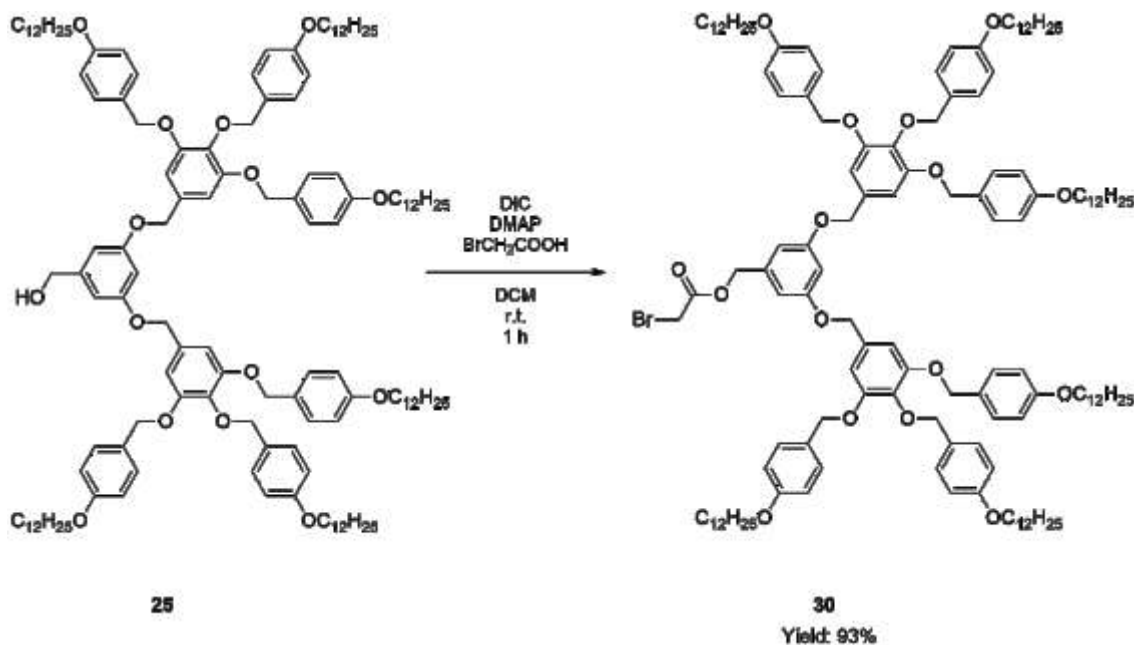


Figure 3.56 Synthesis of **30**.

The following nucleophilic substitution between DPP, **22**, and substrate **30**, as occurred for the synthesis of **G2-DPP** did not lead to the molecular target, **31**.

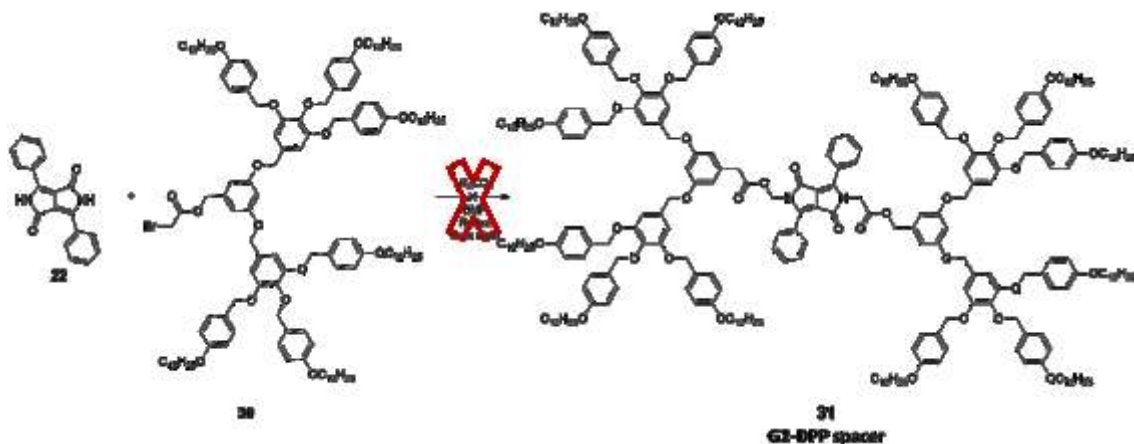


Figure 3.57 Synthesis of **31**.

In order to obtain pure **31**, other synthetic paths were exploited. At first, the diacid derivative of DPP, **32**, was used to conduct a nucleophilic substitution with molecule **26**, as shown in Scheme 3.58. The reaction was performed in a mixture of dry DMF and THF and using K₂CO₃, as base. Unfortunately product **31** could not be isolated.

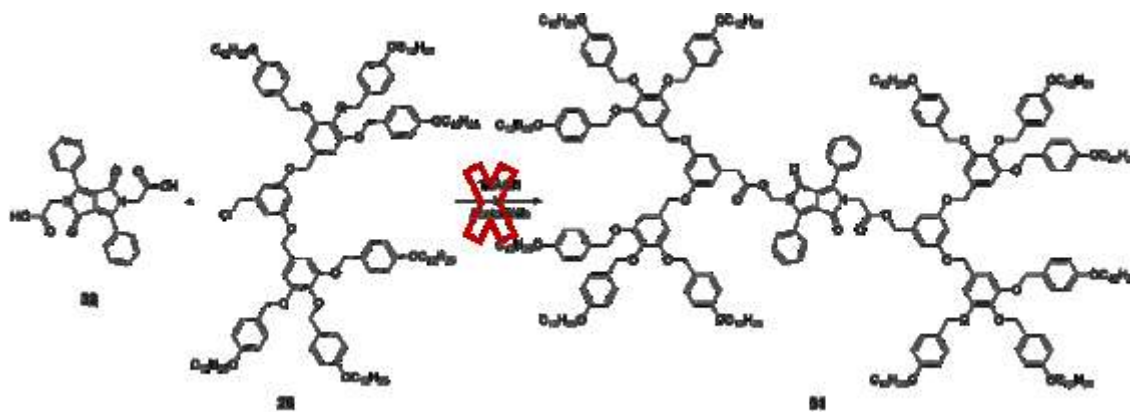


Figure 3.58 Synthetic strategy to obtain **31**.

Thus, the active ester of DPP **33**, was used in place of **32** but also in this case the pure product **31** could not be isolated.

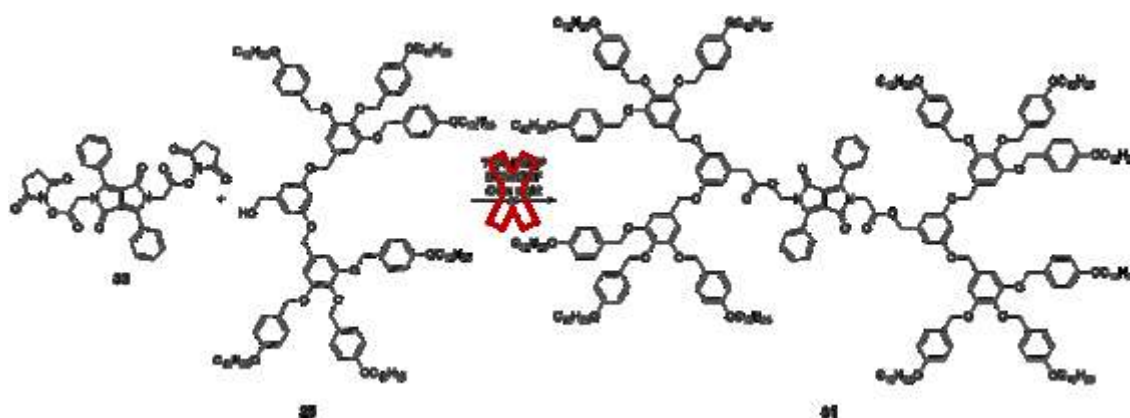


Figure 3.59 Synthetic strategy to obtain **31**.

The low yield of the reactions, probably due to the steric hindrance of second generation, together with the formation of by-products and the low solubility of the molecular target made difficult the isolation of **31** and it was not possible to achieve the necessary purity to conduct POM and DSC analysis.

3.8 Conclusions

In this work we have used dendrimers as tool to explore other possible supramolecular organizations of DPP compounds. Poly(benzylether) dendrimers of first and second generation have been synthesized using the convergent synthetic approach and **4**, **11**, **16** compounds have been obtained (Figure 3.60).

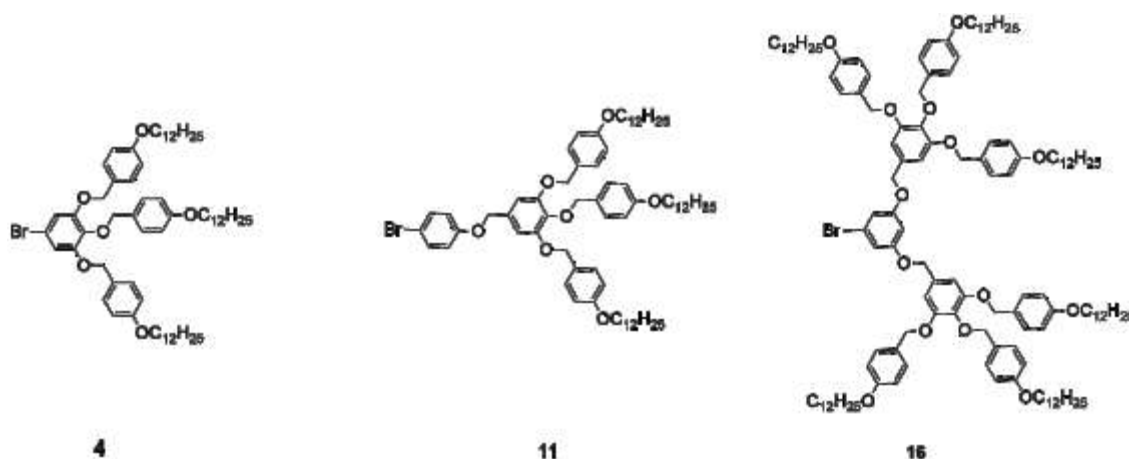


Figure 3.60 New substrates synthesized using convergent synthesis.

These new molecules have been characterized by elemental analysis, POM and DSC. Compounds **4** and **11** do not develop mesomorphic phase, while for **16**, it is possible to distinguish the typical columnar mesophase of poly (benzyl ether) dendrimers. The molecules **4**, **11**, **16** have been converted to the corresponding three pinacol boronic esters as shown in Figure 3.61, using Myaura borylation reaction. These compounds have been used in cross-coupling reaction with **BrDPP-Boc**.

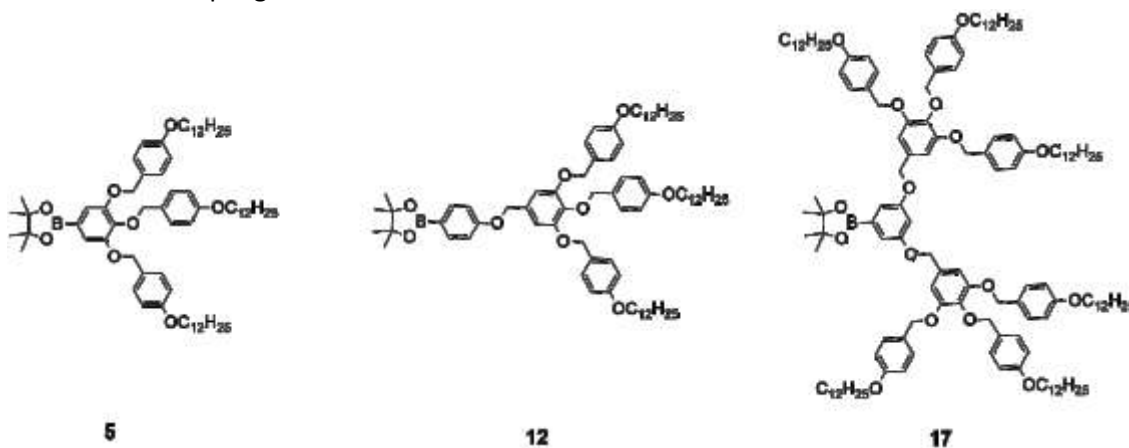


Figure 3.61 Pinacol boronic esters of first generation (**5**, **12**) and of second generation (**17**).

These molecular structures do not exhibit mesophase. Moreover once in a liquid phase, the pinacol boronic esters need long time to return in the solid state and for this reason the DSC spectra, for all the three samples, display only a peak in the first heating process.

The use of the Suzuki cross coupling reactions, to attach the dendrimers to **BrDPP-Boc**, has shown a significant disadvantage: the pure products cannot be isolated without hydrolysing them. Moreover, the hydrolysis cannot be conducted in the traditional way with 5 % of TFA

because the dendrimeric structures collapse even in weak acid conditions. Thus the three compounds are left to be absorbed on silica gel to conduct the hydrolysis and then purified through FC. This synthetic approach shows two disadvantages: long time of deprotection reaction and the low yields due to the decomposition of a part of the products in silica gel. The substrates **7**, **14**, **18b**, shown in Figure 3.62, have been isolated and characterized.

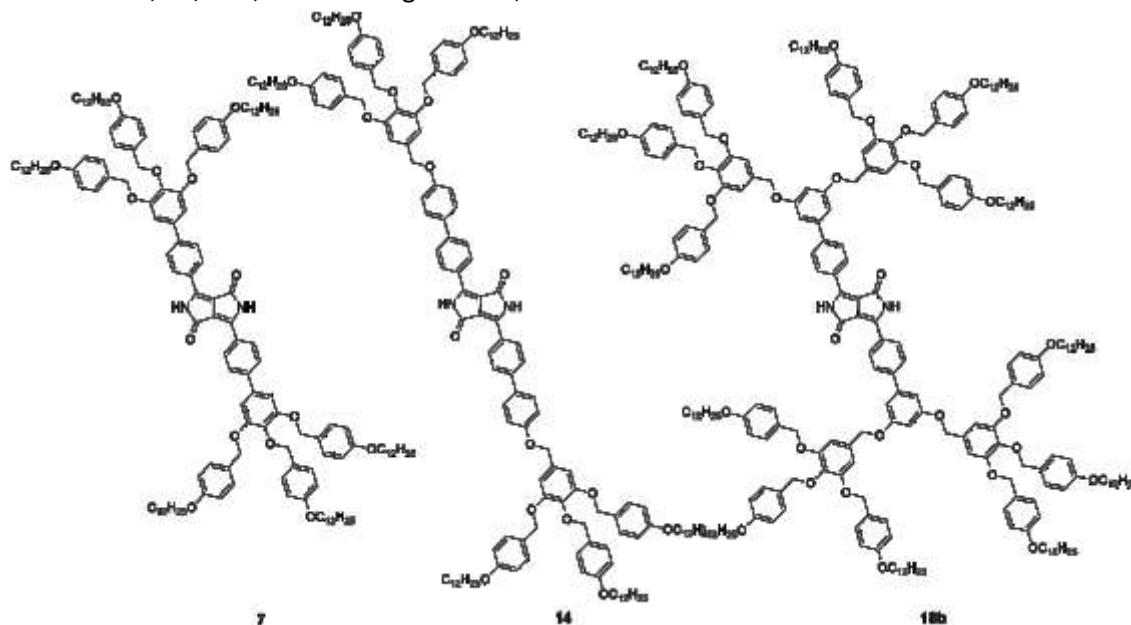


Figure 3.62 Molecular targets based on deprotected DPP.

For these three molecules, it is not possible to observe a transition phase. At room temperature they have a viscous and rubbery aspect letting us to suppose the presence of a mesophase even at low temperature, but the textures are too thick to distinguish any kind of mesomorphic phase. Moreover, they feature high melting points (>240° C) and the structures collapse before to reach the liquid state and for this reason DSC did not give any information.

On the basis of these results we have decided to modify the dendrimer's core substituting the **BrDPP-Boc** in the Suzuki cross coupling reaction with the Br DPP protected with methyl groups. With this substitution products **20** and **21** are obtained, shown in Figure 3.63, in better yields (from 16 % of molecule **14** to 47 % of molecule **20**).

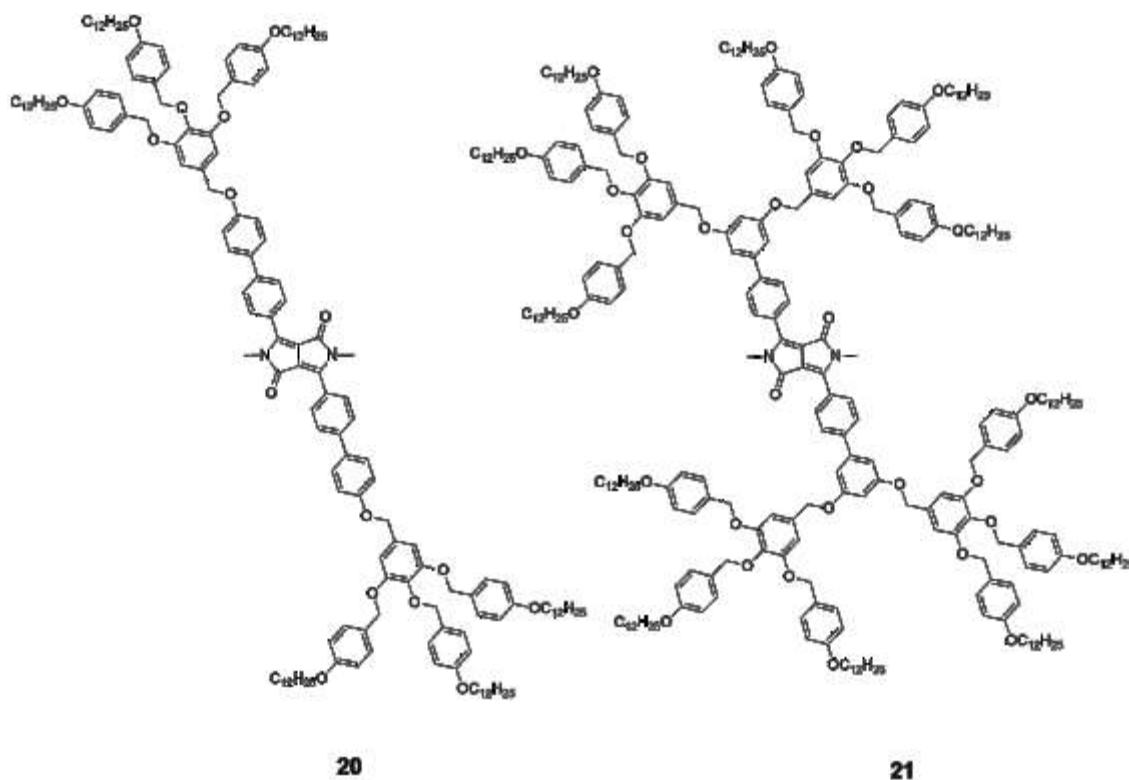


Figure 3.63 Molecular targets based on methyl-DPP.

Molecules **20** and **21** observed at POM show a birefringent, viscous and rubbery aspect as shown from molecules **7**, **14**, **18b** and in this case the presence of a mesomorphic state already at room temperature can be supposed. Changing temperature the substrate **20** develops a stable columnar mesophase, as displayed in Figure 3.64, (a), while the texture formed by **21** is too thick to identify any phase, as shown in Figure 3.64, (b).

An important consideration concerns the isotropization temperature: for **20** and **21** this value is lower than that of **7**, **14**, **18b** (175° C for **20** and more than 240° C for **14**). This significant change can be due to the supramolecular contribution that hydrogen bonds induce in structures **7**, **14**, **18b**.

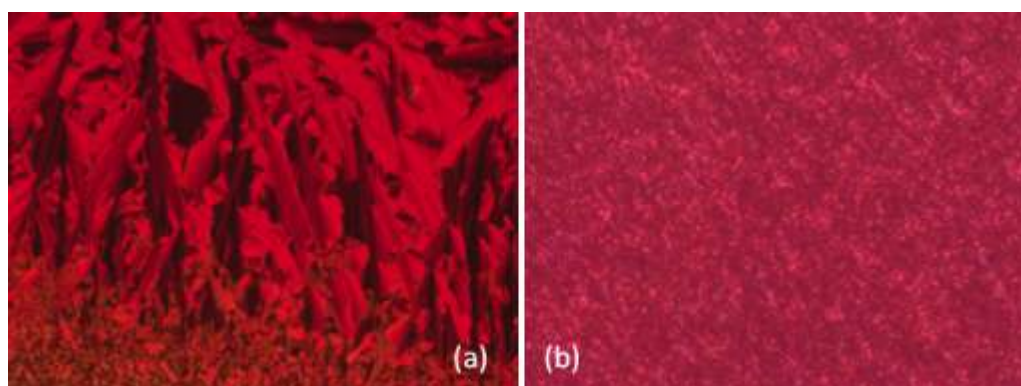


Figure 3.64 Substrate 20 (a) and 21 (b) observed at POM.

With this information new DPPs N-functionalised with G1 and G2 dendrimers are synthesized to verify how the molecules' behaviour changes. Product **23** is isolated while product **27** is

formed in too small quantity to obtain a sample with a sufficient purity for the characterization (Figure 3.65).

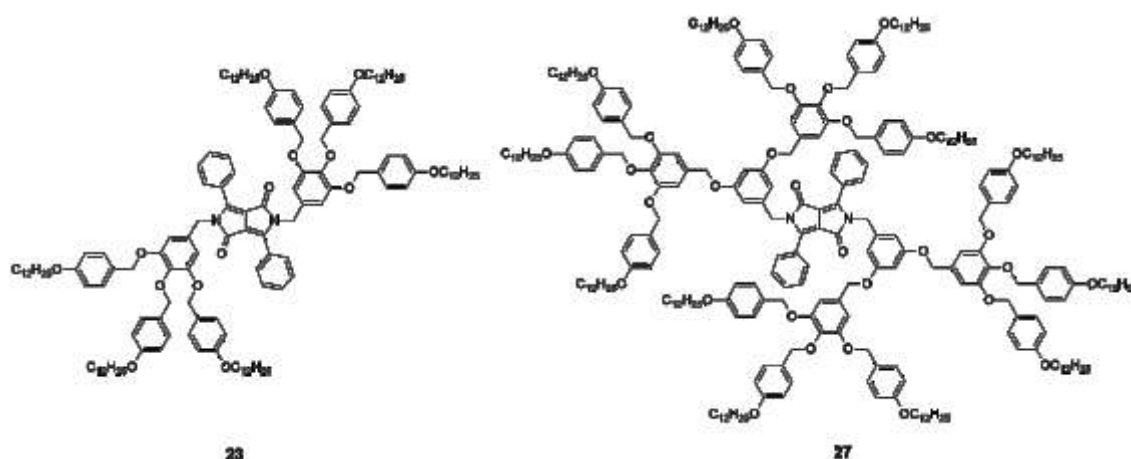


Figure 3.65 N-functionalised DPP with G1 and G2.

For this reason a spacer is introduced to obtain an unhindered and more reactive system, but also in this attempt only the dendrimer of first generation, shown in Figure 3.66, **29**, is isolated. The low yield of the reaction, probably due to the steric hindrance of second generation, together with the formation of by-products and the low solubility of the molecular target make difficult the isolation of **31** in good purity.

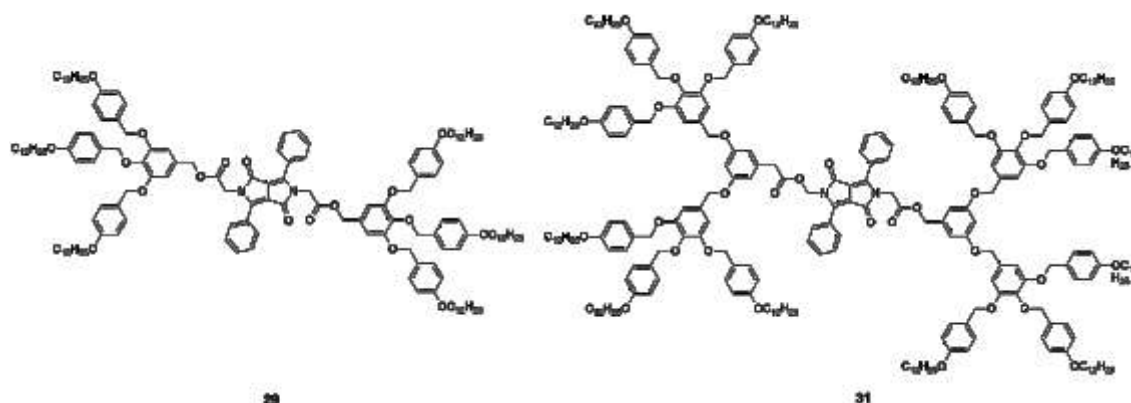


Figure 3.66 N-functionalized DPP with G1 and G2 spacer.

Product **23** and **29** have been characterized: for both structures the DSC spectra seem to show the presence of a mesophase and the isotropization occurs at lower temperature (120° C for **24** and 145° C for **30**). POM experiments reveal that the two textures are too thick to be distinguished.

Unfortunately, also X-Ray experiments do not give information: the high viscosity of these substrates and their high thermal stability make their analysis difficult to be performed.

3.9 Experimental Section

3.9.1 General

Solvents and reagents were used as purchased. Column chromatography was performed on silica gel MERK 60, 0.04-0.063 mm/230-400 mesh and thin layer chromatography (TLC) was conducted on Alugram silica gel UV₂₅₄ (Macherey-Nagel).

¹H-NMR spectra were recorded on a Bruker AMX-400 MHz using TMS (δ :0 ppm), CDCl₃ (δ :7.26 ppm), (CD₃)₂SO (δ :2.55 ppm) and CD₂Cl₂ (δ :5.3 ppm) as internal standard. Coupling constants (J) were denoted in Hz and chemical shifts (δ) in ppm. Multiplicities were denoted as follows: s= singolet, d= doublet, m= multiplet.

POM studies were conducted through an Axio Scope Zeiss with THMS600 based on Linkam 93 system. Photos are taken with a AxioCam MRc (Zeiss) and visualised with Axio Vision Rel 4.8.

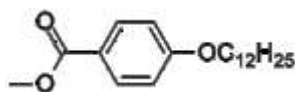
DSC analysis were recorded on a METTLER DSC 822 or METTLER DSC 1. The instrument was calibrated with a sample of indium ($F_{In} = 156.6^\circ \text{C}$, $\Delta_f(\text{In}) = 28.45 \text{ J/g}$) and zinc ($F_{Zn} = 419.6^\circ \text{C}$, $\Delta_f(\text{Zn}) = 28.45 \text{ J/g}$). Samples were analysed in aluminium capsules (40 μl) under nitrogen atmosphere. Samples were analysed with a cooling and heating speed of $10^\circ \text{C}/\text{min}$. Transition temperatures were extrapolated by onset values and enthalpies were calculated by the area of peaks.

Elemental Analysis were conducted in collaboration with the Swiss Federal Institute of Technology of Zurich.

Maldi-TOF mass spectra were conducted in collaboration with the University of Fribourg, whereas mass spectra were carried out with a *Finnigan LCQ* ion trap mass spectrometer equipped with an *electrospray ionization (ESI)* source.

3.9.2 Synthetic procedures

Synthesis of methyl 4-(dodecyloxy)benzoate, **1**

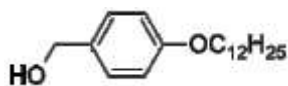


1

A mixture of methyl 4-hydroxybenzoate (12 g, 0.078 mol), K_2CO_3 (21.70 g, 0.157 mol) in acetone (72 mL) was stirred at room temperature for 45 minutes under argon. After bromododecane was added and the mixture was heated at reflux over night. After cooling to room temperature the mixture was filtered to remove K_2CO_3 . The filtrate was concentrated and extracted with diethyl ether. The organic phase was washed with brine and dried with $MgSO_4$ and the solvent was evaporated. The product was purified by crystallization into heptane (100 mL) to give compound **1** (22.40 g, yield: 90 %).

1H NMR (400 MHz, CD_2Cl_2), δ (ppm): 7.93 (d, $J = 8.7$ Hz, 2H, H_{arom}), 6.89 (d, $J = 8.7$ Hz, 2H, H_{arom}), 3.99 (t, $J = 6.6$ Hz, 2H, OCH_2), 3.82 (s, 3H, OCH_3), 1.79-1.73 (m, 2H, OCH_2CH_2), 1.47-1.20 (m, 18H, H_{aliph}), 0.86 (t, $J = 16$ Hz, 3H, CH_2CH_3). PM ($C_{20}H_{32}O_3$): 320.47 u.

Synthesis of (4-(dodecyloxy)phenyl)methanol, **2**

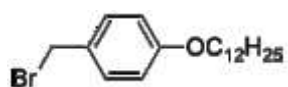


2

Compound **1** (20g, 62.45mmol) was dissolved in dry THF (100mL) and the solution was added in small portion to a solution of $LiAlH_4$ (4.74g, 124.90mmol) in THF at 0° C. The reaction mixture was allowed to room temperature and stirred for 2 hours under argon. The reaction was quenched with ice/water and then extracted with diethyl ether twice. The organic phase was washed with brine and dried with $MgSO_4$ and the solvent was evaporated to give compound **2** (17.90 g, yield: 96 %).

1H NMR (400 MHz, CD_2Cl_2), δ (ppm): 7.24 (d, $J = 8.5$ Hz, 2H, H_{arom}), 6.84 (d, $J = 8.5$ Hz, 2H, H_{arom}), 4.55 (d, $J = 5.8$ Hz, 2H, CH_2OH), 3.92 (t, $J = 6.6$ Hz, 2H, OCH_2), 1.82-1.64 (m, 2H, OCH_2CH_2), 1.57-1.17 (m, 18H, H_{aliph}), 0.86 (t, $J = 6.7$ Hz, 3H, CH_2CH_3). PM ($C_{19}H_{32}O_2$): 292.46 u.

Synthesis of 1-(bromomethyl)-4-(dodecyloxy)benzene, **3**

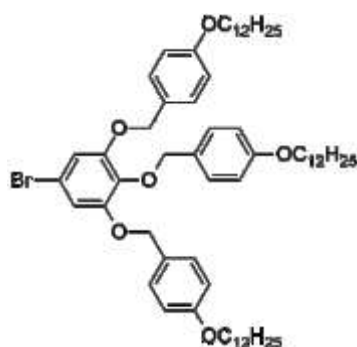


3

A mixture of **2** (15 g, 51.28 mmol) and PBr_3 (2.45 mL, 25.64 mmol) in dry DCM (300 mL) was stirred at reflux for 18 hours under argon. The reaction was quenched with water and extracted with DCM twice. The organic phase was washed with brine, dried with MgSO_4 and the solvent was evaporated to give compound **3** (17.98 g, yield: 98 %).

^1H NMR (400 MHz, CD_2Cl_2), δ (ppm): 7.29 (d, $J = 8.5$ Hz, 2H, H_{arom}), 6.83 (d, $J = 8.5$ Hz, 2H, H_{arom}), 4.50 (s, 2H, CH_2Br), 3.93 (t, $J = 6.6$ Hz, 2H, OCH_2), 1.83–1.62 (m, 2H, OCH_2CH_2), 1.50–1.19 (m, 18H, H_{aliph}), 0.86 (t, $J = 16$ Hz, 3H, CH_2CH_3). PM ($\text{C}_{19}\text{H}_{31}\text{BrO}$): 335.35 u.

Synthesis of 4,4',4''-(((5-bromobenzene-1,2,3-triyl)tris(oxy))tris(methylene))tris((dodecyloxy)benzene), **4**

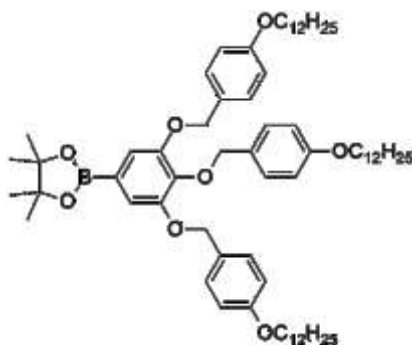


4

A solution of 5-bromobenzene-1,2,3-triol (2.0 g, 9.75 mmol), K_2CO_3 (10.78 g, 78 mmol) in acetone (130 mL) was stirred for 45 minutes at room temperature under argon. A solution of **3** (13.86 g, 39 mmol) in acetone (80 mL) was added. The reaction mixture was heated at reflux over night. The reaction mixture was filtered and the solvent was evaporated. The crude product was extracted with DCM. The organic phase was washed with brine, dried with MgSO_4 and evaporated under reduced pressure. The crude product was purified by crystallisation in acetone to give compound **4** (5.51 g, yield: 55 %).

EA: [C] 73.52 %, [H] 9.33 %. ^1H NMR (400 MHz, CD_2Cl_2), δ (ppm): 7.30 (d, $J = 8.4$ Hz, 4H, H_{arom}), 7.18 (d, $J = 8.5$ Hz, 2H, H_{arom}), 6.78 (s, 2H, H_{arom}), 6.88 (d, $J = 8.5$ Hz, 4H, H_{arom}), 6.74 (d, $J = 8.5$ Hz, 2H, H_{arom}), 4.94 (s, 4H, OCH_2), 4.84 (s, 2H, OCH_2), 3.96–3.88 (m, 6H, OCH_2), 1.88–1.80 (m, 6H, OCH_2CH_2), 1.46–1.28 (m, 54H, H_{aliph}), 0.86 (t, $J = 6.8$ Hz, 9H, CH_2CH_3). ^{13}C NMR (100 MHz, CDCl_3), δ 204.48, 204.34, 159.10, 158.92, 153.78, 130.25, 129.13, 128.36, 116.13, 114.44, 114.05, 111.78, 71.24, 68.02, 31.87, 29.62, 29.59, 29.56, 29.38, 29.30, 29.24, 26.02, 22.64, 14.07. PM ($\text{C}_{65}\text{H}_{95}\text{BrO}_6$): 1028.33 u. MS (ESI) m/z : 1050.1 ($\text{M}^+ + \text{Na}^+$, 100 %).

Synthesis of 4,4,5,5-tetramethyl-2-(3,4,5-tris((4-(dodecyloxy)benzyl)oxy)phenyl)-1,3,2-dioxaborolane, 5, G1 pinacol ester



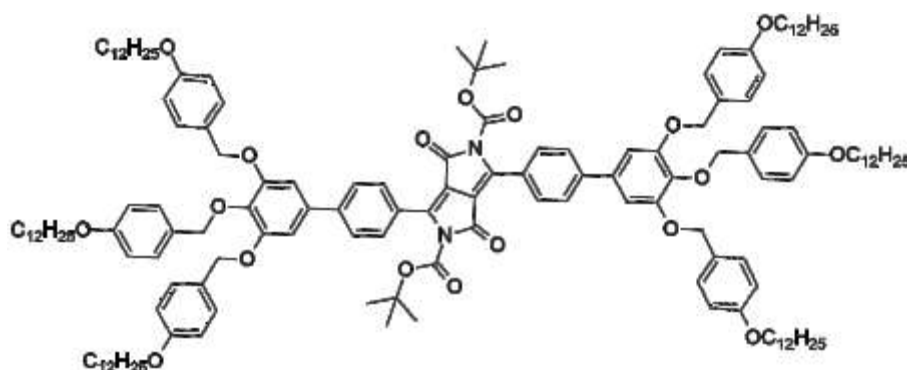
5

G1 pinacol boronic ester

Compound **4** (1.00 g, 0.97 mmol), dichlorobis(triphenylphosphine)palladium (22 mg, 0.032 mmol), bis(pinacolato)diboron (370 mg, 1.45 mmol), and potassium acetate (285 mg, 2.91 mmol) were flushed with argon and charged with a mixture of degassed dioxane (12 mL). The mixture was heated at 80° C for 12 hrs, cooled, and then extracted with DCM. The combined extracts were dried over anhydrous MgSO₄ and evaporated. The crude product was purified by precipitation (acetone/MeOH) to give compound **5** as a colourless solid (0.731 g, yield: 70 %).

EA: [C] 76.67 %, [H] 9.98 %. EA: [C] 76.67 %, [H] 9.98 %. ¹H NMR (400 MHz, CD₂Cl₂), δ (ppm): 7.30 (d, J = 8.4 Hz, 4H, H_{arom}), 7.18 (d, J = 8.5 Hz, 2H, H_{arom}), 7.08 (s, 2H, H_{arom}), 6.88 (d, J = 8.5 Hz, 4H, H_{arom}), 6.74 (d, J = 8.5 Hz, 2H, H_{arom}), 4.94 (s, 4H, OCH₂), 4.84 (s, 2H, OCH₂), 3.96-3.88 (m, 6H, OCH₂), 1.88-1.80 (m, 6H, OCH₂CH₂), 1.46-1.28 (m, 66H, H_{aliph}+C(CH₃)₂), 0.86 (t, J = 6.8 Hz, 9H, CH₂CH₃). ¹³C NMR (100 MHz, CDCl₃), δ (ppm): 158.87, 158.79, 152.74, 130.20, 129.29, 129.16, 114.35, 114.00, 83.83, 71.08, 68.01, 31.89, 29.66, 29.59, 29.57, 29.55, 29.41, 29.39, 29.34, 29.26, 26.03, 24.76, 22.67, 14.11. PM (C₆₉H₁₀₇BO₇): 1075.39 u. MS (ESI) m/z: 1098.2 (M⁺+Na⁺, 100 %).

Synthesis of di-tert-butyl 1,4-dioxo-3,6-bis(3',4',5'-tris((4-(dodecyloxy)benzyl)oxy)-[1,1'-biphenyl]-4-yl)pyrrolo[3,4-c]pyrrole-2,5(1H,4H)-dicarboxylate, 6



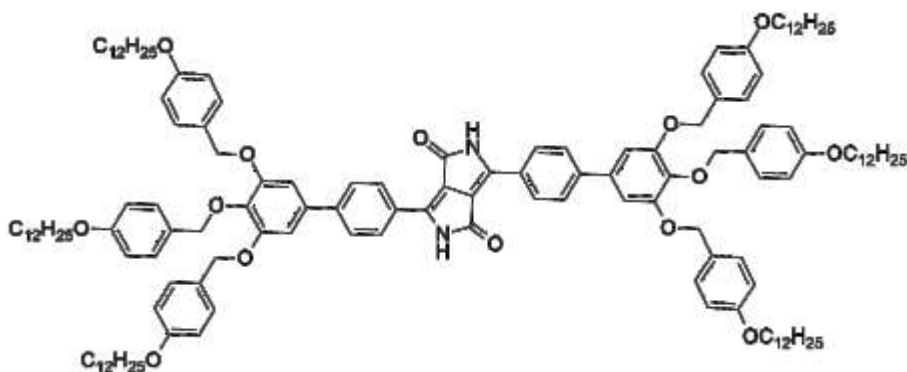
6

G1-pDPP Boc

To a suspension of degassed toluene (12.0 mL) and K_2CO_3 (2.3 mL of a 2 M aqueous solution) were added, under argon atmosphere, Br DPP-Boc (50 mg, 0.084 mmol), product **5** (188 mg, 0.177 mmol) and a catalytic amount (1 % m/m) of $Pd(PPh_3)_4$. The resulting mixture was heated at 80° C for 27 hours, cooled and then extracted with DCM. The combined extracts were dried over anhydrous $MgSO_4$ and evaporated under reduced pressure. The crude product was not purified (Crude: 200 mg).

1H NMR (400 MHz, CD_2Cl_2), δ (ppm): 7.79 (d, $J = 8.1$ Hz, 4H, H_{arom}), 7.65 (d, $J = 8.3$ Hz, 4H, H_{arom}), 7.35 (d, $J = 8.5$ Hz, 8H, H_{arom}), 7.25 (d, $J = 8.2$ Hz, 4H, H_{arom}), 6.94 (s, 4H, H_{arom}), 6.89 (m, 8H, 8H), 6.74 (d, $J = 8.4$ Hz, 4H), 5.05 (s, 8H, OCH_2), 4.93 (s, 4H, OCH_2), 3.97-3.88 (m, 12H, OCH_2), 1.78-1.69 (m, 12H, OCH_2CH_2), 1.42-1.22 (m, 126H, $H_{aliph} + C(CH_3)_3$), 0.85 (t, 12H, 18H, CH_2CH_3). PM ($C_{154}H_{216}N_2O_{18}$): 2383,37 u.

Synthesis of 3,6-bis(3',4',5'-tris((4-(dodecyloxy)benzyl)oxy)-[1,1'-biphenyl]-4-yl)pyrrolo[3,4-c]pyrrole-1,4(2H,5H)-dione, **7**, G1-pDPP

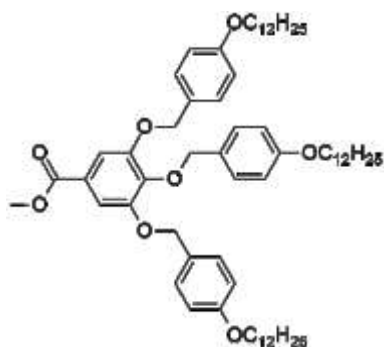


7
G1-pDPP

A mixture of compound **6** (200 mg, 0.08 mmol) and silica-gel (5 g) in DCM was evaporated under reduced pressure. The compound was left in silica for 10 days. The crude product was purified by column chromatography (100 % DCM) to obtain the desired product (16 mg yield of two steps: 9 %).

1H NMR (400 MHz, $CDCl_3$), δ (ppm): 7.25 (d, $J = 4.0$ Hz, 4H, H_{arom}), 8.06 (s, 2H, NH), 7.68 (d, $J = 8.4$ Hz, 4H, H_{arom}), 7.34 (d, $J = 8.0$ Hz, 8H, H_{arom}), 7.31 (d, $J = 8$ Hz, 4H, H_{arom}), 6.93-6.88 (s+d, 12H, H_{arom}), 6.79 (d, $J = 8.0$ Hz, 4H, H_{arom}), 5.08 (s, 8H, CH_2Ph), 5.00 (s, 4H, CH_2Ph), 4.00-3.91 (m, 12H, OCH_2), 1.83-1.73 (m, 12H, OCH_2CH_2), 1.51-1.21 (m, 108H, H_{aliph}), 0.88 (t, $J = 6.5$ Hz, 18H, CH_2CH_3). ^{13}C NMR (100 MHz, CD_2Cl_2), δ (ppm): 204.33, 154.45, 150.75, 130.03, 129.25, 128.89, 114.31, 113.90, 68.03, 53.87, 53.60, 53.33, 53.05, 52.78, 31.85, 29.60, 29.57, 29.38, 29.28, 25.98, 22.61, 13.79. PM ($C_{144}H_{200}N_2O_{14}$): 2183,13 u. MS (MALDI-TOF) m/z: 2205.49($M^+ + Na^+$, 100 %).

Synthesis of methyl 3,4,5-tris((4-(dodecyloxy)benzyl)oxy)benzoate, **8**

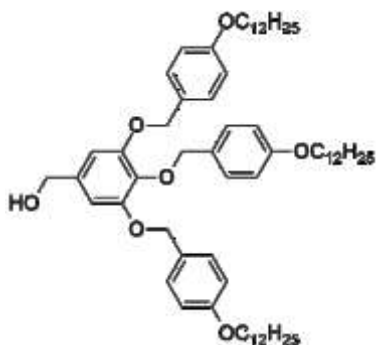


8

A mixture of methyl 3,4,5-trihydroxybenzoate (4.20 g, 22.80 mmol), K_2CO_3 (25.21 g, 182.40 mmol) in acetone (300 mL) was stirred at room temperature for 30 minutes under argon. A solution of compound **3** (32.40 g, 91.20 mmol) in acetone (200 mL) was added. The mixture was heated at reflux over night. The reaction mixture was filtered and the solvent was evaporated. The crude product was extracted with DCM twice. The organic phase was washed with brine and dried with $MgSO_4$, the solvent was evaporated. The product was purified by crystallization in acetone (300 mL) to give compound **8** (17.37, yield: 75 %).

1H NMR (400 MHz, CD_2Cl_2), δ (ppm): 7.32 (d+s, 6H, H_{arom}), 7.20 (d, $J = 8.6$ Hz, 2H, H_{arom}), 6.88 (d, $J = 8.5$ Hz, 4H, H_{arom}), 6.72 (d, $J = 8.4$ Hz, 2H, H_{arom}), 5.01 (s, 4H, OCH_2), 4.94 (s, 2H, OCH_2), 4.00–3.86 (m, 6H, OCH_2), 3.84 (s, 3H, OCH_3), 1.78–1.71 (m, 6H, OCH_2CH_2), 1.46–1.22 (m, 54H, H_{aliph}), 0.86 (t, $J = 6.5$ Hz, 9H, CH_2CH_3). PM ($C_{65}H_{98}O_8$): 1007,47 u.

Synthesis of (3,4,5-tris((4-(dodecyloxy)benzyl)oxy)phenyl)methanol, **9**

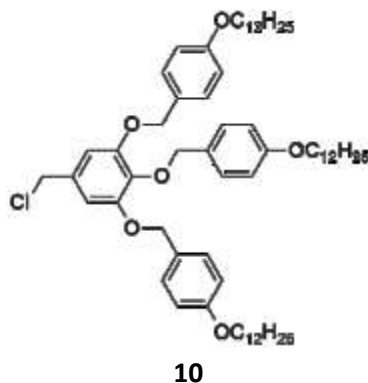


9

Compound **8** (17.37 g, 17.73 mmol) was dissolved in dry THF (110 mL) and the solution was added in small portions to a solution of $LiAlH_4$ (1.34 g, 35.46 mmol) and dry THF at $0^\circ C$. The reaction mixture was allowed to room temperature and stirred for 2 hours under argon. The reaction was quenched with ice/water and then extracted with diethyl ether twice. The organic phase was washed with brine, dried with $MgSO_4$ and the solvent was evaporated to give compound **9** (16 g, yield: 92 %).

^1H NMR (400 MHz, CD_2Cl_2), δ (ppm): 7.32 (d, $J = 8.5$ Hz, 4H, H_{arom}), 7.22 (d, $J = 8.5$ Hz, 2H, H_{arom}), 6.88 (d, $J = 8.5$ Hz, 4H, H_{arom}), 6.73 (d, $J = 8.4$ Hz, 2H, H_{arom}), 6.65 (s, 2H, H_{arom}), 4.99 (s, 4H, OCH_2), 4.86 (s, 2H, OCH_2), 4.55 (d, $J = 6.1$ Hz, 2H, CH_2OH), 3.97-3.88 (m, 6H, OCH_2), 1.82-1.67 (m, 6H, OCH_2CH_2), 1.47-1.22 (m, 54H, H_{aliph}), 0.86 (t, $J = 6.6$ Hz, 9H, CH_2CH_3). PM ($\text{C}_{64}\text{H}_{98}\text{O}_7$): 979,46 u.

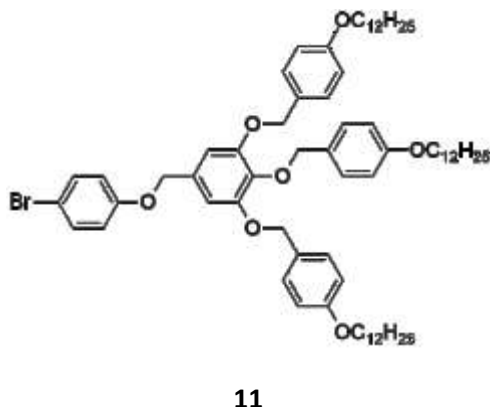
Synthesis of 4,4',4''-(((5-(chloromethyl)benzene-1,2,3 triyl)tris(oxy))tris(methylene)) tris((dodecyloxy) benzene), 10



A solution of SOCl_2 (1.25 mL, 15.42 mmol) in dry DCM (25 mL) was added dropwise to a solution of compound **9** (15 g, 15.31 mmol), DTBP (5.15 mL, 22.96 mmol) in dry DCM (115 mL) under argon. The reaction mixture was stirred for 30 minutes at room temperature. Then the solution was extracted with HCl 2N and the organic phase was washed with brine, dried with MgSO_4 and the solvent was evaporated to give compound **10** (11 g, yield: 73 %).

^1H NMR (400 MHz, CD_2Cl_2), δ (ppm): 7.32 (d, $J = 8.5$ Hz, 4H, H_{arom}), 7.21 (d, $J = 8.4$ Hz, 2H, H_{arom}), 6.88 (d, $J = 8.8$ Hz, 4H, H_{arom}), 6.73 (d, $J = 8.0$ Hz, 2H, H_{arom}), 6.71 (s, 2H, H_{arom}), 4.98 (s, 4H, CH_2Ph), 4.87 (s, 2H, CH_2Ph), 4.52 (s, 2H, CH_2Cl), 3.97-3.87 (m, 6H, OCH_2), 1.79-1.70 (m, 6H, OCH_2CH_2), 1.51-1.29 (m, 54H, H_{aliph}), 0.86 (t, $J = 6.7$ Hz, 9H, CH_2CH_3). PM ($\text{C}_{64}\text{H}_{97}\text{ClO}_6$): 997,90 u.

Synthesis of 4,4',4''-(((5-((4-bromophenoxy)methyl)benzene-1,2,3-triyl)tris(oxy))tris(methylene)) tris((dodecyloxy)benzene), 11

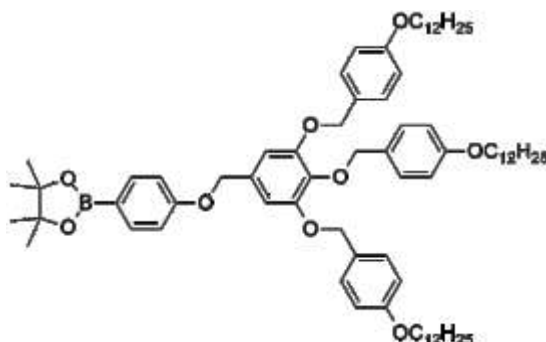


A solution of 4-bromophenol (500 mg, 2.89 mmol), K_2CO_3 (2.79 g, 20.23 mmol) in DMF (12 mL) was stirred for 45 minutes at room temperature under argon. A solution of **10** (3.17 g, 3.79

mmol) in DMF (10 mL) was added. The reaction mixture was heated at reflux over night. The reaction was quenched with water and extracted with DCM. The organic phase was washed with brine, dried with MgSO₄ and evaporated under reduced pressure. The crude product was purified by precipitation (Acetone/MeOH) to give compound **11** (2.7 g, yield: 84 %).

EA: [C] 73.94 %, [H] 8.93 %. ¹H NMR (400 MHz, CD₂Cl₂), δ (ppm): 7.39 (d, *J* = 8.0 Hz, 2H, H_{arom}), 7.33 (d, *J* = 8.0 Hz, 4H, H_{arom}), 7.25 (d, *J* = 8.0, 2H, H_{arom}), 6.90 (d, *J*=8, 4H, H_{arom}), 6.85 (d, *J*=9.2 Hz, 2H, H_{arom}), 6.75 (d, *J*=8, 2H, H_{arom}), 6.71 (s, 2H, H_{arom}), 5.01 (s, 4H, CH₂Ph), 4.94 (s, 2H, CH₂Ph), 4.90 (s, 2H, CH₂Ph), 4.00-3.91 (m, 6H, OCH₂), 1.83-1.71 (m, 6H, OCH₂CH₂), 1.50-1.24 (m, 54H, H_{aliph}), 0.89 (t, *J* = 6.6 Hz, 9H, CH₂CH₃). ¹³C NMR (100 MHz, CDCl₃), δ (ppm) 158.97, 153.12, 132.16, 131.70, 130.27, 129.18, 129.02, 116.67, 114.46, 113.93, 107.31, 71.10, 70.31, 68.02, 67.94, 31.87, 29.62, 29.39, 29.31, 29.26, 26.03, 22.69, 14.07. PM (C₇₀H₁₀₁BrO₇): 1134,45 u. MS (ESI) m/z: 1156.0 (M⁺+Na⁺, 100 %).

Synthesis of 4,4,5,5-tetramethyl-2-(4-((3,4,5-tris((4-(dodecyloxy)benzyl)oxy)benzyl)oxy)phenyl)-1,3,2-dioxaborolane, **12**, G1.1 pinacol ester



12

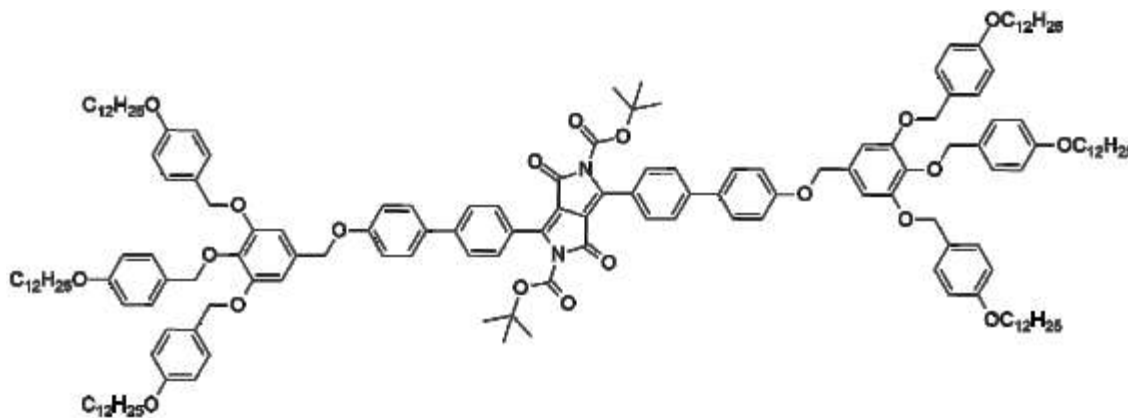
G1.1 pinacol boronic ester

Compound **11** (1.00 g, 0.88 mmol), dichlorobis(triphenylphosphine)palladium (20.35 mg, 0.029 mmol), bis(pinacolato)diboron (335 mg, 1.32 mmol), and potassium acetate (259 mg, 2.64 mmol) were flushed with argon and charged with a mixture of degassed dioxane (11 mL). The mixture was heated at 80° C for 12 hrs, cooled, and then extracted with DCM. The combined extracts were dried over anhydrous MgSO₄ and evaporated. The crude product was purified by column chromatography (9DCM:1Heptane) to give compound **12** as a colourless solid (0.676 g, yield: 65 %).

AE: [C] 77.29 %, [H] 9.70 %. ¹H NMR (400 MHz, CD₂Cl₂), δ (ppm): 7.71 (d, *J* = 8.4 Hz, 2H, H_{arom}), 7.34 (d, *J* = 8.5 Hz, 4H, H_{arom}), 7.25 (d, *J* = 8.4 Hz, 2H, H_{arom}), 6.97 (d, *J* = 8.0 Hz, 2H, H_{arom}), 6.90 (d, *J* = 8.0 Hz, 2H, H_{arom}), 6.78-6.74 (d+s, 4H, H_{arom}), 5.01 (s, 4H, CH₂Ph), 4.99 (s, 2H, CH₂Ph), 4.90 (s, 2H, CH₂Ph), 4.00-3.90 (m, 6H, OCH₂), 1.84- 1.72 (m, 6H, OCH₂CH₂), 1.50-1.24 (m, 66H, H_{aliph}+C(CH₃)₂), 0.89 (t, *J* = 6.7 Hz, 9H, CH₂CH₃). ¹³C NMR (100 MHz, CD₂Cl₂), δ (ppm): 204.54, 161.12, 159.05, 158.91, 152.92, 137.75, 136.31, 132.27, 130.13, 129.89, 129.34, 128.78,

114.29, 114.08, 113.97, 106.71, 83.49, 74.53, 70.93, 69.96, 68.02, 31.86, 29.61, 29.29, 26.10, 24.48, 22.77, 13.77.PM (C₇₆H₁₁₃BO₉): 1181,52 u. MS (ESI) m/z: 1204.2 (M⁺+Na⁺, 100 %).

Synthesis of di-tert-butyl 1,4-dioxo-3,6-bis(4'-((3,4,5-tris((4-(dodecyloxy)benzyl)oxy)benzyl)oxy)-[1,1'-biphenyl]-4-yl)pyrrolo[3,4-c]pyrrole-2,5(1H,4H)-dicarboxylate, 13

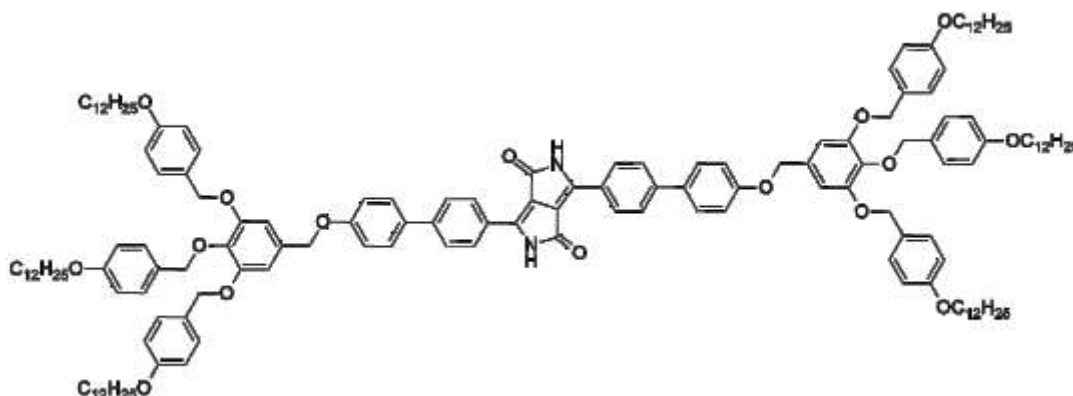


13

To a suspension of degassed toluene (15.0 mL) and K₂CO₃ (3.2 mL of a 2 M aqueous solution) were added, under argon atmosphere, Br DPP-Boc (70 mg, 0.108 mmol), compound **12** (382mg, 0.324mmol) and a catalytic amount (1% m/m) of Pd(PPh₃)₄. The resulting mixture was heated at 80° C for 27 hours, cooled and then extracted with DCM. The combined extracts were dried over anhydrous MgSO₄ and evaporated under reduced pressure. The crude product was not purified (crude: 312 mg).

¹H NMR (400 MHz, CDCl₃), δ (ppm): 7.84 (d, *J* = 8.0 Hz, 4H, H_{arom}), 7.69 (d, *J* = 8.0 Hz, 4H, H_{arom}), 7.62-7.58 (s+d, *J* = 8.0 Hz, 8H, H_{arom}), 7.32 (d, *J* = 16.0 Hz, 8H, H_{arom}), 7.29 (d, *J* = 8.0 Hz, 4H, H_{arom}), 7.05 (d, *J* = 8.0 Hz, 4H, H_{arom}), 6.88 (d, *J* = 8.0 Hz, 8H, H_{arom}), 6.77 (d, *J* = 8.0 Hz, 4H, H_{arom}), 5.04 (s, 8H, CH₂Ph), 4.99 (s, 4H, CH₂Ph), 4.95 (s, 4H, CH₂Ph), 4.00-3.89 (m, 12H, OCH₂), 1.83-1.73 (m, 12H, OCH₂CH₂), 1.40-1.23 (m, 126H, H_{aliph}+ C(CH₃)₃), 0.88 (t, *J* = 16.0 Hz, 18H, CH₂CH₃). PM (C₁₆₈H₂₂₈N₂O₂₀): 2595,61 u.

Synthesis of 3,6-bis(4'-((3,4,5-tris((4-(dodecyloxy)benzyl)oxy)benzyl)oxy)-[1,1'-biphenyl]-4-yl)pyrrolo[3,4-c]pyrrole-1,4(2H,5H)-dione, 14, G1.1-pDPP



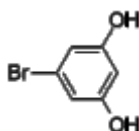
14

G1.1-pDPP

A mixture of compound **13** (312 mg, 0.120 mmol) and silica-gel (5 g) in DCM was evaporated under reduced pressure. The compound was left in silica for 10 days. The crude product was purified by column chromatography (100% DCM) to obtain the desired product (43 mg, yield of two steps: 16%).

PM ($C_{158}H_{212}N_2O_{16}$): 2395.38 u. MS (MALDI-TOF) m/z : 2417.58 ($M^+ + Na^+$, 100 %).

Synthesis of 5-bromobenzene-1,3-diol

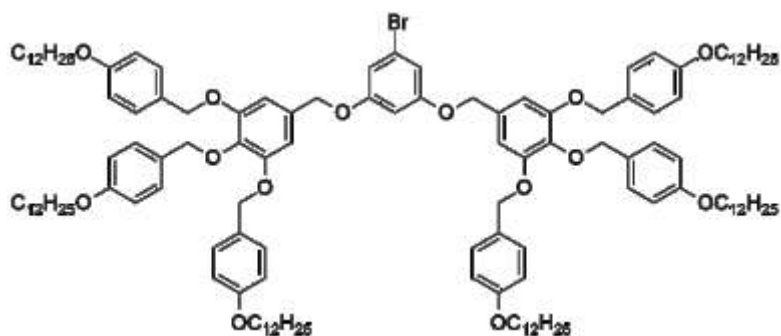


15

A solution of BBr_3 (28.79 mL) was added dropwise to a solution of 1-bromo-3,5-dimethoxybenzene (2.5 g, 11.51 mmol) in dry DCM (15 mL) at $-84^\circ C$. The reaction mixture was allowed to room temperature and stirred for 16 hours under argon. After ice-cold water was added. The mixture was stirred at room temperature for 2 hours and then extracted with ethyl acetate. The organic solution was dried over anhydrous $MgSO_4$, filtered, and evaporated under reduced pressure to give compound **15** as a brown solid (1.85 g, yield: 85%).

1H NMR (400 MHz, $(CD_3)_2SO$), δ (ppm): 9.25 (s, 2H, OH), 8.29 (s, 1H), 6.39 (s, 2H).

Synthesis of 16

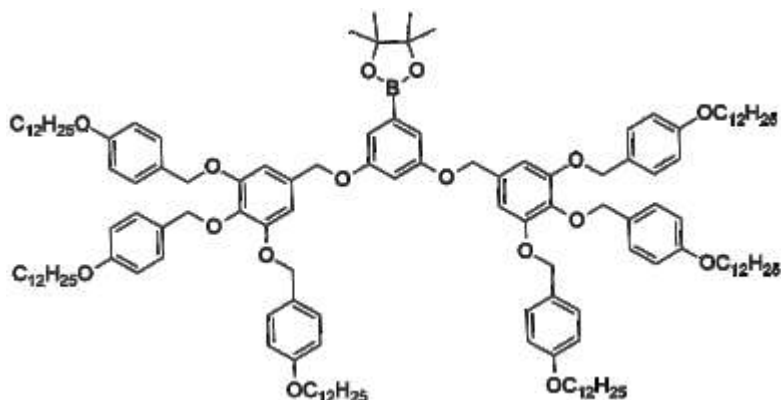


16

A solution of **15** (500 mg, 2.6 mmol), K_2CO_3 (4.31 g, 31.2 mmol) in DMF (11 mL) was stirred for 45 minutes at room temperature under argon then a solution of **9** (5.8 g, 5.81 mmol) in DMF (15 mL) was added at the reaction mixture. The solution was heated at reflux over night. The reaction was quenched with water and extracted with DCM. The organic phase was washed with brine, dried with $MgSO_4$ and evaporated under reduced pressure. The crude product was purified by column chromatography (8DCM:2Heptane) to give compound **16** (4.3 g, yield: 79 %).

AE: [C] 76.43 %, [H] 9.54 %. 1H NMR (400 MHz, CD_2Cl_2), δ 7.34 (d, $J = 8.3$ Hz, 8H, H_{arom}), 7.25 (d, $J = 8.3$ Hz, 4H, H_{arom}), 6.90 (d, $J = 8.5$ Hz, 8H, H_{arom}), 6.78 (d, $J = 8$ Hz, 4H, H_{arom}), 6.76-6.73 (s+d, 6H, H_{arom}), 6.55 (t, $J = 4$ Hz, 1H, H_{arom}), 5.02 (s, 8H, CH_2Ph), 4.94 (s, 4H, CH_2Ph), 4.90 (s, 4H, CH_2Ph), 3.99-3.92 (m, 12H, OCH_2), 1.82-1.73 (m, 12H, OCH_2CH_2), 1.50-1.25 (m, 108H, H_{aliph}), 0.90 (t, $J = 6.7$ Hz, 18H, CH_2CH_3). ^{13}C NMR (100 MHz, CD_2Cl_2), δ (ppm): 158.96, 153.07, 132.14, 130.08, 129.25, 128.91, 114.38, 113.99, 74.59, 70.87, 68.06, 67.94, 31.85, 29.60, 29.54, 29.38, 29.28, 29.24, 25.98, 22.67, 13.82. PM ($C_{134}H_{197}BrO_{14}$): 2111,89 u. MS (MALDI-TOF) m/z: 2134.38 ($M^+ + Na^+$, 100 %).

Synthesis of 2-(3,5-bis((3,4,5-tris((4-(dodecyloxy)benzyl)oxy)benzyl)oxy)phenyl)-4,4,5,5-tetramethyl-1,3,2-dioxaborolane, 17



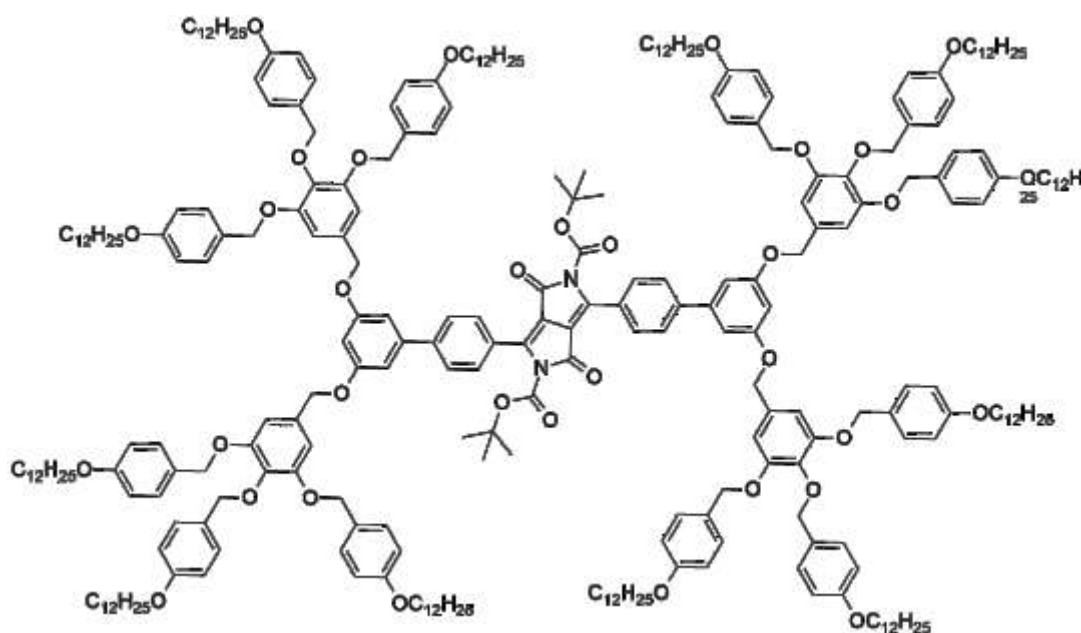
17

G2 pinacol boronic ester

Compound **16** (1.00 g, 0.473 mmol), dichlorobis(triphenylphosphine)palladium (10.00 mg, 0.033 mmol), bis(pinacolato)diboron (180 mg, 0.710 mmol), and potassium acetate (140 mg, 1.419 mmol) were flushed with argon and charged with a mixture of degassed dioxane (6 mL). The mixture was heated at 80° C for 12 hours, cooled, and then extracted with DCM. The combined extracts were dried over anhydrous MgSO₄ and evaporated. The crude product was purified by column chromatography (9DCM:1Heptane) to give compound **17** as a colourless solid (0.694 g, yield: 68 %).

¹H NMR (400 MHz, CD₂Cl₂), δ (ppm): 7.35 (d, *J* = 8.4 Hz, 8H, H_{arom}), 7.26 (d, *J* = 8.4 Hz, 4H, H_{arom}), 7.05 (d, *J* = 4.0 Hz 2H, H_{arom}), 6.91 (d, *J* = 8.5 Hz, 8H, H_{arom}), 6.76 (d+t+s, *J* = 16.69 Hz, 9H, H_{arom}), 5.34 (s, 8H, CH₂Ph), 5.01 (s, 4H, CH₂Ph), 4.92 (s, 4H, CH₂Ph), 4.01-3.90 (m, 12H, OCH₂CH₂), 1.84-1.72 (m, 12H, OCH₂CH₂), 1.50-1.24 (m, 120H, H_{aliph}+C(CH₃)₂), 0.90 (t, *J* = 6.6 Hz, 18H, CH₂CH₃).
¹³C NMR (100 MHz, CD₂Cl₂), δ(ppm): 158.96, 153.07, 132.14, 130.08, 129.25, 128.91, 114.38, 113.99, 74.59, 70.87, 68.06, 67.94, 31.85, 29.60, 29.54, 29.38, 29.28, 29.24, 25.98, 22.67, 13.82. PM (C₁₄₀H₂₀₉BO₁₆): 2158.96 u. MS (MALDI-TOF) *m/z*: 2181.55 (M⁺+Na⁺, 100 %).

Synthesis of di-tert-butyl 3,6-bis(3',5'-bis((3,4,5-tris((4-(dodecyloxy)benzyl)oxy)benzyl)oxy)-[1,1'-biphenyl]-4-yl)-1,4-dioxopyrrolo[3,4-c]pyrrole-2,5(1H,4H)-dicarboxylate, **18a**



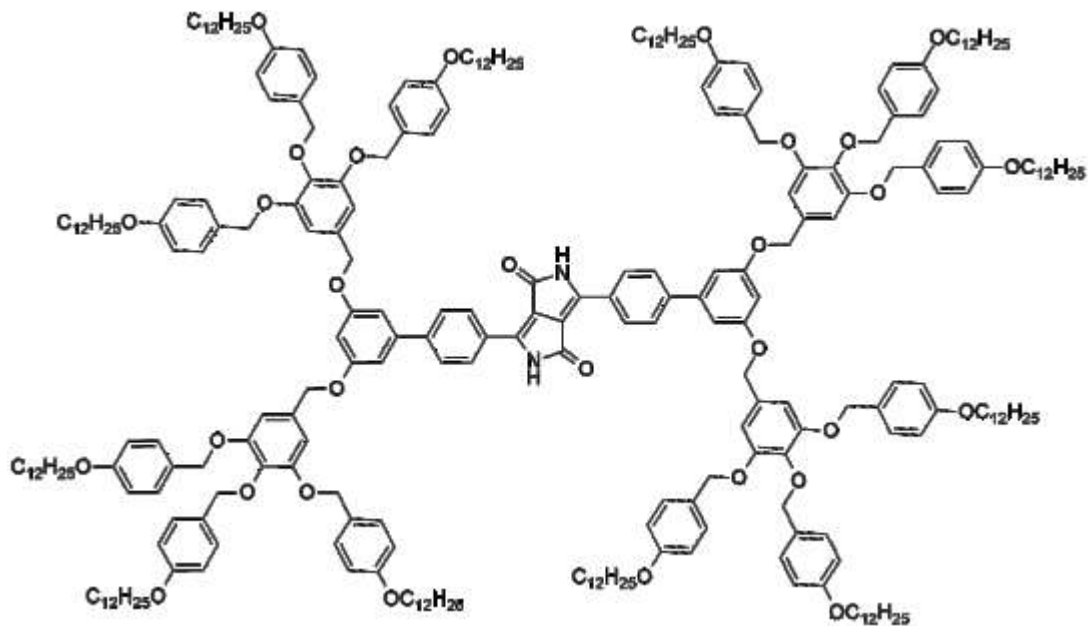
18a

To a suspension of degassed toluene (15.0 mL) and K₂CO₃ (3.2 mL of a 2 M aqueous solution) were added, under argon atmosphere, Br DPP-Boc (70 mg, 0.108 mmol), compound **17** (699 mg, 0.324 mmol) and a catalytic amount (1 % m/m) of Pd(PPh₃)₄. The resulting mixture was heated at 80° C for 27 hours, cooled and then extracted with DCM. The combined extracts were dried over anhydrous MgSO₄ and evaporated under reduced pressure. The crude product was not purified (Crude: 503 mg).

¹H NMR (400 MHz, CDCl₃), δ (ppm): 7.85 (d, *J* = 8 Hz, 4H, H_{arom}), 7.71 (d, *J* = 8 Hz, 4H, H_{arom}), 7.33 (d, *J* = 8 Hz, 16H, H_{arom}), 7.29 (d, *J* = 8 Hz, 8H, H_{arom}), 6.91-6.86 (m, 18H, H_{arom}), 6.79-6.73

(s+d, 16H, H_{arom}), 6.66 (t, $J = 8$ Hz, 2H, H_{arom}), 5.04 (s, 16H, CH_2Ph), 4.99 (s, 8H, CH_2Ph), 4.95 (s, 8H, CH_2Ph), 3.98-3.88 (m, 24H, OCH_2CH_2), 1.82-1.74 (m, 24H, OCH_2CH_2), 1.44-1.22 (m, 234H, $H_{\text{aliph}} + \text{C}(\text{CH}_3)_3$), 0.88 (m, 36H, CH_2CH_3). PM ($\text{C}_{296}\text{H}_{420}\text{N}_2\text{O}_{34}$): 4550,49 u.

Synthesis of 3,6-bis(3',5'-bis((3,4,5-tris((4-(dodecyloxy)benzyl)oxy)benzyl)oxy)-[1,1'-biphenyl]-4-yl)pyrrolo[3,4-c]pyrrole-1,4(2H,5H)-dione, 18 b, G2-pDPP

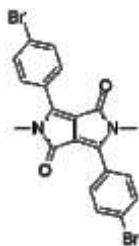


18b
G2-pDPP

A mixture of compound **18a** (503 mg, 0.110 mmol) and silica-gel (5 g) in DCM was evaporated under reduced pressure. The compound was left in silica for 10 days. The crude product was purified by column chromatography (100 % DCM) to obtain the desired product, **18b** (65 mg, yield of two steps: 14 %).

EA: [C] 78.68 %, [H] 9.42 %, [N] 0.61 %. ^1H NMR (400 MHz, CDCl_3), δ (ppm): 8.35 (d, $J = 8.6$ Hz, 4H, H_{arom}), 8.24 (s, 2H, NH), 7.82 (d, $J = 8.4$ Hz, 4H, H_{arom}), 7.34 (d, $J = 8.7$ Hz, 16H, H_{arom}), 7.25 (d, $J = 8.6$ Hz, 8H, H_{arom}), 6.95 (d, $J = 4.0$ Hz, 18H, H_{arom}), 6.89 (d, $J = 8.0$ Hz, 16H, H_{arom}), 6.79 (s, 8H, H_{arom}), 6.76 (d, $J = 8.0$ Hz, 8H, H_{arom}), 6.68 (t, 4H, 2H, H_{arom}), 5.02 (s+s, 24H, CH_2Ph), 4.91 (s, 8H, CH_2Ph), 3.98-3.90 (m, 24H, OCH_2CH_2), 1.81-1.72 (m, 24H, OCH_2CH_2), 1.51-1.24 (m, 216H, H_{aliph}), 0.88 (m, 36H, CH_2CH_3). ^{13}C NMR (100 MHz, CD_2Cl_2), δ (ppm): 204.33, 154.45, 150.75, 130.03, 129.25, 128.89, 114.31, 113.90, 68.03, 31.85, 29.60, 29.57, 29.38, 29.28, 25.98, 22.61, 13.79. PM ($\text{C}_{286}\text{H}_{404}\text{N}_2\text{O}_{30}$): 4350,26 u. MS (MALDI-TOF) m/z : 4373.12 ($\text{M}^+ + \text{Na}^+$, 100 %).

Synthesis of 3,6-bis(4-bromophenyl)-2,5-dimethylpyrrolo[3,4-c]pyrrole-1,4(2H,5H)-dione, 19, methyl BrDPP



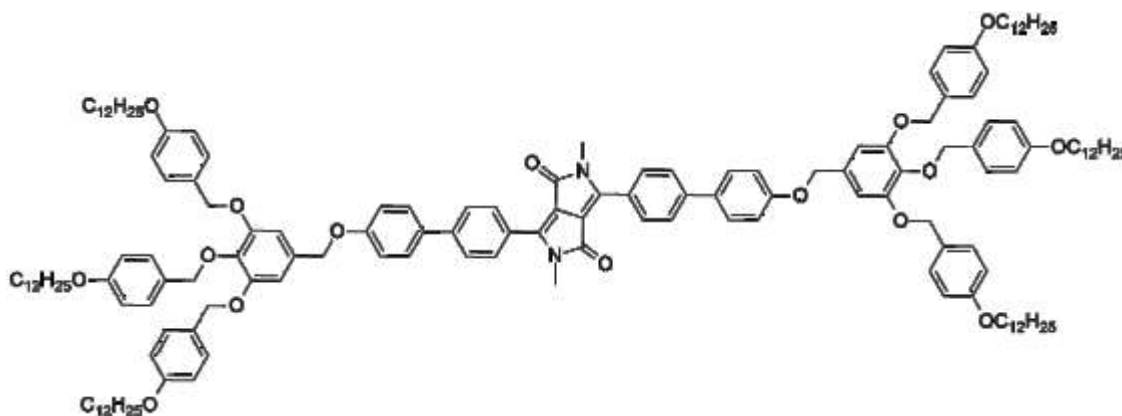
19

Methyl BrDPP

A solution of Br DPP (250 mg, 0.56 mmol) and NaH (0.053 mg, 2.24 mmol) in dry DMF was stirred at room temperature for an hour before adding methyl iodide (365 μ L, 5.93 mmol). After 24 hours the mixture was diluted with water and extracted with DCM. The organic phase was dried over anhydrous $MgSO_4$, filtered, and evaporated under reduced pressure. The crude product was purified by precipitation with ACN to give the desired compound, **19**, as an orange solid (0.167 mg, yield: 63 %).

1H NMR (400 MHz, $CDCl_3$), δ (ppm): 7.71- 7.66 (m, 8H), 3.34 (s, 9H). PM ($C_{20}H_{14}Br_2N_2O_2$): 474,15 u.

Synthesis of 2,5-dimethyl-3,6-bis(4'-((3,4,5-tris((4-(dodecyloxy)benzyl)oxy)benzyl)oxy)-[1,1'-biphenyl]-4-yl)pyrrolo[3,4-c]pyrrole-1,4(2H,5H)-dione, 20, G1.1-methyl DPP



20

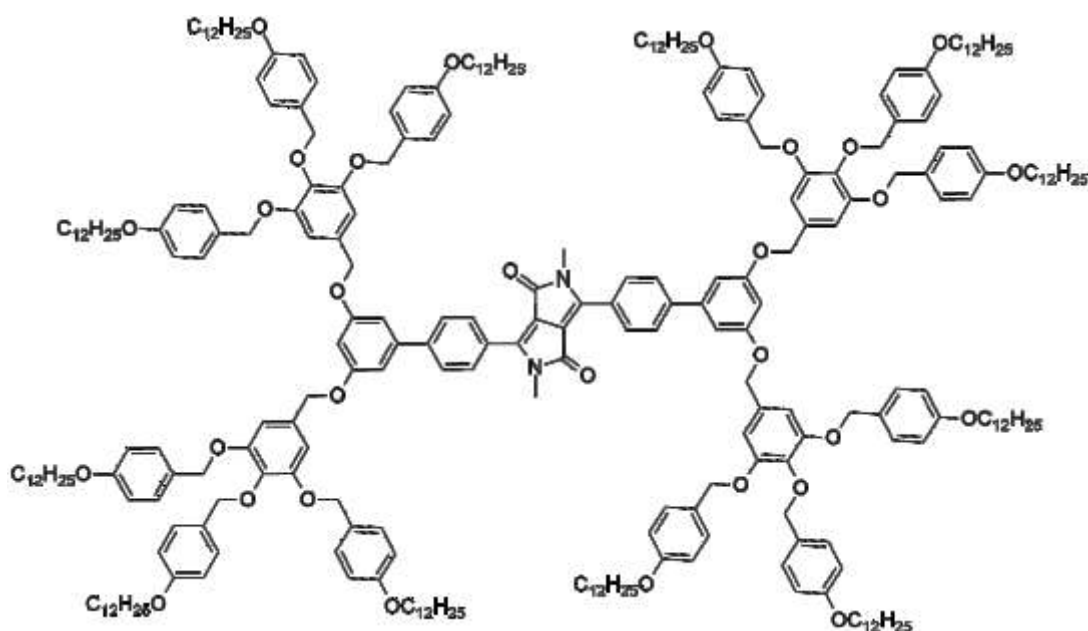
G1.1-methyl DPP

To a suspension of degassed toluene (23.0 mL) and K_2CO_3 (4.0 mL of a 2 M aqueous solution) were added, under argon atmosphere, methyl Br DPP (67 mg, 0.141 mmol), compound **12** (500 mg, 0.423 mmol) and a catalytic amount (1 % m/m) of $Pd(PPh_3)_4$. The resulting mixture was heated at 80° C for 27 hours, cooled and then extracted with DCM. The combined extracts were dried over anhydrous $MgSO_4$ and evaporated under reduced pressure. The crude

product was purified by column chromatography (9.8DCM: 0.2AcOEt) to obtain the desired product, **20**, as a red solid (160 mg, yield: 47 %).

EA: [C] 79.26 %, [H] 8.97 %, [N] 1.10 %. ^1H NMR (400 MHz, CDCl_3), δ (ppm): 8.01 (d, $J = 8.5$ Hz, 4H, H_{arom}), 7.75 (d, $J = 8.5$ Hz, 4H, H_{arom}), 7.61 (d, $J = 8.7$ Hz, 4H, H_{arom}), 7.33 (d, $J = 8.0$ Hz, 8H, H_{arom}), 7.29 (d, $J = 8.0$ Hz, 4H, H_{arom}), 7.06 (d, $J = 8.0$ Hz, 4H, H_{arom}), 6.89 (d, $J = 8.6$ Hz, 8H, H_{arom}), 6.78 (d, $J = 12.0$ Hz, 4H, H_{arom}), 6.75 (s, 4H, H_{arom}), 5.05 (s, 8H, CH_2Ph), 5.0 (s, 4H, CH_2Ph), 4.95 (s, 4H, CH_2Ph), 4.01- 3.86 (m, 12H, OCH_2), 3.42 (s, 6H, $\text{N}(\text{CH}_3)_2$), 1.87-1.60 (m, 12H, OCH_2CH_2), 1.56-1.35 (m, 108H, H_{aliph}), 0.88 (t, $J = 6.8$ Hz, 18H, CH_2CH_3). ^{13}C NMR (100 MHz, CD_2Cl_2), δ (ppm): 162.40, 159.07, 159.00, 158.93, 152.98, 147.73, 143.15, 132.42, 132.27, 130.07, 129.87, 129.63, 129.26, 128.83, 128.16, 126.56, 126.32, 115.29, 114.32, 113.90, 109.19, 106.76, 74.59, 70.84, 70.17, 68.04, 67.94, 31.87, 29.62, 29.58, 29.38, 29.29, 29.25, 25.99, 22.63, 13.81. PM ($\text{C}_{160}\text{H}_{216}\text{N}_2\text{O}_{16}$): 2423,43 u. MS (MALDI-TOF) m/z : 2445.60 ($\text{M}^+ + \text{Na}^+$, 100 %).

Synthesis of 3,6-bis(3',5'-bis((3,4,5-tris((4-(dodecyloxy)benzyl)oxy)benzyl)oxy)-[1,1'-biphenyl]-4-yl)-2,5-dimethylpyrrolo[3,4-c]pyrrole-1,4(2H,5H)-dione, **21, G2-methyl DPP**



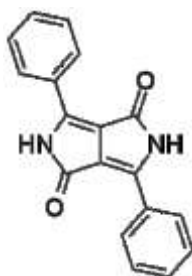
21

G2-methyl DPP

To a suspension of degassed toluene (24.0 mL) and K_2CO_3 (4.41 mL of a 2 M aqueous solution) were added, under argon atmosphere, methyl Br DPP (70 mg, 0.147 mmol), compound **17** (956 mg, 0.44 mmol) and a catalytic amount (1 % m/m) of $\text{Pd}(\text{PPh}_3)_4$. The resulting mixture was heated at 80° C for 27 hours, cooled and then extracted with DCM. The combined extracts were dried over anhydrous MgSO_4 and evaporated under reduced pressure. The crude product was purified by column chromatography (DCM:AcOEt, 9.8:0.2) to obtain the desired product, **21**, as a red solid (328 mg, yield: 51 %).

EA: [C] 78.83 %, [H] 9.64 %, [N] 0.60 %. ^1H NMR (400 MHz, CD_2Cl_2), δ (ppm): 8.04 (d, $J = 8.5$ Hz, 4H, H_{arom}), 7.81 (d, $J = 8.4$ Hz, 4H, H_{arom}), 7.35 (d, $J = 8.6$ Hz, 16H, H_{arom}), 7.26 (d, $J = 8.6$ Hz, 8H, H_{arom}), 6.96 (d, $J = 4.0$ Hz, 4H, H_{arom}), 6.90 (d, $J = 8.0$ Hz, 16H, H_{arom}), 6.82 (s, 8H, H_{arom}), 6.76 (d, $J = 8.0$ Hz, 8H, H_{arom}), 6.69 (t, $J = 4.0$ Hz, 2H, H_{arom}), 5.04 (s, 24H, CH_2Ph), 4.91 (s, 8H, CH_2Ph), 3.99-3.91 (m, 24H, OCH_2), 3.39 (s, 6H, $\text{N}(\text{CH}_3)_2$), 1.82-1.75 (m, 24H, OCH_2CH_2), 1.51-1.22 (m, 216H, H_{aliph}), 0.96-0.84 (m, 36H, CH_2CH_3). ^{13}C NMR (100 MHz, CD_2Cl_2), δ (ppm): 162.46, 160.35, 159.07, 158.93, 153.03, 147.74, 132.20, 130.06, 129.87, 129.58, 129.27, 128.81, 127.26, 114.32, 113.90, 106.79, 74.61, 70.89, 70.34, 68.03, 67.94, 31.86, 29.61, 29.58, 29.38, 29.29, 29.25, 25.99, 22.62, 13.81. PM ($\text{C}_{288}\text{H}_{408}\text{N}_2\text{O}_{30}$): 4378,32 u. MS (MALDI-TOF) m/z : 4401.02 ($\text{M}^+ + \text{Na}^+$, 100 %).

3,6-diphenylpyrrolo[3,4-c]pyrrole-1,4(2H,5H)-dione, **22**, DPP

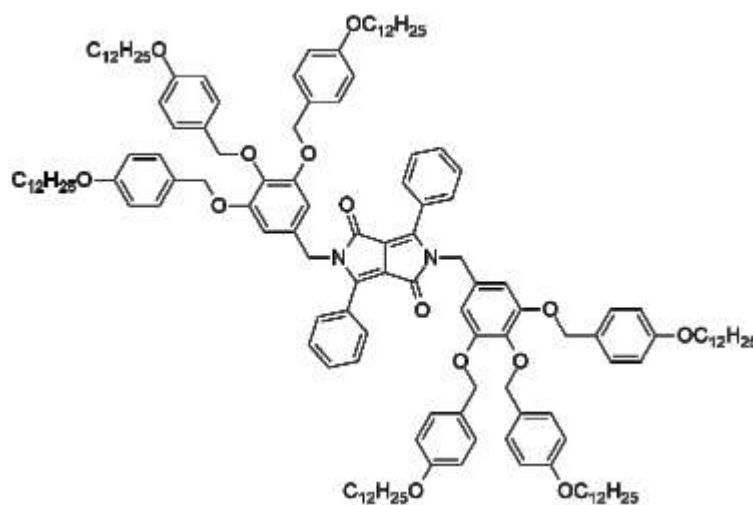


22
DPP

Under argon atmosphere $t\text{-BuOK}$ (g, 126.33 mmol) and tert-amylalcohol (60mL) were heated to reflux. before adding 2-benzonitrile (10 g, 54.93 mmol) in one portion. Then di-iso-propyl succinate (5.55 g, 27.46 mmol) was added dropwise over 8 hours with a syringe pump and then the mixture was vigorously stirred for a night. Therefore, the reaction was quenched by adding at 60°C CH_3OH before and HCl 2M after. The bright red suspension was filtered and washed with water and methanol. This procedure was repeated until the filtrate was clear. The red powder was dried under vacuum to give **22** (7 g, yield: 57 %).

^1H NMR (400 MHz, $(\text{CD}_3)_2\text{SO}$), δ (ppm): 8.47 (m, 4H, H_{arom}), 7.56 (m, 6H, H_{arom}). PM ($\text{C}_{18}\text{H}_{12}\text{N}_2\text{O}_2$): 288,30 u.

Synthesis of 3,6-diphenyl-2,5-bis(3,4,5-tris((4-(dodecyloxy)benzyl)oxy)benzyl)pyrrolo[3,4-c]pyrrole-1,4(2H,5H)-dione, 23, G1-DPP

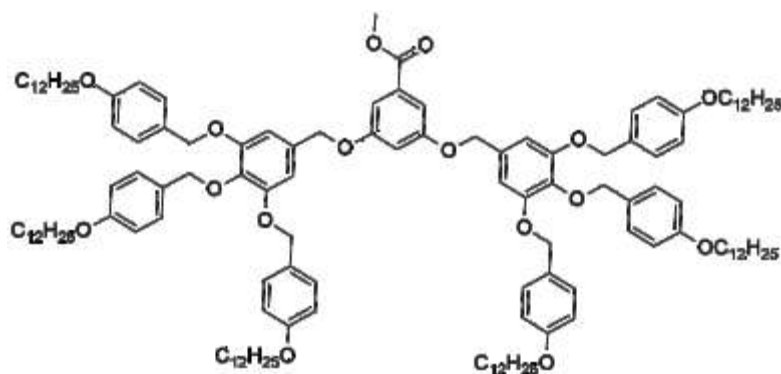


23
G1-DPP

A solution of **DPP** (0.07 g, 0.242 mmol), K_2CO_3 (0.470 g, 3.39 mmol) in DMF (3 mL) was stirred for 45 minutes at room temperature under argon. A solution of **9** (0.362 g, 0.363 mmol) in THF (3 mL) was added. The reaction mixture was heated at reflux over night. The reaction was quenched with water and extracted with DCM. The organic phase was washed with brine, dried with $MgSO_4$ and evaporated under reduced pressure. The crude product was purified by HPLC to give compound **23**, as a orange solid (0.133 g, yield: 25 %).

EA: [C] 79,09 %; [H] 9.43 %; [N] 1.32 %. 1H NMR (400 MHz, $CDCl_3$), δ (ppm): 7.69-7.66 (m, 4H, H_{arom}), 7.51-7.38 (m, 6H, H_{arom}), 7.26-7.19 (d+d, 12H, H_{arom}), 6.79 (d, $J = 8.0$ Hz, 8H, H_{arom}), 6.74 (d, $J = 8.0$ Hz, 4H, H_{arom}), 6.42 (s, 4H, H_{arom}), 4.88 (s+s+s, 16H, CH_2Ph), 3.93-3.84 (m, 12H, OCH_2), 1.81-1.70 (m, 12H, OCH_2CH_2), 1.49-1.22 (m, 108H, H_{aliph}), 0.88 (t, $J = 8.5$ Hz, 18H). ^{13}C NMR (100 MHz, $CDCl_3$), δ (ppm): 162.41, 158.76, 152.96, 148.82, 132.66, 130.09, 128.94, 128.70, 127.92, 114.25, 113.93, 67.88, 31.80, 29.56, 29.52, 29.49, 29.34, 29.23, 25.96, 22.56, 13.99. PM ($C_{146}H_{204}N_2O_{14}$): 2211,19 u.

Synthesis of methyl 3,5-bis((3,4,5-tris((4-(dodecyloxy)benzyl)oxy)benzyl)oxy)benzoate, 24

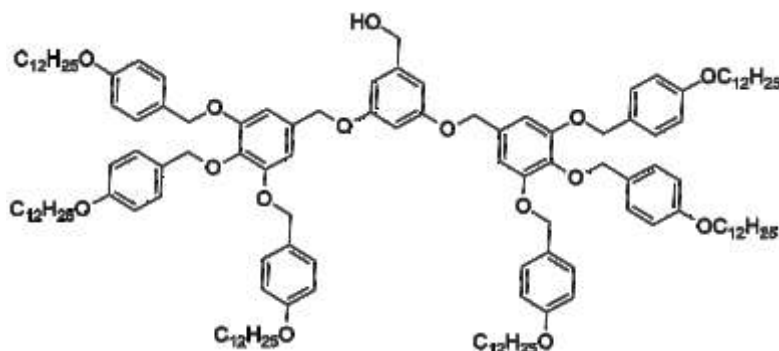


24

A solution of methyl 3,5-dihydroxybenzoate (1.078 g, 6.41 mmol), K_2CO_3 (8.9 g, 64.35 mmol) in DMF (90 mL) was stirred at room temperature for 45 minutes under argon. A solution of **9** (16 g, 16.033 mmol) in dry THF (70 mL) was added. The reaction mixture was heated at 70° C for 18 hours, cooled and extracted with DCM. The organic phase was washed with brine, dried with $MgSO_4$ and evaporated under reduced pressure. The crude product was purified by column chromatography (8DCM:2Heptane) to give compound **24**, as a colourless solid (4.74 g, yield: 55 %).

1H NMR(400MHz, CD_2Cl_2), δ (ppm): 7.33 (d, 8H, H_{arom}), 7.29 (d, 2H, H_{arom}), 7.24 (d, 4H, H_{arom}), 6.89 (d, 8H, H_{arom}), 6.80 (t, 1H, H_{arom}), 6.76 (d, 4H, H_{arom}), 6.75 (d, 4H, H_{arom}), 5.01 (s, 8H, OCH_2), 4.99 (s, 4H, OCH_2), 4.89 (s, 4H, OCH_2), 3.97-3.89 (m, 12H, OCH_2), 3.90 (s, 3H, CO_2CH_3); 1.79-1.74 (m, 12H, OCH_2CH_2); 1.47-1.28 (m, 108H, H_{aliph}); 0.89 (t, 18H, CH_2CH_3). PM ($C_{136}H_{200}O_{16}$): 2091,03 u.

Synthesis of (3,5-bis((3,4,5-tris((4-(dodecyloxy)benzyl)oxy)benzyl)oxy)phenyl)methanol, **25**

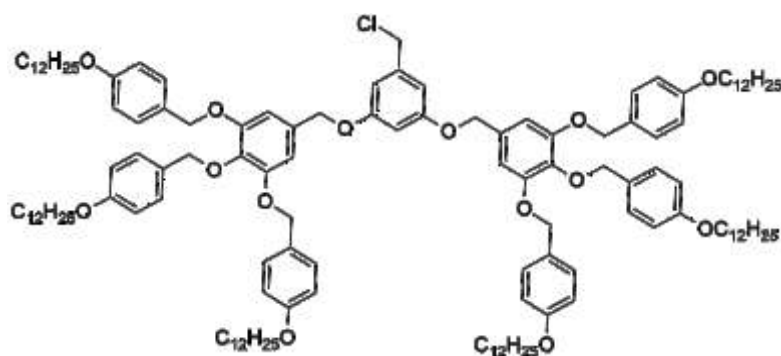


25

Compound **24** (10.88 g, 5.20 mmol) was dissolved in dry THF (50 mL) and the solution was added in small portions to a solution of $LiAlH_4$ (3.94 g, 10.40 mmol) and dry THF (120 mL) at 0° C. The reaction mixture was allowed to room temperature and stirred for 2 hours under argon. The reaction was quenched with ice/water and then extracted with diethyl ether twice. The organic phase was washed with brine, dried with $MgSO_4$ and the solvent was evaporated to give compound **25**, as a colourless solid (10.4 g, yield: 97 %).

1H NMR (400 MHz, $CDCl_3$), δ (ppm): 7.31 (d, $J = 8.0$ Hz, 8H, H_{arom}), 7.28 (d, $J = 8.0$ Hz, 4H, H_{arom}), 6.87 (d, $J = 8.0$ Hz, 8H, H_{arom}), 6.76 (d, $J = 8.0$ Hz, 4H, H_{arom}), 6.69 (s, 4H, H_{arom}), 6.59 (d, $J = 4.0$ Hz, 2H, H_{arom}), 6.52 (t, $J = 4.0$ Hz, 1H, H_{arom}), 5.02 (s, 8H, OCH_2), 4.93 (s, 4H, OCH_2), 4.92 (s, 4H, OCH_2), 3.98-3.90 (m, 12H, OCH_2), 1.81-1.72 (m, 12H, OCH_2CH_2), 1.47-1.18 (s, 108 H, H_{aliph}), 0.88 (t, $J = 6.8$ Hz, 18H, CH_2CH_3). PM ($C_{135}H_{200}O_{15}$): 2063,02u.

Synthesis of 26

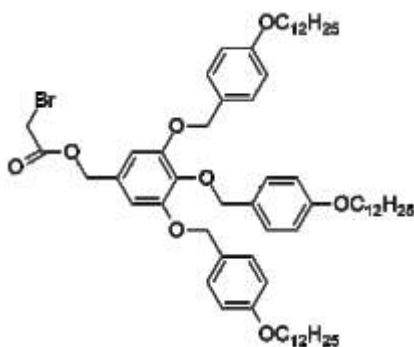


26

A solution of SOCl₂ (374 μL, 5.31 mmol) in dry DCM (20 mL) was added dropwise to a solution of compound **25** (10.54 g, 5.10 mmol), DTBP (2.29 mL, 10.21 mmol) in dry DCM (115 mL) under argon. The reaction mixture was stirred for 30 minutes at room temperature. Then the solution was extracted with HCl 2N and the organic phase was washed with brine, dried with MgSO₄ and the solvent was evaporated to give compound **26**, as a colourless solid. (9.96 g, yield: 94 %).

¹H NMR (400 MHz, CDCl₃), δ (ppm): 7.32 (d, *J* = 10 Hz, 8H, H_{arom}), 7.29 (d, *J* = 8.4 Hz, 4H, H_{arom}), 6.88 (d, *J* = 8.8 Hz, 8H, H_{arom}), 6.77 (d, *J* = 8.8 Hz, 4H, H_{arom}), 6.71 (s, 4H, H_{arom}), 6.63 (d, *J* = 2.4 Hz, 2H, H_{arom}), 6.55 (t, *J* = 4 Hz, 1H, H_{arom}), 5.02 (s, 8H, OCH₂), 4.93 (s, 4H, OCH₂), 4.92 (s, 4H, OCH₂), 4.95 (s, 2H, CH₂Cl), 3.98- 3.87 (m, 12H), 1.83-1.72 (m, 12H, OCH₂CH₂), 1.49-1.21 (m, 108H, H_{aliph}), 0.89 (t, *J* = 6.7 Hz, 18H, CH₂CH₃). PM (C₁₃₅H₁₉₉ClO₁₄): 2081,47 u.

Synthesis of 3,4,5-tris((4-(dodecyloxy)benzyl)oxy)benzyl 2-bromoacetate, 28



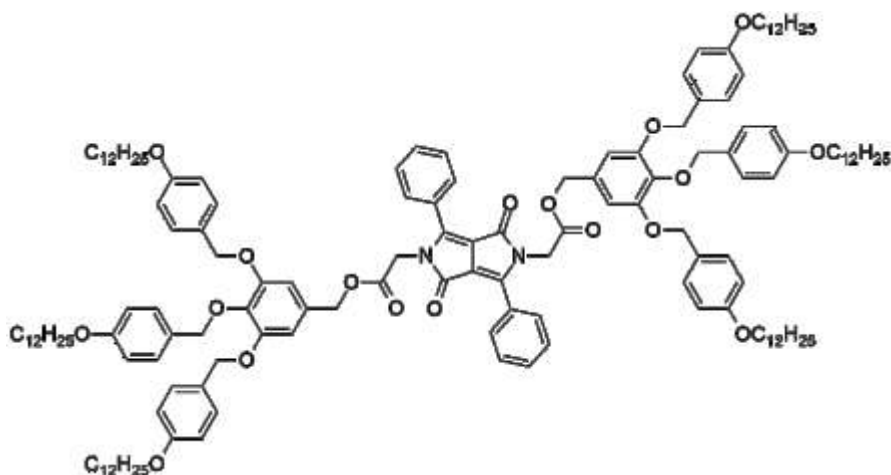
28

Compound **9** (0.600 g, 0.613 mmol) was dissolved in 6 mL of DCM and 2-bromoacetic acid (0.170 g, 1.22 mmol), DIC (189 μL, 1.22 mmol) and a catalytic amount of DMAP (0.030 g, 0.245 mmol) were added. The reaction mixture was stirred at room temperature for 1h. After the solution was evaporated under vacuum, methanol was added to the residue followed by filtration to afford the product **28** (0.645 g, yield: 97 %).

¹H NMR (400 MHz, CDCl₃), δ (ppm): 7.32-7.26 (m, 6H, H_{arom}), 6.88 (d, *J* = 8.6 Hz, 4H, H_{arom}), 6.76 (d, *J* = 8.6 Hz, 2H, H_{arom}), 6.64 (s, 2H, H_{arom}), 5.08 (s, 2H, OCH₂), 5.01 (s, 4H, OCH₂), 4.94 (s, 2H,

OCH₂), 3.99- 3.89 (m, 6H, OCH₂), (3.86, s, CH₂Br), 1.85-1.71 (m, 6H, OCH₂CH₂), 1.46-1.26 (m, 54H, H_{aliph}), 0.88 (t, *J* = 8.0 Hz, 9H, CH₂CH₃). ¹³C NMR (100 MHz, CDCl₃), δ (ppm): 158.70, 152.74, 129.94, 128.86, 128.53, 114.16, 113.83, 108.03, 70.88, 67.79, 31.63, 29.38, 29.35, 29.32, 29.14, 29.06, 25.78, 25.57, 22.40, 13.82. PM (C₆₆H₉₉BrO₈): 1100,39 u.

Synthesis of bis(3,4,5-tris((4-(dodecyloxy)benzyl)oxy)benzyl) 2,2'-(1,4-dioxo-3,6-diphenylpyrrolo[3,4-c]pyrrole-2,5(1H,4H)-diyl)diyl)diacetate, 29, G1-DPP spacer



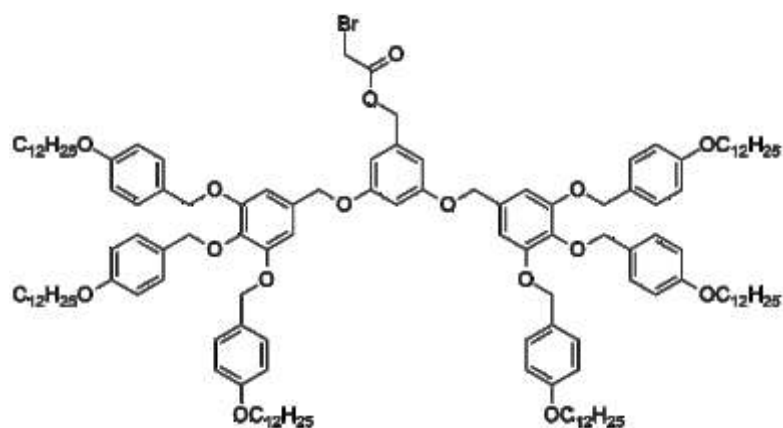
29

G1-DPP spacer

A solution of **DPP** (0.05 g, 0.173 mmol), K₂CO₃ (0.335 g, 2.42 mmol) in dry DMF (2 mL) was stirred for 45' at room temperature under argon. A solution of **28** (0.476 g, 0.433 mmol) in dry DMF (5 mL) was added. The reaction mixture was heated at reflux over night. The reaction was quenched with water and extracted with DCM. The organic phase was washed with brine, dried with MgSO₄ and evaporated under reduced pressure. The crude product was purified by column chromatography (8DCM:2AcOEt) to give compound **29** as a orange solid (0.360 g, yield: 90 %).

EA: [C] 77.49 %; [H] 9.18 %; [N] 1.18 %. ¹H NMR (400 MHz, CDCl₃), δ (ppm): 7.72-7.69 (m, 2H, H_{arom}), 7.46- 7.37 (m, 6H, H_{arom}), 7.31-7.26 (d+d, 12H, H_{arom}), 6.87 (d, *J* = 8.6 Hz, 8H, H_{arom}), 6.75 (d, *J* = 8.6 Hz, 4H, H_{arom}), 6.61 (s, 4H, H_{arom}), 5.05 (s, 4H, OCH₂), 4.96 (s, 8H, OCH₂), 4.94 (s, 4H, OCH₂), 3.98-3.95 (m, 12H, OCH₂), 1.85- 1.54 (m, 12H, OCH₂CH₂), 1.45-1.23 (m, 108H, H_{aliph}), 0.88 (t, *J* = 6.8 Hz, 18H). ¹³C NMR (100 MHz, CDCl₃), δ (ppm): 168.09, 161.93, 158.68, 158.62, 152.75, 147.95, 138.39, 130.05, 129.93, 129.54, 128.92, 128.82, 128.55, 128.38, 127.09, 114.14, 113.83, 109.38, 107.87, 70.81, 67.78, 67.70, 31.63, 29.39, 29.35, 29.33, 29.16, 29.06, 29.03, 25.79, 22.40, 13.82. PM (C₁₅₀H₂₀₈N₂O₁₈): 2327,26 u.

3,5-bis((3,4,5-tris((4-(dodecyloxy)benzyl)oxy)benzyl)oxy)benzyl 2-bromoacetate, **30**

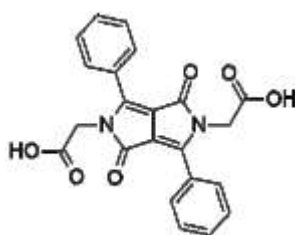


30

Compound **25** (1.2 g, 0.581 mmol) was dissolved in 10 ml of DCM and 2-bromoacetic acid (0.161 g, 1.16 mmol), DIC (180 μ l, 1.16 mmol) and a catalytic amount of DMAP (0.028 g, 0.232 mmol) were added. The reaction mixture was stirred at room temperature for 1h. After the solution was evaporated under vacuum, methanol was added to the residue followed by filtration to afford the product **30** (1.18 g, yield: 93 %).

^1H NMR (400 MHz, CDCl_3), δ (ppm): 7.32-7.25 (d+d, 12H, H_{arom}), 6.87 (d, $J = 8.6$ Hz, 8H, H_{arom}), 6.76 (d, $J = 8$ Hz, 4H, H_{arom}), 6.72 (s, 4H, H_{arom}), 6.60 (d, $J = 2$ Hz, 2H, H_{arom}), 6.57 (t, $J = 4$ Hz, 1H, H_{arom}), 5.14 (s, 2H, OCH_2), 5.01 (s, 8H, OCH_2), 4.92 (s, 4H, OCH_2), 4.91 (s, 4H, CH_2Br), 3.97-3.89 (m, 12H, OCH_2), 1.82-1.72 (m, 12H, OCH_2CH_2), 1.47-1.22 (m, 108H, H_{aliph}), 0.88 (t, $J = 6.7$ Hz, 18H, CH_2CH_3). PM ($\text{C}_{137}\text{H}_{201}\text{BrO}_{16}$): 2183,96 u.

2,2'-(1,4-dioxo-3,6-diphenylpyrrolo[3,4-c]pyrrole-2,5(1H,4H)-diyl)diacetic acid, **32**

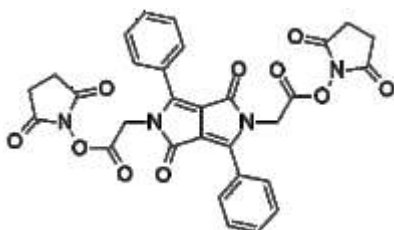


32

Di-tert-butyl ester **32** (78 mg, 0.15 mmol, 1 equiv.) was dissolved in DCM (2.5 mL). TFA (1.39 mL, 18.05 mmol, 120 equiv.) was added and the resulting reaction mixture was stirred for a night. The reaction was checked for completion by TLC (DCM/EtOAc 9 : 1, v/v) and the mixture was evaporated under reduced pressure. The residual TFA was evaporated with DCM and diethyl ether to obtain, **32**, an orange solid (58 mg, yield: 95 %).

^1H NMR (400 MHz, $(\text{CD}_3)_2\text{SO}$), δ (ppm): 7.79 (dd, $J = 6.7, 3.0$ Hz, 4H, H_{arom}), 7.63- 7.53 (m, 6H, H_{arom}), 4.26 (s, 4H, NCH_2). PM($\text{C}_{22}\text{H}_{16}\text{N}_2\text{O}_6$): 404,37 u.

bis(2,5-dioxopyrrolidin-1-yl) 2,2'-(1,4-dioxo-3,6-diphenylpyrrolo[3,4-c]pyrrole-2,5(1H,4H)-diyl)diacetate, **33**



33

Compound **32** (0.450 g, 1.11 mmol), EDAC (0.415 g, 2.67 mmol) and N-hydroxysuccinimide (0.310 g, 2.67 mmol) were stirred in dry DMF (50 mL) for 4 hrs and 30' thus another portion of EDAC (0.070 g, 0.44 mol) was added. After a night the reaction mixture was diluted with ice and water. The orange precipitated was filtered and washed with water to obtain **33** (0.630 g, yield: 95 %).

^1H NMR (400 MHz, $(\text{CD}_3)_2\text{SO}$), δ (ppm): 7.80 (dd, $J = 8.0, 1.6$ Hz, 4H, H_{arom}), 7.70-7.56 (m, 6H, H_{arom}), 4.98 (s, 4H, NCH₂), 2.79 (s, 8H, C(CH₂)₂). PM ($\text{C}_{30}\text{H}_{22}\text{N}_4\text{O}_{10}$): 598,52 u.

- ¹ (a) Mizrahi, A.; Ben-Ner, E.; Katz, M. J.; Kedem, K.; Glusman, J. G.; Libersat, F. *J Comp Neurol* **2000**, *422*, 415-428. (b) Tomalia, D. A.; Naylor, A. M.; Goddard, W. A. *Angew. Chem.*, Int. Ed. Engl. **1990**, *29*, 138-175. (c) Hawker, C. J.; Wooley, K. L.; Fréchet, M. J. *J. Chem. Soc., Perkin Trans.* **1993**, *1*, 1287-1297. (d) Fréchet, M. J. *J. Science* **1994**, *263*, 1710. (e) Tomalia, D. A. *Adv. Mater.* **1994**, *6*, 529-539. (f) Ardoin, N.; Astruc, D. *Bull. Soc. Chim. Fr.* **1995**, *132*, 875-909.
- ² (a) Tomalia, D. A.; Fréchet, M. J. *J. Polym. Chem.* **2002**, *20*, 2719-2726. (b) Tomalia, D. A. Dendrimer molecules *Sci. Am.* **1995**, *272*, 42-46.
- ³ Tripathy, S.; Das, M. K. *J.App.Pharm.Sci.* **2013**, *3* (09); 142-149.
- ⁴ (a) Fréchet, M. J.; Tomalia, D. A. *J. Polym. Sci.* **2002**, *40*, 2719-2728. (b) Farrington, P. J.; Hawker, C. J.; Fréchet, M. J.; Mackay, M. E. *Macromolecules*, **1998**, *31*, 5043-5050.
- ⁵ (a) Flory, P. J. *J. Am. Chem. Soc.* **1952**, *74*, 2718-2723. (b) Flory, P. J. *J. Am. Chem. Soc.* **1941**, *63*, 3083-3090. (c) Flory, P. J. *J. Am. Chem. Soc.* **1941**, *63*, 3091-3096. (d) Flory, P. J. *J. Am. Chem. Soc.* **1941**, *63*, 3096-3100. (e) Flory, P. J. *J. Am. Chem. Soc.* **1942**, *64*, 132.
- ⁶ Buhleier, E.; Wehener, W.; Vögtle, F. *Synthesis*, **1978**, *9*, 155-158.
- ⁷ Newkome, G. R.; Moorefield, F.; Vögtle, F. *Dendritic molecules: concepts, synthesis, perspectives - VCH*, **1996**, 17-20.
- ⁸ (a) Tomalia, D. A. *Prog. Polym. Sci.* **2005**, *50*, 294-324. (b) Balogh, L.; Leuze-Jallouli, A.; Dvornic, P.; Kunugi, Y.; Blumstein, A.; Tomalia, D. A. *Macromolecules* **1999**, *32*, 1036-1042. (c) Topp, A.; Bauer, B. J.; Tomalia, D. A.; Amis, E. J. *Macromolecules*, **1999**, *32*, 7232-7237. (d) Tomalia, D. A.; Baker, H.; Dewald, J.; Hall, M.; Kallos, G.; Martin, S.; Roeck, J.; Ryder, J.; Smith, P. *Polym. J.* **1985**, *17*, 117-132.
- ⁹ Newkome, G. R.; Yao, Z.; Baker, G. R.; Gupta, V. K. *J. Org. Chem.* **1985**, *50*(11), 2003-2004.
- ¹⁰ (a) Hawker, C. J.; Fréchet, M. J. *J. Chem. Soc. Chem. Commun.* **1990**, *112*, 1010-1013. (b) Hawker, C. J.; Fréchet, M. J. *J. Am. Chem. Soc.* **1990**, *112*, 7638-7647. (c) Fréchet, M. J.; Jiang, Y.; Hawker, C. J.; Philippides, A. E. Proceedings of IUPAC International Symposium, *Macromolecules*, Seoul, Korea, **1989**, 19-20.
- ¹¹ Madaan, K.; Kumar, S.; Poonia, N.; Lather, V.; Pandita, D. *J Pharm Bioallied Sci.* **2014**, *6* (3), 139-150.
- ¹² Langereis, S.; Dirksen, A.; Hackeng, T. M.; van Genderen, M. H. P.; Meijer, E. W. *New J.Chem.* **2007**, *31*, 1152-1160.
- ¹³ Astruc, D.; Chardac, F. *Chem. Rev.* **2001**, *101*, 2991-3023.
- ¹⁴ Mia Gi, M.; Im, W.; Hong, S. *Sensors* **2009**, *9*(9), 6730-6751.
- ¹⁵ (a) Sarkar, A.; Carver, P. I.; Zhang, T.; Merrington, A.; Bruza, K. J.; Rousseau, J. L.; Keinath, S. E.; Dvornic, P. R. *Journal of Membrane Science* **2010**, *349*, 421-428. (b) Jong, E. R.; Deloch, N.; Knoll, W.; Turrin, C. O.; Majoral, J. P.; Caminade, A. M.; Köper, I. *New J. Chem.*, **2015**, *39*, 7194-7205.
- ¹⁶ Caminade, A. M.; Cedric-Olivier Turrin, C. O.; (a cura di), Regis Laurent, R.; Armelle Ouali, A.; Delavaux-Nicot, B. *Dendrimers: Towards Catalytic, Material and Biomedical Uses*, Wiley, 1 Ed., **2011**.
- ¹⁷ (a) Eichman, J. D.; Bielinska, A. U.; Kukowska-Latallo, J. F.; Baker, J. R. *PSTT* **2000**, *3* (7), 232-245. (b) Wang, H.; Shi, H. B.; Yin, S. K. *Exp. Ther. Med.* **2011**, *2*, 777-781.
- ¹⁸ (a) Hodge, P. *Nature*, **1993**, *362*, 18-19. (b) Grayson, S. M.; Fréchet, M. J. *J. Chem. Rev.*, **2001**, *101*, 3819-3867.
- ¹⁹ Svenson, S.; D. A. Tomalia, D. A. *Advanced Drug Delivery Reviews*, **2005**, *57*, 2106-2129.
- ²⁰ Mishra, M.; Kobayashi, S. *Star and Hyperbranched Polymers*, **1999**, CRC Press.
- ²¹ (a) Israelachvili, J. *Intermolecular and Surface Forces*, 3rd ed., Academic Press, Burlington, **2010**. (b) Hassan, S.; Rowe, W.; Tiddy, G. J. T. *Handbook of Applied Surface and Colloid Chemistry*, Vol. 1 (Ed.: K. Holmberg), Wiley-VCH, Chichester, **2002**, p. 465. Chandrasekhar, S. *Liquid Crystals*, 2nd edition, Cambridge University Press, **1992**.
- ²² Goodby, J. W.; Collings, P. J.; Gleeson, H.; Raynes, P.; Kato, T.; Tschierske, C. *Handbook of Liquid Crystals*, 2nd ed., Wiley-VCH, Weinheim, **2013**.
- ²³ (a) Tschierske, C. *J. Mater. Chem.* **1998**, *8*, 1485-1508; *J. Mater. Chem.* **2001**, *11*, 2647-2671; *Isr. J. Chem.* **2012**, *52*(10), 935-959.
- ²⁴ http://home.arcor.de/stefan._lange/uni/in_rep_html/
- ²⁵ (a) Laschat, S.; Baro, A.; Steinke, N.; Giesselmann, F.; Hägele, C.; Scalia, G.; Judele, R.; Kapatsina, E.; Sauer, S.; Schreivogel, A.; Tosoni, M. *Angew. Chem.* **2007**, *119*, 4916-4973; *Angew. Chem. Int. Ed.* **2007**,

- 46, 4832-4887. (b) Kumar, S. *Chemistry of discotic liquid crystals—From monomers to polymers*, CRC, Taylor & Francis Group, Boca-Raton, **2011**. (c) Roy, B.; De, N.; Majumdar, K. C. *Chem. Eur. J.* **2012**, *18*,14560-14588.
- ²⁶ (a) Würthner, F.; Thalacker, C.; Diele, S.; Tschierske, C. *Chem. Eur. J.* **2001**, *7*, 2245-2553. (b) *Self-organized Organic Semiconductors - From Materials to Device Applications* (Ed.: Q. Li), Wiley, Hoboken, **2011**.
- ²⁷ Guillon, D.; Deschenaux, R. *Current Opinion in Solid State and Materials Science* **2002**, *6*, 515-525.
- ²⁸ Ponomarenko, S. A.; Boiko, N. I.; Shibaev V. *Polymer Science, Ser. C*, **2001**, *43(1)*, 1-45.
- ²⁹ Baars, M. W. P.L.; Söntjens, S. H. M.; Fischer, H. M.; Peerlings, H. W. I.; Meijer, E.W. *Chem Eur J* **1998**;4, 2456-2466.
- ³⁰ (a) Percec, V.; Chu, P.; Ungar, G.; Zhou, J. *J Am. Chem. Soc.* **1995**, *117*, 11441-11454. (b) Baars, M.W.P.L.; Söntjens, S.H.M.; Fischer, H.M.; Peerlings, H.W.I.; Meijer, E.W. *Chem. Eur. J.* **1998**, *4*, 2456-2466.
- ³¹ Donnio, B.; Barbera, J.; Giménez, R.; Guillon, D.; Marcos, M.; Serrano, J. L. *Macromolecules* **2002**;35, 370-381.
- ³² (a) Gehringer, L.; Bourgogne, C.; Guillon, D.; Donnio, B. *J. Am. Chem. Soc.* **2004**, *126*, 3856-3857; *J. Mater. Chem.*, **2005**, *15*,1696-1703.
- ³³ (a) Percec, V.; Cho, W. D.; Ungar, G.; Yeardley, D. J. P. *Angew. Chem. Int. Ed.* **2000**, *39(9)*, 1597-1602. (b) Percec, V.; Cho, W. D.; Ungar, G. *J. Am. Chem. Soc.* **2000**, *122*, 10273-10281. (c) Percec, V.; Cho, W. D.; Mosier, P. E.; Ungar, G.; Yeardley, D. J. P. *J. Am. Chem. Soc.* **1998**, *120*, 11061-11070. (d) Percec, V.; Cho, W. D.; Möller, M.; Prokhorova, S. A.; Ungar G.; Yeardley, D. J. P. *J. Am. Chem. Soc.* **2000**, *122(17)*, 4249-4250. (e) Balagurusamy, V. S. K.; Ungar, G.; Percec, V.; Johansson, G. *J. Am. Chem. Soc.* **1997**, *119*, 1539-1555. (f) Ungar, G.; Percec, V.; Holerca, M. N.; Johansson G.; Heck, J. A. *Chem. Eur. J.* **2000**, *6*, 1285-1296. (g) Percec, V.; Cho, W. D.; Ungar G.; Yeardley, D. J. P. *J. Am. Chem. Soc.* **2001**, *123*, 1302-1315.
- ³⁴ Tschierske, C. *Annu. Rep. Prog. Chem., Sect. C*, **2001**, *97*, 191-267.
- ³⁵ Fréchet, J. M. *Science* **1994**, *263*, 1710-1715.
- ³⁶ Li, Y.; Lin, S. T.; Goddard, W. A. III *J. Am. Chem. Soc.* **2004**, *126(6)*, 1872-1885.
- ³⁷ Zhang, R.; Zeng, X.; Kim, B.; Bushby, R. J.; Shin, K.; Baker, P. J.; Percec, V.; Leowanawat, P.; Ungar, G. *ACS Nano* **2015**, *9(2)*, 1759-1766.
- ³⁸ Popere, B. C.; Della Pelle, A. M.; Poe, A.; Thayumanavan, S. *Phys. Chem. Chem. Phys.* **2012**, *14*, 4043-4057. (b) Satoh, N.; Nakashima, T.; Yamamoto, K. *J. Am. Chem. Soc.* **2005**, *127*, 13030-13038.
- ³⁹ Elizabeth R. Gillies and Jean M.J. Fréchet DDT • Volume 10, Number 1 • January 2005; Oleh Taratula, Olga B. Garbuzenko, Paul Kirkpatrick, Ipsit Pandya, Ronak Savla, Vitaly P. Pozharov, Huixin He, Tamara Minko *Journal of Controlled Release* **140** (2009) 284-293.
- ⁴⁰ Craig J. Hawker and J. M. J. Fréchet *J. Am. Chem. Soc.* **1990**, *112* (21).
- ⁴¹ Balagurusamy, V. S. K.; Ungar, G.; Percec, V.; Johansson, G. *J. Am. Chem. Soc.* **1997**, *119*, 1539-1555.
- ⁴² Haketa, Y.; Sakamoto, S.; Chigusa, K.; Nakanishi, T.; Maeda, H. *J. Org. Chem.* **2011**, *76*, 5177-5184.
- ⁴³ An, Z.; Yu, J.; Domercq, B.; Jones, S. C.; Barlow, S.; Kippelen, B.; Marder, S. R. *J. Mater. Chem.*, **2009**, *19*, 6688-6698.
- ⁴⁴ Green, T. W.; Wuts, P. G. M. *Protective Groups in Organic Synthesis*, Wiley-Interscience, New York, **1999**, 76-86, 708-711.
- ⁴⁵ Zambounis, J.; Hao, Z.; Iqbal A Canadian Patent. Patent number: CAS.117.865, 1995.
- ⁴⁶ Wunderlich, B.; *J. Chem. Phys.* 1958, *29*, 1395.
- ⁴⁷ Kim, S.; Ikuhisa, T.; Chiba, K. *Chemistry Letters* **2011**;40(10),1077-1078.

Estratto per riassunto della tesi di dottorato

Studente: Ester Vagnozzi

matricola: 810846

Dottorato: Scienze Chimiche

Ciclo: XXVIII

Titolo della tesi : Supramolecular organization of diketopyrrolopyrrole derivatives

Abstract:

Il presente lavoro di tesi riguarda la sintesi di materiali innovativi partendo dalla molecola del dichetopirrolopirrolo (DPP), pigmento organico appartenente alla classe degli High Performance Pigments (HPP). In modo particolare sono stati sintetizzati due derivati del DPP in grado di sviluppare degli aggregati supramolecolari in acqua. Il meccanismo di polimerizzazione è stato individuato e caratterizzato tramite UV-Vis, DLS e $^1\text{H-NMR}$, mentre la morfologia dei substrati è stata analizzata mediante AFM e SEM. Tramite DSC e POM si è verificata la presenza di mesofasi per le strutture sintetizzate. Inoltre nel periodo di stage svolto presso il Laboratorio di chimica macromolecolare dell'Università di Neuchâtel sono stati studiati dei derivati del DPP opportunamente sostituiti con dendrimeri poli(benzil eteri) di prima e seconda generazione. La combinazione del DPP con queste macromolecole ha condotto alla sintesi di nuovi composti con elevata stabilità termica, fluorescenti in soluzione e dalla struttura ramificata ben definita. Le strutture ottenute sono state caratterizzate mediante spettrometria Maldi-Tof, DSC e POM. La mesofasi sono state identificate e opportunamente caratterizzate.

In this dissertation two water soluble dyes based on the diketopyrrolopyrrole skeleton have been prepared via Suzuki cross coupling on 3,6-bis(4-bromophenyl)pyrrolo[3,4-c]pyrrole-1,4(2H,5H)-dione. The two molecules, able to develop supramolecular polymers in solution, have been completely characterised, studying their morphology and liquid crystal properties (POM, DSC, AFM, SEM) and appropriate UV and NMR experiments have been done in order to obtain the thermodynamic constants that describe the mechanisms of polymerization. Moreover UV results are in good agreement with our DLS data. Following in collaboration with the macromolecular lab of the University of Neuchâtel we have combined the poly (benzyl ether) dendrimers of first (G1) and second generation (G2) with DPP molecule to study and characterised the supramolecular organization of these new dendritic architectures. All the synthesised substrates have been characterised through elemental analysis, $^1\text{H-NMR}$ and MALDI-TOF mass spectroscopy, DSC and POM.

Firma dello studente
